



HAL
open science

Development of a Targeted Therapy for Charcot Marie Tooth 1A (CMT1A) Neuropathy Based on siRNA PMP22 Squalene Nanoparticles

Suzan Boutary

► **To cite this version:**

Suzan Boutary. Development of a Targeted Therapy for Charcot Marie Tooth 1A (CMT1A) Neuropathy Based on siRNA PMP22 Squalene Nanoparticles. Biotechnology. Université Paris Saclay (COmUE), 2019. English. NNT: 2019SACLS526 . tel-03934632

HAL Id: tel-03934632

<https://theses.hal.science/tel-03934632v1>

Submitted on 11 Jan 2023

HAL is a multi-disciplinary open access archive for the deposit and dissemination of scientific research documents, whether they are published or not. The documents may come from teaching and research institutions in France or abroad, or from public or private research centers.

L'archive ouverte pluridisciplinaire **HAL**, est destinée au dépôt et à la diffusion de documents scientifiques de niveau recherche, publiés ou non, émanant des établissements d'enseignement et de recherche français ou étrangers, des laboratoires publics ou privés.

Développement d'une Thérapie Ciblée pour la maladie Charcot Marie Tooth 1A (CMT1A) par des Nanoparticules siRNA PMP22 Squalénées

Thèse de doctorat de l'Université Paris-Saclay
Préparée à l'Université Paris-Sud

École doctorale n°568 : Signalisations et réseaux intégratifs en
biologie (Biosigne)

Spécialité de doctorat : recherche clinique, innovation technologique, santé
publique

Thèse présentée et soutenue au Le Kremlin-Bicêtre, le 13 Décembre 2019, par

SUZAN BOUTARY

Composition du Jury:

Elias FATTAL

Professeur, Université Paris Sud (UMR CNRS 8612)

Président

Frederic CHARBONNIER

Professeur, Université Paris Descartes (UMR-S1124)

Rapporteur

Ruth STASSART

MD, PhD, Université de Leipzig, Germany

Rapporteur

Charbel MASSAAD

Professeur, Université Paris Descartes (UMR-S1124)

Examineur

Didier DESMAËLe

Directeur de recherche, Université Paris Sud (UMR CNRS 8612)

Examineur

Liliane MASSADE

Directrice de recherche, Université Paris-Sud (UMR1195)

Directrice de thèse

Development of a Targeted Therapy for Charcot Marie Tooth 1A (CMT1A) Neuropathy based on siRNA PMP22 Squalene Nanoparticles

PhD thesis of Paris-Saclay University
Prepared at Paris-Sud University

*Doctoral School n°568: Signals and integrative networks in biology
(Biosigne)
PhD specialty: Clinical research, Innovation Technology, Public Health*

Thesis presented and defended at Le Kremlin-Bicêtre, 13 December 2019, by

SUZAN BOUTARY

Composition of the Jury:

Elias FATTAL Professor, Paris Sud University (UMR CNRS 8612)	President
Frederic CHARBONNIER Professor, Paris Descartes University (UMR-S1124)	Reporter
Ruth STASSART MD, PhD, University of Leipzig, Germany	Reporter
Charbel MASSAAD Professor, Paris Descartes University (UMR-S1124)	Examiner
Didier DESMAËLE Research Director, Paris Sud University (UMR CNRS 8612)	Examiner
Liliane MASSADE Research Director, Paris-Sud University (UMR1195)	Thesis director

This work was supported by a public grant overseen by the French National Research Agency (ANR) as part of the "Investissements d'Avenir" program (Labex NanoSaclay, reference: ANR-10-LABX-0035)

Table of Contents

LIST of TABLES.....	6
LIST of FIGURES	7
ACKNOWLEDGMENT.....	12
ABBREVIATIONS	15
INTRODUCTION	17
A. Peripheral nervous system myelination and pathologies	18
1. Myelin composition and function.....	18
2. Myelin synthesis.....	19
3. Myelin Pathologies.....	20
B. Charcot Marie Tooth.....	21
1. Epidemiology of Charcot Marie Tooth.....	21
2. Classification and most common genes implicated.....	22
C. Charcot Marie Tooth 1A	27
1. Animal Models of CMT1A	27
2. CMT1A drug therapies and treatments	29
3. CMT1A: involvement of immune cells, autophagy and inflammation.....	37
4. Conclusions	38
D. RNA interference: History, encapsulation and clinical Trials	39
1. History of RNAi.....	39
2. Mechanism of action of RNAi	40
3. Barriers to siRNA delivery	41
4. Chemical modifications of siRNA	42
5. Vehicles for siRNA Delivery	43
6. siRNA Therapeutics and Clinical Trials	49
7. Conclusion.....	52
AIM.....	53
MATERIAL AND METHODS	54
1. Screening of siRNA against PMP22.....	54
2. siRNAs and chemical modifications.....	54
3. Bioconjugation of siRNAs.....	55
4. Purification of siRNAPMP22-SQ bioconjugates <i>via</i> HPLC	56
5. MALDI-TOF Mass Spectrometry.....	56

6. Annealing of siRNA-SQ bioconjugates to antisense siRNA strands.....	56
7. Preparation and Characterization of nanoparticles siRNAPMP22-SQ.....	57
8. Cell line.....	57
9. <i>In vitro</i> cell transfection.....	58
10. mRNA extraction and Real time PCR (RT-qPCR).....	58
11. Immunoblotting.....	58
12. Cell Viability Test.....	59
13. CMT1A mouse models.....	59
14. CMT1A mouse model treatment.....	60
15. CMT1A mice model Genotyping Protocol.....	62
16. Behavioral Tests.....	63
a. Beam Walking Test.....	63
b. Locotronic.....	63
c. Grip strength test.....	64
17. Electrophysiological study.....	64
18. Dissection, fixation and cryo-sectioning of sciatic nerve.....	65
19. Immunohistochemistry staining.....	65
20. Statistical Analysis.....	66
RESULTS.....	67
A. Choice of siRNAs PMP22 and their efficacy score.....	67
B. Inhibitory effect of eight different siRNAs PMP22 on PMP22 and P0 gene and protein expression.....	68
C. Effect of different concentrations of siPMP22 number 7 on PMP22 and P0 gene expression and on cell viability.....	71
D. Characterization of siPMP22-SQ Nanoparticles.....	72
E. Characterization of siRNA-Ct SQ Nanoparticles.....	74
F. <i>In vitro</i> inhibitory effect of siPMP22-SQ NPs on siPMP22 and P0 gene expression as well as cell viability.....	76
G. Genotyping of CMT1 A mice models JP18, JY13 and JP18/JY13 B6.....	77
H. Effect of siPMP22-SQ NPs on the motor and neuromuscular activity of single transgenic JP18B6 mice.....	78
I. Electrophysiological analysis on single transgenic JP18B6 mice.....	80
J. Effect of siPMP22-SQ NPS on pmp22 protein expression in JP18 B6 single transgenic mice.....	81
K. Effect of siPMP22-SQ NPs on Schwann cell myelination markers in JP18 B6 single transgenic mice.....	82
L. Effect of siPMP22-SQ NPs on axonal regeneration factor neurofilament in JP18 B6 single transgenic mice.....	85
M. Effect of siPMP22-SQ NPs on the motor and neuromuscular activity of double	

transgenic JP18/JY13 mice	87
N. Electrophysiological analysis of double transgenic JP18/JY13B6 mice	89
O. Effect of siPMP22-SQ NPs on Schwann cell myelination and axonal regeneration markers in JP18/JY13 B6 transgenic mice	90
P. Long lasting effect of siPMP22-SQ NPs on the motor and neuromuscular activity on double transgenic mice.	92
Q. Localization of NPs in Schwann cells and axons of treated mice	94
DISCUSSION	95
CONCLUSIONS	103
PROSPECTIVE	104
REFERENCES	105
APPENDIX	115
I. Synthèse en français.....	116
II. Review: Charcot Marie Tooth Disease Therapies: from the Classical Approach to Gene Regulation.....	131
Submitted to Journal Neurobiology of disease	131
III. European Patent: Antisense RNA Targeting PMP22 For the Treatment of Charcot Marie Tooth 1A.....	132
IV. International extention of the Patent : Antisense RNA Targeting PMP22 For the Treatment of Charcot Marie Tooth 1A	134
V. Demande de Confidentiality	136

LIST of TABLES

Table 1. Classification, Mode of Inheritance and Number of Causative Genes of CMT	21
Table 2. Genetic epidemiology of CMT in the general population from Barreto et al., 2016 [19].....	22
Table 3. Drugs tested as a treatment for CMT1A disease.....	30
Table 4. siRNA Treatment and clinical Trials	50
Table 5. Primary antibodies used for KROX20, NF and SOX10.....	66
Table 6. Secondary antibodies used for KROX20, NF and SOX10	66
Table 7. Comparison of siPMP22-SQ NPto other CMT1A tested drugs	100
Table 7 continued. Comparison of siPMP22-SQ NPto other CMT1A tested drugs	101

LIST of FIGURES

Figure 1. Peripheral nervous system structure showing myelin sheath, node of Ranvier, myelin protein and GAP junctions.....	18
Figure 2. Schematic diagram showing Schwann cells development and the transcriptional factors affected. ↑: increase; ↓: decrease; +: high secretion; - : low secretion.....	20
Figure 3. Schematic diagram representing gene overlap between CMT disease and other diseases of the CNS and PNS	23
Figure 4. Peripheral myelin protein zero structure	25
Figure 5. Representative diagram showing some of the drugs tested for CMT1A treatments and the pathways involved.....	38
Figure 6. Petunia flower where gene of pigmentation where silenced by RNAi [140].....	39
Figure 7. Timeline of the important events in RNAi discovery.....	40
Figure 8. RNA interference. Long dsRNA introduced into the cytoplasm is processed by the enzyme Dicer into 22-nt pieces with 2-nt single-stranded overhangs on the 3'-ends. The structure of synthetic siRNA mimics that of Dicer products. The siRNA guide strand is loaded into the RNA-induced silencing complex (RISC), and the passenger strand is cleaved by Argonaute-2 (Ago2). The activated RISC–guide-strand complex identifies and cleaves mRNA that is complementary to the guide strand, preventing translation and thereby silencing gene expression[150].....	41
Figure 9. Different types of siRNA delivery systems: (a) siRNA chemical modification, (b) Lipoplexes, (c) stable nucleic acid- lipid particles (SNALPs), (d) Polymer based delivery (Cyclodextrin), (e) conjugate siRNA delivery, (f) aptamer-siRNA chimeras.	42
Figure 10. Copper Free Click chemistry to synthesize siRNA-SQ nanoparticles.	49
Figure 11. Schematic diagram representing the number of siRNA developed for research studies by therapeutic domain.....	49
Figure 12. Chemical Reaction of bioconjugation of siRNA to squalene molecule	55
Figure 13. Injection protocol of siRNA PMP22-SQ NPs and siRNA RNA Ct-SQ NPs in JP18 and JP18/JY13 B6 mice.	61
Figure 14. Long lasting effect injection protocol for JP18/JY13 B6 mice	62
Figure 15. in vitro inhibitory efficacy of eight different siRNA PMP22. MSC80 cells were transfected at 50 nM concentration with siRNA Ct and eight different siRNAs against PMP22 gene: siPMP1, siPMP2, siPMP3, siPMP4, siPMP4, siPMP5, siPMP6, siPMP7 and siPMP8. After 48h, and 72h cells were harvested, then mRNA were extracted to be analyzed for gene knockdown. All siRNA PMP22 significantly inhibited siPMP22 gene expression after 48h except siPMP6 (NS). After 72h only siPMP 5, 6, 7 and 8 showed a long lasting effect with 50% significant inhibition on PMP22 gene expression and no significant effect on P0 gene expression. siPMP7 significantly decreased PMP22 gene after 48 and 72h (red arrow). The experiments was repeated more than 3 times and (*) represent significance between NT group and other groups. (#) represent significance between siRNA Ct group and other groups. *, #: p < 0.05; **, ##: p < 0.01; ***, ###: p < 0.00 1(Anova followed by Bonferroni tests). .	69
Figure 16: Representative images of protein expression of PMP22 after 48h and 72h of transfection of eight different siRNAs against PMP22 (si1, si2, si3, si4, si5, si6, si7 and si8) at 50nM concentration in MSC80 cells. Si7 that represent siPMP22 number 7 showed long lasting protein inhibitory effect on PMP22 and no effect on P0 protein expression. The gels were quantified using image J software (data not presented). Each experiment was repeated three times with biological duplicates.	70
Figure 17. Effect of different concentrations of siPMP22 number 7 on PMP22 and P0 gene expression and Cell viability: MSC80 cells were transfected with siPMP22 number 7 and siRNA Ct at different concentrations: 25 nM, 50 nM and 100 nM. After 72h, cells were	

harvested for mRNA extraction to study the gene expression of PMP22 and P0. Also, an MTT assay was performed to study the effect on cell viability. **50nM concentration showed a 50% inhibition on PMP22 gene expression when compared to siRNA Control (siRNA Ct) and non-treated cells with no effect on P0 gene expression and cell viability.** (*) represent significance between NT group and other groups, **: $p < 0.01$; ***: $p < 0.001$ (Anova followed by Bonferroni tests).71

Figure 18. Characterization of siPMP22-SQ NPs: **A.** HPLC chromatograms of the siPMP22-anti sense strand (AS) (green chromatogram), siPMP22-sense strand (S) (red chromatogram) and siPMP22C6-SQ bioconjugate (Black chromatogram). The elution time of siPMP22C6-SQ bioconjugate is 18 mins higher than that of the both siPMP22 strands antisense and sense (12 and 16 mins respectively). **B.** MALDI-TOF MS spectrum of siPMP22-SQ bioconjugate (sense strand). **C.** Physicochemical characterization of siPMP22-SQ NPs by DLS analysis. Size, Polydispersity Index of siPMP22-SQ nanoparticles monitored over time (one month). Each measure is the mean of 3 independent formulations and 3 independent technical measurements. **D.** CryoTEM image of the siPMP22-SQ-NPs. White arrows indicate the nanoobjects size detected (180 and 200 nm). The scale bar used is 200 nm. Each experiment is repeated at least 3 times.73

Figure 19. Characterization of siRNA Ct-SQ NPs: **A.** HPLC chromatograms of the siRNA Ct-anti sense strand (AS) (green chromatogram), siRNA Ct-sense strand (S) (red chromatogram) and siRNA Ct-SQ bioconjugate (Black chromatogram). The elution time of siRNA Ct-SQ bioconjugate is 18 mins and its higher than that of the both siRNA Ct strands antisense and sense (12 and 16mins respectively). **B.** MALDI-TOF MS spectrum of siRNA Ct-SQ bioconjugate (sense strand). **C.** Physicochemical characterization of siRNA Ct-SQ NPs by DLS analysis. Size, Polydispersity Index and Zeta Potential of siRNA CT-SQ nanoparticles were monitored over time (one month). Each measure is the mean of 3 independent formulations and 3 independent technical measurements. **D.** 4% agarose gel showing siRNA Ct-SQ NPs and naked siRNA Ct (S-AS) stability in 5% FBS solution at 37°C.75

Figure 20. In vitro inhibitory effect of siPMP22-SQ NPs on siPMP22 and P0 gene expression and cell viability: MSC80 cells were transfected at 50nM concentration with siRNA Ct, siRNA Ct-SQ NPs, siPMP22 and siPMP22-SQ NPs. After 48h, and 72h, cells were harvested for either mRNA extraction to analyze gene knockdown or to perform MTT assay to study cell viability. **After 48 and 72h, the siPMP22-SQ NPs significantly inhibited PMP22 gene expression at a 50% level, same as, siPMP22 and showed no significant effect on P0 and cell viability.** siRNA Ct-SQ NPs behaved the same way as siRNA Ct thus proving no effect of squalene and DBCO modification on the efficacy of siPMP22. (*) represent significance between NT group and other groups, **, $p < 0.01$, *** $p < 0.001$ (Anova followed by Bonferroni tests).76

Figure 21. Representative image of genotyping results showing PMP22 and tTA gene after qualitative PCR77

Figure 22. Behavioral test analysis on single transgenic JP18 CMT1A mice: single Transgenic JP18B6 CMT1A mice of 16 weeks age were divided into three groups (n=9 each) receiving the following treatment 5% dextrose, siRNA Ct-SQ NPs and siPMP22-SQ NPs respectively in addition to a wild type B6 group as a control. Beam walking test was performed before starting treatment and after treatment. The time taken by each mouse was recorded over three passages (mean \pm SEM). JP18 siPMP22-SQ NPs group showed normalized time after treatment when compared to the WT-B6 group and were significantly faster than the groups receiving 5% dextrose and siRNA Ct-SQ NPs. Locotronic test was performed after the end of the treatment and it showed significant results as the beam walking test. Three passages were recorded and the data shown is the average of 9 independent mice

(mean \pm SEM). Grip strength test was performed at the end of treatment on both the fore limbs alone and the total limbs. JP18 siPMP22-SQ NPs group showed significant improvement in its muscular strength compared the JP18 5% dextrose and JP18 siRNA Ct-SQ NP groups and became comparable to the muscular strength of the WT-B6 group. (*) represent the significance between WT-B6 and other groups at $P < 0.05$. ***, ###: $p < 0.001$ (Anova followed by Bonferroni tests).79

Figure 23. Electrophysiological analysis on single transgenic JP18 CMT1A mice:

Compound Muscle Action potential (left panel) and sensory nerve action potential (right panel). Data represent mean \pm SD. (*) represent the significance between WT-B6 and other groups and # represent significance between JP18 5% dextrose and the other two groups at a $P < 0.05$. #: $p < 0.05$; ** : $p < 0.01$, ***, ###: $p < 0.001$ (Anova followed by Bonferroni tests).80

Figure 24. Western blot analysis on JP18B6 single transgenic mice. A. representative image of western blot showing pmp22, p0 and tubulin protein expression in the WT, JP18 B6 5% dextrose, JP18 siRNA CT-SQ NPs and JP18 siPMP22-SQ NPs. **B** and **C** are quantitative analysis of pmp22 and p0 protein expression using image J software. Each protein was normalized on tubulin as a reference (number of animals analyzed is 3 per group).Data represent mean \pm SD. Anova analysis followed by Bonferroni post hoc analysis. * $P < 0.05$ between Wt-B6 and the other groups. # $P < 0.05$ between siPMP22-SQ NPs and JP18 B6.....81

Figure 25. SOX10 transcriptional factor immuno staining on sciatic nerve of single transgenic JP18 mice . (A) Representative confocal microscopy images of immunostained sciatic nerve sections of 5 μ m thickness showing Schwann cells marker SOX10 in the studied mice groups. DAPI staining was used to colorize the nucleus. **(B)** Quantification analysis showed that the levels of transcriptional factor SOX 10 were diminished in the JP18 5% dextrose and siRNA Ct groups. Notably, siPMP22-SQ NPs treatment significantly increased its levels compared to the JP18 5% dextrose group. Data represents mean \pm SD and each group consists of three different mice. * at $P < 0.05$ represents the significance between WT-B6 group and the other groups and # represent significance between JP18 5% dextrose and JP18siPMP22-SQ NPs. *: $p < 0.05$; *** : $p < 0.001$, ###: $p < 0.001$ (Anova followed by Bonferroni tests). Magnification lens 20X. Scale bar 100 μ m83

Figure 26. KROX20 transcriptional factor immuno staining on sciatic nerves of single transgenic JP18 mice . (A) Representative confocal microscopy images of immunostained sciatic nerve sections of 5 μ m thickness showing Schwann cells myelination marker KROX20 (green) and in the studied mice groups. DAPI staining was used to colorize the nucleus. Collocation between blue and green represent myelinating schwann cells.**(B)** Quantification data showed that the levels of the myelination factor KROX20 were diminished in the JP18 5% dextrose and siRNA Ct groups. Notably, siPMP22-SQ NPs treatment significantly increased its levels compared to the JP18 5% dextrose group. Data represents mean \pm SD and each group consists of three different mice. * $P < 0.05$ represents the significance between WT-B6 group and the other groups and # represent significance between JP18 5% dextrose and JP18siPMP22-SQ NPs. *: $p < 0.05$; *** : $p < 0.001$, ###: $p < 0.001$ (Anova followed by Bonferroni tests). Magnification lens 20X. Scale bar 100 μ m.84

Figure 27. Axonal regeneration factor neurofilament immuno staining on sciatic nerves of single transgenic JP18 mice . Representative confocal microscopy image of immunostained sciatic nerve sections of 5 μ m thickness showing axonal regeneration factor neurofilament in the studied mice groups. DAPI staining was used to colorize the nucleus. **(A).** Quantification analysis **(B)** showed that the levels of NF were significantly decreased in the JP18 5% dextrose and siRNA Ct groups. Notably, siPMP22-SQ NPs treatment significantly elevated its levels compared to the JP18 5% dextrose group. Data represents mean \pm SD and each group consists of three different mice. * $P < 0.05$ represents the

significance between WT-B6 group and the other groups and # represent significance between JP18 5% dextrose and JP18siPMP22-SQ NPs. *: $p < 0.05$; *** : $p < 0.001$, ###: $p < 0.001$ (Anova followed by Bonferroni tests). Magnification lens 20X. Scale bar 100 μ m.86

Figure 28. Behavioral test analysis on double transgenic JP18/JY13 B6 CMT1A mice: double Transgenic JP18/ JY13 B6 CMT1A mice of 12 wks age were divided on three groups (n=6 each) receiving the following treatment 5% dextrose, siRNA Ct-SQ NPs and siPMP22-SQ NPs respectively in addition to a wild type B6 group as a control. Beam walking test was performed before starting treatment and after treatment. The time taken by each mouse was recorded over three passages (mean \pm SD). JP18/JY13 siPMP22-SQ NPs group showed normalized time after treatment when compared to the WT-B6 group and were significantly faster than the mice in groups receiving 5% dextrose and siRNA ct-SQ NPs. Locotronic test was performed after the end of the treatment and it showed significant results as the beam walking test. Three passages were recorded and the data shown is the average of 6 independent mice. Grip strength test was performed at the end of treatment on both the fore limbs alone and the total limbs. JP18/JY13 mice receiving siPMP22-SQ NPs group showed significant improvement in their muscular strength compared the JP18/JY13 5% dextrose and JP18/JY13 siRNA Ct-SQ NP groups and became comparable to the muscular strength of the WT-B6 group. (*) represent the significance between WT-B6 and other groups. (#) represents the significance between WT-B6 and other groups. (#) represent the significance between JP18/JY13 5% dextrose and JP18/JY13 siPMP22-SQ NPs. ***, ###: $p < 0.001$ (Anova followed by Bonferroni tests).88

Figure 29. Electrophysiological analysis on double transgenic JP18/JY13 CMT1A mice: Compound Muscle Action potential (left panel) and sensory nerve action potential (right panel). Data represent mean \pm SD. (*) represents the significance between WT-B6 and other groups. (#) represent the significance between JP18/JY13 5% dextrose and JP18/JY13 siPMP22-SQ NPs. *#: $p < 0.05$; ** : $p < 0.01$, ***, ###: $p < 0.001$ (Anova followed by Bonferroni tests).....89

Figure 30. Immuno staining analysis of myelination and axonal regeneration factors on sciatic nerves of double transgenic JP18/JY13 CMT1A mice. Representative images of immuno stained sciatic nerve sections of 5 μ m thickness showing collocation between the Schwann cells nucleus stained with DAPI (blue) and Schwann cell markers SOX10 (Red) and KROX20 (green). Axonal regeneration marker neurofilament is shown in green.91

Figure 31. Immuno staining analysis of myelination and axonal regeneration factors on sciatic nerves of double transgenic JP18/JY13 CMT1A mice. Quantification analysis (B-D) showed that siPMP22-SQ NPs treatment increased myelination transcription factors (SOX10 and KROX20) and enhanced axonal regeneration compared to the JP18/JY13 5% dextrose group. Data shows mean \pm SD and each group consist of three different mice * at $P < 0.05$ represents the significance between WT-B6 group and the other groups and # represent significance between JP18/JY13 5% dextrose and JP18/JY13 siPMP22-SQ NPs. *: $p < 0.05$; ** : $p < 0.01$; *** : $p < 0.001$, ###: $p < 0.001$ (Anova followed by Bonferroni tests). Magnification lens 20X. Scale bar 100 μ m.....91

Figure 32. Long lasting effect analysis of Beam walking and locotronic on double transgenic JP18/JY13 transgenic mice. JP18/JY13 B6 mice received two cycles of treatment of 2.5mg/Kg per cycle. Treatment was stopped for 21 days in between the two cycles to study the relapse Data of Beam walking test (left panel) represent time spent to cross the bar (mean \pm SD). Data of Locotronic test (right panel) represent time recorded by the computerized program (mean \pm SD). The mice were followed weekly to analyze the recovery and relapse periods. (*) represents the significance between WT-B6 and other groups. (#) represent the significance between JP18/JY13 5% dextrose and JP18/JY13 siPMP22-SQ NPs. **, $p < 0.01$, *** $p < 0.001$ (Anova followed by Bonferroni tests).....93

Figure 33: Long lasting effect analysis of Grip strength test on double transgenic JP18/JY13 transgenic mice. JP18/JY13 B6 mice received two cycles of treatment of 2.5mg/Kg per cycle. Treatment was stopped for 21 days in between the two cycles to study the relapse. Data of grip strength test (left panel) represent force exerted by the mice on the fore limbs (mean \pm SD). Data of grip strength test (right panel) force exerted by the mice on the total limbs (mean \pm SD). The mice were followed weekly to analyze the recovery and relapse periods. (*) represents the significance between WT-B6 and other groups. (#) represent the significance between JP18/JY13 5% dextrose and JP18/JY13 siPMP22-SQ NPs. **, p < 0.01, *** p < 0.001 (Anova followed by Bonferroni tests).....93

Figure 34. TEM micrographs of ultrathin section of sciatic nerves from single transgenic JP18 mice. TOP: represent TEM micrographs on longitudinal sections of JP18 siPMP22-SQ NPs at low and higher magnifications respectively. The nanoparticles are localized in the cytoplasm of Schwann cells, N = Nucleus. Down represent a low and higher magnifications focus of the Ranvier node. The nanoparticles can enter the nerve via the Ranvier nodes. The red square represents the part of the micrograph that was observed at higher magnification.94

Figure 35. Hypothetical representation of the transport of siPMP22-SQ NPs through the blood stream to reach the sciatic nerve where they enter Schwann cells through the Nodes of Ranvier..... 102

ACKNOWLEDGMENT

This work was supported by a public grant overseen by the French National Research Agency (ANR) as part of the "Investissements d'Avenir" program (Labex NanoSaclay, reference: ANR-10-LABX-0035). Hence, I would like to acknowledge the ANR agency for funding my project and giving me the opportunity to continue my studies.

I would like to thank my thesis advisor Dr. Liliane Massade for giving me this great opportunity to pursue my graduate studies and accepting me as a member of her team. I would like to express my sincere gratitude for all the help and support that she gave me along the duration of my studies. She was always present to follow up the project and to give scientific advice that helped in the advancement of the project and led to a smooth finalization of the experimental plan. It was really a great pleasure to work under her supervision.

I like to express my gratitude to all the jury members who accepted to participate in this thesis evaluation. Thank you Dr. Frederic Charbonnier for being part of my thesis committee from my first year of PhD until the end and for accepting to review my thesis as a reporter. Thank you for all the scientific advice that you gave me during our meetings to ameliorate our experiments. Thank you Dr. Ruth Stassart for revising my thesis manuscript and for your scientific advice. Also, I want to thank Drs. Elias Fattal, Didier Desmaele and Charbel Massaad for accepting to evaluate my manuscript as an examiners.

I would like to express my deep gratitude for Dr. Charbel Massaad and his team in UMR-S 1124 for opening their laboratory for me and providing me with all the support needed to pursue my work at Paris Descartes University. Specifically, I want to thank Celine Becker for her help and advice in how to manage the animal models. Thank you Julien Grenier for all the scientific advice. Equally, I want to thank Venkat for his help and advice on IHC experiment.

I am also thankful for Dr. Michael Schumacher who was also part of my thesis committee from the beginning of my PhD. Thank you for your continuous support, encouragement and scientific advice. Especially thank you for welcoming our team as part of the unit 1195 Disease and hormones of the nervous system. Thanks for all the members of unit 1195 for welcoming us and accepting us among you. Thank you for all the help that you provided us during my last year of PhD as part of your unit.

I am equally thankful for all the members of our former unit UMR8203 Vectorology and Anticancer Therapeutics at Gustave Roussy hospital. The time I spent at this place was unforgettable and I enjoyed every moment of it. Thank you for all the support and the happy time. Thank you Isabelle Croquison, Lena Zig and Linda Larabi-Cherif. I want to especially thank Céline Gracia. We came to the lab in the same period and she was always supportive and helpful. Thank you Celine for your continuous help, advice and support. Thank you Giorgia Urbinati for your scientific help and advice. Amina Ghorbel my friend our small chats during coffee breaks made my journey smooth.

For our lab members thank you so much for the enjoyable time that I spent during three years and few month in the lab. Marie Caillaud, my friend, my French translator, my supporter, a big thank you for all the encouragement and help. No words can express my gratitude. You were always there whenever I needed any kind of help. Your smile, positive attitude and our conversations always enlightened our long days in the lab. Mevidette El Madani your presence is an elegance. Your calmness, your smile and your support made my journey less stressful. Thank you for everything you have done during your one year stay among us. Julien Loisel-duwattez your presence enriched our days and made our lunch break livelier. Thank you for the scientific help, support and continuous encouragement. Thank you Celia Dupain for the support and encouragement. The time that we spent together was unforgettable. You were the first to help me in the laboratory with all the administrative and non-administrative papers. Thank you for giving me part of your time to translate every paper for me. You always helped me with a smile and I am grateful. You don't know how much you made my life easier while I was feeling frustrated in the beginning of my journey with zero knowledge of French language.

I am also thankful for Dr. David Adams and Andoni Echaniz Laguna members of Team 3 U1195 for their time and scientific advice in the project to ameliorate the work.

I want to thank the EOPS members of the animal facility at Faculty of Medicine of Paris Descartes University. Thank you Claire Mader, Maja Adamsen and Camille Delair for your help and your cheerful welcome. You made my experiments pass smoothly in the animal facility.

To my Lebanese friends who I have met at Gustave Roussy hospital, thank you for being part of my journey. Our outings and the time that we spent together is the most valuable and precious one. I hope that we will always stay connected wherever we go. Thank you from the heart Rawan El amine, Carla Dib, Mira El khoury, Tracy Dagher, Desire Tannous, Walaa,

Diana, Hanna Fakhry and Hussein Ghamloush. I also want to thank my friends Rasha Barakat and Mohammad El Masry who were always supportive and together we spent a joyful time.

I especially want to thank my first friend in France and house mate Veronica Guiance. Veronica the helpful, cheerful and nice girl that I met during my first day in France. My first tour guide and first person to ask information from, thank you for helping me and standing by my side during the happy and sad time.

To my family in Lebanon, without your support and understanding I wouldn't be here. You gave me the chance to discover a new life. Thanks to my father Saadeldine who is my role model. You always supported me in all my decisions and encouraged me to continue my studies to have a brighter future. My mother May El Khoury you left us early. I hope that I was able to make you proud of me. I dedicate this work to you for being the best mom ever. Hope that you were with me during this time else, you will always look over us from the sky. We love you. My brothers Ziad and Ahmed my pillars in this life, my support thank you. Thank you Nivine, Hikmat, ahlam and my uncle khodor for standing by myside. My niece and nephew May and Saad who always asked about their aunt. And a special thanks for all my extended family in Lebanon.

Finally, thank you for France and its people for hosting me during the past three years and for giving me the opportunity to pursue my studies. I am really grateful for this country that welcomed me. In this country, I was exposed to different cultures and met people from different origins.

ABBREVIATIONS

Charcot Marie Tooth disease / Maladie de Charcot Marie Tooth (CMT)
Charcot-Marie-Tooth 1A (CMT1A)
Peripheral myelin protein / myéline périphérique de 22 kDa (PMP22)
Myelin Protein Zero (P0)
Myelin Basic Protein (MBP)
Connexin 32 (Cx32)
Myelin Associated Glycoprotein (MAG)
Early Growth Response 2 (EGR2 or KROX-20)
Guillain-Barré syndrome (GBS)
Chronic Inflammatory Demyelinating Polyradiculo-Neuropathy (CIDP)
Mycobacterium Leprae (*M. Leprae*)
Nerve Conduction Velocity (NCV)
Motor Nerve Conducting Velocity (MNCV)
Compound Muscle Action Potential (CMAP)
Gap Junction β 1 (GJ β 1)
Mitofusin 2 (MFN2)
Hereditary Neuropathy with Liability to pressure Palsies (HNPP)
tetracycline Transactivator (tTA)
Charcot-Marie-Tooth Neuropathy Scores (CMTNS)
Neurotrophin-3 (NT-3)
NT-3 adeno-associated viruses (AAV1-NT3)
cyclic Adenosine Mono Phosphate (cAMP)
Overall Neuropathy Limitations Scale (ONLS)
Small interfering RNA (siRNA)
double stranded RNA (dsRNA)
micro RNA (miRNA)
small hairpin RNA (shRNA)
RNA-Induced Silencing Complex (RISC)
Hereditary Transthyretin Amyloidosis (hATTR)
Transthyretin Amyloid (TTR)
hATTR with Polyneuropathy (hATTR-PN)
Synthetic Antisense Oligonucleotides (ASO)

Heat-Shock-Proteins (HSP)
Monocyte Chemoattractant Protein-1 (MCP-1/CCL2)
Age-Related Macular Degeneration (AMD)
Food and Drug Administration (FDA)
European Commission (EC)
Locked nucleic acid (LNA)
Dinitrophenol (DNP)
Polyethylene Glycol (PEG)
Cyclodextrin polymers (CDP)
Stable Nucleic Acid Lipid Particles (SNALP)
Dioleoyl-3-Trimethyl Ammonium Propane (DOTAP)
N-(1-(2,3-dioleoyloxy)propyl)-N,N,N-trimethylammonium methyl sulfate (DOTMA)
dibenzocyclooctyne (DBCO)
High-Performance Liquid Chromatography (HPLC)
Matrix Assisted Laser Desorption/Ionization Time-of-Flight Mass spectrometr (MALDI-TOF MS)
siRNA PMP22-squalene (siRNA PMP22-SQ)
Nanoparticles (NPs)
Dynamic Light Scattering (DLS)
Cryogenic Transmission Electron Microscopy (cryo-TEM)
Mouse Schwann Cell (MSC80)
Low density Lipoprotein (LDL)

INTRODUCTION

Charcot Marie Tooth disease (CMT) is one of the most frequent diseases of the peripheral nervous system in the world; 1 of 2500 individual is affected by this neuropathy. It is also known as hereditary motor and sensory neuropathy and was discovered in late 19th century by three pathologist Charcot and Marie from France and Tooth from England. More than 90 genes were discovered lately to cause the pathology thus, leading to heterogeneous disorder with many types.

CMT1A represent 50-60 % of all the CMTs and occurs due to a duplication in on ch17p12 that leads to over expression of PMP22 gene. Since its discovery, several molecules were tested on different CMT1A animal models. Some reached clinical trials but failed to give positive results while one is still ongoing but facing problems in the formulation. The only present treatments for CMT1A patient are based on relieving the symptoms by physiotherapy, orthopedics or surgical corrections. Therefore, up to date there is no significant treatment for CMT1A pathology hence this project was designed and aimed to develop a treatment using siRNA technology based on squalene nanoparticles.

siRNAs are small molecules of 21-23 nucleotides. They are natural processes present in the cells and have many advantages in gene inhibition. Since their discovery, 20 years ago they gained a lot of interest and were used in research for gene silencing. They were tested as gene therapy for several diseases including cancer, Alzheimer and amyloids diseases. Nevertheless, they have disadvantages as low plasmatic half-life time, degradation but endonucleases and off target effect. Thus, they require modification and encapsulation to increase their stability *in vivo* without affecting their efficacy. In this project, the encapsulation method used is the click-chemistry where siRNA was conjugated to squalene in a 1:1 ratio. Squalene is a cholesterol precursor that was first discovered in the shark liver extracts in 1903. Since then it gained the interest of many researches for its beneficial biological role as an antioxidant, antitumor and cytoprotective effects.

The introduction of the thesis will focus on discussing (1) the peripheral nervous system myelination and pathologies, (2) CMT pathology and the most affected genes, (3) CMT1A animal models and drugs tested as a suspected treatment and (4) siRNA discovery, vectorization and clinical trials.

A. Peripheral nervous system myelination and pathologies

1. Myelin composition and function

Schwann cells are the glia cells of the peripheral nervous system, discovered in the mid nineteenth century by Theodore Schwann [1]. Their main function is to produce a highly rich lipid plasma membrane that is wrapped several times around the axon thus forming the myelin sheath. The latter consists of 70-80% lipids (as neutral lipids, phospho-glycerides and sphingolipids) [2, 3] and 20-30% proteins (60% glycoproteins, 20-30% basic proteins and 10-20% other proteins) [3].

The myelin sheath permits electrical insulation around the axon, allowing saltatory conduction of nerve impulses. The action potential jumps from one node of Ranvier (the non-insulated parts of the axon) to the other. At the nodes of Ranvier, the density of voltage sensitive sodium channels is elevated. This type of transmission leads to faster conduction of nerve impulse and saves energy and space. The myelin sheath consists of two areas: the compact and non-compact one. The compact area is located between two nodes of Ranvier and includes cholesterol, sphingolipids, peripheral myelin protein (PMP22), myelin protein zero (P0) and myelin basic protein (MBP). The non-compact area is formed by the juxta paranodal region, that comprises the potassium channels, and the paranodal region, that contains the major gap junction protein connexin 32 (Cx32) and myelin associated glycoprotein (MAG) [3], (Figure 1).

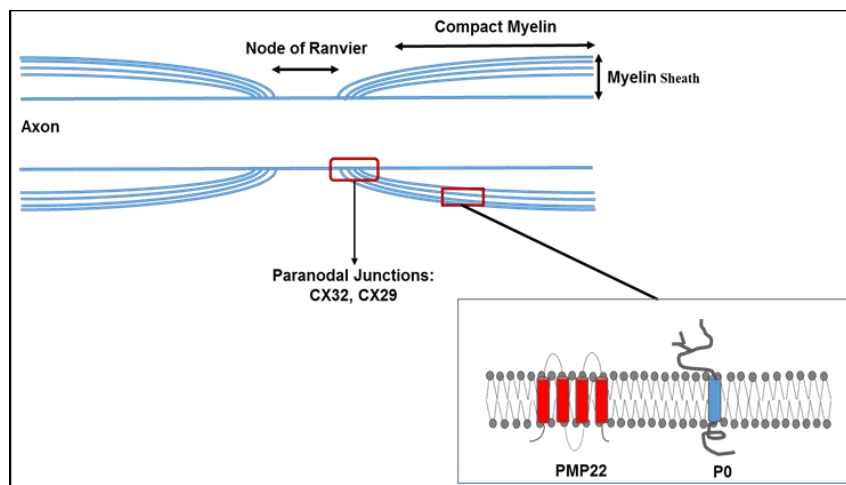


Figure 1. Peripheral nervous system structure showing myelin sheath, node of Ranvier, myelin protein and GAP junctions

Moreover, it is noteworthy that the role of Schwann cells goes beyond myelin formation and insulation of axons. They also provide the necessary metabolic support for axons, which is particularly important for the long axons of the peripheral nerves [4, 5].

2. Myelin synthesis

Myelination in the peripheral nervous system starts during early embryonic life when Schwann cells originate from the neural crest. The latter undergoes two differential steps to produce precursor or immature Schwann cells until birth. After birth, the immature Schwann cells, under the effect of neuregulin differentiate into either myelinating or non-myelinating Schwann cells. Myelination phenotypes are gained upon interaction with large diameter axons ($\geq 1\mu\text{m}$), secreting high levels of neuregulin. Small diameter axons produce lower levels of neuregulin, thus inducing direct ensheathment, with single unmyelinated Schwann cells wrapping several small axons separated by single layers of plasma membrane, forming the so-called Remak fibers [6].

To allow the synthesis of myelin, the expression of several transcriptional factors is either upregulated as for EGR2 (Early Growth Response 2, also termed KROX-20) or downregulated as for OCT-6 (POU class 3 homeobox 1) and SOX 10 (SRY-related HMG-box). Oct-6, expressed in immature Schwann cells, acts a repressor of P0 and MBP genes [3]. KROX20, is an important transcriptional factor for the differentiation of immature Schwann cells into mature ones [7]. SOX 10 is needed for the generation of glial cells from neural crest; it works synergistically with Oct-6 and represses KROX20 expression [8]. SOX 10 mutations provoke CMT-like neuropathies due to formation of irregular myelin or demyelination [9]. In addition, Schwann cells produce progesterone that upregulates gene expression of the myelin proteins P0, PMP22 and MBP, while MAG expression is not affected [10, 11], (**Figure 2**).

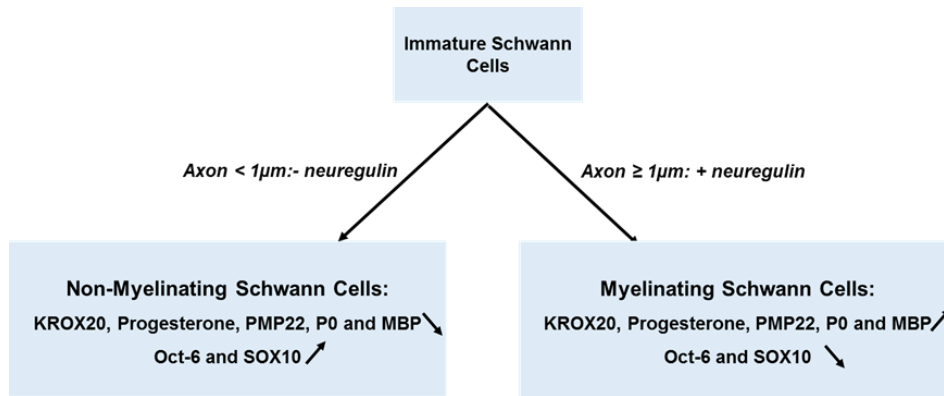


Figure 2. Schematic diagram showing Schwann cells development and the transcriptional factors affected. ↑: increase; ↓: decrease; +: high secretion; -: low secretion

3. Myelin Pathologies

Diseases affecting the myelin sheath in the peripheral nervous system can be categorized into three different entities: nerve injury, inflammatory polyneuropathies and inherited neuropathies. Some nerve injuries cause damage to the myelin sheath, sparing axons, but disrupting the blood nerve barrier and downregulating mRNA levels of major constituents of the tight junction complexes that regulate the permeability of epithelia: *CLAUDIN-1*, *CLAUDIN-5* and *OCCLUDIN* [12, 13]. Autoimmune polyneuropathies include the acute Guillain-Barré syndrome (GBS) [14] and chronic inflammatory demyelinating polyradiculoneuropathy (CIDP) [15]. GBS causes severe paralysis with 20-30% of the cases showing severe respiratory problems [14]. CIDP is an acquired peripheral neuropathy, in which macrophages, T lymphocytes and autoantibodies attack the peripheral nerve components, eventually leading to myelin sheath damage [15]. *Mycobacterium Leprae* (*M. Leprae*) is a bacterium that causes demyelination by infecting Schwann cells. Alpha-dystroglycan receptor serves as the binding site of *M. Leprae* that once inside the Schwann cells take over the MAPK pathway to initiate demyelination and proliferation of Schwann cells thus increase the number of infected cells and worsen the case [16]. Finally, inherited neuropathies such as Charcot-Marie-Tooth disease are due to mutations in several genes, amongst the myelin genes like *P0* and *PMP22*. Mutations of the latter are responsible of Charcot-Marie-tooth 1A (CMT1A), the commonest demyelinating inherited neuropathy.

B. Charcot Marie Tooth

Charcot-Marie-Tooth (CMT), which is also known as «hereditary motor and sensory neuropathy», was discovered in 1886 by three physiologist: J.M. Charcot, P. Marie and H.Tooth. It is one of the most frequent inherited diseases of the peripheral nervous system with a prevalence of 1 in 2500 worldwide [17, 18]. CMT is a neuromuscular disorder characterized by degeneration of the peripheral nerves leading to muscle atrophy, weakness in the distal limbs, absence of deep tendon reflexes, *pes cavus* deformity of the foot and in severe cases, by claw hand deformities. Its early onset ranges from childhood to late adolescence and the severity of the symptoms differs between patients [18]. Its mode of inheritance can be autosomal dominant or recessive or X- linked (**Table 1**).

Table 1. Classification, Mode of Inheritance and Number of Causative Genes of CMT

CMT Types	Mode of inheritance	Electrophysiology	Number of Causative Genes
CMT1	Autosomal Dominant	Demyelinating NCV<35m/s	6
CMT2	Autosomal Dominant	Axonal NCV > 45m/s	20
	Autosomal Recessive		9
CMT4	Autosomal Recessive	Demyelinating NCV<35m/s	13
CMTX	X-Linked	Axonal NCV > 45 m/s	4
CMTRI	X-Linked	Intermediate 35<NCV<45m/s	4
DI-CMT (Dominant intermediate CMT)	Autosomal recessive	Intermediate 35<NCV<45m/s	5

* Different mutation in the same gene can take place leading to either mild, moderate or severe subtype of CMT

1. Epidemiology of Charcot Marie Tooth

Epidemiological studies on CMT diseases in different parts of the world are rare and insufficient especially with the growing interest in CMT research [19]. The primary epidemiological studies reported that the prevalence of CMT is 1:2500 people worldwide [20, 21]. Most of these studies were done in European countries may be due to the availability of CMT Diagnostic centers in Europe. Recently, Barreto et al., to analyze the epidemiological studies on CMT, did a systematic review. They reported 10 studies performed in different countries including Egypt, England, Germany, Iceland, Italy, Japan, Norway, Serbia, Sweden, Turkey and the United Kingdom. Results showed a prevalence

range of CMT disease from 9.7/100,000 in Serbia to 82.3/100,000 in Norway (**Table 2**). CMT1 was the most frequent sub- type in different countries with a range varied from 37.6% (Norway) to 84 % (Iceland) whereas the CMT2 subtype percentage ranges from 12% (UK) to 35.9% (Norway)[19]. In the Auckland region of New Zealand, a point-prevalence epidemiological study was designed lately and the primary outcome was that the age-standardized prevalence of all CMT cases was 15.7 per 100,000. The prevalence was higher in males of 16.6 per 100,000 compared to 14.6 per 100,000 in females. CMT1A frequency was 6.4 per 100000[22]. In France 30,000 people are affected by CMT disease (France CMT Association www.cmt-france.org).

Table 2. Genetic epidemiology of CMT in the general population from Barreto et al., 2016 [19]

Country	Affected individuals, n	Families, n	CMT prevalence/ 100,000 population	CMT1, % (prevalence/ 100,000) (n)	CMT2, % (prevalence/ 100,000) (n)	Others, % (n)
Norway	245	116	82.3	37.6 (-) (92)	35.9 (-) (88)	2.9 (intermediate CMT: 7) 23.6 (unknown neurophysiological phenotype: 58)
Sweden	104	52	20.1	81 (16.2) (84)	15 (-) (16)	4 (4)
UK	133	49	18.1	56 (10.9) (69)	12 (2.7) (15)	31 (CMT3: 1; CMT5: 7; spinal CMT: 9; not classified: 22)
Italy	58	13	17.5	64 (-) (37)	25 (-) (15)	1 (6)
Turkey		33	16	52 (-) (18 families)	33 (-) (11 families)	15 (intermediate CMT: 4 families)
Egypt	5	-	12	-	-	-
Iceland	37	18	12	84 (10) (31)	16 (2) (6)	-
England	352	275	11.8	56.7 (-) (126)	17.6 (-) (39)	25.8 (57)
Japan	19	11	10.8	-	-	-
Serbia	161	-	9.7	73 (7.1) (119)	23 (2.3) (37)	4 (5)
Germany	776 (589*)	-	-	60 (-) (355)	26 (-) (151)	14 (HNPP: 83)
Italy	100	30	-	- (9.37) (100)	-	-
Total	1,990	597				

* Five hundred eighty nine patients with nerve conduction studies.

2. Classification and most common genes implicated

CMT is classified into several types depending on electrophysiological studies and mode of inheritance. CMT1 is the autosomal dominant demyelinating form characterized by a moderate to low motor nerve conducting velocity (MNCV) less than 38 m/s, absence of muscle stretch reflexes and onion bulb nerves [13], (**Table 1**). CMT2 is the autosomal dominant axonal form that shows normal MNCVs > 45m/s, decrease in the compound muscle action potential amplitude (CMAP) and normal muscle stretch reflexes [17]. CMT4, a rare subtype of CMT, is the autosomal recessive demyelinating form while CMTX is the X-linked resulting from

mutations in the gap junction $\beta 1$ (GJ $\beta 1$) gene [23]. Beneath each type, there are several subtypes depending on the genes implicated. In fact, more than 90 genes with different types of alterations have been identified. The majority of the cases are caused by modification in four genes: PMP22, P0, GJ $\beta 1$ and Mitofusin 2 (MFN2) [17].

Interestingly, several genes responsible for CMT are also involved in other neurological and neuromuscular disorders such as myopathy, spastic paraplegia, and motor neuron disorders. Genes like VCP, KIF5A, HSPB1, HSPB8, BAG3, SURF1, CHCHD10 and RAB7 illustrate the fact that Central nervous system, PNS and muscle disease disorders share common pathophysiological pathways [24], (**Figure 3**).

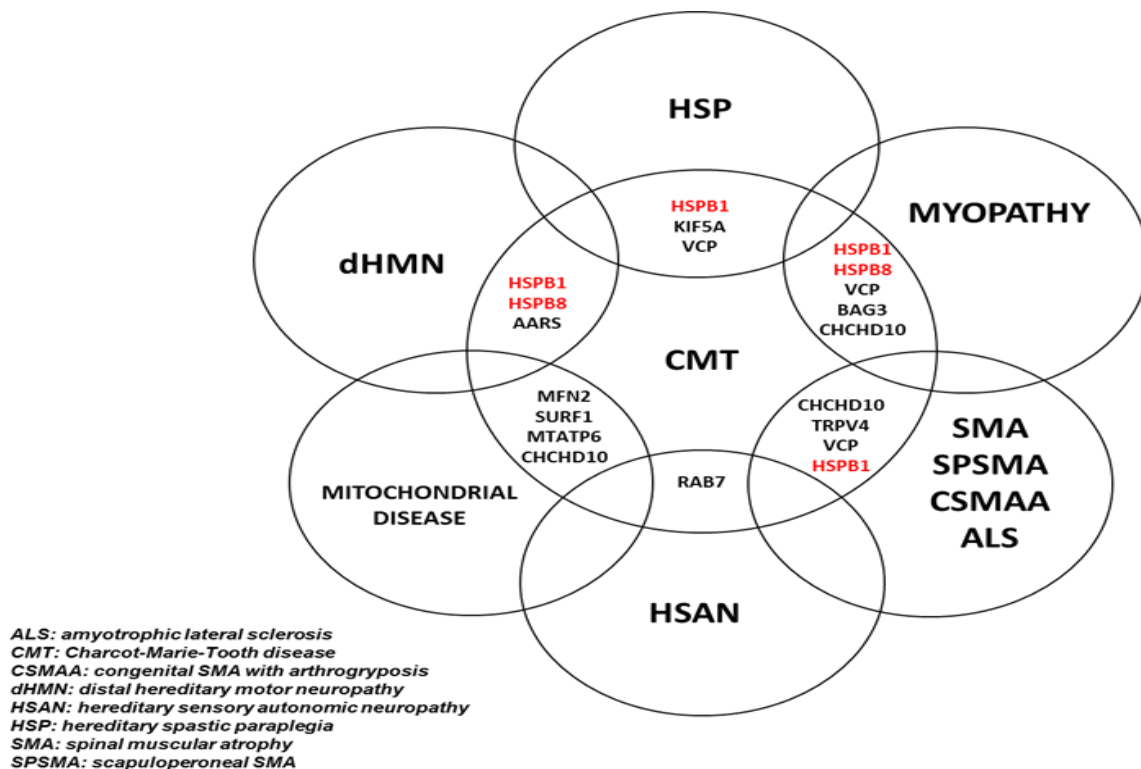


Figure 3. Schematic diagram representing gene overlap between CMT disease and other diseases of the CNS and PNS

i. Peripheral myelin protein 22

PMP22 is a 22kDa glycoprotein of 160 amino acids produced by Schwann cells [25]. It was identified in two systems: in the PNS where it was reported that PMP22 protein is down regulated after sciatic nerve injury [26] and, in fibroblast, as an mRNA that is upregulated in growth arrested NIH3T3 cells named *GAS3* gene [27]. Later, it was reported to be expressed in the intestines, lungs, heart [28] and the central nervous system [29]. In the peripheral nervous system, it was found in the compact region of the myelin sheath as well as in the plasma membrane of the Schwann cells of the unmyelinated axons. It comprises 2- 5% of the total

myelin proteins. The PMP22 gene has two promoters that lead to translation of two transcripts containing different exons, A and B, which makes it tissue-specific and highly regulated [30, 31]. Promoter one is active in the myelinating Schwann cells while, promoter two is expressed in tissues that do not produce myelin [32]. PMP22 expression is regulated at the gene level as well as at the step of protein synthesis and translocation. The majority of PMP22 protein is degraded in the endoplasmic reticulum while only few proteins are glycosylated and reach the Golgi apparatus [33]. PMP22 gene is involved in several diseases that affect the PNS including CMT1A, Dejerine Sottas syndrome and hereditary neuropathy with liability to pressure palsies (HNPP) [34]. A duplication in the PMP22 gene results in CMT1A where as a deletion causes HNPP [29].

Other than its role in the formation of myelin, studies have shown that PMP22 is involved in different cellular functions such as adhesion and cell proliferation since it was first discovered to be upregulated in growth arrested fibroblasts [35, 36]. Also Rao *et al.*, have shown that PMP22 protein expression was elevated in the proliferative phase of human endometriosis [37].

ii. Myelin protein zero

P0 is a transmembrane protein that belongs to the immunoglobulin gene superfamily. It consists of 219 amino acids distributed as follow: 124 a.a. in the extracellular domain, 25 a.a in the transmembrane domain and 69 a.a. in the cytoplasmic domain [38]. Post-transcriptional modifications of P0 include the addition of an N-linked oligosaccharide at the extracellular domain, as well as the addition of sulphate, acyl and phosphate groups [39], (**Figure 4**).

Several studies have shown that P0 is a hemophilic adhesion molecule that plays an important role in myelination by adhering the adjacent myelin wraps to each other [40-42]. This adhesion phenomenon not only involves the extracellular region, but also the cytoplasmic one. In 1999, Fiblin *et al.*, have shown that deletion of 28 amino acids from the carboxyl terminal of the P0 protein decreased adhesion *in vitro* [43]. Also non-sense mutations in the cytoplasmic region caused demyelinating peripheral neuropathies [43]. In particular, genetic alterations within the region where protein kinase C substrate motif is located, between amino acids 198 and 201 causes CMT disease [41]. In addition to adhesion, P0 has a role in the regulation of myelin since its knock-out disrupts the localization and expression of myelin specific genes in Schwann cells [44].

P0 mutations in humans can cause a severe disease in infants called Dejerine-Sottas syndrome, which is characterized by a very slow nerve conduction velocity and weakness at the neonatal period. They can also cause CMT1B that develops during that first two decades

of life. Also, other mutation may cause CMT2 with an onset of the disease at the 4th decade of life with normal conduction velocity. In a clinical study conducted by Shy et al., (2004), 13 patients from 12 different families with eight different MPZ mutations were recruited and 64 cases of CMT1B were reanalyzed from the literature to correlate their phenotypes with their genotypes. It was found that the neonatal neuropathy occurs when the MPZ mutation disrupts the tertiary structure of P0, while late onset of neuropathy occurs when there is disruption in Schwann cell-axon interactions [40].

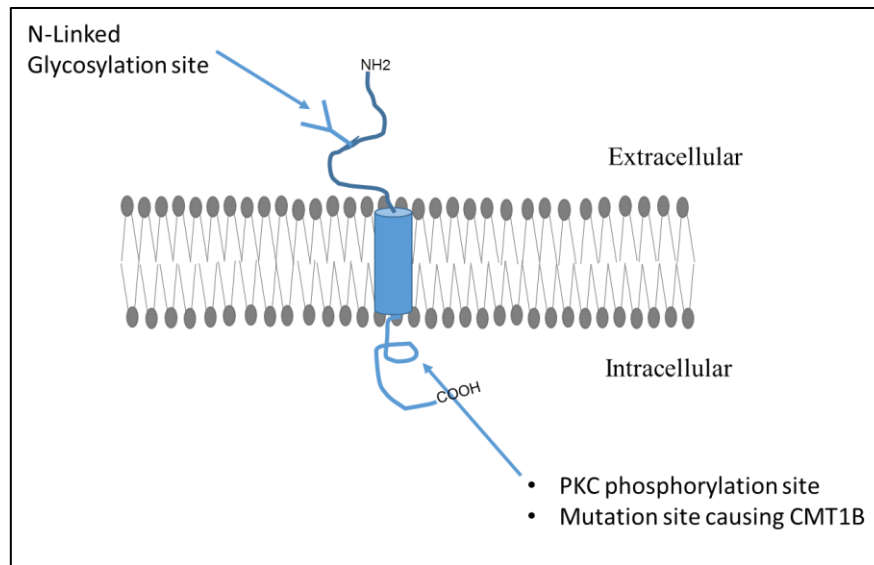


Figure 4. *Peripheral myelin protein zero structure*

iii. Gap Junction Beta 1 (Connexin 32)

Gap junctions are channels that connect to each other adjacent cells or different layers of the same cell as in the case of the myelin sheath [45-47]. Their main function is to allow the diffusion of ions and small molecules since the diameter of each channel is 1.2 nm [45]. Gap junctions are formed from two opposing hemichannels or connexons that are composed of six molecules of connexin located around a central pore [48]. In the PNS, GJB1 encodes connexin 32 (Cx32) and is expressed in Schwann cells. The presence of Cx32 has been confirmed by immunohistochemistry studies and freeze fracture electron microscopy at the paranodal myelin loops and Schmidt-Lanterman clefts of the myelin sheath [49, 50]. In addition, it has been reported that Cx32 plays an important role in the function of myelinating Schwann cells as mutations in the GJB1 gene lead to Charcot –Marie-Tooth 1X which is, the second most frequent type of CMT [51-53]. Moreover, Cx32 null mice showed a phenotype similar to CMT1X where sciatic nerves showed formation of onion bulb with slow MNCV [54, 55].

Most of the mutations in GJB1 lead to homogeneous clinical severity in CMT1X patients. These mutations can be classified into: (1) lack of synthesis of Cx32 protein; (2) mutation of

Cx32 that decrease its expression; (3) normal Cx32 synthesis but not transported to the plasma membrane; (4) mutations in the Cx32 protein that form nonfunctional channels; (5) mutations in the Cx32 protein that form channels with altered properties [56].

iv. Mitofusin 2

Mitofusin proteins (MFN) were first characterized in the fruit fly *Drosophila melanogaster* as “fuzzy onion protein”. MFN1 and MFN2 proteins are the mammalian homologs that belong to a large family of mitochondrial GTPases [57]. They share 80% similarity and consist of 737 and 757 amino acids respectively [58]. They are located on the outer mitochondrial membrane, where they mediate mitochondrial fusion through the large GTPase domain that transverses the outer mitochondrial membrane with both the amino and the carboxy terminals facing the cytoplasm [59]. Notably, the main difference between MFN1 and MFN2 is that the latter has a proline rich domain that is necessary for protein-protein interaction [58]. MFN2 plays an important role in cell metabolism. Its loss of function can lead to the following problems: (1) decrease in the membrane potential of the mitochondria; (2) low oxygen consumption; (3) inhibition of glucose, pyruvate and fatty acid oxidation, and (4) reduction in the respiratory chain enzymatic activity [60-63]. Whereas the gain of function leads to an increase in mitochondrial membrane potential and glucose oxidation [62]. In addition, mutations in MFN2 leads to CMT2A, which accounts for 40% of the cases of the axonal form of CMT [64]. To date more than 100 mutation of MFN2 gene were reported that cause CMT2A [65]. These mutations are either missense or small deletions that take place in all the domains of the MFN2 gene but with higher percentage near or in the GTPase domain [66, 67]. MFN2 mutations are autosomal dominant so mutation in one allele can cause the disease [68], but the severity of the clinical spectrum ranges from loss of motor functions to sensorimotor phenotypes, and the patients suffer from muscle weakness and cramps [69]. MFN2 is involved in other neurodegenerative diseases including Alzheimer’s, Parkinson and Huntington’s diseases [70-72]. Moreover, changes in MFN2 expression can lead to obesity and diabetes due to altered glucose metabolism and oxidation [60, 62] and to vascular proliferative disease since MFN2 plays an important role in vascular smooth muscle cell proliferation and growth [73].

C. Charcot Marie Tooth 1A

CMT1A is the most common subtype representing 60-70% of all CMT cases [74]. It is caused by duplication of a 1.4 mega base (Mb) region on chromosome 17p11.2 of the PMP22 gene [17, 74] due to unequal crossover during meiosis [75]. The PMP22 gene as mentioned previously, encodes for a 22-kDa hydrophobic transmembrane protein that is produced by Schwann cells and corresponds to 2-5% of all myelinated proteins. Mutation in *PMP22* genes cause the formation of PMP22 aggregates that block wild-type PMP22 transportation to the membrane by a dominant negative effect [17]. Several therapeutic approaches were tested for CMT1A in the last 20 decades but none was effective until now. Numerous drugs reached clinical trials, but failed to show positive results. Nowadays, there is a clinical trial with a multidrug treatment and hope is built on to be available in market for CMT1A patients. The only effective treatments that are available nowadays for CMT1A patients are either supportive care or surgical corrections. The following paragraphs are intended to show the most relevant animal models and then to describe the treatments developed to date in preclinical and clinical trials for CMT1A.

1. *Animal Models of CMT1A*

i. C22 mouse model

The C22 mouse model was generated by pronuclear injection of 560 kb YAC called 49H7 that carries one copy of the human *PMP22* gene. Approximately eight copies of this YAC were integrated in the C22 mouse model, resulting in a strong and fully dominant CMT1A phenotype over four generations. At three weeks of age C22 mice, are unsteady during walking, shake when hold up and are more sensible to noises. As they grow older, they show severe disabilities in their hind limbs. Female mice are fertile, while males rarely mate and their death rate ranges from two to five months of age [76].

ii. TgN248 mouse model

The TgN248 mouse model was generated by a pronuclear injection of a purified 43Kb insert of cosmid PTCF-6.1 containing the PMP22 sequence into a fertilized mouse oocyte of B6C3F1 hybrid strain. This strain carries around 16 copies of the *PMP22* gene. The first behavioral abnormalities were shivering of the babies, starting two weeks of age, followed by poor gait after four weeks of age. Between the age of two to three months, muscle atrophy starts progressing with age to reach paralysis of the hind limbs. Mice survive up to eight months

of age. At the electrophysiological level, this mouse model shows increased latency and decreased amplitude of CMAP responses. Also, they show reduced muscle conduction velocity at the age of twelve weeks [77].

iii. Tetracycline conditional mouse models

Using the tetracycline responsive system, Perea *et al.* generated two transgenic mouse models of CMT1A named JY13 and JP18 [78]. The JY13 mouse model was created with a construct that is based on a modified 560 Kb yeast artificial chromosome 49G7, which carries both the human *PMP22* gene and a tetracycline transactivator (tTA) open reading frame on the second exon of the *PMP22* gene. On the other hand, the JP18 mouse model was made with a plasmid, pJP7m, which carries the open reading frame of mouse *PMP22* cDNA under the control of the PhCMV*.1 promoter that has seven copies of the tetracycline operator sequence [79]. Both mouse strains were generated by pronuclear injection of the construct into F2 fertilized eggs of CBA/Ca and C57BL/6J background [79]. Moreover, the two mouse models were crossed together to form a double transgenic strain that shows over expression of the *PMP22* gene in the absence of tetracycline [78]. Testing this mouse model showed that in the absence of tetracycline since birth, the *PMP22* gene is overexpressed, thus leading to demyelination. Then, after one week of administration of tetracycline myelin starts to recover. In addition, tetracycline administration to these mice since birth leads to normalization of *PMP22* gene expression. After discontinuing tetracycline administration, active demyelination starts after one week and reaches maximal levels after 8 weeks [78, 79]. The tetracycline on/off model can be a good model for gene targeted therapy. RNA interference approach against *PMP22* gene can be used to inhibit *PMP22* gene expression and to study the pathways that are implicated in CMT1A pathology. In addition, this model proves that inhibition of *PMP22* gene overexpression results in a re-myelination and correction of the different disease phenotypes.

iv. CMT1A Rat model

Sereda *et al.* designed a rat model with an elevated expression of *PMP22* [80]. To increase levels of *PMP22* in rats, the gene was cloned from a cosmid gene library of the 129Sv mouse. Then a 43Kb fragment consisting of the *PMP22* transcription domain was cut 7 kb upstream exon A and 4 kb downstream exon five using restriction enzymes. Oocytes of Sprague- Dawley rats were fertilized by DNA-microinjection, resulting in one male carrying three copies of *PMP22*. This male rat was considered the founder of the transgenic strain. The rats showed unsteady gait at two month of age, out-ward positioning of the hind feet when walking on a

straight surface and muscle weakness. Also, they showed reduced nerve conduction velocity and hypomyelination in the peripheral and the cranial nerves. When these rats were bred to homozygosity, they showed severe demyelination and retardation in their development, resulting in the death of many rats [81]. Individual variability in this model mimics the phenotypic variation among CMT1A patients that range from normal to severely affected. Hence, it was used later on to study the disease inconsistency and it provided biomarkers of axonal loss in CMT1A patients [82].

2. CMT1A drug therapies and treatments

Since CMT1A discovery, several drugs were tested. However, most of the drugs were symptomatic rather being curative and were not able to reverse the Charcot-Marie-Tooth Neuropathy Scores (CMTNS). The only solution that is present till nowadays is to relieve the pain through physical therapy or surgical corrections. This is the main cause why CMT is considered as economic burden with an annual cost of around 10286€ per patient according to a recent German study done by Schorling *et al.*, [83].

The drugs that were tested for CMT1A can be classified as either symptomatic or curative. Symptomatic drugs are those that relieve the pain symptoms in CMT1A patients as for example FLX-787. FLX-787 is a drug produced by Flex Pharma and was tested in CMT1A patient suffering from muscle cramps (<https://clinicaltrials.gov/ct2/show/NCT03254199>) but phase II COMMIT trial was stopped due to oral intolerability of the dose. ADX71441 from Addex therapeutics is a modulator of GABA B receptor. Scientists believe that activating GABA B receptor will reduce PMP22 gene production. Other drugs are further discussed to reach the curative gene therapy (**Table 3**). It is noteworthy that the average duration to find a cure for CMT1A is around 5 years in basic research and around 8 years in clinical trials.

Table 3. *Drugs tested as a treatment for CMT1A disease*

Drug Nomenclature	Receptor and Pathway	Animal Models	Number of PMP22 genes and age at start of treatment	Administration Mode and duration	Studies
Onapristone	Progesterone receptor 1 antagonist	CMT1A Rat	3 Copies P5	Subcutaneous Six weeks	Research
Ascorbic acid	Sodium-Dependent VitaminC Transporter Reduce Adynelate Cyclase Activity cAMP pathway	C22	7 Copies P5	Force feeding Once per week till death	Research, Preclinical and Clinical
Neurotrophin-3 & SCAAV1.tMCK.NTF3	Nerve growth factor Tyrosine Kinase receptor	Trembler J	Point mutation 6-8 weeks	Intramuscular 20 and 40 weeks	Research, preclinical and clinical study recruiting
PXT3003	GABA _B receptor agonist narcotic antagonist muscarinic receptor antagonist cAMP pathway	CMT1A Rat	3 copies 4 weeks	Oral gavage daily For 4 month	Research, Preclinical and Clinical (Phase II and Phase III ongoing trials)
siRNA Leu¹⁶Pro	Leu ¹⁶ PMP22 point mutation siRNA machinery	Trembler J	Point mutation P5 or P6	Intraperitoneal 2 weeks	Research
ASO against PMP22	PMP22 mRNA expression Watson Crick Base pairing	C22 CMT1A Rat	7 copies/ 5 weeks 3 copies/ 6 weeks	Subcutaneous 9 weeks for C22 12 weeks for rats	Research

i. Progesterone antagonist

Progesterone has been found to promote myelination of the rat sciatic nerve after injury through the progesterone receptor, which is present in the PNS and in Schwann cells [84]. It exerts its effect by activating promoter one of PMP22 as well as the P0 promoter thus making its action very specific [11]. Melcangi *et al.* have also shown that a metabolite of progesterone, 5 α -dihydroprogesterone, affects the gene expression of both PMP22 and P0 [10]. Based on these data, Sereda *et al.*, showed that the administration of 20mg/kg of progesterone to CMT1A rats for 7 weeks deteriorated the clinical and neuropathic outcomes, whereas administration of the same dose of the progesterone receptor antagonist onapristone for 7 weeks improved the CMT1A phenotype and decreased PMP22 mRNA expression [80]. Onapristone is a type one progesterone receptor antagonist that prevents progesterone receptor dimerization, which is required for its transcriptional activity [85, 86]. Subsequently, another study was conducted during 5 month to examine the long-term effect of onapristone treatment. This study confirmed the beneficial effects of antiprogesterone treatment and showed that it prevents axonal loss without any side effects [80, 87]. Unfortunately, the observed liver

toxicity of onapristone has precluded its clinical use [17, 69, 88] (<https://clinicaltrials.gov/ct2/show/NCT02600286>).

ii. **Neurotrophin-3**

Neurotrophin-3 (NT-3) belongs to the neurotrophin family, whose members bind to membrane tyrosine kinase receptors and play important roles in the development, functioning and plasticity of the nervous system [89, 90]. It is also highly expressed in Schwann cells and plays an important role in their survival and differentiation [91]. NT-3 treatment in animal models either having xenografts from patients of CMT1A or in TremblerJ mice improved axonal regeneration; also it significantly increased the number of solitary myelin fiber as well as their diameter [92, 93]. However, since NT-3 has short plasmatic half-life time, it is not effective for a long-term treatment. For this reason, NT-3 has been administered by gene therapy. Its delivery via lentiviral vectors promoted axonal regeneration after peripheral nerve injury [94, 95]. Sahenik *et al.* have administered NT-3 *via* adeno-associated viruses (AAV1-NT3) to Trembler J mice. Results showed that intramuscular injection of AAV1NT-3 increased the serum levels of NT3 and significantly improved the sensory and motor functions [92]. Therefore, Sarepta Therapeutics, acquired rights to “CMT Gene Therapy Program” from Nationwide Children’s Hospital with a hope to use of AAV1-NT3 for future CMT1A clinical trials.

iii. **Ascorbic acid**

Ascorbic acid, known as Vitamin C, is a water-soluble compound composed of six carbons with two ionizing acid groups. It is an essential nutrient in the human diet that is required for the synthesis of collagen in fibrous tissues, bones, teeth, capillaries and skin. It is a reducing agent and a powerful antioxidant. It gained interest for its two neurobiological roles as a neuroprotector and neuromodulator. Ascorbic acid was pharmacologically tested as antidepressant, antipsychotic and antiepileptic drugs as well as for Alzheimer, Parkinson and Huntington diseases [96]. Noteworthy, it was tested as a treatment of CMT1A for the following reasons. Firstly, it promotes myelination of Schwann cells *in vitro* [97-99]. Secondly, in case of ascorbic acid deficiency, there is evidence of femoral neuropathies. Thirdly, ascorbic acid is easily synthesized and commercially available. Finally, it was approved by the FDA as a treatment for vitamin C deficiency since 1981 [100]. Ascorbic acid regulates the level of PMP22 mRNA by inhibiting the adenylate cyclase activity thus reducing the level of cAMP in

a dose-dependent manner [101, 102]. Ascorbic acid exerts its effect on Schwann cells through sodium-dependent vitamin C transporter [103, 104]

Passage *et al.*, have shown that weekly treatment of CMT1A mice (C22) with 1.12 mg of ascorbic acid improved locomotion, myelination and the life span of mice and decreased PMP22 mRNA levels [100]. Based on *in vitro* and *in vivo* studies, several clinical trials have been completed. A study conducted by Shy *et al.* showed that daily administration of 1g of ascorbic acid for one year had no significant effect on the motor and sensory symptoms in CMT1A patients [105]. Micallef *et al.* observed the same results even with 3 g of ascorbic acid. In this study, which also lasted one year, a large cohort (195 patients were recruited, 180 patients of which were enrolled) was randomized into three groups: (1) placebo, (2) 1 g ascorbic acid and (3) 3 g ascorbic acid [106]. In the same year, another clinical trial was conducted on young CMT1A patients' age below 25 years. In this study, 29 patients were assessed for eligibility, but only 13 met the inclusion criteria and were randomized into two groups: placebo and ascorbic acid treatment. No significant improvement in myelination between both groups was shown [107]. To assess the efficacy and safety of ascorbic in CMT1A patients a multicenter two-year study was conducted in UK and Italy. It was found that ascorbic acid treatment had no significant effect on neuropathy when compared to the placebo group [108]. Taken together, these data shows that ascorbic acid is not an effective treatment for CMT1A patients. Perhaps in the future, ascorbic acid could be tested in combination with gene therapy to ameliorate CMT1A phenotypes.

iv. PXT3003

Based on systematic analysis from the literature, Chumakov *et al.* defined several pathways that are involved in CMT1A pathology and affect myelination including cyclic adenosine mono phosphate (cAMP)-dependent mechanism, neurosteroid signaling and AKT/ERK pathway. Accordingly, the following three commercially available drugs were chosen to be tested for a combination therapy named PXT3003: (RS)-baclofen, a selective GABA_B receptor agonist and a skeletal muscle relaxant, naltrexone, a noroxy morphine derivative with competitive opioid and narcotic antagonistic activities and D-sorbitol, a muscarinic receptor antagonist and laxative. These drugs work synergistically to affect the intracellular levels of cAMP either directly or indirectly. This combination was tested in the CMT1A transgenic rat model, where PXT3003 treatment down-regulated PMP22 gene expression and improved nerve conduction velocity and CMT1A clinical phenotype. PXT3003 also enhanced axonal regeneration and myelination in a mouse nerve crush model [109]. These preclinical data led

to a one year randomized double-blind and placebo-controlled phase II clinical study of PXT3003 in patients with CMT1A to confirm its safety and tolerability. In this study, 80 patients were recruited from six hospital sites in France and randomized into four groups: (1) placebo, (2) low dose (0.6 mg baclofen, 0.07 mg naltrexone and 21 mg sorbitol), (3) intermediate dose (1.2 mg baclofen, 0.14 mg naltrexone and 42 mg sorbitol) and (4) high dose (6 mg baclofen, 0.7 mg naltrexone and 210 mg sorbitol). The efficacy of the treatment was shown in the high dose group, where there was significant improvement in electrophysiological outcomes compared to the placebo group. Particularly, PXT3003 showed improvement in the Overall Neuropathy Limitation scale (ONLS) which is the primary efficacy end point in clinical trials for CMT1A as suggested by the American FDA. This suggests an improvement in myelin function. The overall outcome supported further clinical studies on PXT3003 [110]. Later, a meta-analysis of randomized double blind clinical trials of a one-year period that compared placebo, ascorbic acid and PXT3003 treatment was performed. PXT3003 showed improvement of Charcot-Marie-Tooth Neuropathy Score (CMTNS) and the Overall Neuropathy Limitations Scale (ONLS) in comparison to ascorbic acid patients that were stable but not significantly different from the placebo group [111]. Recently, short-term treatment of PXT 3003 has shown that it can delay the early onset of the disease in postnatal CMT1A rats. Two weeks treatment of CMT1A rats of six days age ameliorated their motor activity as well as decreased *PMP22* mRNA expression and regulated the misbalance downstream the PI3K-AKT/MEK-ERK signaling pathway [112]. The Phase III PLEO-CMT clinical trial is being conducted in Europe and the United States to study the efficacy and the tolerability of two doses of PXT3003 in 323 patients suffering from mild and moderate CMT 1A phenotypes and to check the long-term safety and tolerability of PXT3003. In this follow-up study, patients will be treated for 9 months in addition to the 15 months of the original Phase III trial. DATA from Phase II and III clinical trials confirmed that PXT3003 is safe and well tolerated. Overall, they showed significant improvement on the ONLS scale. Another clinical trial will be done on CMT1A pediatric patients as declared by the pharnext company (Pharnext website). Unfortunately, recent press release (pharnext press release august, 2019) declared that the high dose arm of PXT3003 was stopped in phase III PLEO-CMT study due to problems in the formulation and the FDA advised the company to launch another phase III study and further discuss the study design.

v. IFB-088

A new molecule, IFB-088, developed by Inflectis Bioscience, has been designated as an orphan drug by the American (Food and Drug Administration or FDA) and European (European Medicines Agency or EMA) health authorities. IFB-088 (or sephin 1) is a molecule that is involved in controlling the correct folding of certain myelin proteins. Mis folding of myelin proteins occurs due to stress (mechanical, thermal, oxidative...). Preclinical studies have shown that the administration of sephine 1 to mouse models of CMT1A or CMT1B restores their motor functions [113].

Inflectis Bioscience announced in May 2018 that it had received approval to start a Phase I trial of IFB-088 on 72 healthy volunteers. If the results are positive, a Phase II trial will be conducted in patients with CMT (CMT1A and/or CMT1B). The development of this drug candidate (preclinical and phase I) is supported by AFM-Telethon.

vi. Small interfering RNA (siRNA) against Leu16 Point mutation in Trembler] mouse model

RNA interference is a fundamental mechanism found in all eukaryotic cells and since its discovery by Fire and his colleagues in 1998 [114] it became an attractive tool for both *in vivo* and *in vitro* studies [115, 116]. Long dsRNA were the first to be tested in *Caenorhabditis elegans* where a 742 base pair segment was introduced to silence the *unc-22* gene [117]. It is a post-transcriptional gene silencing process which is activated by the introduction of small double stranded RNA (dsRNA) of 19-25 bp that leads to gene inhibition in a highly sequence-specific manner. RNA interference technology is precise, specific and highly efficient for gene silencing [118]. The reagents used in RNAi technology are dsRNA, small interfering RNA (siRNA), micro RNA (miRNA) and small hairpin RNA (shRNA).

siRNAs are double stranded nucleotide molecules of 19-21 base pair length [119]. They are naturally occurring processes that regulate specific gene expression in eukaryotic cells. Inside the cell cytoplasm, siRNAs are produced when double stranded RNAs are cleaved by the RNase III endonuclease dicer. They then interact with the protein Argonaute-2, forming the activated RNA-induced silencing complex (RISC). The activated RISC releases the sense siRNA strand and the antisense strand binds to its complementary mRNA strand leading to its cleavage. As a result, the gene expression and protein expression are down regulated [115, 117, 120]. Concerning the synthetic siRNA, they can be delivered into the cells *via* a lipid-based transfection. They then use the same cytoplasmic machinery as the endogenous siRNA.

miRNAs are another reagent that utilize the same intracellular machinery as siRNA, but the main difference is that long dsRNA are first cleaved by Drosha endonuclease, that also belongs to the RNase III superfamily, to produce a pre-miRNA of 70 nucleotides length in the nucleus. In the cytoplasm, the pre-miRNA is cleaved by a dicer to form the activated miRNA of 22-nucleotide length. After that miRNA is incorporated into the RISC complex harboring the Ago-1 protein. miRNA require partial complementarity with their targeted RNA [117, 121]. shRNA consist of inverted repeats of 19-29 base pairs separated by a loop of 6-9 nucleotides. shRNAs are synthesized to resemble pre-miRNA Drosha products that are inserted in the Dicer to be cleaved to a product of 21-25 nucleotides[115, 117].

siRNA therapeutic approach was used for curing gene disorders, cancers and viral infections. However, their short plasmatic half-life time and hydrophilic character represent limitation for their use in clinic. So far, several approaches have been investigated to counteract these hurdles and to enhance target cell uptake [122]. Their viral delivery has been effective in several disease models including Alzheimer, Parkinson's disease and many other diseases. In our laboratory, we are using an efficient and safe (bio) material for drug delivery: squalene, a cholesterol precursor. We proved its efficiency to deliver siRNA and down regulate the junction oncogene in prostate [123] and papillary thyroid carcinoma [124]. In Hereditary Transthyretin Amyloidosis (hATTR), which is a lethal disease caused by transthyretin amyloid (TTR) accumulation, preclinical data has shown that inhibition of hepatic TTR gene by siRNA reduced systematic levels of TTR thus stabilizing TTR deposits in several tissues [125]. Apollo phase III clinical study was done on ONPATRO (Patisiran), a siRNA against TTR and results have shown that it improved clinical disease manifestations [126, 127]. Nowadays, Patisiran is the first FDA and EMA approved siRNA for treatment of hATTR with polyneuropathy (hATTR-PN), which raises hope for other siRNAs to reach clinical trials.

Recently Lee *et al.*, introduced the siRNA approach for CMT1 disease. They designed 19 siRNAs specific for the mutation Leu¹⁶Pro responsible for the development of CMT1E. First, they tested their efficiency on Schwann Cells, and then identified one siRNA able to counteract the effects of Leu¹⁶Pro mutation. After that, the siRNA Leu¹⁶Pro was encapsulated by a non-viral approach and then administered *via* intraperitoneal injection to TremblerJ mice carrying the mutation at postnatal age of six. Interestingly, improvement in motor function and muscle volume paralleled with an increase in nerve muscle conductive velocity and CMAP was observed. In addition, myelination was augmented in the sciatic nerve with a simultaneous increase in the expression of the myelin genes MBP and P0. They concluded that suppression

of PMP22 mutant allele by non-viral delivery of siRNA could reconstitute CMT1 neuropathic phenotypes [128].

vii. Antisense oligonucleotide against PMP22 gene expression

Synthetic antisense oligonucleotides (ASO) are 12-30 base pairs in length. They bind to their complementary part on the RNA through Watson Crick Base pairing modulating RNA functions by different mechanisms. Based on the design of the ASO, the position where the ASO binds to the RNA and the function of the RNA, ASO can either lead to degradation of the RNA or silencing its translation. If it is designed against miRNA, it can increase the protein translation mechanism. Most of the designed ASO utilize the RNase H1 nuclease to induce RNA degradation. Those ASO must consist of five consecutive DNA nucleotides to bind to RNase H1 endonuclease that is present in the nucleus, mitochondria and the cytoplasm. For better understanding of the mechanism of action of ASO, please refer to recent reviews [129, 130].

Like siRNA, ASO are unstable *in vivo* and they require modifications. Phosphothioate modification is the first and most common modification used to date. ASO bearing phosphothioate-modified DNA and 2'-sugar modifications are water soluble, and show increased stability, and uptake by cells [131, 132]. Recently, ASO Tegsedi® obtained marketing authorization for hATTR-PN by FDA and EMA (<http://www.fda.gov/drugs/drug-approvals-and-databases/drug-trial-snapshot-tegsedi>)

Zhoa *et al.* designed two ASO against PMP22 gene expression. ASO 1 recognizes human/mouse *PMP22* and was used to treat C22 CMT1A mice that contain seven copies of *PMP22* from a YAC. ASO 6 recognizes rat *PMP22* gene and was used for a treatment of a moderate CMT1A rat model that contains three extra copies of *PMP22*. In the C22 CMT1A mouse model the selected ASO1 was administered weekly at different concentrations (25, 50 and 100 mg/kg) *via* the subcutaneous route. Treatment started at 5 weeks of age and continued for 9 weeks. For the rat CMT1A model, treatment started at 6 weeks of age when the symptoms start to appear and lasted for 12 weeks. Interestingly, *PMP22* gene expression was reduced in both rodent models in a dose dependent manner while the highest inhibition of about 50 % was observed in the high dose group (100mg/kg). Notably, most of the neuropathy end point such as myelination, MNCV and CMAP were restored at the high dose of ASO [132]. Taken together, result show that the ASO approach can improve both severe and moderate forms of CMT1A. Unfortunately, systemic toxicology of ASO (thrombocytopenia, nephrotoxicity, hepatotoxicity, proinflammatory effects) is a major limiting factor for long term human use

[133] thus justifying a periodic practice and drastic biological monitoring of platelets and kidney function (https://www.accessdata.fda.gov/drugsatfda_docs/label/2018/211172lbl) .

Although studies by Lee *et al.* using siRNA and Zhao *et al.* using ASO against *PMP22* give hope to patients with CMT1A, further investigation is required to define the optimal conditions and sequence of siRNA to be used as a treatment for CMT1A. Safety and pharmacokinetics studies must be completed to insure the tolerability of the siRNA and to achieve tight regulation of *PMP22* gene expression since its inhibition below the normal levels can lead to HNPP resulting from a deletion in the *PMP22* gene. Overall, the siRNA approach should be widely studied since it opens a new era not only for CMT1A disease, but also for other hereditary neuropathies.

3. CMT1A: enolement of immune cells, autophagy and inflammation

Intracellular trafficking, misfolding and aggregation of *PMP22* in Schwann cells play a role in the underlying mechanisms of CMT1A. They lead to suppression of proteasome activity, leading to apoptosis. Misfolding enhances autophagy and chaperones, which are called heat-shock-proteins (HSP). In the TremblerJ mouse model of CMT1A, the enhancement of autophagy or HSP decreased aggresome formation and accumulation of *PMP22* aggregates in Schwann cells [134]. In another study, the authors investigated the role of HSP70, in reducing *PMP22* aggregates by using fibroblasts from HSP70 deficient mice and skin biopsies of CMT1A patients. To enhance the heat-shock pathway, they used an inhibitor of HSP90 and found that HSP70 improved proteasome activity and prevented aggregation of *PMP22* [135]. Ethoxyquin, which is an antioxidant used to protect against neurotoxicity of chemotherapeutic drugs and a modulator of heat HSP90 [136] can be effective as a treatment for CMT1A patients that require chemotherapy [137]. In addition, macrophages and monocytes are thought to be involved in the progression of CMT1A. For this purpose, an animal model of CMT1A with reduced or diminished levels of monocyte chemoattractant protein-1 (MCP-1/CCL2) was generated. Studies of this model have shown that mice with normal levels of MCP-1/CCL2 have high numbers of macrophages in their nerves whereas in the mutant mice, there were 50% or greater reduction in the number of microphages depending on the expression of MCP-1/CCL2 [138]. Furthermore, in order to test if T- and B-lymphocytes are involved in CMT1A pathology, as previously shown for CMT1B and CMT1X, Kohl *et al.* crossbred *pmp22* mutant mice (C61) with mice lacking mature T- and B-lymphocytes (RAG-1-deficient mice). Their findings strongly support that lymphocytes are not involved in the pathogenesis of CMT1A disease [139]. More studies should be done on HSP, autophagy and inflammation pathways in

CMT1A pathology. Finding treatments that target these systems may become beneficial for improving the phenotype of the disease.

4. Conclusions

The once incurable CMT1A disease may become curable in the upcoming years. The poly therapeutic approach PXT3003 may be facing a slight problem at the high dose level but pharnext co-founders are optimistic about their results. They are continuing the currently performed phase III clinical trial in Europe and China and are working with the FDA to design a new phase III clinical study to bring PXT3003 to U.S CMT1A patients as stated by pharnext press release. Another approach, which is opening its way toward clinical trials, is the use of siRNA machinery. Until now, most of the studies focused on reducing the cAMP activity upstream of PMP22 instead of targeting directly PMP22 gene expression (**Figure 5**). Regulation of PMP22 gene expression using siRNA can be beneficial once proven safe and tolerable in CMT1A patients. This genetic approach paves the way for treatment of other inherited neuropathies especially with the recent approval of the first siRNA as a treatment for amyloid disease by the FDA and EMA.

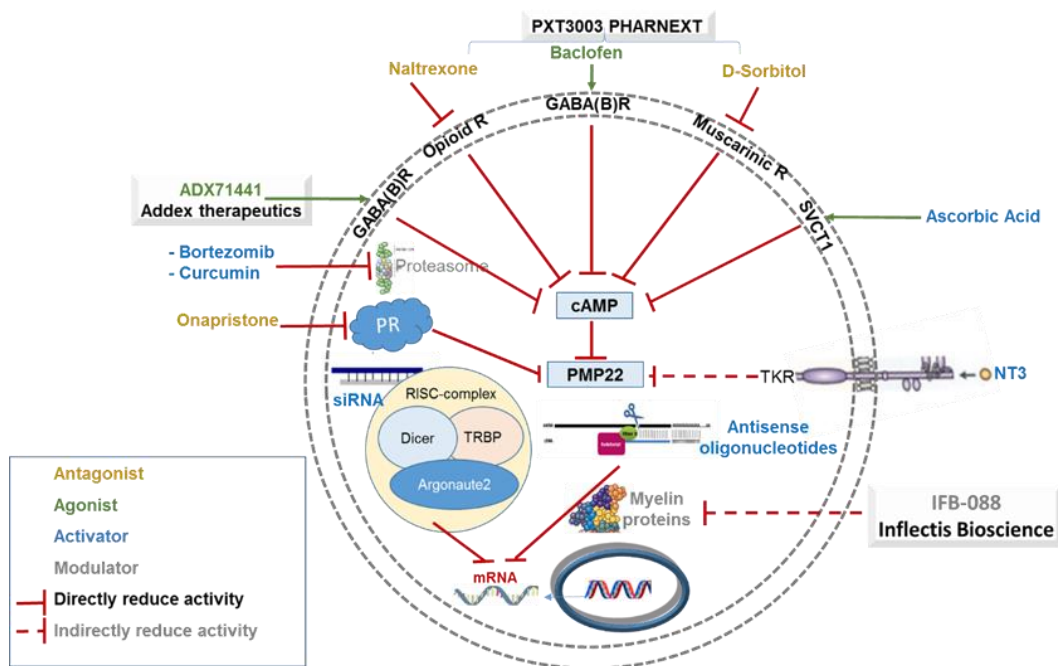


Figure 5. Representative diagram showing some of the drugs tested for CMT1A treatments and the pathways involved.

D. RNA interference: History, encapsulation and clinical Trials

1. History of RNAi

The first observation of gene silencing phenomenon was reported by Jorgensen and colleagues in petunias flower in the 1990s [140], (**Figure 6**).



Figure 6. *Petunia* flower where gene of pigmentation where silenced by RNAi [140].

In 1998, Fire and Mello were the first to report that double stranded RNA can cause potent and specific gene silencing in the nematode worm *Caenorhabditis elegans* [114]. Few years later, Elbashir *et al.*, demonstrated that synthetic siRNA are effective tools for studying gene functions in mammalian cells in vitro and can be used for gene therapeutics. In their study they showed that synthetic siRNA duplex of 21 nucleotides can down regulate specifically the expression of different genes in several kinds of cells including human embryonic kidney and HELA cells [141]. Shortly after, the first successful siRNA for gene silencing in vivo was achieved for hepatitis C Virus [142]. In 2005, an siRNA named siRNA 027 developed for age-related macular degeneration (AMD) was the first to enter phase I clinical trial as a local siRNA based human therapeutic. AMD is the main cause of vision impairment in the developed world. siRNA 027 targets vascular endothelial growth factor receptor-1 in the pathway that mediates blood vessels growth. Its aim is to decrease the pathological effect on blood vessels growth associated with AMD [143]. In 2006, Fire and Mello won the noble prize for the discovery of RNAi [144]. Since then RNAi has been extensively studied as a treatment for many diseases including Hepatitis C, HIV and cancer. Later on Davis *et al.*, launched the first phase I clinical trials using systematic delivery of siRNA nanoparticles to target solid tumors in cancer patients [145]. After that, the field of RNAi continued growing as siRNA is used for both basic and therapeutic research in different fields [6]. Recently, ONPATTRO (Patisiran) which is an oligonucleotide therapeutic based on RNAi was approved by the FDA and the European

Commission (EC) as a treatment for peripheral nerve disease polyneuropathy caused by hereditary transthyretin-mediated amyloidosis in adult patients. It is the first FDA and EC approval of siRNAs as a drug for treatment (**Figure 7**). This approval means that all the obstacles facing RNAi therapeutics can be paved away [146].

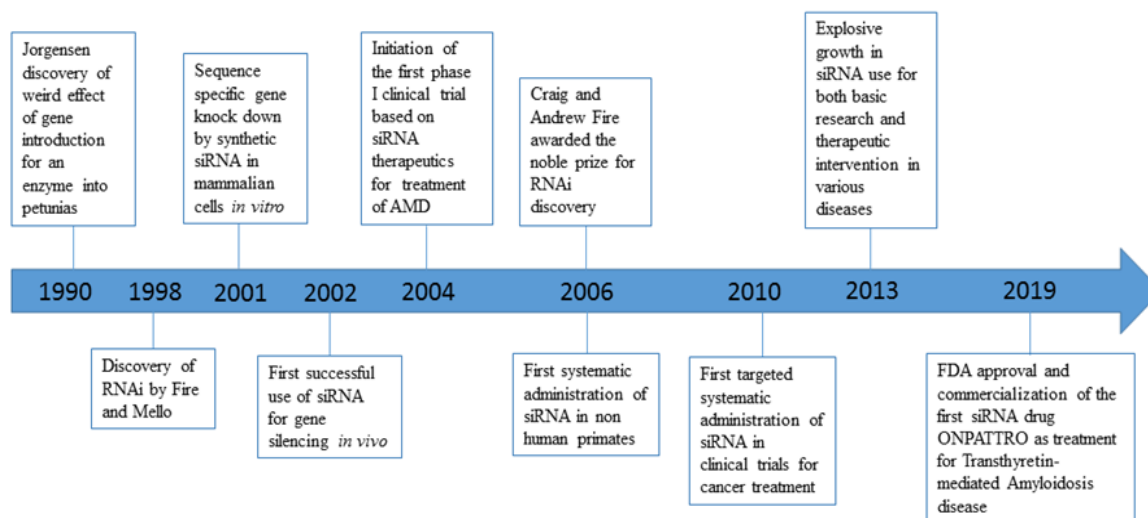


Figure 7. Timeline of the important events in RNAi discovery

2. Mechanism of action of RNAi

RNAi, which is a specific post-transcriptional gene silencing mechanism, is an important pathway present in many eukaryotic cells [141]. In the cell cytoplasm, RNAi machinery is triggered by the presence of long double stranded RNA which is cleaved by the endonuclease dicer into small fragments of 21-23 nucleotides [147] harboring 5'-phosphate and 3'-hydroxyl groups with 2 overhangs-end in the 3'-end known as small interfering RNA (siRNA) [148]. siRNA is recognized by the RNA-induced silencing complex (RISC). RISC has Argonaute protein 2 that unbind the double stranded siRNA and remove the passenger strand, which is also called the sense strand. The leading strand or the antisense strand with the RISC directs the specific recognition of the mRNA complementary sequence [147]. Argonaute 2 degradation of the complementary mRNA [120] starts between bases 10 and 11 from the 5'-end of the antisense strand thus preventing translation and silencing the gene expression [144, 149]. Synthetic siRNA is incorporated in the siRNA machinery downstream of the dicer enzyme [150], (**Figure 8**).

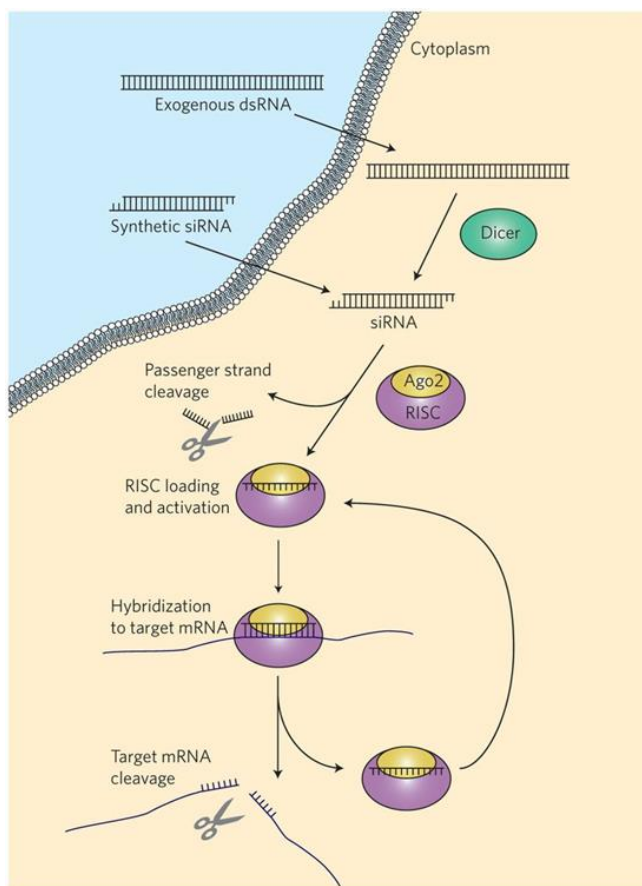


Figure 8. RNA interference. Long dsRNA introduced into the cytoplasm is processed by the enzyme Dicer into 22-nt pieces with 2-nt single-stranded overhangs on the 3'-ends. The structure of synthetic siRNA mimics that of Dicer products. The siRNA guide strand is loaded into the RNA-induced silencing complex (RISC), and the passenger strand is cleaved by Argonaute-2 (Ago2). The activated RISC-gui-der strand complex identifies and cleaves mRNA that is complementary to the guide strand, preventing translation and thereby silencing gene expression[150].

3. Barriers to siRNA delivery

siRNAs are promising agents for gene therapeutics but they still face a lot of hurdles in terms of efficient and controlled systematic delivery *in vivo* and this limit their success in clinics [151]. After injection, the naked siRNA faces several biological barriers that plays a role in reducing its plasmatic half life time from one hour to several minutes [152]. The first biological barrier is the nuclease activity that is present in blood and tissues. The second is the renal filtration where biodistribution studies showed that the highest concentration of siRNA is up taken by the kidney. The third is the uptake of siRNA by the reticuloendothelial system that are composed of phagocytic cells [153].

In addition, one of the most challenging barrier of siRNA delivery is the off target effect that can occur at high siRNA concentration. siRNA has miRNA-like off-target silencing effect where they can inhibit genes with partial similar sequence [154]. Another barrier or challenge is the immune system stimulation. siRNA activate the immune system through protein kinase R, inflammatory cytokines and interferon regulatory factors and NF-kB [155]. Naked siRNAs are hydrophilic double stranded molecules that cannot be readily taken by the cells and hence,

they cannot cross the biological blood barriers. Therefore, to overcome these barriers or difficulties, correct dosing, chemical modifications and 2'-OH methylation of siRNA should be taken into consideration [144] in addition to encapsulation and vectorization that improve its stability [156].

4. Chemical modifications of siRNA

Chemical modifications to siRNA strands improve their stability and performance. The sites of siRNA modifications may include the sugar group, base group, phosphorus group, strand ends or the backbones of the sense and the antisense strands [144], [Figure 9.(a)]. One of the most common modifications is the substitution of phosphodiester group by phosphorothioate (PS) at the 3'-end [157]. PS modification of siRNA enhanced its stability, increased siRNA blood concentration after injection [158] and improved its gene silencing effect although it is position dependent. PS modification at position 3, 5 and 17 from the 5'-end of the sense strand enhanced the antisense RISC complex loading hence improving the gene silencing effect [159]. Another chemical modification is the replacement of phosphate oxygen by boranophosphate. This modification increased siRNA nuclease resistance and serum stability[160].

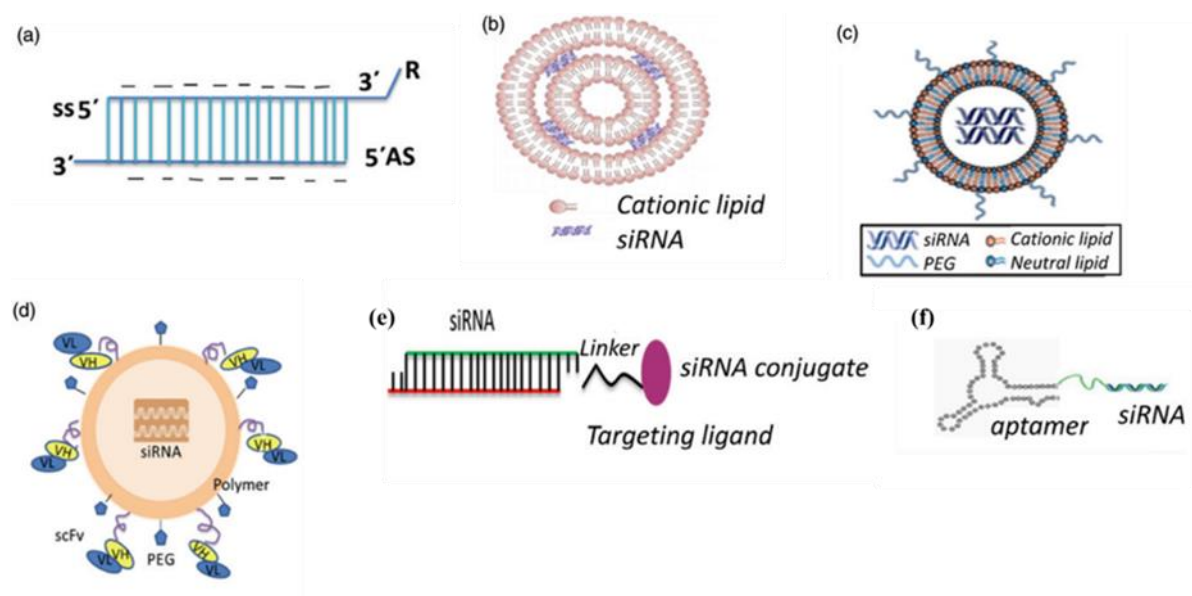


Figure 9. Different types of siRNA delivery systems: (a) siRNA chemical modification, (b) Lipoplexes, (c) stable nucleic acid- lipid particles (SNALPs), (d) Polymer based delivery (Cyclodextrin), (e) conjugate siRNA delivery, (f) aptamer-siRNA chimeras.

Moreover, one of the most attractive modification sites is on the 2'-OH ribose which is not essential for the activation of the RISC complex and the cleavage of the mRNA. 2'-OH ribose

can be substituted by 2'-O methyl, 2'-F or 2'-H. 2'-O-methyl modification increased the resistance of siRNA against endonucleases and improved their thermal stability. This modification should be done only on the sense strand since modification on both siRNA strands abolished siRNA activity. On the other hand, 2'-F modification can be done on both the sense and the antisense strand without affecting the silencing activity of the siRNA [161]. 2'-H modification is tolerable on the sense strand as well as the 3' overhangs or 5' end of the antisense strand. Furthermore, LNA (Locked nucleic acid) modification at the 3'-overhangs amended siRNA serum stability thus protecting it from 3' exonucleases [162]. 2, 4-dinitrophenol (DNP) modification also enhanced siRNA resistance against nucleases along with increasing its membrane permeability [160].

Another strategy to improve the efficacy of siRNA is to conjugate small molecules or peptide to the sense strand of the siRNA such as polyethylene glycol (PEG) and membrane permanent peptide in particular cholesterol-modified siRNAs [144, 163]

5. Vehicles for siRNA Delivery

a. Properties of siRNA vehicles

To facilitate the systemic transport and uptake of siRNA by their targeted tissues, delivery vehicles were designed. The important characteristic of the delivery materials are listed below:

i. Surface properties:

The charge on the surface of the nanoparticle carrying the siRNA affects the way it interact with the target cells and other physiological molecules. *In vitro*, positively charged vehicles can easily interact with the negatively charged cell membrane [164]. While *in vivo*, the situation is more complicated where they can interact with the negatively charged serum proteins thus losing their efficiency. This can be solved by encapsulating the nanoparticle with hydrophilic molecules such as PEG [165]. PEG encapsulation helps the nanoparticle to escape the immune system and phagocytes. In general it enhances the stability and protection of the siRNA [156].

ii. Biodistribution:

Molecules of less than 50kDa in size are easily excreted or eliminated by the kidney [156]. Intravenous injection of naked siRNA in mice showed that siRNA was accumulated in the kidney and urine after 5 minutes of injection [166]. Therefore, the formulation of siRNA delivery vehicles may significantly influence the biodistribution of the siRNA. Increasing the size of the nanoparticle can reduce the glomerular filtration rate and hence render the delivery of nanoparticle for alternative organs [167].

During systemic delivery of siRNA nanoparticles, it was found that most of the nanoparticles accumulate in the organs of the reticuloendothelial system: Liver, kidney, spleen and lungs. This explains why the most effective results of siRNA delivery were seen when targeting diseases affecting these organs [167]. In addition, it was found that some of the nanoparticle delivery systems can accumulate in subcutaneous tumors due to the cancer cells phenomena of enhanced permeability and retention effect [156]

iii. Toxicity:

One of the most important characteristic of siRNA delivery vehicle is not to trigger cellular or systematic toxicity. Viral delivery vehicles were the first to be used for siRNA delivery but it was discovered that they trigger the immune response and induce unacceptable levels of toxicity. Therefore, synthetic lipids and polymers replaced them later on. The latter were formulated to avoid stimulation of the immune system. Also siRNA delivery vehicles have to be biodegradable and easily cleared to reduce toxicity [156].

b. Delivery Materials

i. Cyclodextrin Polymer Nanoparticles

The Cyclodextrin-siRNA delivery system is the first targeted non-viral delivery system to enter clinical trials for cancer, [Figure 9 (d)]. It was adapted for siRNA transport years after its successful introduction for plasmid DNA in 1999. Cyclodextrin polymers (CDP) are polycationic oligomers bearing amidine functional groups [168] that allows efficient condensation of nucleic acids [169]. Although CDP nanoparticles improved siRNA delivery *in vitro*, they still needed additional components to increase stability and efficacy *in vivo*. For this purpose, adamantane-PEG and adamantane-PEG-Transferrin were incorporated in the CDP-siRNA complex to improve the characteristics of the nanoparticle [170]. Adamantane is a hydrophobic molecule that stabilize the cyclodextrin structure while transferrin is a protein linked to the free end of adamantane-PEG to improve cell targeting [138]. The CDP-siRNA nanoparticles were tested in xenografts model for Ewing's sarcoma [169] and other mouse tumor model where it showed its antineoplastic efficacy. The tolerability of CDP-siRNA complex was evaluated in cynomolgus monkeys where they were tolerated up to 27mg/kg of body weight and they reached clinical trial [150].

The CDP delivery system of siRNA harbored the following characteristics: low toxicity of cationic polymers, easy encapsulation of siRNA, enhanced stabilization through linkage to PEG molecule and high efficacy and uptake [150].

ii. Lipid based siRNA Nanoparticles

Lipid based nanoparticles for siRNA Delivery are categorized as liposomes and stable nucleic acid lipid particles (SNALP) [Figure 9 (b & c respectively)]. Liposomes have been studied for more than twenty years as a delivery vectors for nucleic acids [150, 156, 171, 172]. They are composed of simple or multiple types of lipids [173, 174] that are able to form a spherical lipid bilayer with aqueous core in water via hydrophobic association [156, 173]. Liposomes used for siRNA delivery are made of cationic and helper lipids (neutral adjuvant lipids). The role of the cationic lipids is to provide the positive charge that initiate the electrostatic interaction between the liposome and negatively charged siRNA molecule thus forming the lipoplexes complex [144, 150]. Cationic lipids of 100-300nm size [144] increase the siRNAs circulating half-life time, cellular uptake and protect them from endonucleases [144, 150]. Helper lipids are used in the formulation to increase the efficacy of the cationic liposomes and decrease their toxicity. Lipids are composed of three parts: the amine head group, a linker group and hydrophobic tail [150]. Cationic lipids such as 1,2-dioleoyl-3-trimethylammonium propane (DOTAP) and N-(1-(2,3-dioleoyloxy)propyl)-N,N,N-trimethylammonium methyl sulfate (DOTMA) are commonly used along with neutral adjuvant lipid 1,2-dioleoyl-sn-glycero-3-phosphoethanolamine (DOPE) to form liposomes that interact with the negatively charged siRNA forming lipoplexes [144, 175]. Lipoplexes enter the cell by endocytosis thus forming endosomes [173, 176]. Cholesterol is another neutral adjuvant lipid molecule [173] that helps in lowering liposomal transition temperature thus aiding in the release of siRNA from the liposome [150, 177]. The transition temperature is the temperature at which the lipid membrane converts from the stable lamellar phase to the less stable hexagonal phase [173, 178].

Stable nucleic acid lipid particles (SNALP) are the most widely used lipid based material for siRNA delivery [144, 173, 179, 180] [Figure 9 (c)]. They are small particles of 120 nm diameter that are composed of ionizable lipids, fusion/helper/fusogenic lipids, and cholesterol coated with diffusible polyethylene glycol. In the SNALP formulation, siRNA is present in the center surrounded by the lipid layer [144, 173]. SNALPs were the first to be used for siRNA delivery in non-human primates [144, 179]. Several studies have demonstrated the efficacy of siRNA-SNALP complexes *in vivo* [144, 156]. A study done by Morrissey *et al.*, showed that HBV replication was inhibited when targeted using siRNA-SNALPs complex against HBV RNA at a dose of 3 mg/Kg/day. This inhibition was dose dependent, specific and lasted for 7 day after treatment [181]. In another study, siRNA-SNALPs complex designed against Apo B mRNA were used in *cynomolgus* monkey. The siRNA-SNALP complex was able to silencing

ApoB mRNA after 48 h at a single dose injection in a dose dependent manner with a long lasting effect of 11 days after the highest dose administration of 2.5mg/Kg [182]. Also, SNALPs were used in a study to control *Ebola* virus where guinea pigs treated with siRNA contained within SNALP formulation were protected from *viraemia* and death [183].

iii. Bioconjugated siRNAs

An alternative approaches for targeted siRNA delivery is bioconjugation. In this approach siRNA is covalently linked to biological agents such as peptides, cholesterol, antibodies, aptamers and biopolymers of different physical and chemical properties to improve their stability, increase their half-life time and facilitate their cellular uptake [144, 173, 184] [**Figure 9(e)**].

➤ *Aptamer- siRNA conjugate*

Aptamers are synthetic oligonucleotides of 20-80bp length [173, 185] that become promising agents in diagnosis and treatment [186]. They were studied for targeted siRNA delivery because of their chemical stability throughout heat and pH changes, high affinity and specificity for targeting cell receptors and low toxicity and immunogenicity [144, 173, 187, 188]. siRNAs can be combined to aptamers in three different ways: (1) aptamer can be combined directly to the 5' end of the siRNA, (2) siRNA can be bound to aptamer by a linker molecule, (3) a dual nanoparticle can be synthesized as the aptamer acting as the targeting ligand and the siRNA synthesized by the formation of a complex [189]. Recently, aptamer-siRNA chimeras [**Figure 9(f)**] were developed to target prostate cancer cells that express prostate-specific membrane antigen. Results have shown that aptamer-siRNA was able to decrease the targeted protein and induce cell death. Another aptamer-siRNA was also developed against epithelial breast cancer cells and it was successful in suppressing the tumor initiating cells [190].

➤ *Peptide-siRNA conjugates*

Another form of bioconjugation is to link the siRNA to a cell penetrating peptides (CPP) which can facilitate the internalization of siRNA to the cells. CPPs are cationic or amphiphilic peptides of approximately 30 amino acids long [191]. They have been used as carriers of small and large molecules such as antibodies, protein and nucleic acids due to their ability to cross the plasma membrane and the blood brain barrier. This activity is determined by the electrostatic interaction of CPPs with the phosphate in the cell membrane [192]. CPPs are used in siRNA delivery due to their clear structure, biological function and convenient chemical

conjugation. To produce peptide-siRNA conjugates many strategies have been utilized with various linkages including: disulfide bond, amide bond and thioester bond [173].

➤ *Squalene-siRNA bioconjugate*

Squalene is a polyunsaturated triterpene of a chemical formula $C_{30}H_{50}$ [193-195]. It was first discovered by Dr. Tsujimoto in 1903 in the shark liver extract from where it received its name (*Squaluss spp.*) and since then it has been extensively investigated [195, 196]. In addition to shark olive oil, squalene is widely found in nature among olive oil (7mg/g), wheat germ, rice bran and human sebum [194, 197, 198]. Moreover, it was found to be synthesized in the cell by squalene synthase that converts two farnesyl diphosphate molecules, which are direct precursors of terpenes and steroids, into squalene [193, 195]. Squalene is a biochemical precursor of cholesterol and other steroids that is not only synthesized in liver and skin cells, but also taken indirectly from the human diet consumption [194, 195]. It is secreted in large quantities from sebaceous glands in the skin and transported *via* very low density lipoprotein (VLDL) and low density lipoproteins (LDL) in blood [194, 198].

Squalene is further studied for its beneficial biological role as an antioxidant, antitumor and cytoprotective effects [194, 195]. Squalene as an antioxidant acting as singlet oxygen scavenger that protect human skin from lipid peroxidation caused by skin UV light exposure or other oxidative stress[199]. Several studies have shown that squalene treatment protects skin from oxidative cell damage [199-201]. Moreover, the high percentage of squalene in shark liver and low frequency of cancer in sharks suggest that there is a correlation between the two [202]. Therefore, squalene can be a major player that enhance tumor suppression effect of cancer drug treatment and may act as a chemoprotective agent [195]. Furthermore, squalene is preferred for skin care as it can be easily absorbed by the skin [203] and it can maintain skin hydration and moisture without giving an oily residue [204].

Notably, squalene also have been studied for its ability to deliver drugs either by emulsion or conjugates [194, 195]. Squalene emulsion increased the half-life time of drugs [205] as in the case of squalene emulsion carrying morphine prodrug [195, 206]. On the other hand, “Squalenoyl nanomedicine” is a remarkable example of squalene-drug conjugates. In the squalenoylation technology, scientist took advantage of squalene natural folding conformation to bio conjugate this compound to anti-cancer drugs, antiviral nucleoside analogues and siRNA. This resulted in the formation of nanoassemblies of 100-300 nm size in water. The nucleoside anticancer drug gemcitabine was the first example of this conjugation [194, 195, 207]. Squalene-gemcitabine nanoassemblies showed more cytotoxicity when compared to

gemcitabine treatment alone in human nasopharyngeal carcinoma and human breast carcinoma cells [208].

In our laboratory, we are using the squalenylation technique to bioconjugate squalene to siRNA. Our first approach was to use the hetero-Michael addition reaction of 3'thiol siRNA to maleimide squalene to treat several fusion oncogenes in cancer. These fusion oncogenes included RET/PTC1 that is highly expressed in papillary thyroid carcinoma and TMPRSS2-ERG that is found in more than 50% of prostate cancer cases. The resulting squalene-siRNA nanoparticles were of 160 nm diameter and were able to inhibit the growth of both thyroid and prostate carcinoma in xenograft mice [123, 124, 209, 210]. Nevertheless, this synthesis procedure consumed a lot of time and gave low yield after HPLC purification that leads us to explore new technique for bioconjugation to simplify the synthesis scheme and increase the over all synthesis yield. For this purpose, we recently developed the conjugation of siRNA to squalene using copper-free click chemistry synthesis. In this reaction, the 5'-end of the sense strand of the siRNA was modified by a dibenzocyclooctyne (DBCO) group and linked to a squalene molecule modified by azide group (**Figure 10**). This reaction is held in one step, it is fast and the yield is almost complete (100% of squalene conjugated to siRNA). After purification by High-performance liquid chromatography (HPLC) followed by freeze drying steps, the yield of the bioconjugate siRNA-SQ is around 75%. The resulted siRNA-Squalene nanoassemblies were of around 200 nm size. The siRNA-SQ nanoparticles were tested *in vitro* on VCaP cells harboring the TMPRSS2-ERG fusion oncogene and BHP 10-3 and TPC-1 cell line expressing the RET/PTC1 fusion oncogene. Results showed that the siRNA-Squalene nanoassemblies were able to inhibit the mRNA and protein expression of both TMPRSS2-ERG and the RET/PTC1 fusion oncogenes. In addition, *in vivo* injection of siRNA TMPRSS2-ERG- Squalene nanoparticles were able to inhibit tumor growth of about 50-60% [211]. For better understanding of the Click Chemistry synthesis, please refer to ANNEX article 1.

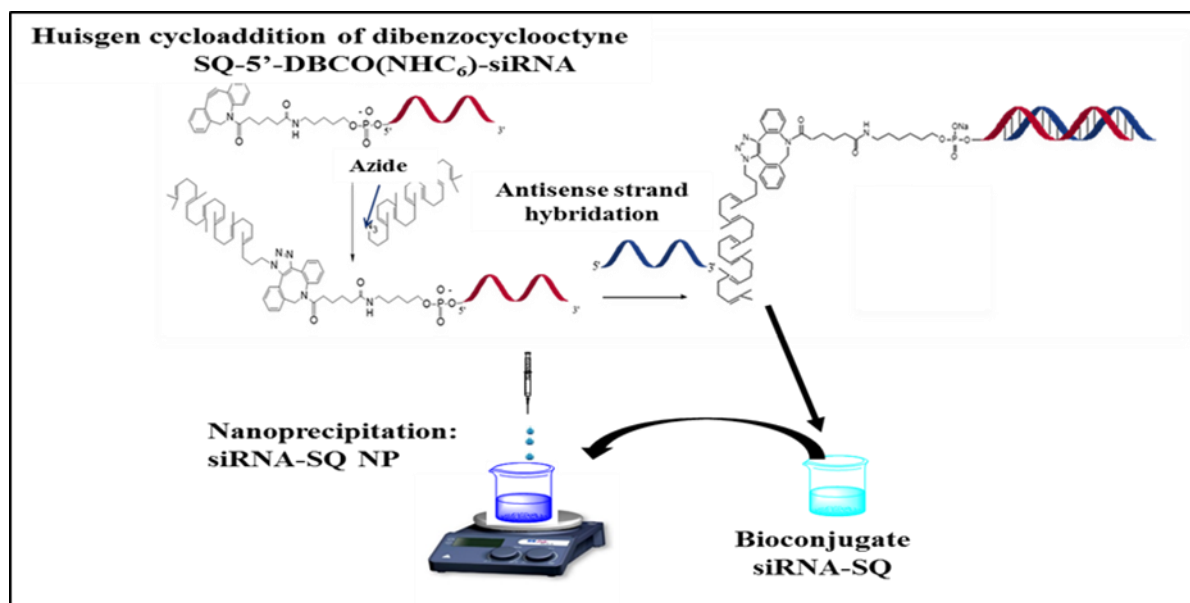


Figure 10. Copper Free Click chemistry to synthesize siRNA-SQ nanoparticles.

6. siRNA Therapeutics and Clinical Trials

Although siRNA therapeutic is considered new, its significant achievement provided the pharmaceutical industry a new approach for disease treatment and control. siRNA research studies included many diseases (**Figure 11**). **Table 4** lists some of the representative clinical studies done using siRNA drugs [146, 173].

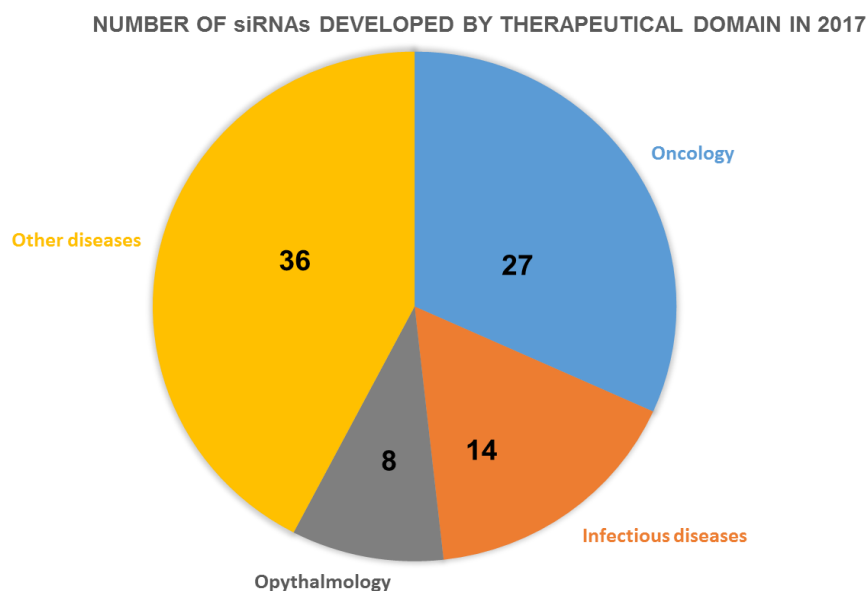


Figure 11. Schematic diagram representing the number of siRNA developed for research studies by therapeutic domain

Table 4. siRNA Treatment and clinical Trials

Drug	Modification	Delivery System	Administration route	Indications	Targets	Clinical Status	Company
ONPATTRO (Patisiran)	2'-Ome, 2'-F	LNP	<i>i.v.</i>	Transthyretin-Mediated Amyloidosis	TTR	FDA Approved	Alnylam Pharmaceuticals
Fitusiran (ALN-AT3sc, ALN-APC)	PS, 2' OME, 2'-F	GAINAC-siRNA conjugate	<i>s.c.</i>	Hemophilia A and B	Thrombin	Clinical Phase III (Recruiting)	Alnylam Pharmaceuticals
Inclisiran (ALN-PCSc)	PS, 2' OME, 2'-F	GAINAC-siRNA conjugate	<i>s.c.</i>	Hypercholesterolemia	PCSK9	Phase III (recruiting)	Alnylam Pharmaceuticals
Givorsiran (ALN-AS1)	PS, 2' OME, 2'-F	GAINAC-siRNA conjugate	<i>s.c.</i>	Acute Intermittent Porphyria	ALAS-1	Phase II	Alnylam Pharmaceuticals
Lumasiran (ALN-GO1)	PS, 2' OME, 2'-F	GAINAC-siRNA conjugate	<i>s.c.</i>	Primary Hyperoxaluria Type I	HAO1	Phase III (recruiting)	Alnylam Pharmaceuticals
Vutrisiran (ALN-TTRsc02)	PS, 2' OME, 2'-F	GAINAC-siRNA conjugate	<i>s.c.</i>	Transthyretin-Mediated Amyloidosis	TTR	Phase III (Recruiting)	Alnylam Pharmaceuticals
QPI-1002 (15NP)	2' OME	Naked siRNA	<i>i.v.</i>	Acute Kidney injury	p53	Phase II (completed)	Quark Pharmaceuticals
QPI-1002	2' OME	Naked siRNA	Intravitreal	Nonarteritic Anterior Ischemic Optic Neuropathy	Caspase 2	Phase II and III (Recruiting)	Quark Pharmaceuticals
Tivansiran (SYL1001)	undisclosed	Naked siRNA	Ophthalmic Topical	Ocular pain and Dry eye	TRPV1	Phase III (completed)	Sylentis, S.A.
Cemdisiran (ALN-CC5)	PS, 2' OME, 2'-F	GAINAC-siRNA conjugate	<i>s.c.</i>	Paroxysmal Nocturnal Hemoglobinuria	C5a Receptor	Phase II (recruiting)	Alnylam Pharmaceuticals
ALN-AAT02	PS, 2' OME, 2'-F	GAINAC-siRNA conjugate	<i>s.c.</i>	Antitrypsin Deficiency Liver Disease	AAT	Phase II (recruiting)	Alnylam Pharmaceuticals
ARO-HBV	PS, 2' OME, 2'-F	GAINAC-siRNA conjugate		Hepatitis B	HBV gene	Phase II (recruiting)	Arrowhead Pharmaceutical
TKM-080301	undisclosed	LNP	<i>i.v.</i>	Adreno cortical carcinoma II, Hepatocellular carcinoma, Neuroendocrine Tumor and Solid Tumors	PLK1	Phase II (completed)	Arbutus Biopharma Corporation
ND-L02-s0201	undisclosed	LNP	<i>i.v.</i>	Hepatic fibrosis	HSP47	Phase II (Recruiting)	Bristol-Myers Squibb, Nitto Denko Corporation
Atu027	2' OME		<i>i.v.</i>	Metastatic pancreatic cancer II, Solid Tumors, Head and Neck cancer	PKN3	Phase II completed	Silence Therapeutics GmbH
SYL040012	undisclosed	Naked siRNA	Ophthalmic Topical	Open Angle Glucoma, Ocular Hypertension	ADRB2	Phase II (completed)	Sylentis, S.A.
Bevasiranib	Unmodified	Naked siRNA	Intravitreal	Diabetic Maculae Edema	VEGF	Phase III (withdrawn)	Opko Health, Inc.

ONPATTRO (Patisiran) is the first siRNA therapeutic to be approved by the FDA for adult patients suffering from peripheral nerve neuropathy caused by hereditary transthyretin-mediated amyloidosis. This approval is due to the positive results reported from the APOLLO phase III clinical study. APOLLO study is a huge global double-blind placebo randomized trial in hATTR amyloidosis patients. Two hundred twenty five patients were enrolled in this trial. Those were randomized to 77 patients in the Placebo group and 148 in the ONPATTRO treated

group. Results from this trial showed that in the ONPATTRO treatment group the modified Neuropathy Impairment Score +7 (mNIS+7), which is the primary end point of APOLLO study, was significantly improved when compared to the patient in the placebo group. The mNIS+7 assess motor strength, reflexes, sensory activity, nerve conduction and postural blood pressure. The secondary end-point of the trial was Norfolk Quality of Life Diabetic Neuropathy (QoL-DN) and it was demonstrated that in terms of quality of life, the patients in the ONPATTRO treatment group showed better exercise intensity, walking speed, nutritional status and autonomic symptoms than the patients in the placebo group [127]. Administration of ONPATTRO showed good safety, tolerance and efficacy results [173]. ONPATTRO is a liposome formulation composed of modified siRNA against TTR gene of molecular weight 14,304 Da. It was administered to patient *via* intravenous infusion at a rate of 1ml/min for the first 15 minutes (min) and then 3ml/min for 55 min at a dose of 0.3mg/kg once every three weeks for 18 months. Patient were given a premedication to reduce the side effects of infusion related reactions [126].

TEGSEDI (Inotersen) is another nucleic acid treatment that has been approved by the European commission for hATTR amyloidosis for adults. TEGSEDI is an antisense oligonucleotide developed by IONIS and AKCEA pharmaceuticals and degrade TTR mRNA through RNase H cleavage and block protein synthesis. It was administered by subcutaneous injection once per week but may cause some side effect such as low platelet count and kidney inflammation [212].

siRNA therapeutic has also been studied for treatment of eye diseases such as age-related macular degeneration, diabetic macular edema and glaucoma. Bevasiranib and SYL040012 are two siRNA drugs tested targeting vascular endothelial growth factor and Beta 2- adrenergic receptors respectively. Both showed good results in phase II clinical trials but Bevasiranib was withdrawn in phase III trial [173].

In cancer, the use of siRNA therapy permits the inhibition of specific cancer-related genes such as epidermal growth factor receptor, p53, or histone deacetylase thus inhibit tumor growth, angiogenesis or tumor metastasis. Most of the siRNA that target tumors are delivered as:(i) liposomes or lipid nanoparticles since the enhanced permeability and retention effect in tumor helps the nanoparticles to target and passively enter tumor tissues. (ii) Bioconjugated-siRNA in which the siRNA is conjugated to various targeting molecule such as peptides, folic acid, galactose residues and antibodies that are specifically expressed in tumor cell surface. (iii) Combination therapy such as use of siRNA with chemotherapy. Several siRNA drugs are now in clinical trials for different kind of cancer (**Table 4**). siRNA therapeutic is also tested for

treatment of respiratory diseases such as asthma associated inflammatory reaction, influenza infections, cystic fibrosis, and respiratory syncytial virus as well as small cell lung cancer[173]. In the liver, siRNAs has a strong capacity to treat hepatitis virus infections [213] and Ebola virus infection [214].

7. Conclusion

Since the discovery of siRNAs, 20 years ago it captured the interests of many researches especially after the Nobel Prize declaration in 2006. In the year 2010, a financial crisis took place in the field of siRNA research due to bad pharmaceutical investments and uncertainties about the beneficial effects of siRNA therapeutic in humans (due to stimulation of the immune system by the delivery material rather than inhibition of the genes). Later this crisis was resolved with the development of new nanomaterial that are less toxic, more efficient and most importantly succeeded in inhibiting the targeted genes. Taken together, this helped the recovery of the pharmaceutical industry in this field [215-217]. Recently and after all the up and downs that faced siRNA technology, the first siRNA drug ONPATRO has been approved by the FDA and this open a new era for RNAi research and development. The next years are the primordial in the siRNA field. Firstly, to see the long-term efficiency and safety of siRNA drug. Secondly to develop new nano-carriers able to reach other non-liver or non-tumor tissues. In addition, the evolvement of the genetic field where new genes are discovered daily. This will also nourish the siRNA field were more genes can be tested to study their effect on the basic research arm as wells as on the therapeutic arm.

AIM

Until nowadays, CMT1A has unmet medical needs despite all the research effort done in the last few decades. The only treatment present is palliative not curative. Therefore, **the aim of this project is to take advantage of RNA interference strategy to downregulate PMP22 gene expression, which is the main cause of the disease.**

The first objective was to **design different siRNAs against PMP22 gene expression and choose among them the best siRNA with 50% inhibition capability.** In addition, the selected siRNA should have no effect on P0 expression and cell viability. It is a fine regulation where inhibition of PMP22 expression more than the normal can lead to HNPP disease and dysregulation of P0 gene expression leads to CMT1B.

The second objective of the study was **to overcome the hurdles that face *in vivo* usage of siRNA.** It is well known that siRNA has limited use *in vivo* due to their short plasmatic half-life time, degradation by endonuclease activity and off-target effect. In this part, **our aim is to synthesize an siRNA-SQ nanoparticle solution,** which has an injectable size, escape endogenous endonucleases, can reach the sciatic nerve, and most importantly don't lose its inhibitory effect.

The third objective and the focus point of this project is to test siPMP22-SQ NPs in CMT1A mouse model. The aim of this part is to study **the effect of siPMP22-SQ NP on motor function, electrophysiological parameters, myelination and axonal regeneration factors in moderate and severe models of CMT1A mice.**

MATERIAL AND METHODS

1. Screening of siRNA against PMP22

To restore the basal levels of PMP22 gene expression, we first obtained the mRNA PMP22 sequence for both human and mice, then defined the homology part between these two sequences. After that different siRNA were designed and then blasted to check their specificity. After that the siRNA were checked for scoring by using three different methods (Tafer software, Thermofisher software and Reynold method). Reynold scores were calculated respecting different criteria [218]. Only eight siRNAs against PMP22 were chosen to continue our study on in addition to an siRNA control (siRNA Ct, a scrambled sequence).

NB. Because of the confidentiality, we can not present the sequences and the scores of the siRNAs designed

2. siRNAs and chemical modifications

The designed sequences of sense and antisense siRNA strands were then purchased from Eurogentec, France. They were synthesized then characterized by matrix assisted laser desorption/ionization time-of-flight mass spectrometry (MALDI-TOF MS) and purified by Reverse Phase-high performance liquid chromatography (RP-HPLC). Single-stranded RNAs were synthesized as 19-mers with two 3'-overhanging 2'-deoxynucleotides residues to provide stabilization against nucleases as described by Tuschl *et al.* [219]. To preserve the functionality, a dibenzocyclooctyne (DBCO) reactive group was introduced at the 5'-end of the sense strand of each siRNA sequence through a *N*-(hexamethylenyl)-6-oxohexanamide spacer (C₆). To generate siRNA from RNA single strands, equimolar amounts of both sense and antisense strands were annealed in annealing buffer [30 mM HEPES-KOH (pH 7.4), 2 mM Mg acetate, 100 mM K acetate] for 3 min at 95 °C and then incubated for 45 min at room temperature before storing at -20 °C.

3. Bioconjugation of siRNAs

To avoid any degradation of siRNA by ribonucleases, precautions were taken before each synthesis. The bioconjugates siRNA PMP22-squalene (siRNA PMP22-SQ) was obtained by the 1,3-dipolar cycloaddition of azides and dibenzocyclooctynes, also known as Cu-free click chemistry where the DBCO modification on the sense strand is conjugated to the azide modified squalene molecule [211].

The protocol to obtain the bioconjugates siRNA PMP22-SQ is described as follows. One nmole of the 5'-end modified sense strand DBCO-C₆ of the siRNA PMP22 (1 mg/mL in DNase/RNase-free water) was mixed with 50 nmoles of SQ-N₃ (1 mg/mL in DMSO) in a glass vial containing DMSO (286 μ L) and acetone (65 μ L). The solution was then incubated at room temperature for 12 h under stirring to obtain the bioconjugate siRNA PMP22-SQ. In the next day, excess acetone was removed under nitrogen flow for 30 min followed by lyophilization step to remove the solvents.

Purification of the bioconjugate from the excess of unconjugated SQ was performed by RP-HPLC on a polymeric column as described below. The identity of the bioconjugates siRNA PMP22-SQ was confirmed by MALDI-TOF mass spectrometry. Purified products were lyophilized, and then solubilized in RNase free water at the desired molar concentration of 10 μ M. The same protocol was performed to obtain the siRNA Ct-SQ bioconjugate (**Figure 12**).

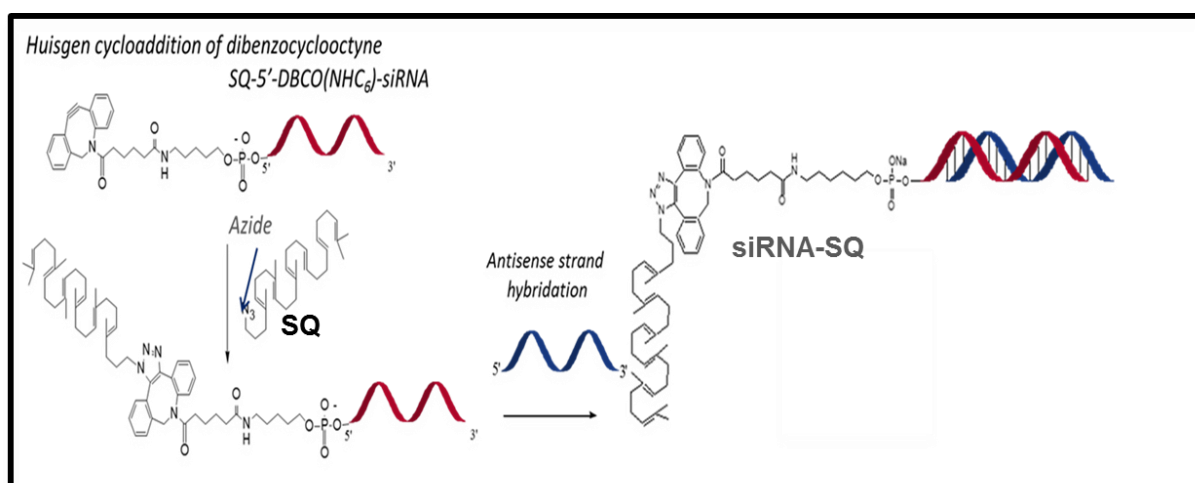


Figure 12. Chemical Reaction of bioconjugation of siRNA to squalene molecule

4. Purification of siRNAPMP22-SQ bioconjugates via HPLC

HPLC purification was performed on a thermoscientific high-performance liquid chromatography system (UltiMAte3000) equipped with a photodiode array detector whose wavelength range between 190 and 800 nm, a pump, and a manual injector. The stationary phase consisted of a nonporous, alkylated polystyrene divinylbenzene column (Hamilton PRP-3 10 μm , 4.6 x 250 mm, PEEK, Ref: 79574) protected by pre-column (Hamilton). Thermofisher Chromeleon software was used for data acquisition with a flow rate of 1.2 mL/min and injection volumes of 100 μL . A gradient of mobile phases A and B was applied. Mobile phase A composed of: 0.2 M TEAA (5%), pH 7.0, with 5% acetonitrile, water 90% while mobile phase B consisted of 95% acetonitrile with 5% TEAA, 5% of water. The gradient applied for purification was as follow: 0 - 8 min linear gradient from 0% to 24% of phase B; 8 - 16 min linear gradient from 24% to 90% of phase B; 16 - 18 min linear gradient from 90% to 100% of phase B; 18 - 30 min 100% of phase B; 30 - 32 min linear gradient from 100% of phase B to 100% of phase A and 32 - 42 min re-equilibration with 100% phase A. Bioconjugates siRNA-SQ were purified by manual peak collection. Fractions were collected for 2 min, corresponding to a fraction volume of 2.4 mL, and then lyophilized. All lyophilized siRNA fractions were reconstituted in RNase free water.

5. MALDI-TOF Mass Spectrometry

A MALDI-TOF/TOF UltrafleXtreme mass spectrometer (Bruker Daltonics, Bremen) was used for all experiments. Mass spectra were obtained in linear positive ion mode. The laser intensity was set just above the ion generation threshold to obtain peaks with the highest possible signal-to-noise (S/N) ratio without significant peak broadening. All data were processed using the Flex Analysis software package (Bruker Daltonics).

6. Annealing of siRNA-SQ bioconjugates to antisense siRNA strands

Annealing of both strands of siRNA PMP22 and siRNA Ct was performed after the bioconjugation of the sense strand to SQ according to the manufacturer protocol and the same as mentioned before for the generation of siRNA from single RNA strands. Precisely, Equimolar amounts of both siPMP22C6-SQ bioconjugate and antisense siPMP22 were mixed with an annealing buffer [30 mM HEPES-KOH (pH 7.4), 2 mM Mg acetate, 100 mM K acetate]

and incubated at 95 °C for 3 min then incubated for 45 min at room temperature. The same protocol was performed to obtain siRNA Ct-SQ bioconjugate..

7. Preparation and Characterization of nanoparticles siRNAPMP22-SQ

Nanoparticles (NPs) siRNAPMP22-SQ and siRNA Ct-SQ were prepared by nanoprecipitation in acetone: water (1:2). One phase was slowly added to the other, under stirring *i.e.* 10 nmole of siRNA-SQ were dissolved in 1ml of DEPC treated water and added drop wisely over 500 ml of acetone under stirring. Then the two solution were kept under stirring for 5 min after which acetone was completely evaporated using nitrogen flux to obtain an aqueous suspension of pure siRNA-SQ nanoassemblies at 10 μ M concentration.

The hydrodynamic diameter (nm) was measured by Dynamic Light Scattering (DLS) Malven Zeta Sizer NANO. Samples were analyzed at 10 μ M concentration in H₂O. Three measures of 5 min for each sample were performed and the average diameter \pm S.D. of three independent samples was calculated.

Cryogenic Transmission Electron Microscopy (cryo-TEM) was performed with the JEOL 2100 electron microscope at the Electronic Microscopy Platform (IBPS/Institut de Biologie Paris-Seine, Université P. et M. Curie, Paris, FRANCE). A drop of 4 μ L of siRNA PMP22-SQ NPs (concentration of 2.2 mg/mL) was deposited on a carbon-coated copper grid. Excess of the liquid was removed with blotting filter paper, and the samples were quickly vitrified by plunging them into liquid ethane using a guillotine-like frame. The samples were then transferred to a cryo-sample holder. Observations were made at an acceleration voltage of 200 kV under a low electron dose. Analysis was performed with Image J software.

8. Cell line

MSC80 cell line (mouse schwann cell line) that expresses myelin genes PMP22 and P0 was used in this study. Cells were grown in a DMEM medium (1X) (Gibco Life Technologies Ref: 11960-044) supplemented with 10% fetal bovine serum, (Gibco Life Technologies Ref:10500-064,), 1% Penicillin/Streptomycin (Gibco Life Technologies Ref:15070-063), 1% Sodium Pyruvate 1 (Thermo Scientific Ref: SH30239.01), 1% L-Glutamine 100X, (Life Technologies Ref: 25030-024) and 2.5 μ g/ml of Fungizone Amphotencin B,(Gibco Life Technologies Ref: 15290-026). Cells were incubated at 37°C in a humidified atmosphere containing 5% CO₂.

9. *In vitro* cell transfection

Studies from our laboratory have shown that NPs siRNA-SQ cannot spontaneously enter the cells *in vitro* [209, 220]. Therefore, lipofectamine 2000 (Invitrogen, Ref # 11668) was used to assess the efficacy of naked siRNA and siRNA-SQ nanoparticles and to study if the conjugation affected the kinetic of the gene down regulation.

To choose the best siRNA PMP22, 350×10^5 MSC80 cells were seeded in six-well plates containing complete medium until 60-70% confluence then, transfection was carried out using Lipofectamine-2000[®] according to manufacturer's instructions in Opti-MEM reduced serum free medium. Eight different siRNAs against PMP22 and siRNA CTRL were transfected at 50 nM concentration. Four hours later, the medium was replaced with a complete medium. After 48 h and 72 h cells were harvested, then mRNA and proteins were extracted to study the gene and protein expression respectively.

After choosing the best siRNA PMP22 sequence, MSC80 cells were seeded and transfected with different concentrations of siPMP22 of 25, 50 and 100 nM. Cells were collected after 48 and 72h for gene expression analysis. To study the efficacy of siRNA PMP22-SQ NPs the same protocol as mentioned above was performed and cell were harvested. Each experiment was performed three times and in duplicates.

10. mRNA extraction and Real time PCR (RT-qPCR)

Total RNA was extracted from MSC80 cells using RNeasy mini-kit (Qiagen, Courtaboeuf, France). First-strand cDNA was generated with M-MLV RT buffer pack (Invitrogen, Charbonnières-les-Bains, France). Real-time PCR (qPCR) was carried out with StepOnePlus PCR System (AB Applied Biosystems, Villebon-sur-Yvette, France) using Maxima Syber Green Rox qPCR master Mix (Thermo Scientific, Villebon-sur-Yvette, France) according to the manufacturer's instructions. Samples were run in triplicate; gene regulation was determined by $2^{-\Delta\Delta C_t}$ method and normalized to 18S levels.

11. Immunoblotting

Total protein extracts from both MSC 80 cells and sciatic nerve tissue were obtained using RIPA buffer (Sigma R0278) supplemented with a protease inhibitor cocktail (Roche, Neuilly sur Seine, France). Sciatic nerve tissues were then homogenised using precellys 24[®] lysis and homogenizer (Bertin, Technologies, France). Samples were then incubated for 2 h under

rotation at 4 °C for complete protein extraction then centrifuged at 13000 rpm for 20 min. Supernatant was stored at -80°C.

Proteins were quantified by Bio-RAD Assay according to manufacturer's instructions. 20 µg of MSC80 protein and 5µg for sciatic nerve proteins were then loaded on a gradient gel of 8-12% polyacrylamide gel (Invitrogen, Ref: NW04120) then transferred to a nitrocellulose membrane using the iBlot Dry Blotting System (Invitrogen iBLOT 2, Cat# IB21001). Membranes were blocked with 5% BSA solution for 1h and then incubated overnight at 4 °C with the following primary antibodies: anti PMP22 (1:750, Sigma: SAB4502217), anti-myelin protein zero (1/1000 abcam: ab31851) and Monoclonal mouse GAPDH-HRP (1:1000, Cell Signalling technology, Saint Quentin in Yvelines, France. Ref: 3683) was used as internal control. Blots were then washed and incubated with the corresponding secondary anti-rabbit antibody conjugated to HRP (horseradish peroxidase, 1:3000, Cell Signalling technology). Bands were visualized by enhanced chemiluminescence reagent (Invitrogen, France) and quantified using image J software.

12. Cell Viability Test

The effect of siRNA PMP22, siRNA Ct, siRNA PMP22-SQ NPs and siRNA Ct-SQ NPs were tested on the viability of cells using MTT assay. 20 x 10⁵ MSC80 cells were seeded in 96 well plate containing complete medium. When the cells reached 60-70% confluence, they were transfected using lipofectamine 2000 as mentioned before. After 72 h the cells were incubated for 2h at 37°C with MTT solution according to the manufacturer's instructions. Then the medium was removed and replaced with DMSO. Absorbance was read at 570 nm and the mean of three independent experiments was recorded ±SD.

13. CMT1A mouse models

Two separate lines of transgenic mice JP18 and JY13 established by Perea et al., 2001 [78] were used in this study. Transgenic mice were purchased after reviviscence from "Transgenesis, Archiving and Animal Models (TAAM-UPS44)". Both strains were archived by cryopreservation and generated on the C57BL/6J (B6) background.

For the JP18 mouse model, the mouse pmp22 cDNA was introduced under control of the PhCMV*-1 promoter, therefore, mice overexpressed pmp22 throughout life. Whereas, the JY13 mouse model carried the intact human PMP22 gene under a tTA open reading frame that give Schwann cell-specific expression of tTA [78]. JY13 strain was found to have little adverse effect on myelination. Double transgenic mouse model (JP18/JY13) was generated by crossing

JP18 and JY13 mice. In absence of tetracycline PMP22 overexpression occur throughout the mice lifespan [78].

In this project, breeding for the JP18 B6 strain was started with one female and one male to generate a stock of mice, and also for the JY13 B6 mice one male and one female were crossed together to generate a large number of mice. After that, the number of breeding couples increased to increase the number of mice of both strains. At ten days of age, mice were systematically genotyped as previously described by Robertson et al., by using specific primers for PMP22 and tTA sequences [79]. After determining the genotype of the mice, we made a new breeding line where we crossed the JP18 B6 mice to the JY13 B6 mice to generate the JP18/JY13 B6 double transgenic mouse model.

14. CMT1A mouse model treatment

According to Perea *et al.* we used JP18 mice at 16 weeks of age. This age showed a high proportion of thin fibres or demyelinating fibres [78]. Therefore, JP18B6 mice were divided into the following three groups of 9 mice each: (1) mice in group one received a vehicle of 5% dextrose solution, (2) mice of group two were treated with siRNA Ct-SQ NPs and (3) mice of the third group were treated with siPMP22-SQ NPs. In addition to one group of wild type B6 mice as a control. All the treatments were administered by retro orbital *IV* injection of a cumulative dose of 2.5 mg/kg at an interval of 0.5 mg/kg per injection twice per week. Beam walking test was performed before and after treatment while locomotor and grip strength tests were performed after treatment. After that, mice were sacrificed and the sciatic nerve was collected for further studies, **Figure 13**. The experiment was repeated twice.

In another similar experiment to test siPMP22-SQ NPs on a more affected CMT1A mouse model, the double transgenic model (JP18/JY13) that harbour two extra copies of PMP22 genes were used. At 12 weeks of age JP18/JY13 mice were divided into three groups similar to the groups of JP18 mice. The same protocol of treatment was performed and 6 mice per group were used in addition to a Wild type B6 group. Behavioural tests were performed as mentioned for the JP18 B6 mice and sciatic nerves were collected after then (**Figure 13**).

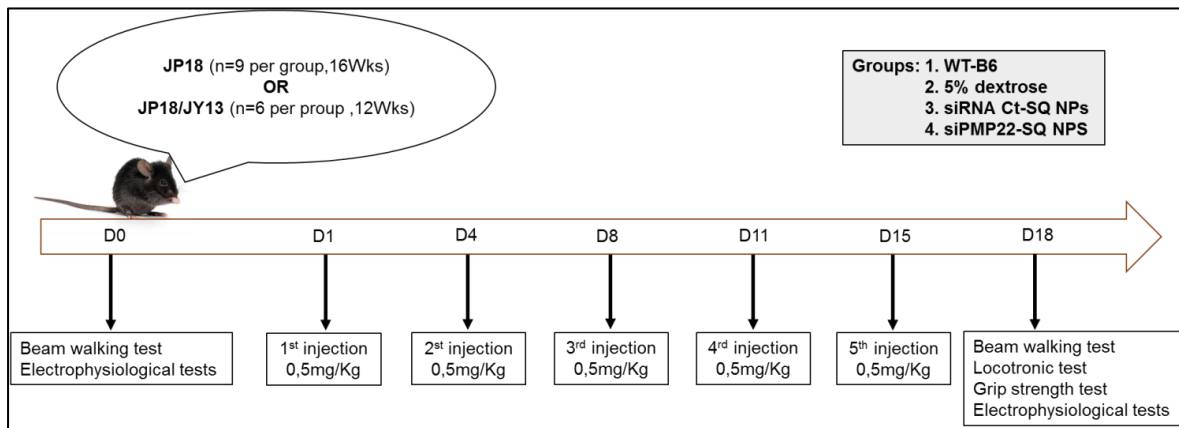


Figure 13. Injection protocol of siRNA PMP22-SQ NPs and siRNA RNA Ct-SQ NPs in JP18 and JP18/JY13 B6 mice.

To study the long lasting effect of siPMP22-SQ NPs JP18/JY13 B6 mice of 12 weeks age were used. Mice were again divided into three groups of 6 mice each: JP18/JY13 vehicle, JP18/JY13 siRNA Ct-SQ NPs and JP18/JY13 siPMP22-SQ NPs in addition to a wild type B6 group as a control. Two cycles of treatment were administered. The first cycle of treatment represents a cumulative dose of 2.5 mg/kg of siPMP22-SQ NPs and siRNA Ct-SQ NPs at an interval of 0.5mg/Kg per injection twice per week. Then treatment were stopped for three weeks to check the relapse period and three mice per group were sacrificed at the end of the first treatment cycle and sciatic nerve were collected for further analysis. At week four, the new cycle of treatment was initiated for another cumulative dose of 2.5mg/kg of siPMP22-SQ NPs and siRNA Ct-SQ NPs at an interval of 0.5mg/Kg per injection twice per week. Behavioural tests were performed before treatment, at 1.5mg/kg of first treatment cycle, at 2.5mg/kg of first treatment cycle, two weeks after stopping the first cycle treatment, three weeks after stopping the first cycle treatment, 1.5mg/kg of second treatment cycle and 2.5mg/kg of second treatment cycle (**Figure 14**). Sciatic nerves were extracted at the end of the second cycle for further analysis.

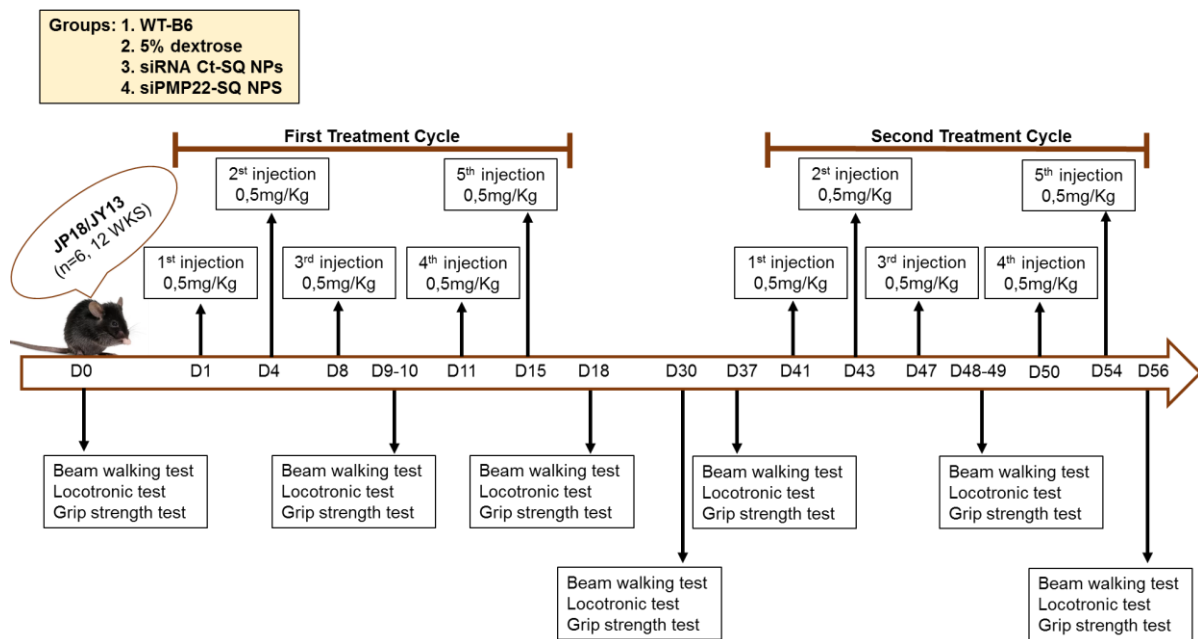


Figure 14. Long lasting effect injection protocol for JP18/JY13 B6 mice

All animal experiments were approved by the institutional Ethics Committee of Animal Experimentation (CEEA) and research council, registered in the French Ministry of Higher Education and Research (Ministère de l'Enseignement Supérieur et de la Recherche; MESR) and carried out according to French laws and regulations under the conditions established by the European Community (Directive 2010/63/UE). Investigation has been conducted in accordance with the ethical standards and according to the Declaration of Helsinki. All efforts were made to minimize animal suffering. Administration of treatments was performed under isoflurane anesthesia and animals were sacrificed by cervical dislocation. All animals were housed in sterilised laminar flow caging system. Food, water and bedding were sterilized before being placed in the cages. Food and water were given *ad libitum*

15. CMT1A mice model Genotyping Protocol

At P7 the fingers of the mice were cut for labelling the number of each mice and the finger tissue was taken for genotyping. Each tissue was placed in an eppendorf tube containing 200µl lysis buffer (200mM NaCl, 5mM SDS, 5mM EDTA pH 8, 100mM TRIS pH 8.5) and 2µl proteinase K. sample were homogenized overnight at 55°C. In the second day the sample were vortexed followed by centrifugation at 13000 rpm for 7 min. The supernatant was then taken and placed over a tube containing 200µl of cold isopropanol. The mixture was shaken vigorously by the hand until the formation of thread like structures that represent the DNA. Then the DNA was suspended in 40µl of ddH₂O and incubated at 55°C for at least 1h. This

was followed by quantification of the cDNA to measure the concentration of each sample on the Nano drop. Five nano gram of DNA was then taken from each sample to perform qPCR using KAPPA2G fast hot start genotyping Mix (KAPA BIOSYSTEM ref# KK5621) and primers of PMP22 and tTA genes at 10 μ M. The pmp22 cDNA construct was assayed for with the primers JPCA 5'GTAGAATTCTGAGATAGCTGTCCCTTTG and JPCF 5, GCGGATGTGGTACAGTTCTG while The tTA-containing constructs were assayed for with the primers tTA807 5'GACGAGCTCCACTTAGACGG and tTA1006 5'-TACTCGTCAATTCCAAGGGC . After qPCR the sample were then RUN on 1.5% agarose gel (105g of agarose prepared in 100ml of 1% TBE solution and 5 μ l of beta mercaptoethanol added after cooling down of the gel) for 30 mins at 150 V in 1% TBE solution and the bands were seen under UV light.

16. Behavioral Tests

a. Beam Walking Test

To test the gait of JP18 and JP18/JY13 mice beam walking was performed. Mice were allowed to walk on a platform with a rod of 3 cm diameter, 70 cm length and around 30 cm above a flat surface [221]. At one end of the rod we set a secure platform to house the animal. First, the mouse was allowed to adapt and then trained to cross the beam from one side to the other. After which the time taken to traverse, the number of pauses and the number of left or right hind paw faults/slips were recorded for analysis. Each animals was tested for three trials per session before starting the treatment and at the end of the experiment for the set of mice of two and half week treatment. For the long lasting effect experiment beam walking test was performed at different time points. The behavior task repeated three times per animal was recorded using a high definition digital camera. Data were presented as average time spent by the mice per group \pm SD. Also the errors and pauses were also recorded.

b. Locotronic

The locotronic apparatus was used to test motor coordination when walking. The mice crossed a 75 \times 5 \times 20 cm flat ladder with bars (7 mm in diameter), which were set 2 cm apart. Infrared photocell sensors situated above and below the bars monitored paw errors. The locotronic apparatus is linked to a software that automatically record the time taken by the mouse to cross the path as well as the paws errors. The time and the errors were assessed in three trials, with 20 min rest between trials. Statistical analysis of obtained data was performed by calculating the mean of three trials for each group. Data are presented as the mean \pm SD.

For the regular treatment strategy the test was performed at the the end of the treatment while for the long lasting experiment it was performed at different time points.

c. Grip strength test

Neuromuscular force was assessed by using the Grip strength test [222]. This test was performed using an automated grip strength meter. The apparatus consisted of a T-shaped metal bar and a rectangular metal bar connected to a force transducer. To measure force in the fore paws of the mice, each mouse was held gently by the base of the tail, allowing the animal to grasp the T shaped metal bar with its forepaws. As soon as the mice grasped the transducer metal bar with their forepaws, the mouse was pulled backwards by the tail until grip was lost. This step was repeated three times and the highest force was automatically recorded in grams (g) by the device. To measure the force on both limbs, each mouse was allowed to grasp the rectangular metal by the fore and hind limbs. After that, it was gently pulled by its tail perpendicular to the axes of the apparatus until the mouse loses the grip. The highest force was recorded automatically by the device. For the regular treatment strategy the test was performed at the end of the treatment while for the long lasting experiment it was performed at different time points. Data represent average force per group \pm SD

17. Electrophysiological study

The test was done with a standard EMG apparatus (Natus /EMG) in accordance with the guidelines of the American Association Of Neuromuscular And Electrodiagnostic Medicine. Anesthesia was performed by isoflurane inhalation where mice were place in an induction chamber containing 1.5-2% isoflurane in pure oxygen. During the whole procedure, anesthesia was maintained on the same level through a face mask. Mice were placed on their frontal side on a heating pad to maintain their body temperature between 34 and 36 °C. For recording the compound muscle action potential, the stimulator needle electrode was inserted at the sciatic nerve notch level, the anode electrode was inserted in the upper base part of the tail while the receptor needle or the recording needle was inserted in the medial part of the gastrocnemius muscle. A supramaximal square wave pulse of 8 mA was delivered through the stimulator needle and recorded through the muscle as amplitude. For the measurement of sensory nerve conduction velocity multiple stimulation of the caudal nerve was delivered through the stimulator needles that were located at the 2/3 of the length of the tail with a distance of 2-2.5cm from the receptor needles. The ground electrode was inserted half way between the

stimulator and the receptor electrodes. The sensory nerve conduction velocity was calculated from the latency of the stimulus and the distance between the stimulator and receptor electrodes [223].

18. Dissection, fixation and cryo-sectioning of sciatic nerve

Immediately upon dissection, sciatic nerves were exposed and few drops of 4% paraformaldehyde were added to start fixation. Then the sciatic nerves were collected carefully and incubated in 4% paraformaldehyde solution at 4°C for 2h. After fixation samples were washed three times 5 min each by phosphate buffer 1X solution followed by 5 min incubation with 5% sucrose prepared in PBS 1X. Then overnight incubation with 20% sucrose was done. In the next day, each sciatic nerve was embedded in O.C.T. Tissue-Tek (Sakura 4583) using cryomolds to orient the segments in an appropriate orientation for transverse sections, and immediately snap-frozen in ice cold isopentane solution place in liquid nitrogen and then stored at -80°C. Frozen sections of 5µm thickness were prepared with a cryostat at -20°C and placed on (3-Aminopropyl) triethoxysilane (Merck, 440140) coated super frost slides. Slides were either directly used or stored at -80° C.

19. Immunohistochemistry staining

To let the OCT melt and the tissue stick well on the slides, slides were left at room temperature for approximately 30 min to equilibrate before starting the permeabilization step. For nuclear proteins SOX10 and KROX20, permeabilization step was done using 0.2% Triton X and 0.1% Tween 20 solution in PBS 1X for 30 min. While samples for cytoplasmic protein as neurofilaments (NF) were permeabilized using ice cold methanol for 10 min. All samples were then blocked for 1 h using blocking buffer consisting of 2% BSA, 0.1% Tween 20 and 5% FBS (replaced by normal donkey serum for SOX10). Subsequently, samples were immunostained for markers specific for myelinating Schwann cells (KROX20), myelinating and non-myelinating Schwann cells (SOX10) and axonal fibers (NF). Primary antibodies are listed in **Table 5** and prepared in their respective blocking buffer and samples were incubated overnight at 4°C. In the second day, samples were washed by PBS 1X three times 5 min each followed by complimentary secondary antibodies incubation (**Table 6**) for 1 h at room temperature. Then three washes of PBS1X 5 min each were done. Cell nuclei were stained with 5µg/ml DAPI in PVA mounting medium (Inova Diagnostics, San Diego,CA). Digital images were obtained using Olympus IX70 fluorescence microscope (Olympus, Tokyo, Japan)

equipped with Leica DFC340 FX camera using Leica Application Suite. Images were analyzed using image J software.

Table 5. Primary antibodies used for KROX20, NF and SOX10

Primary Antibodies	Dilution	Company	Catalog Number
ERG2 (rabbit polyclonal)	1 : 500	Thermofischer Scientific, Waltham, Massachusetts, USA	PA5-27814
Anti-neurofilament H (rabbit polyclonal)	1 :1000	EMD Millipore, Temecula, USA	AB1989
SOX10 (goat polyclonal)	1 :100	R&D systems, Abingdon, UK	AF2864

Table 6. Secondary antibodies used for KROX20, NF and SOX10

Secondary Antibodies	Dilution	Company	Catalog Number
Goat anti-rabbit IgG /Alexa Fluor 488 conjugate	1 :500 KROX20 1:1000 NF	Invitrogen Carlsbad, Californie, USA	A32731
Donkey antigoat IgG/CY3-conjugated	1 :500	Jackson Immuno Research Newmarket, UK	AP194C

20. Statistical Analysis

All data are presented as mean \pm standard deviation (SD). To compare the effects of the different treatments groups *in vitro* and *in vivo*, two-ways ANOVA analysis followed by Bonferroni post-tests for multiple comparison was applied using “Prism” software. $p < 0.05$ was considered as a statistically significant level.

RESULTS

A. Choice of siRNAs PMP22 and their efficacy score

The first step in designing siRNAs is to search for the PMP22 mRNA sequence homologies between Homo sapiens and Mus Musculus PMP22 mRNA sequences. The homology sequences were **Homo sapiens PMP22 variant 1-8, Homo sapiens PMP22 transcript variant X1 and MUS Musculus PMP22 variant 1-7**. Then many siRNA sequences were designed and blasted on the homologous PMP22 mRNA sequence. The scores of each siRNA was calculated according to tafer and Reynold methods. Several criteria were respected to have a good quality of siRNA such as GC ratio between 32% -50 %, at least 3 A/U bases at positions 15-19, and a U base at position 10. Finally, eight different siRNAs were chosen. Sequences number 1 till 8 represent the sense strand of each siRNA. While sequences 12 to 19 represent the antisense strands. All the designed strands are of 19 nucleotide with homology to **human and murine siPMP22 mRNA** and the position was chosen to be at either the beginning, middle or end of the homologous PMP2 sequence (highlighted in the PMP22 mRNA sequence). Also, the selected siRNAs were found to have different scores ranging from 3 till 8. The score is very important since it determine the inhibitory efficiency of the siRNA. Since we did not want a complete inhibition of PMP22 gene all the siRNAs were later tested on MSC-80 cells.

Homology sequence of PMP22 mRNA among mice and human

```
ACACCCCTTCTGCAGCGACGCAAATAGGGCGTAGTTCCCGTTAAAGGGGAACACCGGGAGCCTCCCCTGCCCCCT
TGCTTTGCGCGCGCGCTGACCCGACGACAGCTGTCTTTGGGGACGCCAGCAACCCAGTGGACGCACCGGAGTTT
GTGCCGAGGCTAATCTGCTCTGAGATAGCTGTCCCTTTGAACTGAAACAGGCACCGCTCCTCTGATCCCCGAGCCC
AACTCCCAGCCACCATGCTCCTACTCTTGTGGGGATCCTGTTCCCTGCACATCGCGGTGCTAGTGTGCTCTTCG
TCTCCACCATCGTCAGCCAATGGCTCGTGGGCAATGGACACACGACTGATCTCTGGCAGAACTGTACCACATCCG
CCTTGGGAGCCGTCCAACACTGCTACTCCTCATCAGTGAGCGAATGGCTGCAGTCTGTCCAGGCCACCATGATCC
TGTCTGTCATCTTCAGCGTCCCTGGCTCTGTTCCCTGTTCTTCTGCCAGCTCTTCACTCTCACAAAGGCGGCCGGT
TTTACATCACTGGATTCTTCCAAATCCTTGCTGGTCTGTGCGTGATGAGTGCAGCGGCCATCTACACAGTGAGGC
ACAGTGAGTGGCATGTCAACACTGACTACTCCTATGGCTTCGCCTACATCCTGGCCTGGGTGGCCTTTCCCCTAG
CCCTCCTCAGTGGTATCATCTATGTGATCCTGCGGAAACGCGAATGAGGCGCCGACGACGCACCGTCCGTCTAG
GCTCTGAGCGCGCATAGGGTCCACAGGGAGGGAGGAAGGAAACCAGAGAACAAAACCAACCAACCAAAAAAGAGC
TAGCCCCAAACCCAAACGCAAGCCAAACCAACAGAACGCAGTTGAGTGGGGATTGCTGTTGATTGAAGATGTAT
ATAATATCTATGGTTTTATAAAACCTATTTATAACACTTTTTTACATATATGTACATAGGATTGTTTTGCTTTTTTAT
GTTGACCGTCAGCCTCGTGTGAATCTTAAACAACCTTACATCCTAACACTATAACCAAGCTCAGTATCTTTGTT
TTGTTTTCGTTTTTTTTTTTAAATCTTTTTGTTTTGCTCAGACATAAAAACTCCACGTGGCCCCCTTTCATCTGAAA
GCAGATACCTCCCTCCCCTCAACCTCATAGGATAACCAAAGTGTGGGGACAAACCCAGACAGTTGAAGACCTT
TACACTATGGGTGACCCAGTGCATTTAGCAGGAGTATCCACTGCCCGAATCCATGTGTGAAGCCCTAAGCACTCA
```

CAGACGAAAAGCCCTGACCGGAACCCCTCTGCAAAAACAGTAATAGCTGGTGGCTCCTGAACACTTGACCCTGTAG
ACGGAGTACTGGGGCCACACGTTTTAAATGAGAAGTCAGAGACAAGCAATCTGTGAAATGGTGCTATAGATTTACC
ATTCTTTGTTATTACTAATCGTTTTAAACCCTCACTGGAAACTCAATTAACAGTTTTTATGCGATACAGCAGAATG
GAGACCCGATACAAACGGTTCATAACTGCTTTCATACCTAGCTAGGCTGTTGTTATTACTACAATAAATAAATCT
CAAAGCCTTCGTTCAGTCCCACAGTTTTCTCACGGTTCGGAGCATCAGGACGAGCATCTAGACCCTTGGGACTAGCG
AGTTCCCTGGCTTTCTGGGTCTAGAGTGTCTGTGCCTCCAAGGACTGTCTGGCGATGACTTGTATTGGCCACCA
ACTGTAGATGTATATACGGTGTCCCTTCTGATGCTAAGACTCCAGACCTTCTTGTTTTTGCTTGCTTTCTCTGAT
TTTATACCAACTGTGTGGACTAAGATGCATCAAAAATAAACATCAGAGTAACTCAAAAAAAAAA

NB. Because of the confidentiality, we can not present the sequences and the scores of the siRNAs designed

B. Inhibitory effect of eight different siRNAs PMP22 on PMP22 and P0 gene and protein expression

Eight different siRNAs against PMP22 were tested on MSC80 cells to choose the most effective one. Results have shown that after 48h of transfection all of the tested siRNAs, except the siPMP6, were able to significantly inhibit PMP22 mRNA expression when compared to siRNA Ct and NT cells (**Figure 16**). The long lasting PMP22 mRNA inhibitory effect after 72h of transfection was mostly significant for siPMP4, siPMP5, siPMP6, siPMP7 and siPMP8 when compared to both siRNA Ct treated cell and NT cells (**Figure 15**). As for the protein expression of PMP22, our results have shown that most of the tested siRNA has an inhibitory effect but **interestingly siPMP7 showed an inhibitory effect after 72h of transfection (Figure 17)**.

Also, we studied the effect of these siRNAs on P0 gene expression since any alteration in this myelination protein can lead to another neuropathy as CMT1B. Our data showed no significant change in P0 mRNA siPMP5, siPMP6, siPMP7 and siPMP8 after 48 and 72h of transfection (**Figure 16**). **Based on these results, the best candidates for future studies would be siRNA #5 and #7.** We chose to continue studies with siRNA # 7 because its score of 7 is higher than that of siRNA # 5. **In addition, the siRNA PMP22 #7 met the selection criteria; it was capable of counteracting the 50% overexpression of PMP22 up to 72h, thus restoring the normal expression level of PMP22 (Figure 16).**

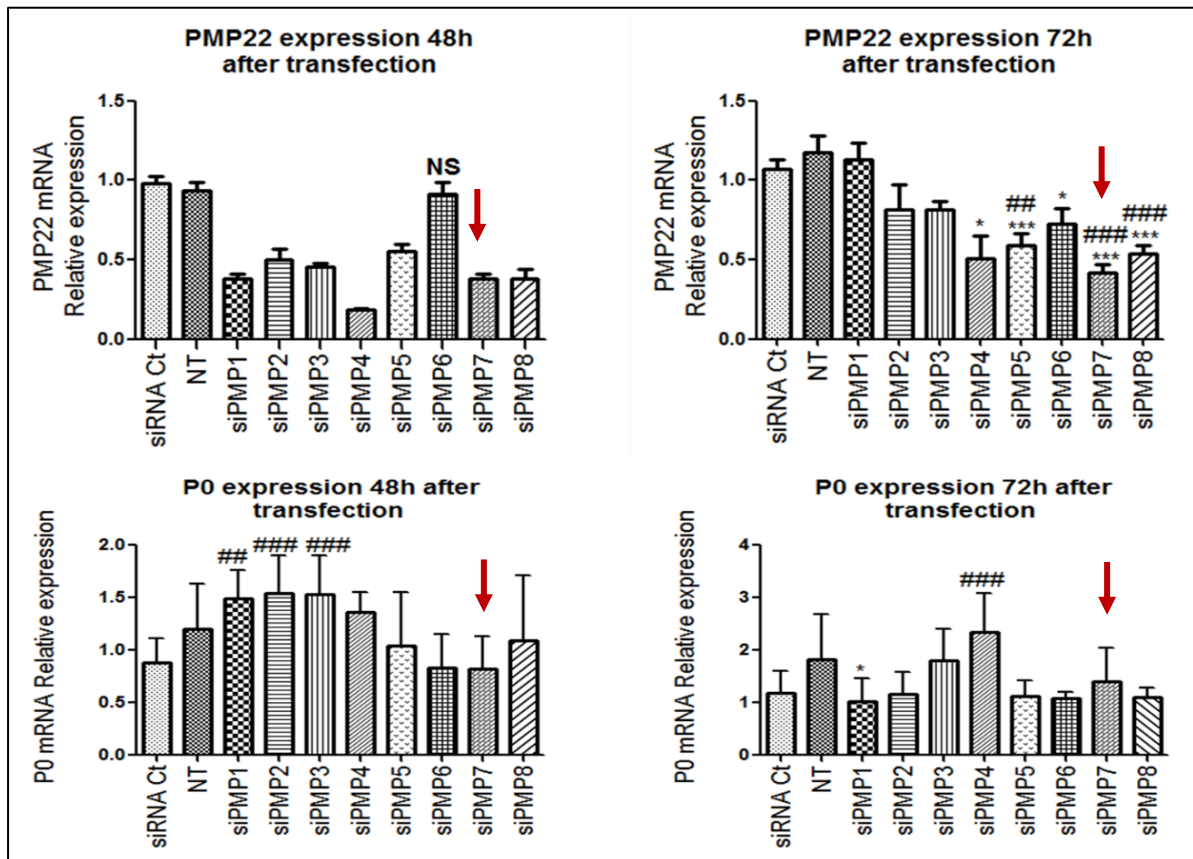


Figure 15. in vitro inhibitory efficacy of eight different siRNA PMP22. MSC80 cells were transfected at 50 nM concentration with siRNA Ct and eight different siRNAs against PMP22 gene: siPMP1, siPMP2, siPMP3, siPMP4, siPMP4, siPMP5, siPMP6, siPMP7 and siPMP8. After 48h, and 72h cells were harvested, then mRNA were extracted to be analyzed for gene knockdown. All siRNA PMP22 significantly inhibited siPMP22 gene expression after 48h except siPMP6 (NS). After 72h only siPMP 5, 6, 7 and 8 showed a long lasting effect with 50% significant inhibition on PMP22 gene expression and no significant effect on P0 gene expression. **siPMP7 significantly decreased PMP22 gene after 48 and 72h (red arrow).** The experiments was repeated more than 3 times and (*) represent significance between NT group and other groups. (#) represent significance between siRNA Ct group and other groups. *, #: p < 0.05; **, ##: p < 0.01; ***, ###: p < 0.001 (Anova followed by Bonferroni tests).

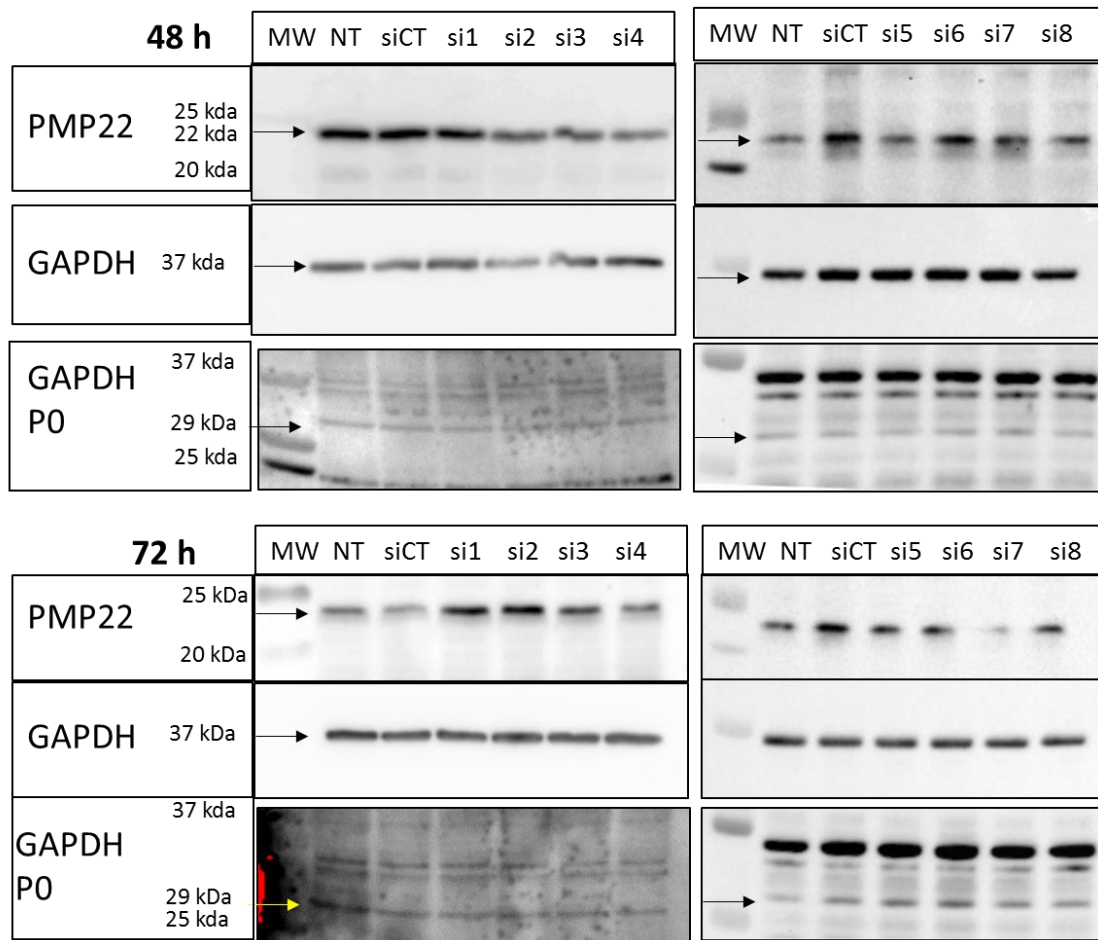


Figure 16: Representative images of protein expression of PMP22 after 48h and 72h of transfection of eight different siRNAs against PMP22 (si1, si2, si3, si4, si5, si6, si7 and si8) at 50nM concentration in MSC80 cells. **Si7 that represent siPMP22 number 7 showed long lasting protein inhibitory effect on PMP22 and no effect on P0 protein expression.** The gels were quantified using image J software (data not presented). Each experiment was repeated three times with biological duplicates.

C. Effect of different concentrations of siPMP22 number 7 on PMP22 and P0 gene expression and on cell viability

After determining the best siRNA candidate which is siPMP22 number 7, different concentration of siRNA PMP22 #7 (25 nM, 50 nM and 100 nM) were studied on MSC80 cells to determine the optimal dose that was considered later on for *in vivo* studies. **We observed that 50 nM concentration reduced the mRNA levels of PMP22 gene and had no effect on P0 gene expression and cell viability.** Precisely, after 72h of transfection, data have shown that siPMP22 #7 at 25 nM concentration inhibited PMP22 gene expression by approximately 35 % while at the 50 nM and 100 nM concentrations were able to inhibit it by 50% when compared to the NT group and had no effect on P0 gene expression. In addition, the siPMP22 25 nM group showed no significant difference in the PMP22 gene expression when compared to the siRNA Ct 25 nM group. siPMP22 100 nM showed a significant effect on cell viability as it demonstrated induction of cell death. **Therefore, based on these observations siPMP22 50 nM were pursued for *in vitro* and *in vivo* studies (Figure 17).**

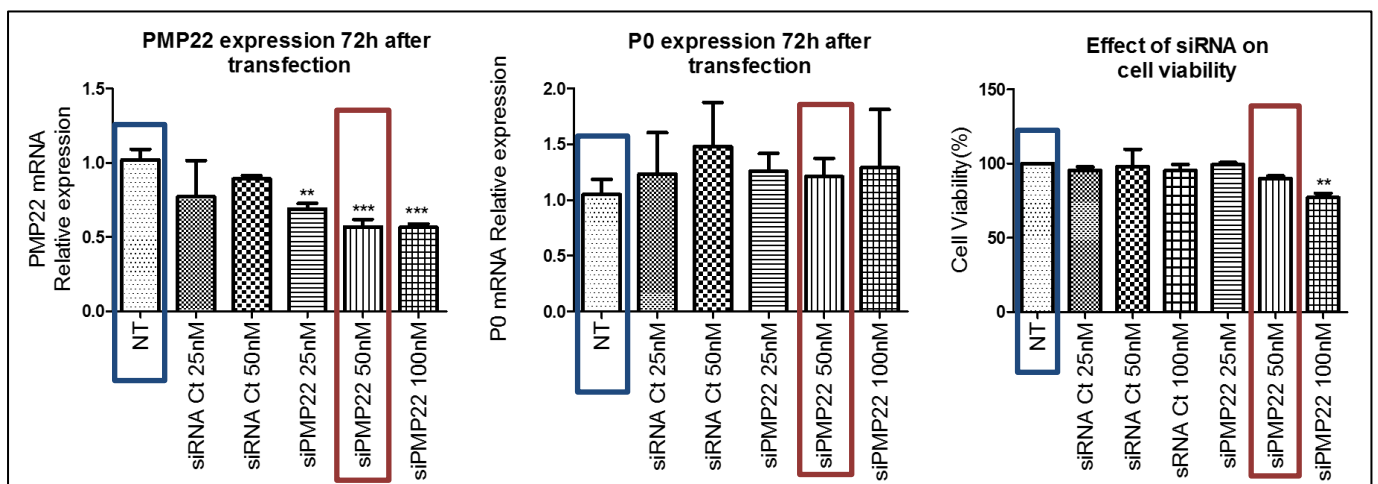


Figure 17. Effect of different concentrations of siPMP22 number 7 on PMP22 and P0 gene expression and Cell viability: MSC80 cells were transfected with siPMP22 number 7 and siRNA Ct at different concentrations: 25 nM, 50 nM and 100 nM. After 72h, cells were harvested for mRNA extraction to study the gene expression of PMP22 and P0. Also, an MTT assay was performed to study the effect on cell viability. **50nM concentration showed a 50% inhibition on PMP22 gene expression when compared to siRNA Control (siRNA Ct) and non-treated cells with no effect on P0 gene expression and cell viability.** (*) represent significance between NT group and other groups, **: $p < 0.01$; ***: $p < 0.001$ (Anova followed by Bonferroni tests).

D. Characterization of siPMP22-SQ Nanoparticles

After selecting the best siRNA candidate and concentration to pursue for *in vivo* studies and due to our previous knowledge that siRNA has to be conjugated to overcome all the hurdles, siPMP22 was conjugated to squalene using copper-free click chemistry method to produce nanoparticles. Several experiments were performed to study the characteristics and stability of siRNA PMP22-SQ nanoparticles. To determine the purity and lipophilicity of the synthesized siPMP22-SQ NPs, RP-HPLC purification was performed and chromatograms of three different compounds representing siPMP22-S (**sense strand in Red**), siPMP22-AS (**anti sense in green**) and siPMP22-S-SQ (**sense strand squalene bioconjugate in black**) were displayed in **Figure 19, A**. **This significantly implied that the synthesized siPMP22-SQ bioconjugates were pure and more lipophilic with an elution time of 18 mins different from that of the siPMP22-S and siPMP22 AS strands (elution time: 16 mins and 12 mins respectively)**. Moreover, MALDI-TOF MS spectrum of siPMP22-SQ bioconjugate showed that the collected bioconjugate had the same molecular weight as the initially injected molecules which further indicated the **purity of the synthesized siPMP22-SQ bioconjugates (Figure 19, B)**. Furthermore, to check the diameter of the siPMP22-SQ NPs DLS measurements were performed and Cryo-TEM images were analyzed. Both techniques determined a nanoparticles size of 180 nm (**Figure 18, C&D**). In addition, DLS measurements over the period of one month showed that siPMP22-SQ NPs **were stable over time with a size ranging between 170-180 nm (Figure 18, C) with a polydispersity index (PDI) less than 0.2**. A PDI value below 0.3 represents the homogeneity of the samples. **Zeta potential measurement was around -48 ± 1 mv.**

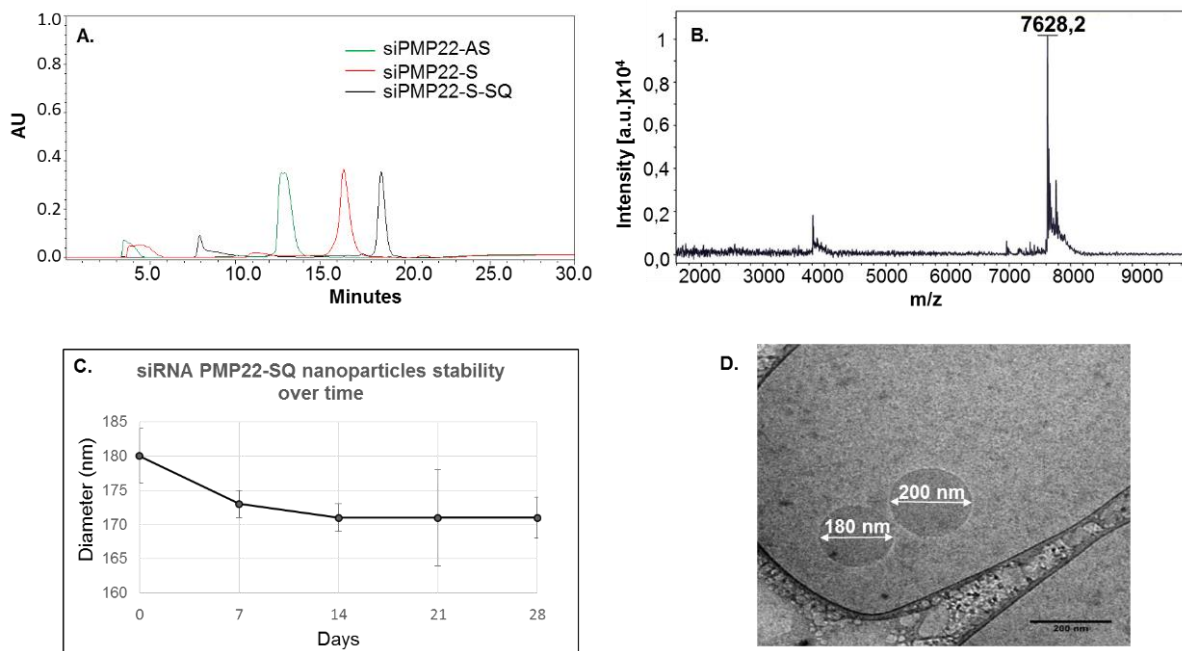


Figure 18. Characterization of siPMP22-SQ NPs: **A.** HPLC chromatograms of the siPMP22-anti sense strand (AS) (green chromatogram), siPMP22-sense strand (S) (red chromatogram) and siPMP22C6-SQ bioconjugate (Black chromatogram). The elution time of siPMP22C6-SQ bioconjugate is 18 mins higher than that of the both siPMP22 strands antisense and sense (12 and 16 mins respectively). **B.** MALDI-TOF MS spectrum of siPMP22-SQ bioconjugate (sense strand). **C.** Physicochemical characterization of siPMP22-SQ NPs by DLS analysis. Size, Polydispersity Index of siPMP22-SQ nanoparticles monitored over time (one month). Each measure is the mean of 3 independent formulations and 3 independent technical measurements. **D.** CryoTEM image of the siPMP22-SQ-NPs. White arrows indicate the nanoobjects size detected (180 and 200 nm). The scale bar used is 200 nm. Each experiment is repeated at least 3 times.

E. Characterization of siRNA-Ct SQ Nanoparticles

siRNA Ct-SQ nanoparticles were also synthesized using the same protocol as that used for the formation of siPMP22-SQ NPs. Same steps of characterization and purification using the same techniques were performed. RP-HPLC purification showed that the siRNA Ct-SQ bioconjugates are more lipophilic than siRNA Ct sense (siRNA Ct S) and antisense strands (siRNA Ct AS). The elution time for siRNA Ct-SQ bioconjugate is 18 mins and **Figure 19, A** showed that its different from the elution time of siRNA Ct-AS (12 mins, green chromatogram) and siRNA Ct S (16min, Red chromatogram). MALDI-TOF MS spectrum of siRNA Ct-SQ bioconjugate showed that the collected bioconjugate had the same molecular weight as the initially injected molecules which further indicated the purity of the synthesized siRNA Ct-SQ biconjugates (**Figure 19, B**). Moreover, DLS analysis was done to check the size of siRNA Ct-SQ nanoparticles directly after synthesis and over the period of one month. Our data showed that the size of the synthesized nanoparticles was around 240 nm with a polydispersity index between 0.1 and 0.2. **This indicated that the nanoparticles were homogeneous and stable over the period of one month (Figure 19, C)**. To check the stability of the siRNA Ct-SQ nanoparticle in serum, the NPs were incubated in 5% FBS solution at 37°C and then loaded on 4% agarose. Results have shown that siRNA Ct-SQ NPs are more stable when incubated at 37°C compared to intact siRNA and their presence lasted up to 4h before complete degradation (**Figure 19, D**). **Therefore, conjugation of siRNA to squalene increased its plasmatic half-life time compared to naked siRNA.**

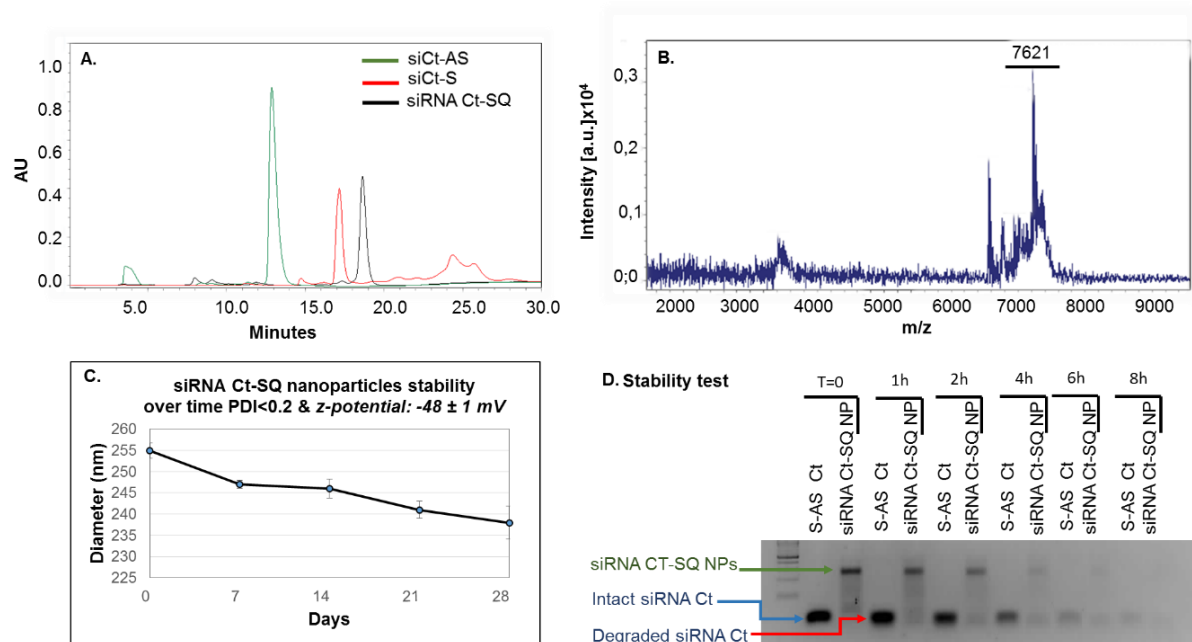


Figure 19. Characterization of siRNA Ct-SQ NPs: **A.** HPLC chromatograms of the siRNA Ct-anti sense strand (AS) (green chromatogram), siRNA Ct-sense strand (S) (red chromatogram) and siRNA Ct-SQ bioconjugate (Black chromatogram). The elution time of siRNA Ct-SQ bioconjugate is 18 mins and its higher than that of the both siRNA Ct strands antisense and sense (12 and 16mins respectively). **B.** MALDI-TOF MS spectrum of siRNA Ct-SQ bioconjugate (sense strand). **C.** Physicochemical characterization of siRNA Ct-SQ NPs by DLS analysis. Size, Polydispersity Index and Zeta Potential of siRNA CT-SQ nanoparticles were monitored over time (one month). Each measure is the mean of 3 independent formulations and 3 independent technical measurements. **D.** 4% agarose gel showing siRNA Ct-SQ NPs and naked siRNA Ct (S-AS) stability in 5% FBS solution at 37°C.

F. *In vitro* inhibitory effect of siPMP22-SQ NPs on siPMP22 and P0 gene expression as well as cell viability

siPMP22-SQ NPs and siRNA Ct-SQ NPs were tested on MSC80 cells to study the effect of the chemical modification and the bioconjugation of squalene to siRNA PMP22 and siRNA Ct on both PMP22 and P0 mRNA expression. Our results in **Figure 20** have shown that siPMP22-SQ NPs maintained the 50% inhibitory effect on PMP22 mRNA expression as the naked siPMP22 after 48 and 72h of transfection when compared to NT, siRNA Ct and siRNA Ct-SQ NPs. Moreover, siPMP22-SQ NPs revealed no effect on P0 mRNA expression and cell viability similarly to siPMP22. Interestingly, siRNA Ct-SQ NPs showed no effect on siPMP22 and P0 gene expression as well as cell viability similar to siRNA Ct (**Figure 20**). **This proves that both squalene and the DBCO modification done on the sense strand of both the siRNA Ct and siPMP22 have no effect on the activity of the siRNA.**

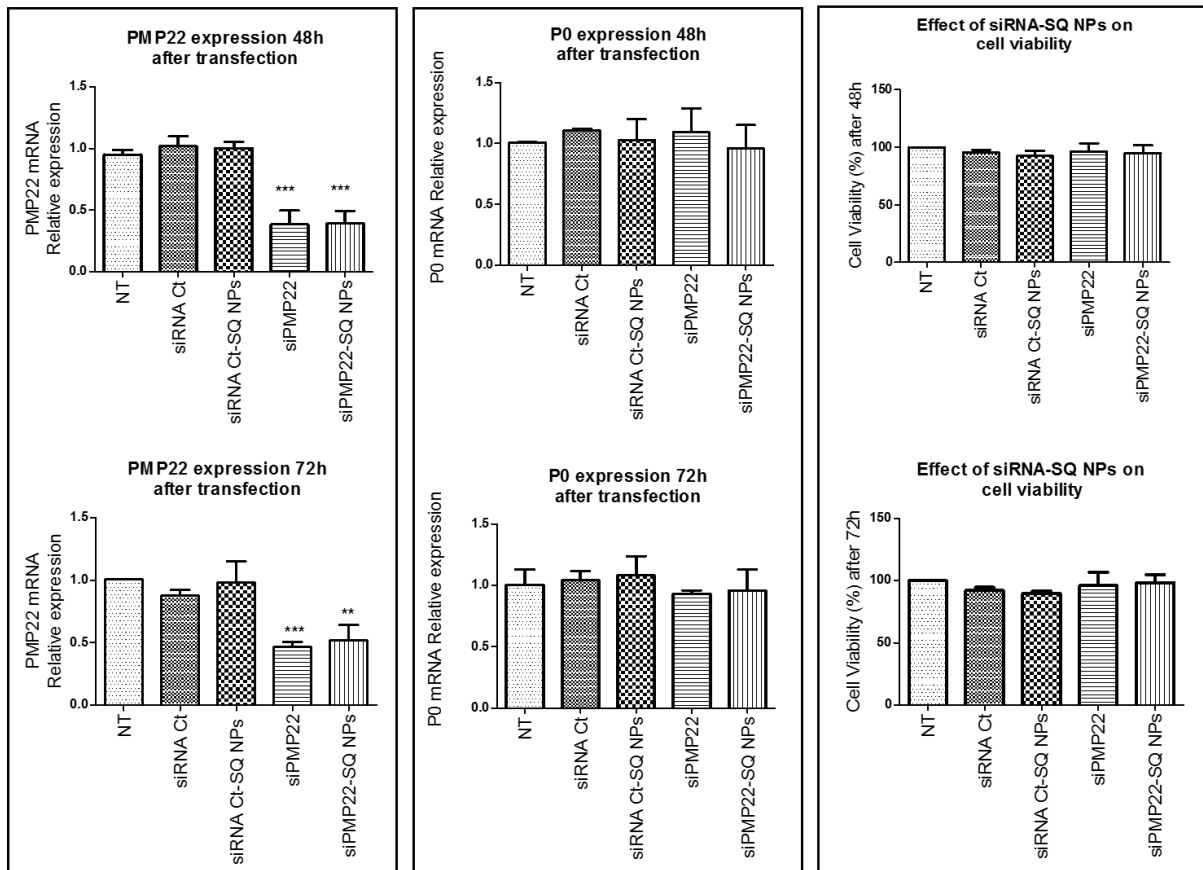


Figure 20. In vitro inhibitory effect of siPMP22-SQ NPs on siPMP22 and P0 gene expression and cell viability: MSC80 cells were transfected at 50nM concentration with siRNA Ct, siRNA Ct-SQ NPs, siPMP22 and siPMP22-SQ NPs. After 48h, and 72h, cells were harvested for either mRNA extraction to analyze gene knockdown or to perform MTT assay to study cell viability. **After 48 and 72h, the siPMP22-SQ NPs significantly inhibited PMP22 gene expression at a 50% level, same as, siPMP22 and showed no significant effect on P0 and cell viability.** siRNA Ct-SQ NPs behaved the same way as siRNA Ct thus proving no effect of squalene and DBCO modification on the efficacy of siPMP22. (*) represent significance between NT group and other groups, **, $p < 0.01$, *** $p < 0.001$ (Anova followed by Bonferroni tests).

G. Genotyping of CMT1 A mice models JP18, JY13 and JP18/JY13 B6

Before the initiation of each in vivo experiment, mice were genotyped to check the expression of the inserted PMP22 and tTA gene. For the JP18 B6 mice, PMP22 gene expression was checked and it showed one band on the agarose gel. The same for the JY13 B6 mice that were used for breeding of JP18/JY13 B6 mice they showed one band representing the tTA gene insert. Whereas for the JP18/JY13 B6 both tTA gene and PMP22 gene expression was studied. Hence, it showed two bands one for PMP22 and the other for tTA depending on the primers used (**Figure 21**). The JP18/JY13 B6 strain was bred in the animal facility from two strains JP18 and JY13 therefore, it has the two constructs: the YAC that carry one copy of the human PMP22 gene under the control of tTA transactivator and Plasmid that carry mouse PMP22 cDNA. The wild type B6 mice do not carry any of the transcripts and were also genotyped to be sure of our results. Since the mice are heterozygote, the number of mice obtained on the double transgenic model is 25 % of the total number while the other 75 % represent the JP18, JY13 and the WT mice. Therefore, to obtain the double transgenic mice we had to increase the number of the breeding couples. It was not possible to do breeding using both double transgenic males and females.

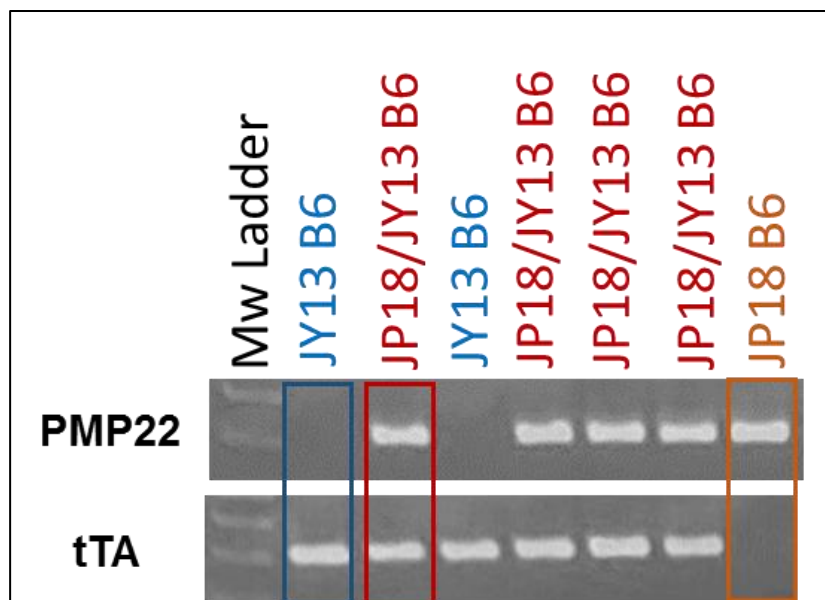


Figure 21. Representative image of genotyping results showing PMP22 and tTA gene after qualitative PCR

H. Effect of siPMP22-SQ NPs on the motor and neuromuscular activity of single transgenic JP18B6 mice

siPMP22-SQ NPs were tested *in vivo* on a single transgenic CMT1A JP18 B6 mouse model and behavioral tests were performed to study the effect of the treatment on the motor and neuromuscular activity of these mice. Results from the beam walking test (**Figure 22**) have shown that before treatment the motor activity of the mice was reduced and the mice in all JP18 B6 group took longer time (**t=25 sec**) to cross the beam from one side to the other when compared to the WT-B6 group (**t=10 sec**). After Treatment the mice treated with **siPMP22-SQ NPs showed a positive results where the time taken by the mice to cross the beam was reduced (t=12 sec) and became comparable to that of the mice in the WT-B6 group.** Mice treated with 5% dextrose vehicle and siRNA Ct NPs still showed a delayed time of 24 sec. Moreover, Results from the locotronic test confirmed the previous data from the beam walking test where the time spent by the JP18 **siPMP22-SQ NPs group was normalized after treatment (t=9 sec) similar to the WT-B6 group.** The time spent by the mice of JP18 5% dextrose and JP18 siRNA Ct-SQ NPs groups was significantly higher than that of the mice of the WT-B6 group (**Figure, 22**).

To analyze the neuromuscular strength of these mice grip strength force was recorded on both the forelimbs and the total limbs (**Figure, 22**). Results from the forelimbs test showed that mice of JP18B6 5% dextrose and JP18 siRNA Ct-SQ NPs groups significantly **have weaker** fore limbs force than the mice of the WT-B6 group. The force on the fore limbs was 40% lower than that of the WT. **Notably, the forelimbs force of the mice of siPMP22-SQ NPs group significantly increased (P<0.05) when compared to JP18 5% dextrose and JP18 siRNA Ct-SQ mice thus reaching the normal levels similar to WT mice after treatment.** For the strength on the total limbs, also our results showed significant weakness in the neuromuscular strength in the groups treated with 5% dextrose and siRNA Ct-SQ NPs when compared to the WT mice. **This activity was normalized in the JP18 siPMP22-SQ NPs group where the force reached 250 g comparable to the WT group.**

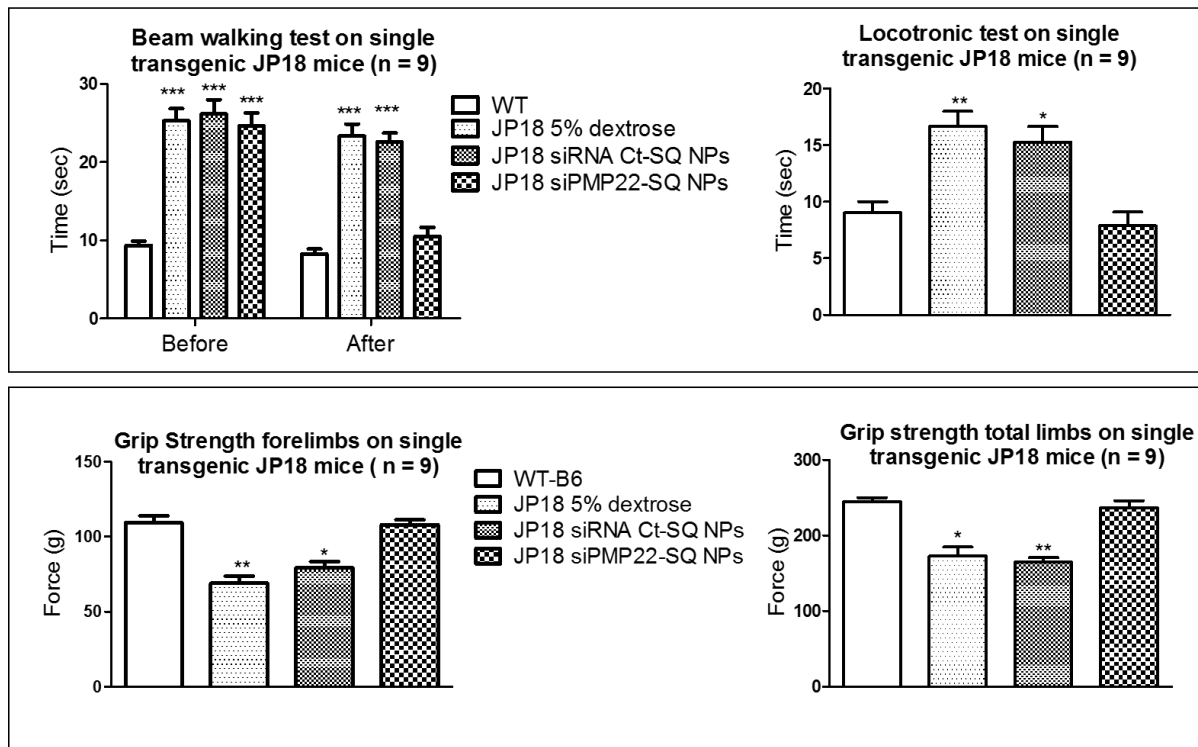


Figure 22. Behavioral test analysis on single transgenic JP18 CMT1A mice: single Transgenic JP18B6 CMT1A mice of 16 weeks age were divided into three groups (n=9 each) receiving the following treatment 5% dextrose, siRNA Ct-SQ NPs and siPMP22-SQ NPs respectively in addition to a wild type B6 group as a control. Beam walking test was performed before starting treatment and after treatment. The time taken by each mouse was recorded over three passages (mean \pm SEM). JP18 siPMP22-SQ NPs group showed normalized time after treatment when compared to the WT-B6 group and were significantly faster than the groups receiving 5% dextrose and siRNA Ct-SQ NPs. Locotronic test was performed after the end of the treatment and it showed significant results as the beam walking test. Three passages were recorded and the data shown is the average of 9 independent mice (mean \pm SEM). Grip strength test was performed at the end of treatment on both the fore limbs alone and the total limbs. JP18 siPMP22-SQ NPs group showed significant improvement in its muscular strength compared the JP18 5% dextrose and JP18 siRNA Ct-SQ NP groups and became comparable to the muscular strength of the WT-B6 group. (*) represent the significance between WT-B6 and other groups at $P < 0.05$. ***, ###: $p < 0.001$ (Anova followed by Bonferroni tests).

I. Electrophysiological analysis on single transgenic JP18B6 mice

Electromyography test was conducted on WT-B6, JP18 5% dextrose and JP18 siPMP22-SQ NPs treated mice to record the compound muscle action potential on the gastrocnemius muscle near to sciatic nerve and tail sensory nerve conduction velocity. Results revealed that before treatment JP18 mice arranged for the treatment groups of 5% dextrose and siPMP22-SQ NPs have significantly CMAP of amplitude 10 mv Lower than that of the WT-B6 mice (CMAP amplitude= 22 mv). After treatment, mice of the **siPMP22-SQ NPs group displayed a significant increase in the CMAP** but the level was still significantly lower than that of the WT-B6 group (**Figure, 23**). As for the sensory nerve conduction velocity (NCV) JP18 mice before treatment showed a SNCV of approximately 35m/s significantly less than that of the WT-B6 mice (45 m/s). **After treatment, JP18 siPMP22-SQ NPs mice group revealed a normalization effect on NCV levels of approximately 45 m/s.** JP18 B6 mice receiving 5% dextrose showed no significant changes on the SNCV speed that remained around 35 m/sec.

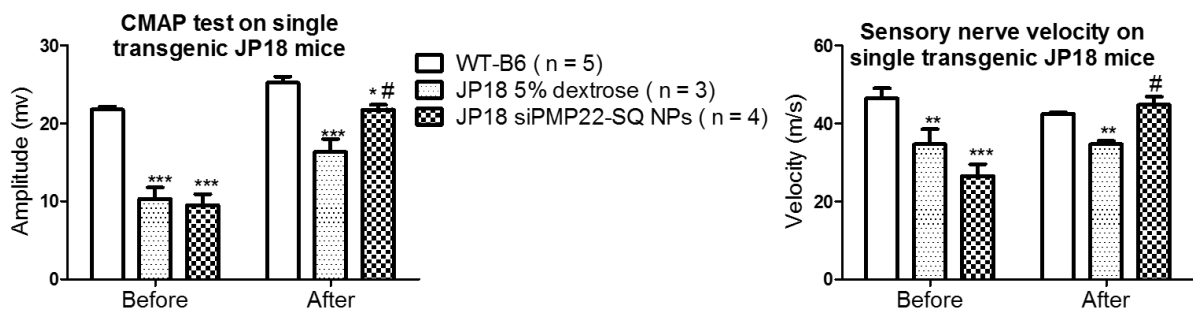


Figure 23. Electrophysiological analysis on single transgenic JP18 CMT1A mice: Compound Muscle Action potential (left panel) and sensory nerve action potential (right panel). Data represent mean \pm SD. (*) represent the significance between WT-B6 and other groups and # represent significance between JP18 5% dextrose and the other two groups at a $P < 0.05$. *#: $p < 0.05$; **: $p < 0.01$, ***, ###: $p < 0.001$ (Anova followed by Bonferroni tests).

J. Effect of siPMP22-SQ NPs on pmp22 protein expression in JP18 B6 single transgenic mice

Western blot analysis was done on JP18 B6 mice and WT-B6 mice to study the inhibitory effect of siPMP22-SQ NPs on pmp22 and p0 protein expression. Our results have shown that siPMP22-SQ NPs were able to normalize the protein level of pmp22 in comparison to WT mice and JP18 B6 5% dextrose and JP18 mice treated with SiRNA Ct-SQ NPs. On the P0 protein levels our results demonstrated regulation in the group treated with the siPMP22-SQ NPs (Figure, 24). This proof that our siPMP22-SQ NPs inhibit PMP22 gene as a consequence the protein expression to a level comparable to that of the WT.

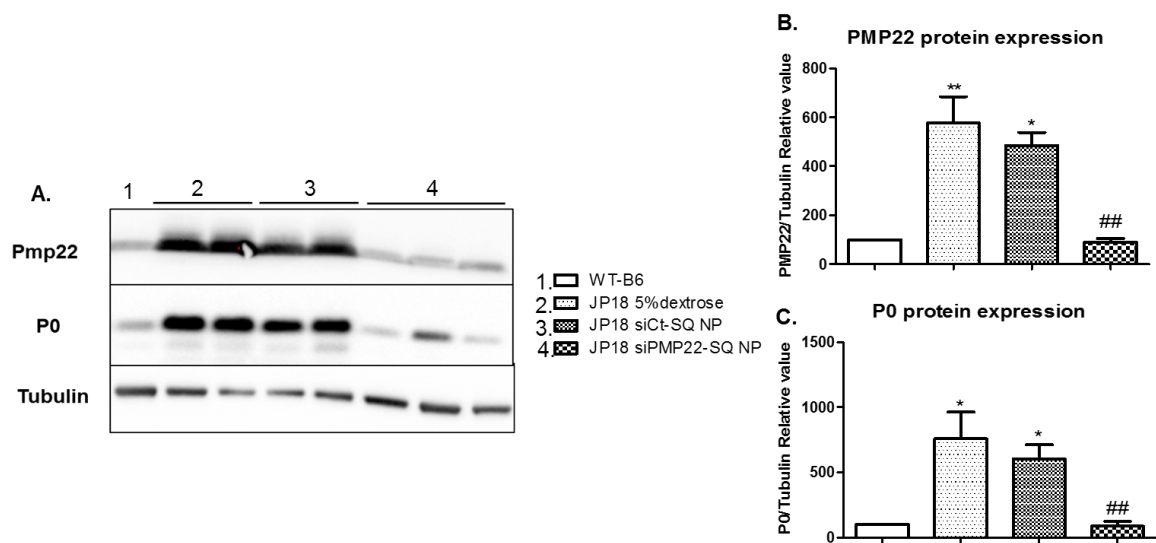


Figure 24. Western blot analysis on JP18B6 single transgenic mice. A. representative image of western blot showing pmp22, p0 and tubulin protein expression in the WT, JP18 B6 5% dextrose, JP18 siRNA CT-SQ NPs and JP18 siPMP22-SQ NPs. B and C are quantitative analysis of pmp22 and p0 protein expression using image J software. Each protein was normalized on tubulin as a reference (number of animals analyzed is 3 per group). Data represent mean \pm SD. Anova analysis followed by Bonferroni post hoc analysis. * $P < 0.05$ between Wt-B6 and the other groups. # $P < 0.05$ between siPMP22-SQ NPs and JP18 B6.

K. Effect of siPMP22-SQ NPs on Schwann cell myelination markers in JP18 B6 single transgenic mice

Immunohistochemistry analysis was done on JP18 B6 and WT-B6 mice to study the effect of siPMP22-SQ NPs on myelination. For this purpose, SOX 10 and KROX 20 which are transcriptional factors playing an important role in myelination were investigated. Confocal images showing the expression of SOX10 (images in Red) in sciatic nerve sections in proportion to stained nuclei of total sciatic nerve cells (DAPI blue) were analyzed. **Figure 25, A**, displayed representative images of SOX10 expression in WT-B6 mice and JP18 mice treated with 5% dextrose, siRNA Ct-SQ NPs or siPMP22-SQ NPs. Quantitative analysis of these images (**Figure 25, B**) showed that JP18 5% dextrose and JP18 siRNA Ct SQ NPs groups when compared to WT-B6 group had lower percentages of SOX10 expression of about 40%. The expression of SOX10 in WT-B6 mice was present in 80% of all the nucleated cells. **Interestingly, mice treated with siPMP22-SQ NPs showed an elevation in the percentage of cells that express SOX10 protein reaching around 70 % of the total number of cells.**

As for the KROX20 expression, which is only present in myelinating Schwann cells, representative confocal images of all the mice group were displayed in **Figure 26, A**. Quantitative analysis of these images showed that KROX20 is expressed in 45% of total sciatic nerve cells in WT-B6 group. This percentage decreased in the JP18 5% dextrose and JP18 siRNA Ct-SQ NPs group till 20% and 25% respectively. JP18 siPMP22-SQ NPs group showed an increase in KROX20 expression where the percentage of cells expressing KROX20 reached 40% after treatment. The level was slightly significant when compared to WT-B6 group but still showed high significance compared to other JP18 groups that had lower levels (**Figure 26, B**). **Therefore, the number of myelinating cells was increased in the group treated with siPMP22-SQ group thus favoring myelination.**

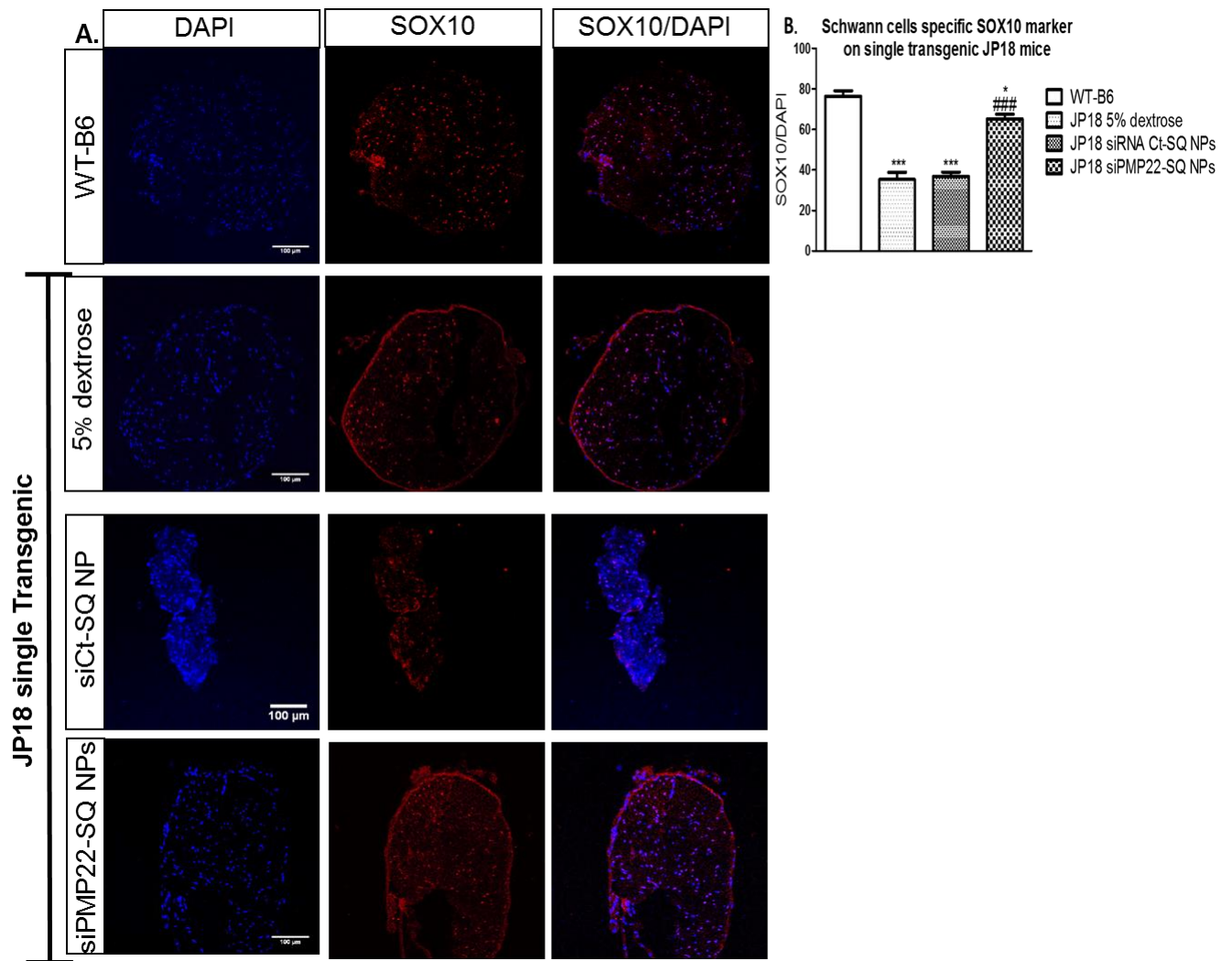


Figure 25. SOX10 transcriptional factor immuno staining on sciatic nerve of single transgenic JP18 mice. (A) Representative confocal microscopy images of immunostained sciatic nerve sections of 5 μ m thickness showing Schwann cells marker SOX10 in the studied mice groups. DAPI staining was used to colorize the nucleus. (B) Quantification analysis showed that the levels of transcriptional factor SOX 10 were diminished in the JP18 5% dextrose and siRNA Ct groups. Notably, siPMP22-SQ NPs treatment significantly increased its levels compared to the JP18 5% dextrose group. Data represents mean \pm SD and each group consists of three different mice. * at $P < 0.05$ represents the significance between WT-B6 group and the other groups and # represent significance between JP18 5% dextrose and JP18siPMP22-SQ NPs. *: $p < 0.05$; ***: $p < 0.001$, ###: $p < 0.001$ (Anova followed by Bonferroni tests). Magnification lens 20X. Scale bar 100 μ m

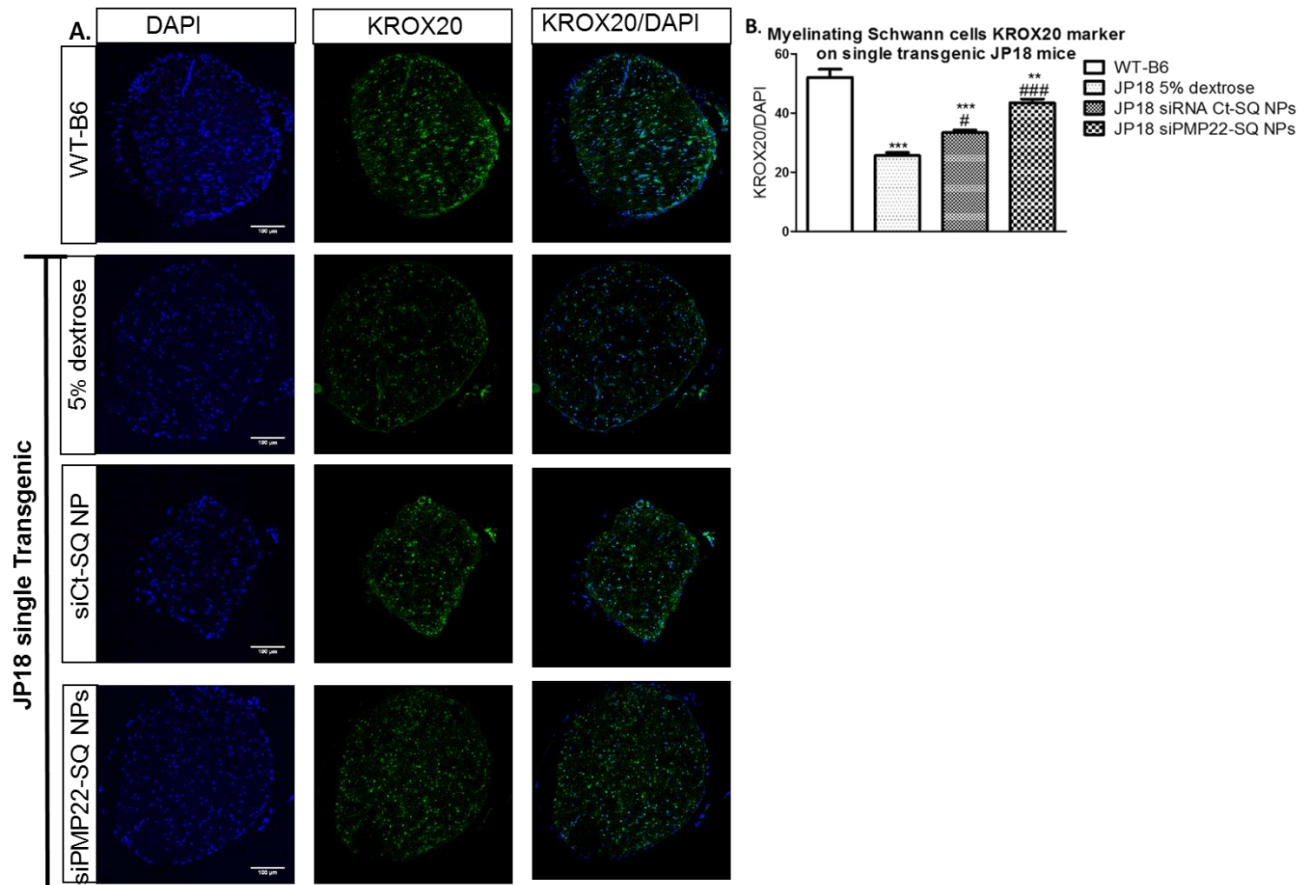


Figure 26. KROX20 transcriptional factor immuno staining on sciatic nerves of single transgenic JP18 mice. (A) Representative confocal microscopy images of immunostained sciatic nerve sections of 5 μ m thickness showing Schwann cells myelination marker KROX20 (green) and in the studied mice groups. DAPI staining was used to colorize the nucleus. Collocation between blue and green represent myelinating schwann cells.(B) Quantification data showed that the levels of the myelination factor KROX20 were diminished in the JP18 5% dextrose and siRNA Ct groups. Notably, siPMP22-SQ NPs treatment significantly increased its levels compared to the JP18 5% dextrose group. Data represents mean \pm SD and each group consists of three different mice. * $P < 0.05$ represents the significance between WT-B6 group and the other groups and # represent significance between JP18 5% dextrose and JP18siPMP22-SQ NPs. *: $p < 0.05$; *** : $p < 0.001$, ###: $p < 0.001$ (Anova followed by Bonferroni tests). Magnification lens 20X. Scale bar 100 μ m.

L. Effect of siPMP22-SQ NPs on axonal regeneration factor neurofilament in JP18 B6 single transgenic mice

To check if siPMP22-SQ NPs can induce axonal regeneration immunohistochemistry analysis on neurofilament (NF) protein was performed on WT-B6 mice and JP18 mice treated with 5% dextrose, siRNA Ct-SQ NPs or siPMP22-SQ NPs. Representative confocal images of sciatic nerve sections showing NF expression (green) and cell nuclei (DAPI blue) were displayed in **figure 27, A**. Quantitative analysis of these images using ImageJ software (**Figure 27, B**) showed that the expression of NF significantly decreased in JP18 5% dextrose and siRNA Ct-SQ mice groups compared to WT-B6 NF expression. This level was normalized in JP18 mice treated with siPMP22-SQ NPs and was significantly higher than the mice treated with 5% dextrose only and siRNA Ct-SQ NPs *i.e.* **siPMP22 SQ NPs can induce axonal regeneration factors after normalizing the levels of PMP22.**

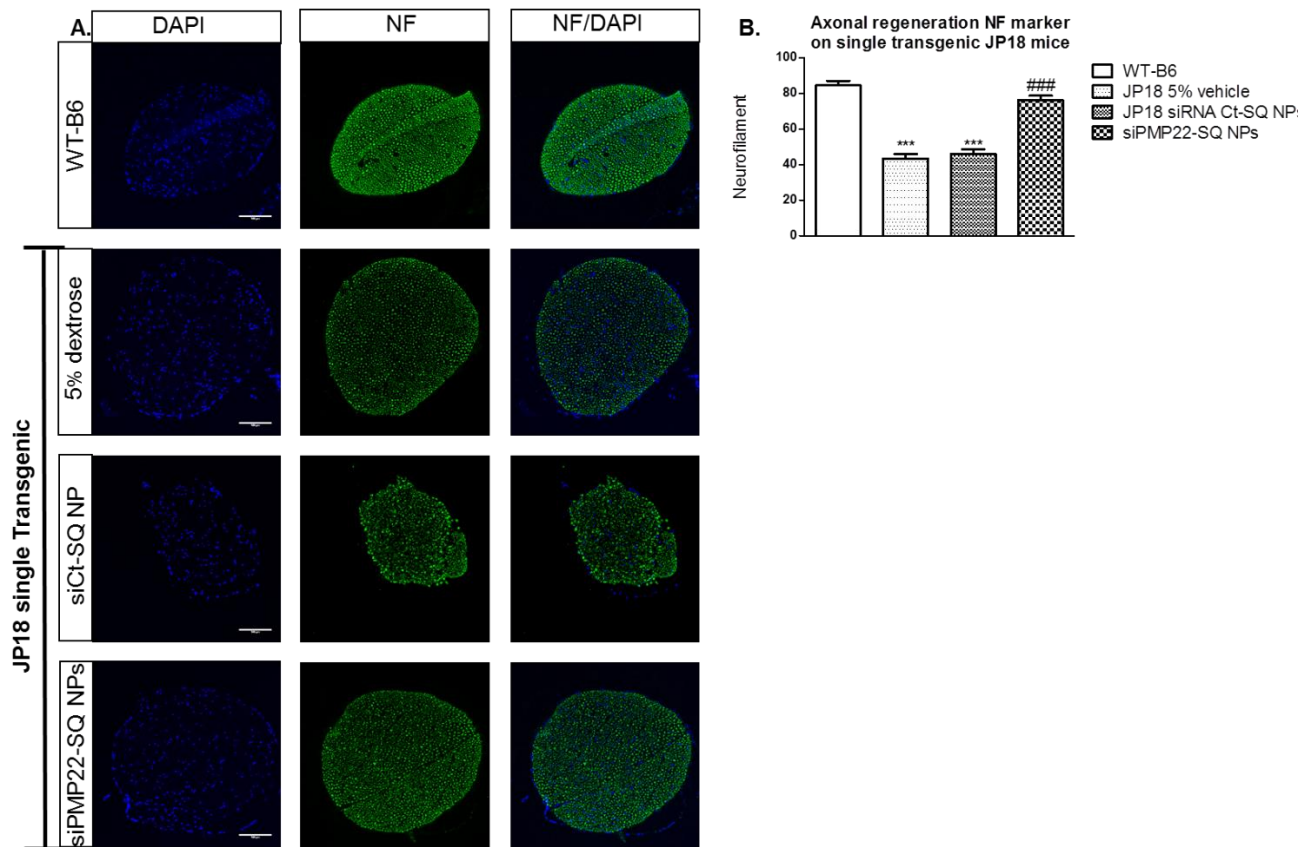


Figure 27. Axonal regeneration factor neurofilament immuno staining on sciatic nerves of single transgenic JP18 mice . Representative confocal microscopy image of immunostained sciatic nerve sections of 5 μ m thickness showing axonal regeneration factor neurofilament in the studied mice groups. DAPI staining was used to colorize the nucleus. (A). Quantification analysis (B) showed that the levels of NF were significantly decreased in the JP18 5% dextrose and siRNA Ct groups. Notably, siPMP22-SQ NPs treatment significantly elevated its levels compared to the JP18 5% dextrose group. Data represents mean \pm SD and each group consists of three different mice. * $P < 0.05$ represents the significance between WT-B6 group and the other groups and # represent significance between JP18 5% dextrose and JP18siPMP22-SQ NPs. *: $p < 0.05$; *** : $p < 0.001$, ###: $p < 0.001$ (Anova followed by Bonferroni tests). Magnification lens 20X. Scale bar 100 μ m.

M. Effect of siPMP22-SQ NPs on the motor and neuromuscular activity of double transgenic JP18/JY13 mice

To study the effect of siPMP22-SQ NP on a double transgenic CMT1A JP18B6 mouse model that carries two extra copies of PMP22 gene representing a more severe CMT1A model the same behavioral tests as those done on the single transgenic mice were performed. We investigated the effect of the treatment on the motor and neuromuscular activity of JP18/JY13B6 mice. Results from the beam walking test showed that before treatment the **motor activity of JP18/JY13 mice was reduced and they took a longer time (t=30 sec) to cross the beam from one side to the other when compared to the WT-B6 group (t=10 sec) (Figure 28) and JP18 B6 5% dextrose (Figure 22)**. In addition, the mice have done more pauses and errors during the test. **This reflects that the double transgenic model is more severe than the single one.** After Treatment the mice treated with siPMP22-SQ NPs showed a positive results where the time taken by the mice to cross the beam was reduced (t=10 sec) and became comparable to that of the mice in the WT-B6 group. Mice treated with 5% dextrose vehicle and siRNA Ct NPs still showed a delayed time of 25-30 sec. Moreover, Results from the locotronic test confirmed the data obtained from the beam walking test where the time spent by the JP18/JY13 siPMP22-SQ NPs group was normalized after treatment (t=9 sec) similar to the WT-B6 group. The time spent by the mice of JP18/JY13 5% dextrose and JP18 siRNA Ct-SQ NPs groups was significantly higher than that of the mice of the WT-B6 group (Figure 28). **Therefore, siPMP22SQ NPs were able to normalize the motor activity of JP18/JY13 mice similar to JP18B6 mice.**

To analyze the neuromuscular strength of the JP18/JY13 mice of the tested groups grip strength force was recorded on both the forelimbs and the total limbs (Figure 28). Results on forelimbs showed that mice of the three JP18/JY13 tested groups showed a significant decrease in their force when compared to the WT-B6 mice but with a tendency to a normal strength in the group treated with siPMP22-SQ NPs. For the strength on the total limbs, our results showed significant weakness in the neuromuscular strength of the groups treated with 5% dextrose and siRNA Ct-SQ NPs when compared to the WT mice. **This activity was normalized in the JP18/JY13 siPMP22-SQ NPs group where the force reached 250 g comparable to the WT group.**

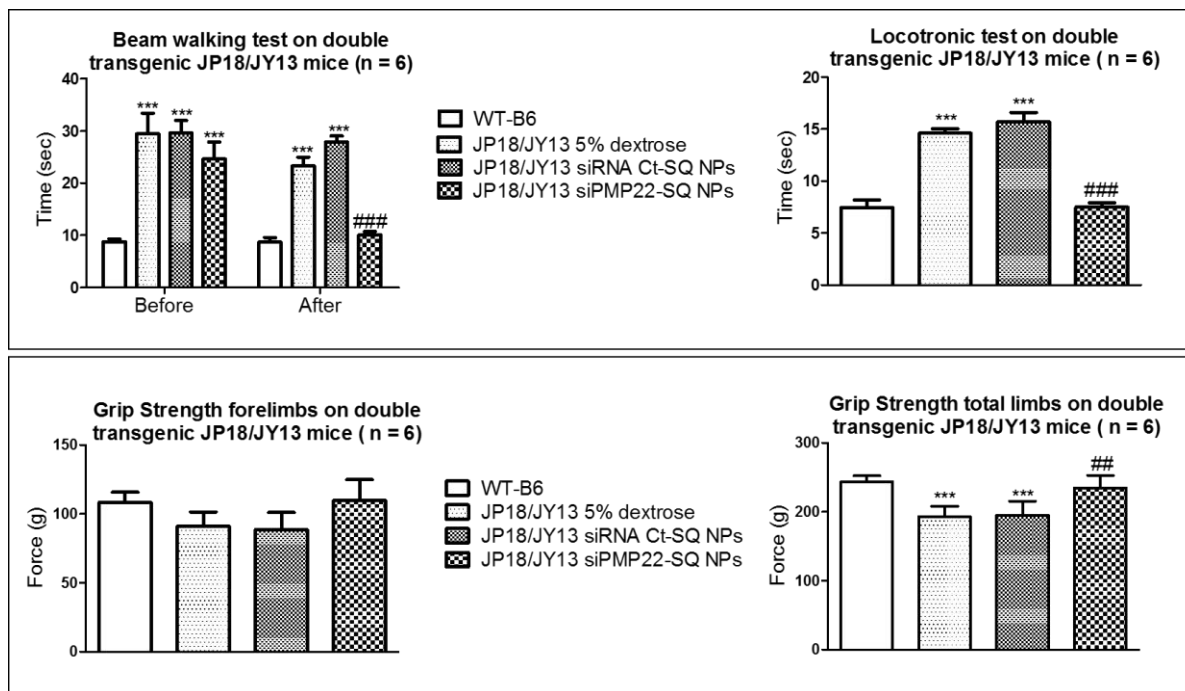


Figure 28. Behavioral test analysis on double transgenic JP18/JY13 B6 CMT1A mice: double Transgenic JP18/JY13 B6 CMT1A mice of 12 wks age were divided on three groups (n=6 each) receiving the following treatment 5% dextrose, siRNA Ct-SQ NPs and siPMP22-SQ NPs respectively in addition to a wild type B6 group as a control. Beam walking test was performed before starting treatment and after treatment. The time taken by each mouse was recorded over three passages (mean \pm SD). JP18/JY13 siPMP22-SQ NPs group showed normalized time after treatment when compared to the WT-B6 group and were significantly faster than the mice in groups receiving 5% dextrose and siRNA ct-SQ NPs. Locotronic test was performed after the end of the treatment and it showed significant results as the beam walking test. Three passages were recorded and the data shown is the average of 6 independent mice. Grip strength test was performed at the end of treatment on both the fore limbs alone and the total limbs. JP18/JY13 mice receiving siPMP22-SQ NPs group showed significant improvement in their muscular strength compared the JP18/JY13 5% dextrose and JP18/JY13 siRNA Ct-SQ NP groups and became comparable to the muscular strength of the WT-B6 group. (*) represent the significance between WT-B6 and other groups. (*) represents the significance between WT-B6 and other groups. (#) represent the significance between JP18/JY13 5% dextrose and JP18/JY13 siPMP22-SQ NPs. ***, ###: $p < 0.001$ (Anova followed by Bonferroni tests).

N. Electrophysiological analysis of double transgenic JP18/JY13B6 mice

Electromyography test was conducted on WT-B6, JP18/JY13 5% dextrose, JP18/JY13 siRNA Ct-SQ NPs and JP18/JY13siPMP22SQ-NPs mice to record the compound muscle action potential on the gastrocnemius muscle near to sciatic nerve and tail sensory nerve conduction velocity. Results revealed that before treatment JP18/JY13 mice arranged for the treatment groups have significantly lower CMAP with amplitude signal ranging between 10-15 mv when compared to WT-B6 mice (amplitude signal of 22 mv). After treatment, mice of the siPMP22-SQ NPs group displayed a significant increase in the CMAP amplitude when compared to JP18/JY13 mice receiving 5% dextrose and siRNA Ct-SQ NPS, respectively (**Figure 29, left panel**). Interestingly the level of the increase in amplitude in the siPMP22-SQ treatment group is comparable to the WT-B6 group with a value of 20-21. As for the sensory nerve conduction velocity (NCV) JP18/JY13 mice before treatment showed an NCV of approximately 30 m/s significantly less than that of the WT-B6 mice (NCV=45 m/s). **After treatment, JP18/JY13 siPMP22-SQ NPs mice group revealed a normalization effect on NCV levels of approximately 40-42 m/s. JP18 B6 mice receiving 5% dextrose showed no changes in the NCV speed that remained around 30 m/s (Figure 29, right panel).**



Figure 29. Electrophysiological analysis on double transgenic JP18/JY13 CMT1A mice: Compound Muscle Action potential (left panel) and sensory nerve action potential (right panel). Data represent mean \pm SD. (*) represents the significance between WT-B6 and other groups. (#) represent the significance between JP18/JY13 5% dextrose and JP18/JY13 siPMP22-SQ NPs. *#: $p < 0.05$; **: $p < 0.01$, ***, ###: $p < 0.001$ (Anova followed by Bonferroni tests).

O. Effect of siPMP22-SQ NPs on Schwann cell myelination and axonal regeneration markers in JP18/JY13 B6 transgenic mice

Same as previously mentioned for JP18 B6 mice immunohistochemistry analysis was done on JP18/JY13 and WT mice to study the effect of siPMP22-SQ NPs on myelination and axonal regeneration. Two Schwann cells markers SOX10 and KROX20 were analyzed to differentiate myelinating from unmyelinating Schwann cells and one axonal regeneration factor NF was studied. Confocal images showing the expression of SOX10 (images in Red) in sciatic nerve sections in proportion to stained nuclei of total sciatic nerve cells (DAPI blue) then analyzed by Image J software. **Figure 30**, displays representative images of SOX10 (Red), KROX20 (green), NF (green) and DAPI stained nuclei (blue) in WT-B6 mice in comparison to JP18/JY13 mice treated with 5% dextrose, siRNA Ct-SQ NPs or siPMP22-SQ NPs.

Quantitative analysis of SOX 10 images (**Figure 31, A**) showed that JP18/JY13 5% dextrose and JP18/JY13 siRNA Ct SQ NPs mice significantly have lower percentages of SOX10 of about 20% when compared to WT-B6 group that showed that 75% of all the nucleated cells express SOX10. Interestingly, mice treated with siPMP22-SQ NPs showed a normalization in the percentage of cells that express SOX10 transcriptional factor reaching around 75 % of the total number of cells.

As for the KROX20 expression which is only present in myelinating Schwann cells, quantitative analysis of confocal images showed that KROX20 is expressed in 45% of total sciatic nerve cells in WT-B6 group. This percentage decreased in the JP18/JY13 5% dextrose and JP18/JY13 siRNA Ct-SQ NPs group as the total percentage of cells expressing KROX20 was approximately 25%. JP18/JY13 siPMP22-SQ NPs group showed an increase in KROX20 expression where the percentage of cells expressing KROX20 reached around 60% of the total number of cells (**Figure 31, B**). Therefore, **the number of myelinating cells was increased in the group treated with siPMP22-SQ group thus favoring myelination. These results show similarity with the result on the JP18B6 single transgenic mice.**

In addition, quantitative analysis of NF immunohistochemistry images (**Figure 31, C**) showed that the expression of NF significantly decreased in JP18/JY13 5% dextrose and siRNA Ct-SQ mice groups compared to WT-B6. This level was normalized in JP18/JY13 mice treated with siPMP22-SQ NPs and was significantly higher than the mice treated with 5% dextrose only and siRNA Ct-SQ NPs, *i.e.* that **siPMP22-SQ NPs can induce axonal regeneration factors after normalizing the levels of PMP22.**

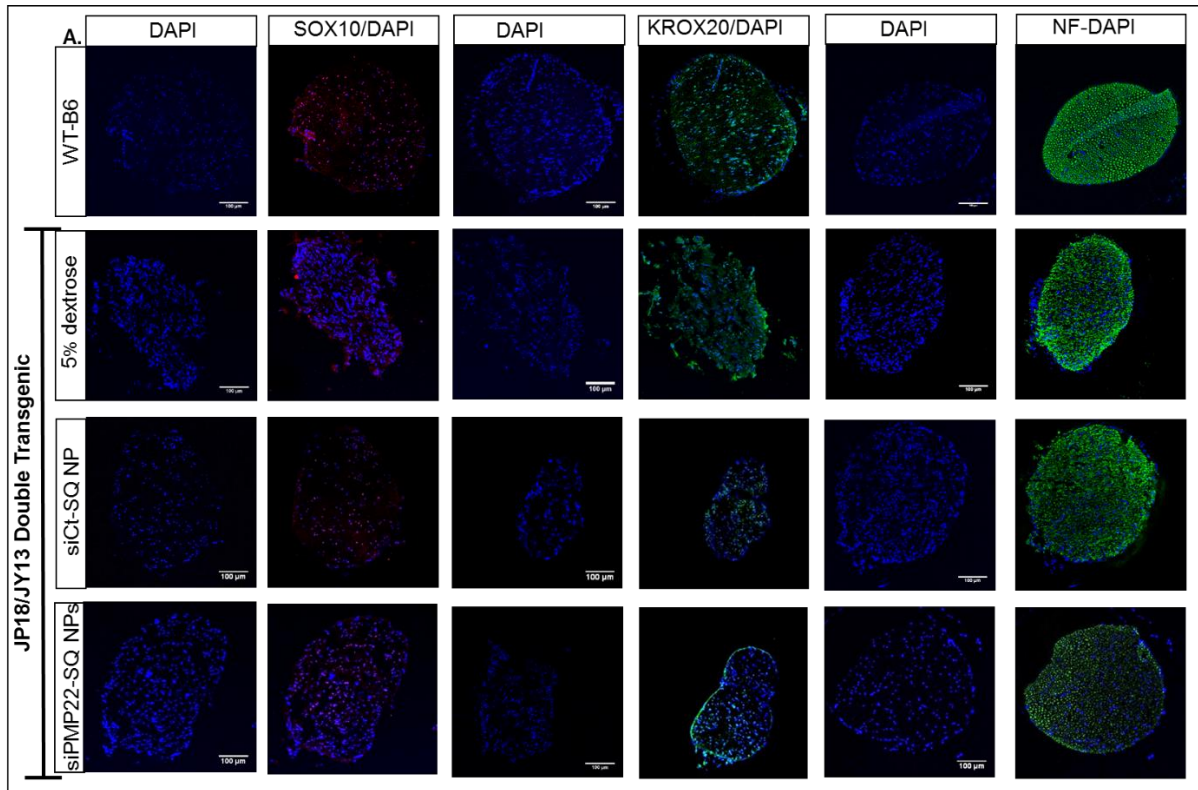


Figure 30. Immuno staining analysis of myelination and axonal regeneration factors on sciatic nerves of double transgenic JP18/JY13 CMT1A mice. Representative images of immuno stained sciatic nerve sections of 5μm thickness showing collocation between the Schwann cells nucleus stained with DAPI (blue) and Schwann cell markers SOX10 (Red) and KROX20 (green). Axonal regeneration marker neurofilament is shown in green.

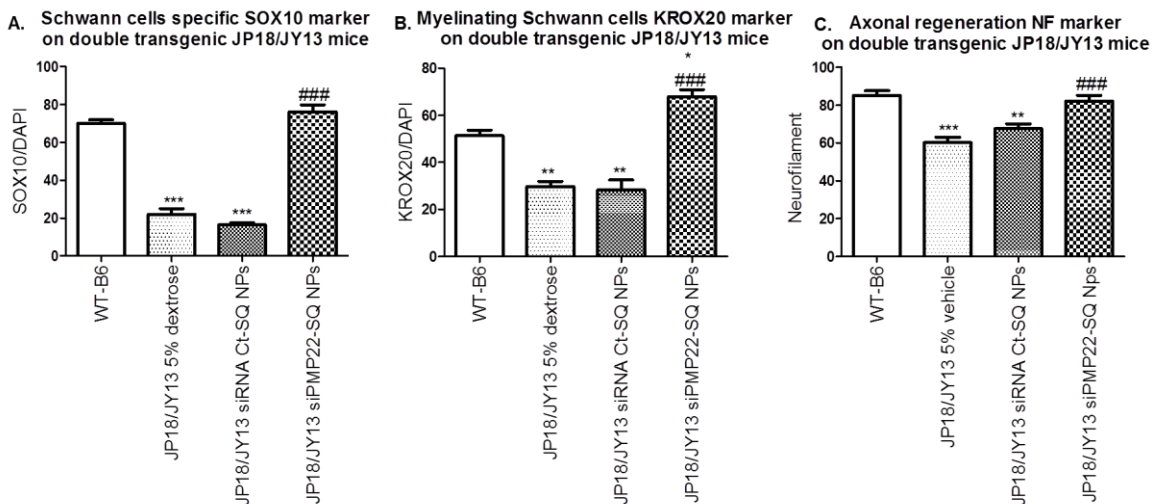


Figure 31. Immuno staining analysis of myelination and axonal regeneration factors on sciatic nerves of double transgenic JP18/JY13 CMT1A mice. Quantification analysis (B-D) showed that siPMP22-SQ NPs treatment increased myelination transcription factors (SOX10 and KROX20) and enhanced axonal regeneration compared to the JP18/JY13 5% dextrose group. Data shows mean±SD and each group consist of three different mice * at $P < 0.05$ represents the significance between WT-B6 group and the other groups and # represent significance between JP18/JY13 5% dextrose and JP18/JY13 siPMP22-SQ NPs. *: $p < 0.05$; **: $p < 0.01$; ***: $p < 0.001$, ###: $p < 0.001$ (Anova followed by Bonferroni tests). Magnification lens 20X. Scale bar 100μm

P. Long lasting effect of siPMP22-SQ NPs on the motor and neuromuscular activity on double transgenic mice.

To study the long lasting effect of siPMP22-SQ NPs on the motor activity of double transgenic mice (JP18/JY13) behavioral tests that monitor the locomotor activity of the mice and their muscular strength as mentioned previously were performed. Briefly and as mentioned in the material and methods part, the mice were treated with 2.5 mg/kg siPMP22-SQ NPs for the first cycle and the behavioral test were performed before, mid-way of treatment (1.5mg/kg) and end of cycle 1 (2,5 mg/kg dose). Then, the mice were monitored for 3 weeks after end of 1st treatment cycle which is the relapse point before the initiation of the second cycle of treatment at the 4th week and monitoring till the end of the treatment (please refer to the protocol figure 15 in materials and methods chapter). During the first cycle of treatment, results of both locomotor test showed that after 1.5mg/kg dose of siPMP22-SQ NPs the motor activity of the mice was increased where the time taken by JP18/JY13 is normalized ($t = 10$ sec, **Figure 32**). This effect became more significant as the dose reached 2.5mg/kg while the mice receiving 5% dextrose and siRNA Ct-SQ NPs showed no change in the time they take to perform the tests. These results of the first cycle confirm the results of the experiment done before on double transgenic mice (**Figure, 28**). After stopping treatment for 3 to 4 weeks, we noticed that effect of siPMP22 SQ-NP on motor activity could last between 14-21 days after which there was a relapse period where the effect is lost and the mice of the JP18/JY13siPMP22-SQ NPs group took around 20-28 secs to perform the tests similar to the other two JP18/JY13 groups. **Interestingly, when we wanted to test if the siPMP22-SQ NPs could induce resistance after the 1st cycle of treatment we started the 2nd cycle and our results showed that same pattern as the results of the 1st cycle where after three injections the mice started to be faster and have less faults when performing the tests. After the fifth injection of the second cycle, the mice took 10 sec to perform the beam walking or the locotronic test (Figure, 32).**

Notably, results from the neuromuscular activity test showed the same pattern as that of the locomotor tests. Mice treated with siPMP22-SQ NPs were stronger after three weeks of injections (cumulative dose of 1.5 mg/kg) on both the fore and the hind limbs when compared to the mice of JP18/JY13 5% dextrose and JP18/JY13siRNA Ct-SQ NPs (**Figure, 33**). At the end of the first cycle of treatment, the results were more significant. The effect of siPMP22-SQ NPs also lasted for 3 weeks after that relapse of the mice was recorded on both fore and hind limbs. Also, the same results were obtained for the second cycle of treatment were **the**

mice receiving siPMP22-SQ NPs had a larger force than those of the other groups and comparable to the WT-B6 mice. Therefore, no resistance was detected during the second cycle of treatment.

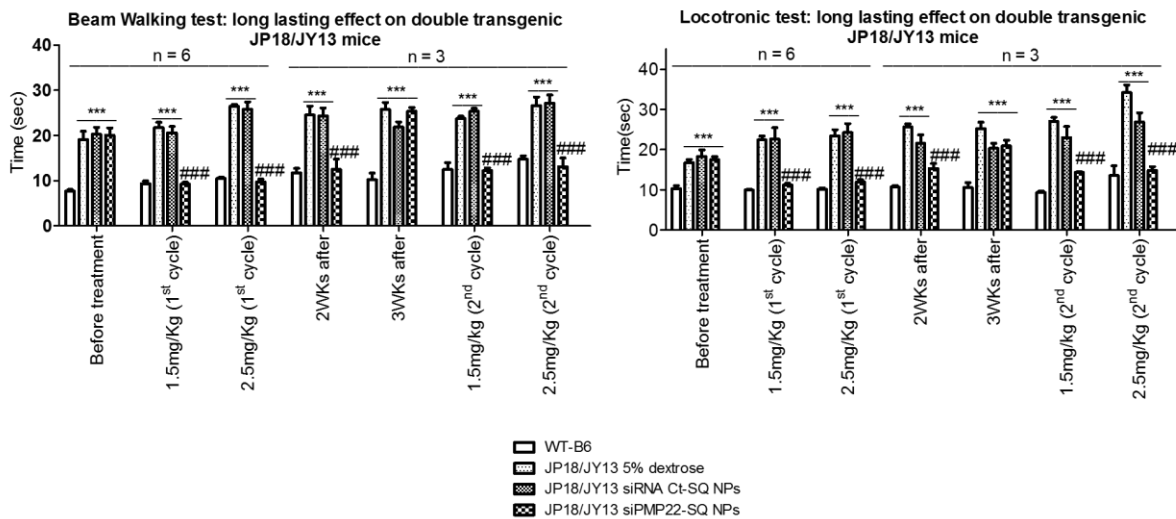


Figure 32. Long lasting effect analysis of Beam walking and locotronic on double transgenic JP18/JY13 transgenic mice. JP18/JY13 B6 mice received two cycles of treatment of 2.5mg/Kg per cycle. Treatment was stopped for 21 days in between the two cycles to study the relapse. Data of Beam walking test (left panel) represent time spent to cross the bar (mean \pm SD). Data of Locotronic test (right panel) represent time recorded by the computerized program (mean \pm SD). The mice were followed weekly to analyze the recovery and relapse periods. (*) represents the significance between WT-B6 and other groups. (#) represent the significance between JP18/JY13 5% dextrose and JP18/JY13 siPMP22-SQ NPs. **, $p < 0.01$, *** $p < 0.001$ (Anova followed by Bonferroni tests).

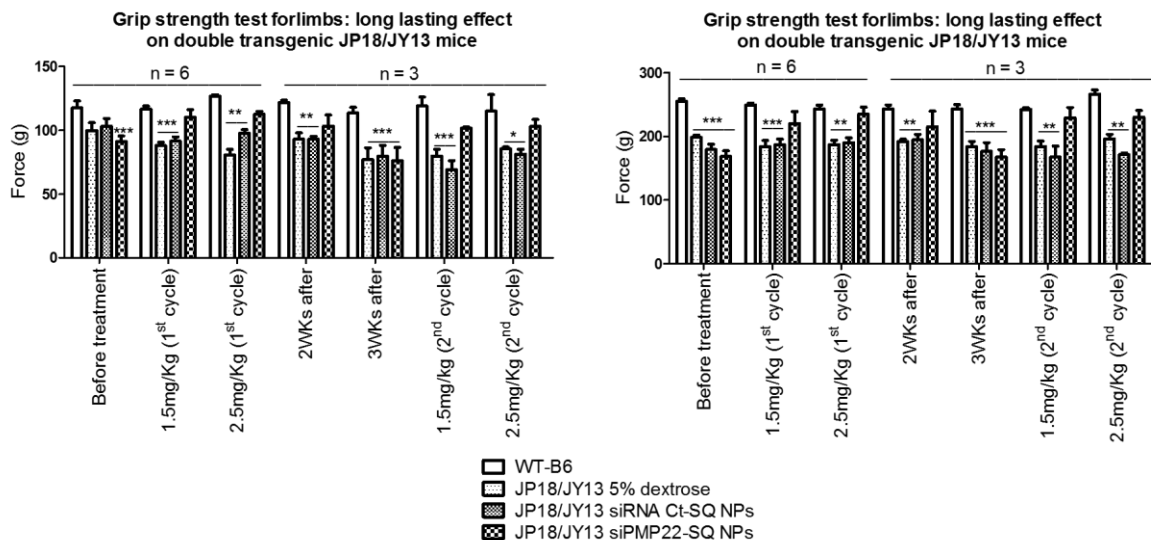


Figure 33: Long lasting effect analysis of Grip strength test on double transgenic JP18/JY13 transgenic mice. JP18/JY13 B6 mice received two cycles of treatment of 2.5mg/Kg per cycle. Treatment was stopped for 21 days in between the two cycles to study the relapse. Data of grip strength test (left panel) represent force exerted by the mice on the fore limbs (mean \pm SD). Data of grip strength test (right panel) force exerted by the mice on the total limbs (mean \pm SD). The mice were followed weekly to analyze the recovery and relapse periods. (*) represents the significance between WT-B6 and other groups. (#) represent the significance between JP18/JY13 5% dextrose and JP18/JY13 siPMP22-SQ NPs. **, $p < 0.01$, *** $p < 0.001$ (Anova followed by Bonferroni tests)

Q. Localization of NPs in Schwann cells and axons of treated mice

To check if the injected NPs reached Schwann cells and axons, high magnification TEM images of sciatic nerve longitudinal sections taken from mice treated with siPMP22-SQ or siRNA CT-SQ NPs were captured (**Figure 34**). **Interestingly, vesicles of 180 nm-220 nm were distinguished in Schwann cells and along the axons. These features were only found in the groups treated with siPMP22-SQ NPs and siRNACT-SQ NPs.** The size of these vesicles was compatible with the size of the injected NPs that had only one lipid layer and could be easily differentiated from other small vesicles and mitochondria. **Notably, high concentration of these NPs were detected near the nodes of Ranvier which made us speculate that they can pass along the axons through this region and cross along the myelin sheath and ultimately reach Schwann cells or *vice versa*.**

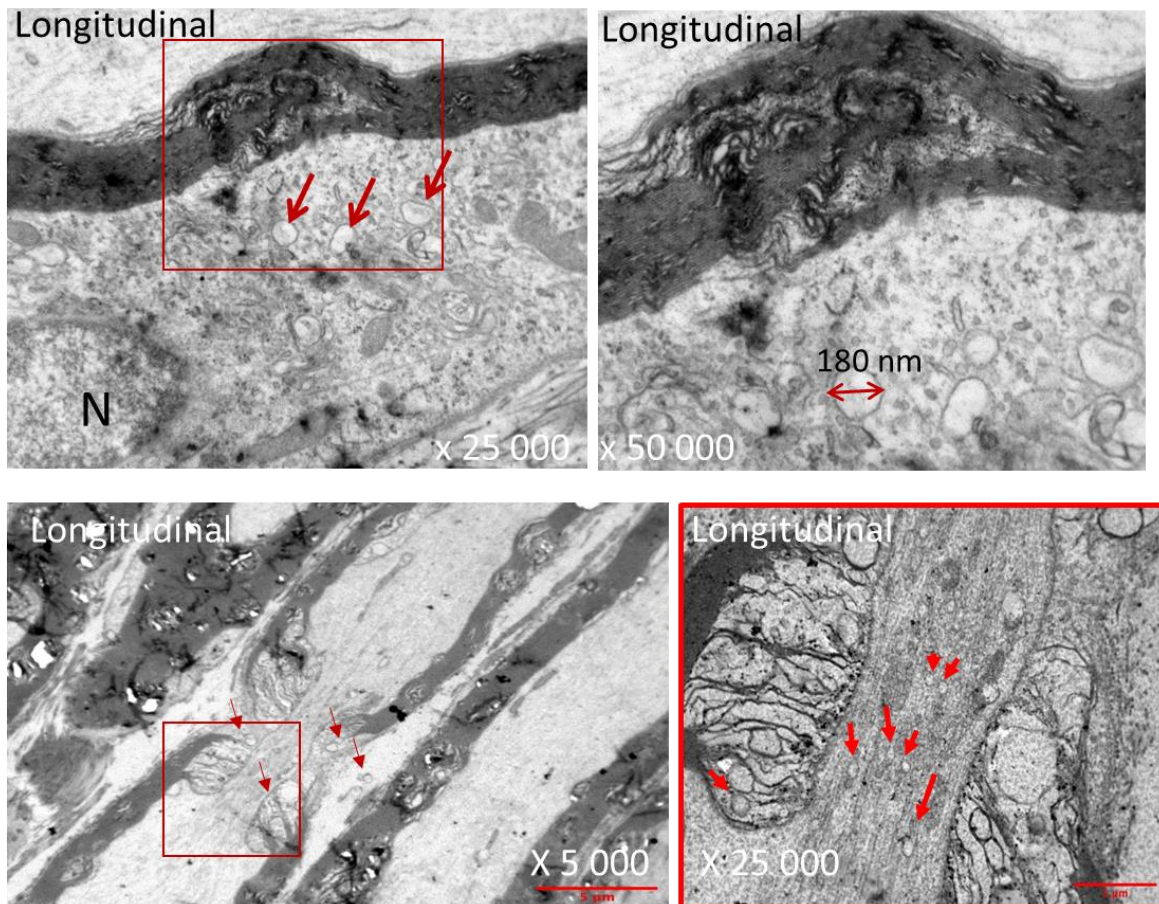


Figure 34. TEM micrographs of ultrathin section of sciatic nerves from single transgenic JP18 mice. TOP: represent TEM micrographs on longitudinal sections of JP18 siPMP22-SQ NPs at low and higher magnifications respectively. The nanoparticles are localized in the cytoplasm of Schwann cells, N = Nucleus. Down represent a low and higher magnifications focus of the Ranvier node. The nanoparticles can enter the nerve via the Ranvier nodes. The red square represents the part of the micrograph that was observed at higher magnification.

DISCUSSION

Charcot Marie Tooth Disease (CMT) is the most frequent inherited neuropathy worldwide where 1 in 2500 people is affected. It is also known as "sensory and motor peripheral neuropathy" to distinguish it from Charcot's disease or amyotrophic lateral sclerosis (ALS). Since its discovery in the 19th century, no drug has been marketed to cure or relieve the symptoms of the disease. The only treatments are based on preventive measures, which are limited to physiotherapy, prosthetics and orthopedic surgery, which can provide relief and maintenance of walking, but do not stop the progression of the disease [224]. Moreover, several drug strategies were studied to find a treatment for CMT1A patients. These strategies focused on different pathways upstream PMP22 genes most importantly cAMP pathway. Hence, a range of drugs was tested. Some gave positive results *in vitro* and *in vivo* but when reached clinical trials failed to prove their beneficial effect on patients. Recently, PXT3003 showed positive results on the CMT1A neuropathy scores in patients but it cannot be considered the most reliable drug. The high dose arm of PXT3003 was stopped in phase III clinical trials due to formulation problems according to Pharnext press release in august. Thus, a new clinical trial will be conducted where the FDA is going to review the study design and it will take few years to have definitive results. Hence, the lack of effective treatment for CMT1A disease has prompted us to work on developing a new therapeutic approach based on RNA interference. Our goal is to develop a targeted therapy that aims to normalize the expression of the PMP22 protein by a small interfering RNA (siRNA).

During the first step of this project, we designed eight different siRNAs against PMP22 using a blast and the siRNAs were given a score according to Tafer and Reynold methods[218]. The eight siRNAs were tested *in vitro* in an immortalized Schwann cell model MSC-80 [225]. The siRNA that best met our inclusion criteria (inhibition between 30% and 50% of PMP22 expression, no effect on P0 expression) was retained. The aim here was not to strongly inhibit the expression of PMP22 but to normalize it. An Inhibition of greater than 70% of PMP22 gene would be responsible for the development of tomacular neuropathy or HNPP, which is a rare condition due to a deletion (17p12) [29]. At the level of P0 gene which ensures cohesion between the spiral turns of the plasma membrane of Schwann cells during myelin formation, an increase in its expression would be responsible for the development of CMT1B [40]. Then, the optimal dose of the selected siRNA PMP22 was determined in *vitro* by real-time PCR after extraction of mRNA and MTT test that was used to study the effects on cell viability. siPMP22 of 50 nM had the best inhibitory effect of 50 % on siPMP22 gene.. Importantly, 50nM

concentration had no significant effect on P0 and MSC 80 cell viability. **Accordingly, siPMP22 of 50 nM was further used for *in vivo* studies.** *In vitro*, our study design is comparable to that performed by lee *et al.*, where they designed several siRNA PMP22 L16P that specifically target the mutation in the trembler J mice and tested them in a Schwann cell model where they introduced the mutation. After that, they were able to choose one siRNA called mTr11 and tested *in vivo* on the preferable concentration [128].

siRNAs have several advantages as they are natural mechanism of gene inhibition, active at low concentration and highly specific, but once they are used *in vivo* several hurdles face them. These limitations includes short plasmatic half-life time [152] due to degradation by systematic endonucleases [153], hydrophilic which make it hard for siRNAs to penetrate the cells [156] and show off-target effect when used at high concentration [154]. Taken together, siRNA cannot be injected directly *in vivo* as they will be directly degraded by endonucleases or eliminated by the kidney. Therefore, a delivery system is required for safe administration of siRNA. In our laboratory, our work focuses on developing a non-viral method for delivery of siRNA in which we used a safe and biodegradable molecule called squalene. This method of delivery was proven efficient in down regulating fusion oncogene in prostate [123] and papillary carcinoma [124]. Recently, we were able to develop a new method to bioconjugate siRNA to squalene by click chemistry, the yield of the reaction was high of around 90-95% and the nanoparticles produced were stable, efficient and preserved the inhibitory effect of the siRNA [211]. Therefore, the click chemistry method was used in this project to produce the siRNA PMP22-SQ and siRNA Ct-SQ NPs.

Characterization studies of both siPMP22-SQ and siRNA Ct-SQ bioconjugates showed that our nanoparticles were stable over the period of one month at 4 °C while when incubated with FBS solution to mimic the serum concentration of blood the siRNA-SQ NPs were stable up to 4 h before degradation at 37°C. The siRNA-SQ NPs became more hydrophilic and their size ranges between 180 nm for siPMP22-SQ NP and 240 nm for siRNA Ct-SQ NPs. These results matches previous results obtained by Massaad-Massade *et al.*, 2018 for siRNA Tmprss2-ERG- SQ and siRNA RET/PTC1-SQ NPs with a size of 250 nm, stable with time and efficient both *in vitro* and *in vivo*. In addition, they were able to show antineoplastic activity [211]. Moreover, the inhibitory effect of siPMP22-SQ NPs on PMP22 gene expression was sustained and showed 50 % down regulation of PMP22 gene similar to the naked siPMP22. Furthermore, siPMP22-SQ NPs had no effect on P0 gene expression and cell viability. Interestingly, siRNA Ct-SQ NPs showed no effect on PMP22 and P0 gene expression as well as on cell viability which proves that the modification that was done on the sense strand of the

siRNA had no effect on the gene expression. In fact, chemical modifications of the siRNA improve their stability and performance [144]. Therefore, the synthesized siPMP22-SQ NPs were active *in vitro* and their size was more than 50 kDa. Molecules with a size greater than 50kDa are less likely to be eliminated by the kidney [156] this proves that our NPs can stay a longer period in the blood stream and thus reach the estimated organ. In addition, the bioconjugation of siRNA to SQ did not generate any toxicity, as it showed no effect on MSC-80 cell viability. One of the most important properties of the siRNA delivery material is not to induce systematic toxicity and trigger the immune system [156]. In fact, squalene is a natural product that is extensively studied for its biological role as antioxidant, antitumor and cryoprotector [195]. Squalene is used also for skin care [204] and as a delivery material of drugs such as morphine and gemcitabine by either emulsion or conjugation [194, 195].

After checking that our nanoparticles are active *in vitro* and gave a preferable inhibition of 50 % on PMP22 gene expression. We tested siPMP22-SQ NPs on two CMT1A mouse models JP18 B6 and JP18/JY13 B6. These two mouse models are tetracycline conditional i.e. when these mice are fed tetracycline they do not develop CMT1A pathology while if they were kept without tetracycline the phenotypes of CMT1A disease appears throughout their life span. The JP18 B6 mouse model is single transgenic model that carry a copy of the mouse PMP22 cDNA under the control of the PhCMV*.1 promotor [78]. This model shows a moderate phenotype of CMT1A pathology. JP18/JY13 B6 is a double transgenic mouse model generated in our laboratory from two animal models the JP18 and JY13 on B6 background. The JY13 B6 model as mentioned by Perea *et al.*, carries the human PMP22 gene [78] . Hence, the double transgenic mouse model carries both the PMP22cDNA and the human PMP22 gene. Thus shows a slightly more severe CMT1A phenotype than JP18B6 mice. If we compare the JP18 and JP18/JY13 to the C22 CMT1A mouse model that carry 7 copies of human PMP22 gene [76] and the rat model that carries 3 extra copies of PMP22[81], we can say that our mouse model show less severe phenotypes. In our mouse models demyelination starts at 16 weeks of age [78] while in C22 and rat model the phenotypic changes start at 5 and 6 weeks respectively and this takes place due to failure of myelination [226]. While in human, the disease phenotype is due to repeated cycles of demyelination and remyelination. Regarding the trembler J mice that has P16L mutation in PMP22 gene they start to show developmental abnormalities and demyelination at postnatal day 4 which is not the case in CMT1A patients [226]. We believe that the mice model used in our study is remarkably comparable to the CMT1A patient regarding the number of copies of the PMP22 genes. it's very important to use a mouse model with moderate increase of PMP22 levels because the effective siRNA must have an adequate

effect on PMP22 levels since our primary aim is to test the chosen siRNA in patient. Herein, it is important to highlight the penetrance phenomenon where the individual harboring the disease genotype may exhibit severe, moderate or no signs of the disease. This phenomenon is due to the variety of different genetic and environmental factors [227]. This explains the heterogeneity of CMT disease and our choice of two mouse models of different disease severity.

The dose of the siPMP22-SQ NPs of 2.5 mg/kg was calculated based on the *in vitro* studies done on MSC-80 cells where the 50 nM concentration gave the best results and on previous studies done in our lab on prostate and thyroid carcinoma [123, 124, 211]. The schedule of treatment was also chosen based on previous data from our research on cancer models. In this project, we wanted to apply our expertise in cancer and siRNA fields on a hereditary neuropathy.

The motor function of the CMT1A single and double transgenic mice was first to be assessed. **Interestingly, the mice treated with siPMP22-SQ NPs showed restoration and normalization of the motor activity in both single and double transgenic models.** In addition, the neuromuscular strength assessed by the grip strength test was normalized on both the fore limbs and the hind limbs of the treated siPMP22-SQ mice group of the single transgenic model and the hind limbs of the double transgenic model. **Thus, in a duration of 21 days and at a cumulative dose of 2.5 mg/kg siPMP22 SQ NPs were able to show a normalization effect on the motor and muscular activity of moderate and severe models of CMT1A.** Importantly the siRNA CT-SQ showed no effect on the motor and muscular activity of the mice. Lee *et al.*, in the Trembler J mouse model that has a mutation in the PMP22 gene showed slight restoration in the muscular activity of the mice after 21 days of siRNA PMP22-L16P treatment. Treatment was started at postnatal age P6 and mice were given 5 intraperitoneal injections of 10µg per mouse [128]. Zhoa et al., in their study where they injected ASO subcutaneously on C22 severe CMT1A model at the age of 5 weeks showed regulation of the motor coordination and muscular strength only in the group treated with a high dose of 100mg/kg per week. The effect on the motor coordination started to appear after 3 weeks of treatment while it was lost after 9 weeks whereas the muscular strength was significantly increased after 9 weeks [132]. Taken together siPMP22-SQ NPs showed better results on the motor coordination and muscular strength than ASO and siRNA PMP22-L16P. In the ASO study, the dose of the ASO is very high compared to siPMP22-SQ NPs so may be what is documented is the off-target effect of ASO. It is necessary to note that the mechanism of action of ASO is different from that of siRNA. In the cells, ASO utilize the RNase H1

nuclease enzyme to initiate RNA degradation [131] while siRNA bind to argonaute 2 protein thus forming the activated RISC complex that direct the cleavage of the complementary mRNA [115].

Further electrophysiological analysis was performed to study abnormal myelination. In fact, the NCV of CMT1A patients is slow (NCV < 38m/s) [13]. The CMAP correlates with the number of fibers that are stimulated during performance of MNCV test [132]. Therefore, CMAP and SNCV were assessed in the single and double transgenic mice and it was notably found that they were affected in both mouse models and upon treatment with siPMP22-SQ NPs these two **electrophysiological end points were restored**. It was noted by Perea *et al.*, that the NCV of double transgenic mice was slower than that of the wild type littermate [78]. In comparison to the studies done on trembler J mice and the C22 severe mouse strain where siRNA PMP22-L16P and ASO were used respectively, an improvement in the electrophysiological ends point were recorded [128, 132]. Interestingly this improvement never reached the WT levels as for the case of siPMP22-SQ NPs. Taken together this proves that a recovery from the pathology can take place using siRNA PMP22-SQ NPs.

One of the pathological characteristics of CMT1A is the presence of demyelinating axons and onion bulbs [13]. Therefore, the structure and integrity of the sciatic nerves of both strains were studied. Preliminary histological analysis was done on electromyograms to assess the quality of the myelin around the axons. Dysregulation of the myelin sheath was observed in both the JP18 and JP18/JY13 and this was rearranged upon treatment with siPMP22-SQ NPs. One of the important roles of PMP22 gene is to regulate the tight junctions and transmembrane adhesions [228] thus any irregularity of PMP22 gene can leads to myelin disruption and this is the case in JP18 and JP18/JY13 mouse model. **Interestingly treatment with siPMP22-SQ NPs regulated this myelin disruption due to normalization of PMP22 expression (data not shown)**. Hence, our results are consistent with Perea *et al.*, who indicated in their study, that histological analysis on double transgenic mice JP18/JY13 mice of 16 weeks age showed that there is demyelination in 26 % of the fibers and upon treatment with tetracycline re-myelination occurred [78].

Since CMT1A is a demyelinating neuropathy, we further studied the expression of two transcriptional factors SOX 10 and KROX 20 that are necessary for proper myelination. Both factors helps to differentiate between mature and immature Schwann cells [1]. In fact, KROX 20 is important for the transition of Schwann cell from the pro-myelinating form to the myelinating form and in case of its absence, myelination does not occur. Furthermore mutations in KROX 20 can lead to CMT1 [229]. We found that in both JP18 and JP18/JY13

mice models there is a decrease in the level of both transcriptional factors i.e. myelination is affected. Myelination was restored upon treatment with siPMP22-SQ NPs. As the number of Schwann cells expressing KROX 20 reached normal levels. Also, to check if the axons are affected in the JP18 and JP18/JY13 mice, neurofilament, which is an axonal regeneration protein that give the cells their shape and determine axonal caliber [26], was examined. It was reported that in both mice model neurofilament level was decreased. This was enhanced upon treatment with siPMP22-SQ NPs. Low levels of neurofilament protein can lead to defects in the axon caliber that further affects myelination and decrease the nerve conduction velocity [26]. **Interestingly, siPMP22-SQ NPs can ameliorate myelination and axonal regeneration factors through inhibition of PMP22 in Schwann cells.**

Since other types of drugs were tested on CMT1A mouse and rat models a table was created to compare the results of siPMP22-SQ NPs to these drugs. **Table 7** summarizes the animal model models used for each treatment, dose, duration of treatment and the most significant results.

Table 7. Comparison of siPMP22-SQ NP to other CMT1A tested drugs

Treatment	Dose	Administration route and Duration of treatment	Animal model	PMP22 expression	Locomotor and Muscular strength	Electrophysiological effect	Myelin structure
<i>siPMP22-SQ NPS</i>	<i>2,5mg/kg (Cumulative dose)</i>	<i>retro-orbital twice weekly for 2,5 weeks</i>	<i>JP18B6 & JP18/JY13 B6</i>	<i>Normalization of protein level</i>	<i>normalization of motor and muscular strength</i>	<i>CMAP and NCV significant normalization</i>	<i>Rearrangement of the myelin sheath</i>
ASO (Zhoa et al., 2018)	25 mg/Kg, 50 mg/Kg & 100 mg/Kg	S.C. once per week for 9 weeks	C22 mouse model CMT1A rat model	35% inhibition of PMP22 mRNA expression at the high dose	Significant improvement on the muscular strength while. Loss of effect after 9 weeks at the high dose arm	slight improvement on the CMAP at the high dose while significant increase on the MNCV at all doses	reduction in the unmyelinated axons after 9 weeks of high dose
siRNA pmp22-L16P (Lee et al., 2017)	2,5mg/Kg (cumulative dose)	<i>i.p. twice per week for 2 weeks</i>	Tr-J mice (postnatal day 6)	Significant decrease in Pmp22-L16P mRNA level but no effect on protein levels	Slightly significant increase in the muscular strength	Slight increase in MNCV and CMAP	Enhanced myelination
PXT3003 (Chumakov et al., 2014)	Baclofen 30 µg/kg , Naltrexone 3.5 µg/kg and D-sorbitol 1.05 mg/kg	oral gavage Once daily for 9 weeks	CMT1A rat model	5% decrease of PMP22 gene expression	Reduce motor and sensory signs of neuropathy	5% increase in MNCV	Slight improvement
PXT 3003 is now in phase III clinical trial but the high dose arm was stopped due to precipitation of the formulation							

Table 7 continued. Comparison of siPMP22-SQ NP to other CMT1A tested drugs

Ascorbic acid (Passage et al., 2004)	57 mg/Kg	Force feeding once per week for 3 month	C22 mice	10 folds decrease in comparison to non-treated mice	Improved locomotion	Not performed	increase in the myelinated axons
<i>Ascorbic acid Reached clinical Trial but failed to show the same effect in CMT1A Patients</i>							
Onapristone (Sereda et al., 2003)	20mg/Kg	Daily S.C. 7 weeks	CMT1A Rats (P7)	19% decrease in mRNA expression	Improved motor performance	Not performed	Significant increase in the # of axons
<i>Onapristone caused liver toxicity in clinical trials so it was not tested in CMT1A patients</i>							
AAV1.NT3 (Sahenk et al., 2014)	1*10 ¹¹	<i>i.m.</i> One injection followed by nerve crush. Follow up:20 and 40 weeks post injection	Tr-J mice	Not tested	Improved performance	50% increase in CMAP	Increase in the myelin thickness in the uncrushed nerve

Notably, in this project we also found that the **curable dose of the siPMP22-SQ NPs is 1.5mg/kg** since this dose showed normalization of the motor and muscular activity of the CMT1A mice in the long lasting follow-up study. In addition, it can be noted that **long lasting effect of the siPMP22-SQ NPs is between two to three weeks** after the end of the treatment. Remarkably, there was **no resistance of the treatment** after initiation of the second cycle of siPMP22-SQ NPs treatment to double transgenic mice. This result can be taken as the base for the transition from the preclinical to the clinical phase of the project where a dose of 1.5mg/kg can be tested on human each 3 weeks. In fact, ONPATRO, which is the first FDA approved siRNA for use in human, is effective at a dose of 0.3 mg/kg every three weeks [127]. In CMT the dose will be higher because of the difference in the destination of the targeted organ since siPMP22-SQ NPs target Schwann cells in PNS while ONPATRO target liver cells. It is widely known that siRNA NPs reach in high quantities liver and kidney tissues [167].

The most remarkable finding of this project is the detection of siRNA-SQ NPs in Schwann cells and along the axons of mice treated with either siPMP22-SQ NPs or siRNA Ct-SQ NPs. The vesicles had one lipid layer with a size ranging between **100 nm to 250 nm same as the size of the siRNA-SQ NPs.** It can be easily differentiated from the mitochondria where the crescent interior can be seen. This proves that siRNA-SQ NPs can reach the peripheral nervous system and exert their effect even when injected at a low concentration of 2.5mg/kg. Since the highest concentration of siRNA-SQ NPs was detected around the area of nodes of Ranvier, we hypothesize that after *i.v.* injection of the siRNA-SQ NPs they will react

with low density lipoprotein molecules present in the blood stream. After that they will be transported to the sciatic nerve region where they can pass through the node of Ranvier to the axons and then reach Schwann cells or circulating between. **Figure 35** shows hypothetical representation of the siRNA PMP22-SQ NPs delivery to the sciatic nerve region which could be in accordance with Sobot *et al.* [230].

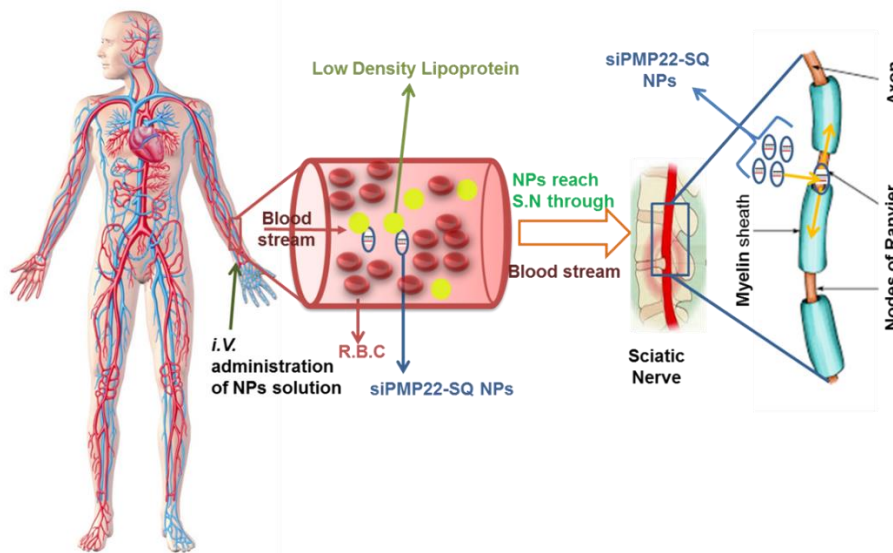


Figure 35. Hypothetical representation of the transport of siPMP22-SQ NPs through the blood stream to reach the sciatic nerve where they enter Schwann cells through the Nodes of Ranvier.

In fact, in their study found that SQ nanoparticles can be transported in the human blood by interacting with Low density lipoproteins (LDL) and accumulate in cancer cells that express high percentage of LDL receptors [230]. To improve this hypothesis, the siRNA antisense strand can be linked to a fluorescent probe then localization and interaction with LDL receptor will be assessed by fluorescent microscopy.

Our study is the first to use siRNA mechanism to downregulate PMP22 gene expression in CMT1A disease. The dose and duration of the treatment was small compared to the study done by Zhoa *et al.*, where they used ASO at a 100mg/kg dose for 9 month. On the other hand, the study done on trembler J mice is for a point mutation in PMP22 and the treatment was started at postnatal age 6 days so it was more used as protection not as a cure. Hence, we are confident that our results are unique and we are the first to show normalization of PMP22 gene expression. Our siPMP22-NPs can be used as a treatment for CMT1A disease were they showed positive result and give proof that a recovery from CMT1A pathology can take place. Finally, all the results are registered in European patent n°18306241.3, September 2018 and under international patent extension since September 2019.

CONCLUSIONS

In this project, we were able to meet our primary goal, which is to find a curable therapy for CMT1A patients. We hope that siPMP22-SQ NPs can progress further on to prove its safety and tolerability *in vivo* and in clinical trials. All the efforts are gathered to go on with this project and carry it to higher levels.

Firstly, we chose one siRNA out of the eight tested siRNAs. This siRNA PMP22 was able to inhibit PMP22 gene expression by 50 %, has no effect on P0 gene expression and no effect on the viability of cells. Secondly, we used the squalenoylation method to synthesize siRNA PMP22- SQ bioconjugate where the reaction yield was around 90-95 %. The siRNA PMP22-SQ or siRNA Ct-SQ bioconjugate was later precipitated to form nanoparticles. The siRNA-SQ NPs produced were active and stable over time. Their size was of injectable diameter and they become more lipophilic after conjugation with squalene. Most importantly, the activity of the siRNA was not affected due to the modification done on the sense strand of the siRNA or squalene.

Thirdly, siRNA PMP2-SQ NPs once injected *in vivo* can improve the end point of CMT1A neuropathy. They normalized the motor and the muscular activity of CMT1A mouse models of moderate and severe phenotypes. siRNA PMP22-SQ NPs restored the CMAP and NCV of both mice models and improve myelination and axonal regeneration factors. Fourthly, it was found that the long lasting effect of siPMP22-SQ NPs is between two to three weeks after the last injection and if the treatment is re-initiated, the mice do not develop any resistance for the therapy.

Finally, siRNA-SQ NPs can reach the peripheral nervous system and this opens a new field of study where siRNAs can be used to treat other inherited neuropathies. We hope that we can extract our expertise from this project and apply it on other inherited neuropathies in the future.

PROSPECTIVE

Our work in this project focuses on developing a new therapy for CMT1A disease based on siRNA technology. Therefore, based on our primary results we were able to provide the proof of concept that a recovery from the pathology can take place using siPMP22-SQ NPs. Hence, our future goal is to do a series of experiments where we define the optimal dose and toxicity of the siPMP22-SQ NPs before going to phase I clinical trial. For this purpose, a maturation project will be done to continue the work.

To obtain the optimal dose several concentrations of siPMP22-SQ NPs are going to be tested in CMT1A mouse models (JP18 B6 and JP18/JY13 B6). Behavioral tests including beam walking, Locotronic, Rota Rod and Grip strength tests will be performed on weekly bases to study the motor and muscular activity of the mice. Sciatic nerves will be collected at each end point where molecular and histological studies will be done to check myelination. In addition, electrophysiological analysis will be performed at the beginning and end of each treatment schedule.

Moreover, Pharmacokinetics and biodistribution study will be done to analyze the delivery of the siRNA-SQ NPs to the sciatic nerve. Furthermore, to study the toxicity of siRNA-SQ NPs *in vivo* blood samples and different organs including the liver, heart, lungs and kidneys will be collected. Several proteins and enzyme levels will be measured to determine the end points of toxicity such as Troponin, Creatinine, Albumin, SGPT and SGOT.

Lastly, we will try to synthesis the siRNA-SQ NPs on a large scale followed by characterization studies to check the size, stability and lipophilicity of the NPs. Taken together, all these studies will help to determine the dose and duration of treatment in case we succeeded to go for a phase I clinical trial.

In case of toxicity due to high quantities of squalene we will do another vectorization method for our siRNA PMP22 followed by several characterization steps. *In vivo* studies will be later performed to check that results of the new formulation followed by toxicity tests.

REFERENCES

1. Bhatheja, K. and J. Field, *Schwann cells: origins and role in axonal maintenance and regeneration*. Int J Biochem Cell Biol, 2006. **38**(12): p. 1995-9.
2. Schmitt, S., L.C. Castelvetti, and M. Simons, *Metabolism and functions of lipids in myelin*. Biochim Biophys Acta, 2015. **1851**(8): p. 999-1005.
3. Garbay, B., et al., *Myelin synthesis in the peripheral nervous system*. Prog Neurobiol, 2000. **61**(3): p. 267-304.
4. Nave, K.A., *Myelination and the trophic support of long axons*. Nat Rev Neurosci, 2010. **11**(4): p. 275-83.
5. Beirowski, B., et al., *Metabolic regulator LKB1 is crucial for Schwann cell-mediated axon maintenance*. Nat Neurosci, 2014. **17**(10): p. 1351-61.
6. Jessen, K.R. and R. Mirsky, *The origin and development of glial cells in peripheral nerves*. Nat Rev Neurosci, 2005. **6**(9): p. 671-82.
7. Topilko, P., et al., *Krox-20 controls myelination in the peripheral nervous system*. Nature, 1994. **371**(6500): p. 796-9.
8. Kuhlbrodt, K., et al., *Sox10, a novel transcriptional modulator in glial cells*. J Neurosci, 1998. **18**(1): p. 237-50.
9. Inoue, K., Y. Tanabe, and J.R. Lupski, *Myelin deficiencies in both the central and the peripheral nervous systems associated with a SOX10 mutation*. Ann Neurol, 1999. **46**(3): p. 313-8.
10. Melcangi, R.C., et al., *Age-induced decrease of glycoprotein Po and myelin basic protein gene expression in the rat sciatic nerve. Repair by steroid derivatives*. Neuroscience, 1998. **85**(2): p. 569-78.
11. Desarnaud, F., et al., *Progesterone stimulates the activity of the promoters of peripheral myelin protein-22 and protein zero genes in Schwann cells*. J Neurochem, 1998. **71**(4): p. 1765-8.
12. Hirakawa, H., et al., *Loss and recovery of the blood-nerve barrier in the rat sciatic nerve after crush injury are associated with expression of intercellular junctional proteins*. Experimental Cell Research, 2003. **284**(2): p. 194-208.
13. Perveen, S., et al., *Charcot-Marie-Tooth type 1A disease from patient to laboratory*. J Pak Med Assoc, 2015. **65**(2): p. 206-12.
14. Willison, H.J., B.C. Jacobs, and P.A. van Doorn, *Guillain-Barré syndrome*. The Lancet, 2016. **388**(10045): p. 717-727.
15. Bright, R.J., J. Wilkinson, and B.J. Coventry, *Therapeutic options for chronic inflammatory demyelinating polyradiculoneuropathy: a systematic review*. BMC Neurol, 2014. **14**: p. 26.
16. Tapinos, N. and A. Rambukkana, *Insights into regulation of human Schwann cell proliferation by Erk1/2 via a MEK-independent and p56Lck-dependent pathway from leprosy bacilli*. Proc Natl Acad Sci U S A, 2005. **102**(26): p. 9188-93.
17. Jerath, N.U. and M.E. Shy, *Hereditary motor and sensory neuropathies: Understanding molecular pathogenesis could lead to future treatment strategies*. Biochim Biophys Acta, 2015. **1852**(4): p. 667-78.
18. Timmerman, V., A.V. Strickland, and S. Zuchner, *Genetics of Charcot-Marie-Tooth (CMT) Disease within the Frame of the Human Genome Project Success*. Genes (Basel), 2014. **5**(1): p. 13-32.
19. Barreto, L.C., et al., *Epidemiologic Study of Charcot-Marie-Tooth Disease: A Systematic Review*. Neuroepidemiology, 2016. **46**(3): p. 157-65.
20. Skre, H., *Genetic and clinical aspects of Charcot-Marie-Tooth's disease*. Clin Genet, 1974. **6**(2): p. 98-118.
21. Martyn, C.N. and R.A. Hughes, *Epidemiology of peripheral neuropathy*. J Neurol Neurosurg Psychiatry, 1997. **62**(4): p. 310-8.

22. Theadom, A., et al., *Prevalence of Charcot-Marie-Tooth disease across the lifespan: a population-based epidemiological study*. *BMJ Open*, 2019. **9**(6): p. e029240.
23. Pareyson, D., C. Marchesi, and E. Salsano, *Hereditary predominantly motor neuropathies*. *Curr Opin Neurol*, 2009. **22**(5): p. 451-9.
24. Echaniz-Laguna, A., *The shifting paradigm of Charcot-Marie-Tooth disease*. *Rev Neurol (Paris)*, 2015. **171**(6-7): p. 498-504.
25. Snipes, G.J., et al., *Characterization of a novel peripheral nervous system myelin protein (PMP-22/SR13)*. *J Cell Biol*, 1992. **117**(1): p. 225-38.
26. Didonna, A. and P. Opal, *The role of neurofilament aggregation in neurodegeneration: lessons from rare inherited neurological disorders*. *Mol Neurodegener*, 2019. **14**(1): p. 19.
27. Manfioletti, G., et al., *A growth arrest-specific (gas) gene codes for a membrane protein*. *Mol Cell Biol*, 1990. **10**(6): p. 2924-30.
28. Patel, C.V., et al., *Molecular cloning of a homeobox transcription factor from adult aortic smooth muscle*. *J Biol Chem*, 1992. **267**(36): p. 26085-90.
29. Chanson, J.B., et al., *Central nervous system abnormalities in patients with PMP22 gene mutations: a prospective study*. *J Neurol Neurosurg Psychiatry*, 2013. **84**(4): p. 392-7.
30. Suter, U., et al., *Regulation of tissue-specific expression of alternative peripheral myelin protein-22 (PMP22) gene transcripts by two promoters*. *J Biol Chem*, 1994. **269**(41): p. 25795-808.
31. Hai, M., S.I. Bidichandani, and P.I. Patel, *Identification of a positive regulatory element in the myelin-specific promoter of the PMP22 gene*. *J Neurosci Res*, 2001. **65**(6): p. 508-19.
32. Wistow, G., *Lens crystallins: gene recruitment and evolutionary dynamism*. *Trends Biochem Sci*, 1993. **18**(8): p. 301-6.
33. Ward, C.L. and R.R. Kopito, *Intracellular turnover of cystic fibrosis transmembrane conductance regulator. Inefficient processing and rapid degradation of wild-type and mutant proteins*. *J Biol Chem*, 1994. **269**(41): p. 25710-8.
34. Suter, U. and G.J. Snipes, *Peripheral myelin protein 22: facts and hypotheses*. *J Neurosci Res*, 1995. **40**(2): p. 145-51.
35. Brancolini, C., et al., *Rho-dependent regulation of cell spreading by the tetraspan membrane protein Gas3/PMP22*. *Mol Biol Cell*, 1999. **10**(7): p. 2441-59.
36. Zoidl, G., et al., *Retroviral-mediated gene transfer of the peripheral myelin protein PMP22 in Schwann cells: modulation of cell growth*. *Embo j*, 1995. **14**(6): p. 1122-8.
37. Rao, R.G., et al., *Peripheral myelin protein-22 (PMP22) modulates alpha 6 integrin expression in the human endometrium*. *Reprod Biol Endocrinol*, 2011. **9**: p. 56.
38. Quarles, R.H., R.G. Farrer, and S.H. Yim, *Structure and Function of Myelin, an Extended and Biochemically Modified Cell Surface Membrane*, in *Cell Biology and Pathology of Myelin: Evolving Biological Concepts and Therapeutic Approaches*, B.H.J. Juurlink, et al., Editors. 1997, Springer US: Boston, MA. p. 1-12.
39. Eichberg, J. and S. Iyer, *Phosphorylation of myelin protein: recent advances*. *Neurochem Res*, 1996. **21**(4): p. 527-35.
40. Shy, M.E., *Charcot-Marie-Tooth disease: an update*. *Curr Opin Neurol*, 2004. **17**(5): p. 579-85.
41. Xu, W., et al., *Mutations in the cytoplasmic domain of P0 reveal a role for PKC-mediated phosphorylation in adhesion and myelination*. *J Cell Biol*, 2001. **155**(3): p. 439-46.
42. Giese, K.P., et al., *Mouse P0 gene disruption leads to hypomyelination, abnormal expression of recognition molecules, and degeneration of myelin and axons*. *Cell*, 1992. **71**(4): p. 565-76.
43. Mandich, P., et al., *Congenital hypomyelination due to myelin protein zero Q215X mutation*. *Ann Neurol*, 1999. **45**(5): p. 676-8.
44. Menichella, D.M., et al., *Protein zero is necessary for E-cadherin-mediated adherens junction formation in Schwann cells*. *Mol Cell Neurosci*, 2001. **18**(6): p. 606-18.
45. Kleopa, K.A. and S.S. Scherer, *Molecular genetics of X-linked Charcot-Marie-Tooth disease*. *NeuroMolecular Medicine*, 2006. **8**(1-2): p. 107-122.

46. Cisterna, B.A., P. Arroyo, and C. Puebla, *Role of Connexin-Based Gap Junction Channels in Communication of Myelin Sheath in Schwann Cells*. Front Cell Neurosci, 2019. **13**: p. 69.
47. Saez, J.C., et al., *Plasma membrane channels formed by connexins: their regulation and functions*. Physiol Rev, 2003. **83**(4): p. 1359-400.
48. Sosinsky, G.E., *Molecular organization of gap junction membrane channels*. J Bioenerg Biomembr, 1996. **28**(4): p. 297-309.
49. Scherer, S.S., et al., *Connexin32 is a myelin-related protein in the PNS and CNS*. J Neurosci, 1995. **15**(12): p. 8281-94.
50. Meier, C., et al., *Connexin32-containing gap junctions in Schwann cells at the internodal zone of partial myelin compaction and in Schmidt-Lanterman incisures*. J Neurosci, 2004. **24**(13): p. 3186-98.
51. Abrams, C.K., et al., *Voltage opens unopposed gap junction hemichannels formed by a connexin 32 mutant associated with X-linked Charcot-Marie-Tooth disease*. Proc Natl Acad Sci U S A, 2002. **99**(6): p. 3980-4.
52. Kleopa, K.A., C.K. Abrams, and S.S. Scherer, *How do mutations in GJB1 cause X-linked Charcot-Marie-Tooth disease?* Brain Res, 2012. **1487**: p. 198-205.
53. Kulshrestha, R., et al., *Deletion of P2 promoter of GJB1 gene a cause of Charcot-Marie-Tooth disease*. Neuromuscul Disord, 2017. **27**(8): p. 766-770.
54. Anzini, P., et al., *Structural abnormalities and deficient maintenance of peripheral nerve myelin in mice lacking the gap junction protein connexin 32*. J Neurosci, 1997. **17**(12): p. 4545-51.
55. Scherer, S.S., et al., *Connexin32-null mice develop demyelinating peripheral neuropathy*. Glia, 1998. **24**(1): p. 8-20.
56. Bortolozzi, M., *What's the Function of Connexin 32 in the Peripheral Nervous System?* Front Mol Neurosci, 2018. **11**: p. 227.
57. Hales, K.G. and M.T. Fuller, *Developmentally regulated mitochondrial fusion mediated by a conserved, novel, predicted GTPase*. Cell, 1997. **90**(1): p. 121-9.
58. Chandhok, G., M. Lazarou, and B. Neumann, *Structure, function, and regulation of mitofusin-2 in health and disease*. Biol Rev Camb Philos Soc, 2018. **93**(2): p. 933-949.
59. Alexander, C., et al., *OPA1, encoding a dynamin-related GTPase, is mutated in autosomal dominant optic atrophy linked to chromosome 3q28*. Nat Genet, 2000. **26**(2): p. 211-5.
60. Bach, D., et al., *Mitofusin-2 determines mitochondrial network architecture and mitochondrial metabolism. A novel regulatory mechanism altered in obesity*. J Biol Chem, 2003. **278**(19): p. 17190-7.
61. Chen, H., A. Chomyn, and D.C. Chan, *Disruption of fusion results in mitochondrial heterogeneity and dysfunction*. J Biol Chem, 2005. **280**(28): p. 26185-92.
62. Pich, S., et al., *The Charcot-Marie-Tooth type 2A gene product, Mfn2, up-regulates fuel oxidation through expression of OXPHOS system*. Hum Mol Genet, 2005. **14**(11): p. 1405-15.
63. Zorzano, A., et al., *Alterations in the mitochondrial regulatory pathways constituted by the nuclear co-factors PGC-1alpha or PGC-1beta and mitofusin 2 in skeletal muscle in type 2 diabetes*. Biochim Biophys Acta, 2010. **1797**(6-7): p. 1028-33.
64. Szigeti, K. and J.R. Lupski, *Charcot-Marie-Tooth disease*. Eur J Hum Genet, 2009. **17**(6): p. 703-10.
65. Stuppia, G., et al., *MFN2-related neuropathies: Clinical features, molecular pathogenesis and therapeutic perspectives*. J Neurol Sci, 2015. **356**(1-2): p. 7-18.
66. Zuchner, S., et al., *Mutations in the mitochondrial GTPase mitofusin 2 cause Charcot-Marie-Tooth neuropathy type 2A*. Nat Genet, 2004. **36**(5): p. 449-51.
67. Feely, S.M., et al., *MFN2 mutations cause severe phenotypes in most patients with CMT2A*. Neurology, 2011. **76**(20): p. 1690-6.
68. Detmer, S.A. and D.C. Chan, *Complementation between mouse Mfn1 and Mfn2 protects mitochondrial fusion defects caused by CMT2A disease mutations*. J Cell Biol, 2007. **176**(4): p. 405-14.

69. Pareyson, D. and C. Marchesi, *Diagnosis, natural history, and management of Charcot-Marie-Tooth disease*. *Lancet Neurol*, 2009. **8**(7): p. 654-67.
70. Su, B., et al., *Abnormal mitochondrial dynamics and neurodegenerative diseases*. *Biochim Biophys Acta*, 2010. **1802**(1): p. 135-42.
71. Wang, H., et al., *Effects of overexpression of huntingtin proteins on mitochondrial integrity*. *Hum Mol Genet*, 2009. **18**(4): p. 737-52.
72. Wang, X., et al., *Impaired balance of mitochondrial fission and fusion in Alzheimer's disease*. *J Neurosci*, 2009. **29**(28): p. 9090-103.
73. Chen, K.H., et al., *Dysregulation of HSG triggers vascular proliferative disorders*. *Nat Cell Biol*, 2004. **6**(9): p. 872-83.
74. Sereda, M.W. and K.-A. Nave, *Animal models of Charcot-Marie-Tooth disease type 1A*. *NeuroMolecular Medicine*, 2006. **8**(1): p. 205-215.
75. Lee, J.H. and B.O. Choi, *Charcot-marie-tooth disease: seventeen causative genes*. *J Clin Neurol*, 2006. **2**(2): p. 92-106.
76. Huxley, C., et al., *Construction of a mouse model of Charcot-Marie-Tooth disease type 1A by pronuclear injection of human YAC DNA*. *Hum Mol Genet*, 1996. **5**(5): p. 563-9.
77. Magyar, J.P., et al., *Impaired differentiation of Schwann cells in transgenic mice with increased PMP22 gene dosage*. *J Neurosci*, 1996. **16**(17): p. 5351-60.
78. Perea, J., et al., *Induced myelination and demyelination in a conditional mouse model of Charcot-Marie-Tooth disease type 1A*. *Hum Mol Genet*, 2001. **10**(10): p. 1007-18.
79. Robertson, A., et al., *Effects of mouse strain, position of integration and tetracycline analogue on the tetracycline conditional system in transgenic mice*. *Gene*, 2002. **282**(1-2): p. 65-74.
80. Sereda, M.W., et al., *Therapeutic administration of progesterone antagonist in a model of Charcot-Marie-Tooth disease (CMT-1A)*. *Nat Med*, 2003. **9**(12): p. 1533-7.
81. Sereda, M., et al., *A transgenic rat model of Charcot-Marie-Tooth disease*. *Neuron*, 1996. **16**(5): p. 1049-60.
82. Fledrich, R., et al., *A rat model of Charcot-Marie-Tooth disease 1A recapitulates disease variability and supplies biomarkers of axonal loss in patients*. *Brain*, 2012. **135**(Pt 1): p. 72-87.
83. Schorling, E., et al., *Cost of illness in Charcot-Marie-Tooth neuropathy: Results from Germany*. *Neurology*, 2019. **92**(17): p. e2027-e2037.
84. Koenig, H.L., et al., *Progesterone synthesis and myelin formation by Schwann cells*. *Science*, 1995. **268**(5216): p. 1500-3.
85. Cottu, P.H., et al., *Phase I study of onapristone, a type I antiprogestin, in female patients with previously treated recurrent or metastatic progesterone receptor-expressing cancers*. *PLoS One*, 2018. **13**(10): p. e0204973.
86. Klein-Hitpass, L., et al., *Two types of antiprogestins identified by their differential action in transcriptionally active extracts from T47D cells*. *Nucleic Acids Res*, 1991. **19**(6): p. 1227-34.
87. Meyer zu Horste, G., et al., *Antiprogestone therapy uncouples axonal loss from demyelination in a transgenic rat model of CMT1A neuropathy*. *Ann Neurol*, 2007. **61**(1): p. 61-72.
88. Pareyson, D. and C. Marchesi, *Natural history and treatment of peripheral inherited neuropathies*. *Adv Exp Med Biol*, 2009. **652**: p. 207-24.
89. Liu, N., et al., *Depleting endogenous neurotrophin-3 enhances myelin formation in the Trembler-J mouse, a model of a peripheral neuropathy*. *J Neurosci Res*, 2007. **85**(13): p. 2863-9.
90. Chao, M.V., *Neurotrophins and their receptors: a convergence point for many signalling pathways*. *Nat Rev Neurosci*, 2003. **4**(4): p. 299-309.
91. Frostick, S.P., Q. Yin, and G.J. Kemp, *Schwann cells, neurotrophic factors, and peripheral nerve regeneration*. *Microsurgery*, 1998. **18**(7): p. 397-405.
92. Sahenk, Z., et al., *AAV1.NT-3 gene therapy for charcot-marie-tooth neuropathy*. *Mol Ther*, 2014. **22**(3): p. 511-521.

93. Sahenk, Z., et al., *NT-3 promotes nerve regeneration and sensory improvement in CMT1A mouse models and in patients*. *Neurology*, 2005. **65**(5): p. 681-9.
94. Liu, S., et al., *Combination of microsurgery and gene therapy for spinal dorsal root injury repair*. *Mol Ther*, 2009. **17**(6): p. 992-1002.
95. Wan, H., et al., *Combination of hypoglossal-facial nerve surgical reconstruction and neurotrophin-3 gene therapy for facial palsy*. *J Neurosurg*, 2013. **119**(3): p. 739-50.
96. Ballaz, S.J. and G.V. Rebec, *Neurobiology of vitamin C: Expanding the focus from antioxidant to endogenous neuromodulator*. *Pharmacol Res*, 2019. **146**: p. 104321.
97. Carey, D.J. and M.S. Todd, *Schwann cell myelination in a chemically defined medium: demonstration of a requirement for additives that promote Schwann cell extracellular matrix formation*. *Brain Res*, 1987. **429**(1): p. 95-102.
98. Eldridge, C.F., M.B. Bunge, and R.P. Bunge, *Differentiation of axon-related Schwann cells in vitro: II. Control of myelin formation by basal lamina*. *J Neurosci*, 1989. **9**(2): p. 625-38.
99. Olsen, C.L. and R.P. Bunge, *Requisites for growth and myelination of urodele sensory neurons in tissue culture*. *J Exp Zool*, 1986. **238**(3): p. 373-84.
100. Passage, E., et al., *Ascorbic acid treatment corrects the phenotype of a mouse model of Charcot-Marie-Tooth disease*. *Nat Med*, 2004. **10**(4): p. 396-401.
101. Kaya, F., et al., *Ascorbic acid inhibits PMP22 expression by reducing cAMP levels*. *Neuromuscul Disord*, 2007. **17**(3): p. 248-53.
102. Bordignon, B., et al., *A derivative of ascorbic acid modulates cAMP production*. *Biochem Biophys Res Commun*, 2013. **439**(1): p. 137-41.
103. Gess, B., et al., *Sodium-dependent vitamin C transporter 2 (SVCT2) is necessary for the uptake of L-ascorbic acid into Schwann cells*. *Glia*, 2010. **58**(3): p. 287-99.
104. Gess, B., et al., *Sodium-dependent vitamin C transporter 2 deficiency causes hypomyelination and extracellular matrix defects in the peripheral nervous system*. *J Neurosci*, 2011. **31**(47): p. 17180-92.
105. Shy, M.E., et al., *Neuropathy progression in Charcot-Marie-Tooth disease type 1A*. *Neurology*, 2008. **70**(5): p. 378-83.
106. Micallef, J., et al., *Effect of ascorbic acid in patients with Charcot-Marie-Tooth disease type 1A: a multicentre, randomised, double-blind, placebo-controlled trial*. *The Lancet Neurology*, 2009. **8**(12): p. 1103-1110.
107. Verhamme, C., et al., *Oral high dose ascorbic acid treatment for one year in young CMT1A patients: a randomised, double-blind, placebo-controlled phase II trial*. *BMC Med*, 2009. **7**: p. 70.
108. Pareyson, D., et al., *Ascorbic acid in Charcot-Marie-Tooth disease type 1A (CMT-TRIAAL and CMT-TRAUK): a double-blind randomised trial*. *The Lancet Neurology*, 2011. **10**(4): p. 320-328.
109. Chumakov, I., et al., *Polytherapy with a combination of three repurposed drugs (PXT3003) down-regulates Pmp22 over-expression and improves myelination, axonal and functional parameters in models of CMT1A neuropathy*. *Orphanet J Rare Dis*, 2014. **9**: p. 201.
110. Attarian, S., et al., *An exploratory randomised double-blind and placebo-controlled phase 2 study of a combination of baclofen, naltrexone and sorbitol (PXT3003) in patients with Charcot-Marie-Tooth disease type 1A*. *Orphanet J Rare Dis*, 2014. **9**: p. 199.
111. Mandel, J., et al., *A meta-analysis of randomized double-blind clinical trials in CMT1A to assess the change from baseline in CMTNS and ONLS scales after one year of treatment*. *Orphanet J Rare Dis*, 2015. **10**: p. 74.
112. Prukop, T., et al., *Early short-term PXT3003 combinational therapy delays disease onset in a transgenic rat model of Charcot-Marie-Tooth disease 1A (CMT1A)*. *PLoS One*, 2019. **14**(1): p. e0209752.
113. Juneja, M., et al., *Challenges in modelling the Charcot-Marie-Tooth neuropathies for therapy development*. *J Neurol Neurosurg Psychiatry*, 2019. **90**(1): p. 58-67.
114. Fire, A., et al., *Potent and specific genetic interference by double-stranded RNA in *Caenorhabditis elegans**. *Nature*, 1998. **391**(6669): p. 806-11.

115. Rao, D.D., et al., *siRNA vs. shRNA: similarities and differences*. *Adv Drug Deliv Rev*, 2009. **61**(9): p. 746-59.
116. Sledz, C.A. and B.R. Williams, *RNA interference in biology and disease*. *Blood*, 2005. **106**(3): p. 787-94.
117. Pare, J.M. and T.C. Hobman, *Dicer: Structure, Function And Role In RNA-Dependent Gene-Silencing Pathways*, in *Industrial Enzymes: Structure, Function and Applications*, J. Polaina and A.P. MacCabe, Editors. 2007, Springer Netherlands: Dordrecht. p. 421-438.
118. Saurabh, S., A.S. Vidyarthi, and D. Prasad, *RNA interference: concept to reality in crop improvement*. *Planta*, 2014. **239**(3): p. 543-64.
119. Zhou, Y., C. Zhang, and W. Liang, *Development of RNAi technology for targeted therapy--a track of siRNA based agents to RNAi therapeutics*. *J Control Release*, 2014. **193**: p. 270-81.
120. Ameres, S.L., J. Martinez, and R. Schroeder, *Molecular basis for target RNA recognition and cleavage by human RISC*. *Cell*, 2007. **130**(1): p. 101-12.
121. Forstemann, K., et al., *Drosophila microRNAs are sorted into functionally distinct argonaute complexes after production by dicer-1*. *Cell*, 2007. **130**(2): p. 287-97.
122. Ali, H.M., et al., *Significance and applications of nanoparticles in siRNA delivery for cancer therapy*. *Expert Rev Clin Pharmacol*, 2012. **5**(4): p. 403-12.
123. Urbinati, G., et al., *Antineoplastic Effects of siRNA against TMPRSS2-ERG Junction Oncogene in Prostate Cancer*. *PLoS One*, 2015. **10**(5): p. e0125277.
124. Ali, H.M., et al., *Effects of siRNA on RET/PTC3 junction oncogene in papillary thyroid carcinoma: from molecular and cellular studies to preclinical investigations*. *PLoS One*, 2014. **9**(4): p. e95964.
125. Butler, J.S., et al., *Preclinical evaluation of RNAi as a treatment for transthyretin-mediated amyloidosis*. *Amyloid*, 2016. **23**(2): p. 109-18.
126. Adams, D., et al., *Trial design and rationale for APOLLO, a Phase 3, placebo-controlled study of patisiran in patients with hereditary ATTR amyloidosis with polyneuropathy*. *BMC Neurol*, 2017. **17**(1): p. 181.
127. Adams, D., et al., *Patisiran, an RNAi Therapeutic, for Hereditary Transthyretin Amyloidosis*. *N Engl J Med*, 2018. **379**(1): p. 11-21.
128. Lee, J.S., et al., *Pmp22 mutant allele-specific siRNA alleviates demyelinating neuropathic phenotype in vivo*. *Neurobiol Dis*, 2017. **100**: p. 99-107.
129. Bennett, C.F. and E.E. Swayze, *RNA targeting therapeutics: molecular mechanisms of antisense oligonucleotides as a therapeutic platform*. *Annu Rev Pharmacol Toxicol*, 2010. **50**: p. 259-93.
130. Bennett, C.F., *Therapeutic Antisense Oligonucleotides Are Coming of Age*. *Annu Rev Med*, 2019. **70**: p. 307-321.
131. Bennett, C.F., et al., *Pharmacology of Antisense Drugs*. *Annu Rev Pharmacol Toxicol*, 2017. **57**: p. 81-105.
132. Zhao, H.T., et al., *PMP22 antisense oligonucleotides reverse Charcot-Marie-Tooth disease type 1A features in rodent models*. *J Clin Invest*, 2018. **128**(1): p. 359-368.
133. Frazier, K.S., *Antisense oligonucleotide therapies: the promise and the challenges from a toxicologic pathologist's perspective*. *Toxicol Pathol*, 2015. **43**(1): p. 78-89.
134. Fortun, J., et al., *The formation of peripheral myelin protein 22 aggregates is hindered by the enhancement of autophagy and expression of cytoplasmic chaperones*. *Neurobiol Dis*, 2007. **25**(2): p. 252-65.
135. Chittoor-Vinod, V.G., et al., *Inducible HSP70 is critical in preventing the aggregation and enhancing the processing of PMP22*. *ASN Neuro*, 2015. **7**(1).
136. Zhu, J., et al., *Ethoxyquin prevents chemotherapy-induced neurotoxicity via Hsp90 modulation*. *Ann Neurol*, 2013. **74**(6): p. 893-904.
137. Ekins, S., et al., *A brief review of recent Charcot-Marie-Tooth research and priorities*. *F1000Res*, 2015. **4**: p. 53.
138. Kohl, B., et al., *MCP-1/CCL2 modifies axon properties in a PMP22-overexpressing mouse model for Charcot-Marie-tooth 1A neuropathy*. *Am J Pathol*, 2010. **176**(3): p. 1390-9.

139. Kohl, B., et al., *Lack of evidence for a pathogenic role of T-lymphocytes in an animal model for Charcot-Marie-Tooth disease 1A*. *Neurobiology of Disease*, 2010. **38**(1): p. 78-84.
140. Jorgensen, R.A., et al., *Chalcone synthase cosuppression phenotypes in petunia flowers: comparison of sense vs. antisense constructs and single-copy vs. complex T-DNA sequences*. *Plant Mol Biol*, 1996. **31**(5): p. 957-73.
141. Elbashir, S.M., et al., *Analysis of gene function in somatic mammalian cells using small interfering RNAs*. *Methods*, 2002. **26**(2): p. 199-213.
142. McCaffrey, A.P., et al., *RNA interference in adult mice*. *Nature*, 2002. **418**(6893): p. 38-9.
143. Whelan, J., *First clinical data on RNAi*. *Drug Discovery Today*, 2005. **10**(15): p. 1014-1015.
144. Singh, A., P. Trivedi, and N.K. Jain, *Advances in siRNA delivery in cancer therapy*. *Artif Cells Nanomed Biotechnol*, 2018. **46**(2): p. 274-283.
145. Davis, M.E., et al., *Evidence of RNAi in humans from systemically administered siRNA via targeted nanoparticles*. *Nature*, 2010. **464**(7291): p. 1067-70.
146. Weng, Y., et al., *RNAi therapeutic and its innovative biotechnological evolution*. *Biotechnol Adv*, 2019.
147. Tolia, N.H. and L. Joshua-Tor, *Slicer and the argonautes*. *Nat Chem Biol*, 2007. **3**(1): p. 36-43.
148. Tuschl, T., et al., *Targeted mRNA degradation by double-stranded RNA in vitro*. *Genes Dev*, 1999. **13**(24): p. 3191-7.
149. Rand, T.A., et al., *Argonaute2 cleaves the anti-guide strand of siRNA during RISC activation*. *Cell*, 2005. **123**(4): p. 621-9.
150. Kanasty, R., et al., *Delivery materials for siRNA therapeutics*. *Nat Mater*, 2013. **12**(11): p. 967-77.
151. Pecot, C.V., et al., *RNA interference in the clinic: challenges and future directions*. *Nat Rev Cancer*, 2011. **11**(1): p. 59-67.
152. Layzer, J.M., et al., *In vivo activity of nuclease-resistant siRNAs*. *RNA*, 2004. **10**(5): p. 766-71.
153. Mosser, D.M. and J.P. Edwards, *Exploring the full spectrum of macrophage activation*. *Nat Rev Immunol*, 2008. **8**(12): p. 958-69.
154. Jackson, A.L., et al., *Widespread siRNA "off-target" transcript silencing mediated by seed region sequence complementarity*. *RNA*, 2006. **12**(7): p. 1179-87.
155. Marques, J.T. and B.R.G. Williams, *Activation of the mammalian immune system by siRNAs*. *Nature Biotechnology*, 2005. **23**(11): p. 1399-1405.
156. Whitehead, K.A., R. Langer, and D.G. Anderson, *Knocking down barriers: advances in siRNA delivery*. *Nat Rev Drug Discov*, 2009. **8**(2): p. 129-38.
157. Czauderna, F., et al., *Structural variations and stabilising modifications of synthetic siRNAs in mammalian cells*. *Nucleic Acids Res*, 2003. **31**(11): p. 2705-16.
158. Braasch, D.A., et al., *Biodistribution of phosphodiester and phosphorothioate siRNA*. *Bioorg Med Chem Lett*, 2004. **14**(5): p. 1139-43.
159. Li, Z.Y., et al., *The effects of thiophosphate substitutions on native siRNA gene silencing*. *Biochem Biophys Res Commun*, 2005. **329**(3): p. 1026-30.
160. Hall, A.H., et al., *RNA interference using boranophosphate siRNAs: structure-activity relationships*. *Nucleic Acids Res*, 2004. **32**(20): p. 5991-6000.
161. Chiu, Y.L., *siRNA function in RNAi: A chemical modification analysis*. *Rna*, 2003. **9**(9): p. 1034-1048.
162. Elmen, J., et al., *Locked nucleic acid (LNA) mediated improvements in siRNA stability and functionality*. *Nucleic Acids Res*, 2005. **33**(1): p. 439-47.
163. Muratovska, A. and M.R. Eccles, *Conjugate for efficient delivery of short interfering RNA (siRNA) into mammalian cells*. *FEBS Letters*, 2004. **558**(1-3): p. 63-68.
164. Torchilin, V.P., et al., *Cell transfection in vitro and in vivo with nontoxic TAT peptide-liposome-DNA complexes*. *Proc Natl Acad Sci U S A*, 2003. **100**(4): p. 1972-7.
165. Auguste, D.T., et al., *Triggered release of siRNA from poly(ethylene glycol)-protected, pH-dependent liposomes*. *J Control Release*, 2008. **130**(3): p. 266-74.

166. van de Water, F.M., et al., *Intravenously administered short interfering RNA accumulates in the kidney and selectively suppresses gene function in renal proximal tubules*. Drug Metab Dispos, 2006. **34**(8): p. 1393-7.
167. Bogdanov, A.A., Jr., *Merging molecular imaging and RNA interference: early experience in live animals*. J Cell Biochem, 2008. **104**(4): p. 1113-23.
168. Gonzalez, H., S.J. Hwang, and M.E. Davis, *New Class of Polymers for the Delivery of Macromolecular Therapeutics*. Bioconjugate Chemistry, 1999. **10**(6): p. 1068-1074.
169. Hu-Lieskovan, S., et al., *Sequence-Specific Knockdown of EWS-FLI1 by Targeted, Nonviral Delivery of Small Interfering RNA Inhibits Tumor Growth in a Murine Model of Metastatic Ewing's Sarcoma*. Cancer Research, 2005. **65**(19): p. 8984-8992.
170. Bellocq, N.C., et al., *Transferrin-containing, cyclodextrin polymer-based particles for tumor-targeted gene delivery*. Bioconjug Chem, 2003. **14**(6): p. 1122-32.
171. Felgner, P.L., et al., *Lipofection: a highly efficient, lipid-mediated DNA-transfection procedure*. Proc Natl Acad Sci U S A, 1987. **84**(21): p. 7413-7.
172. Xu, Y. and F.C. Szoka, Jr., *Mechanism of DNA release from cationic liposome/DNA complexes used in cell transfection*. Biochemistry, 1996. **35**(18): p. 5616-23.
173. Liu, F., et al., *Current Transport Systems and Clinical Applications for Small Interfering RNA (siRNA) Drugs*. Mol Diagn Ther, 2018. **22**(5): p. 551-569.
174. Torchilin, V.P., *Recent advances with liposomes as pharmaceutical carriers*. Nat Rev Drug Discov, 2005. **4**(2): p. 145-60.
175. Kim, H.S., et al., *In vitro and in vivo gene-transferring characteristics of novel cationic lipids, DMKD (O,O'-dimyristyl-N-lysyl aspartate) and DMKE (O,O'-dimyristyl-N-lysyl glutamate)*. J Control Release, 2006. **115**(2): p. 234-41.
176. Severino, P., et al., *Development and characterization of a cationic lipid nanocarrier as non-viral vector for gene therapy*. Eur J Pharm Sci, 2015. **66**: p. 78-82.
177. Takahashi, H., K. Sinoda, and I. Hatta, *Effects of cholesterol on the lamellar and the inverted hexagonal phases of dielaidoylphosphatidylethanolamine*. Biochim Biophys Acta, 1996. **1289**(2): p. 209-16.
178. Zuhorn, I.S., et al., *Nonbilayer phase of lipoplex-membrane mixture determines endosomal escape of genetic cargo and transfection efficiency*. Mol Ther, 2005. **11**(5): p. 801-10.
179. Soutschek, J., et al., *Therapeutic silencing of an endogenous gene by systemic administration of modified siRNAs*. Nature, 2004. **432**(7014): p. 173-8.
180. Shim, M.S. and Y.J. Kwon, *Efficient and targeted delivery of siRNA in vivo*. Febs j, 2010. **277**(23): p. 4814-27.
181. Morrissey, D.V., et al., *Potent and persistent in vivo anti-HBV activity of chemically modified siRNAs*. Nat Biotechnol, 2005. **23**(8): p. 1002-7.
182. Zimmermann, T.S., et al., *RNAi-mediated gene silencing in non-human primates*. Nature, 2006. **441**(7089): p. 111-4.
183. Geisbert, T.W., et al., *Postexposure protection of guinea pigs against a lethal ebola virus challenge is conferred by RNA interference*. J Infect Dis, 2006. **193**(12): p. 1650-7.
184. Jeong, J.H., et al., *siRNA conjugate delivery systems*. Bioconjug Chem, 2009. **20**(1): p. 5-14.
185. Lee, S.H., et al., *Current preclinical small interfering RNA (siRNA)-based conjugate systems for RNA therapeutics*. Adv Drug Deliv Rev, 2016. **104**: p. 78-92.
186. Song, K.M., S. Lee, and C. Ban, *Aptamers and their biological applications*. Sensors (Basel), 2012. **12**(1): p. 612-31.
187. Bhatnagar, I., J. Venkatesan, and S.K. Kiml, *Polymer functionalized single walled carbon nanotubes mediated drug delivery of gliotoxin in cancer cells*. J Biomed Nanotechnol, 2014. **10**(1): p. 120-30.
188. Delac, M., et al., *Aptamer for imaging and therapeutic targeting of brain tumor glioblastoma*. Cytometry A, 2015. **87**(9): p. 806-16.
189. Zhou, J. and J.J. Rossi, *Cell-type-specific, Aptamer-functionalized Agents for Targeted Disease Therapy*. Mol Ther Nucleic Acids, 2014. **3**: p. e169.

190. Gilboa-Geffen, A., et al., *Gene Knockdown by EpCAM Aptamer-siRNA Chimeras Suppresses Epithelial Breast Cancers and Their Tumor-Initiating Cells*. Mol Cancer Ther, 2015. **14**(10): p. 2279-91.
191. Wender, P.A., C.B. Cooley, and E.I. Geihe, *Beyond Cell Penetrating Peptides: Designed Molecular Transporters*. Drug Discov Today Technol, 2012. **9**(1): p. e49-e55.
192. Lee, S.H., B. Castagner, and J.C. Leroux, *Is there a future for cell-penetrating peptides in oligonucleotide delivery?* Eur J Pharm Biopharm, 2013. **85**(1): p. 5-11.
193. Kelly, G.S., *Squalene and its potential clinical uses*. Altern Med Rev, 1999. **4**(1): p. 29-36.
194. Reddy, L.H. and P. Couvreur, *Squalene: A natural triterpene for use in disease management and therapy*. Adv Drug Deliv Rev, 2009. **61**(15): p. 1412-26.
195. Kim, S.K. and F. Karadeniz, *Biological importance and applications of squalene and squalane*. Adv Food Nutr Res, 2012. **65**: p. 223-33.
196. Gershbein, L.L. and E.J. Singh, *Hydrocarbons of dogfish and cod livers and herring oil*. J Am Oil Chem Soc, 1969. **46**(10): p. 554-7.
197. Newmark, H.L., *Squalene, olive oil, and cancer risk: a review and hypothesis*. Cancer Epidemiol Biomarkers Prev, 1997. **6**(12): p. 1101-3.
198. Stewart, M.E., *Sebaceous gland lipids*. Semin Dermatol, 1992. **11**(2): p. 100-5.
199. Kohno, Y., et al., *Kinetic study of quenching reaction of singlet oxygen and scavenging reaction of free radical by squalene in n-butanol*. Biochim Biophys Acta, 1995. **1256**(1): p. 52-6.
200. Warleta, F., et al., *Squalene protects against oxidative DNA damage in MCF10A human mammary epithelial cells but not in MCF7 and MDA-MB-231 human breast cancer cells*. Food Chem Toxicol, 2010. **48**(4): p. 1092-100.
201. Senthikumar, S., et al., *Attenuation of cyclophosphamide induced toxicity by squalene in experimental rats*. Chem Biol Interact, 2006. **160**(3): p. 252-60.
202. Owen, R.W., et al., *Olives and olive oil in cancer prevention*. Eur J Cancer Prev, 2004. **13**(4): p. 319-26.
203. Blasco, L., et al., *Skin Constituents as Cosmetic Ingredients. Part I: A Study of Bio-mimetic Monoglycerides Behavior at the Squalene-Water Interface by the "Pendant Drop" Method in a Static Mode*. Journal of Dispersion Science and Technology, 2006. **27**(6): p. 799-810.
204. Rissmann, R., et al., *Lanolin-derived lipid mixtures mimic closely the lipid composition and organization of vernix caseosa lipids*. Biochim Biophys Acta, 2008. **1778**(10): p. 2350-60.
205. Wang, J.J., et al., *The delivery and antinociceptive effects of morphine and its ester prodrugs from lipid emulsions*. Int J Pharm, 2008. **353**(1-2): p. 95-104.
206. Fang, J.Y., et al., *Lipid nanoparticles as vehicles for topical psoralen delivery: solid lipid nanoparticles (SLN) versus nanostructured lipid carriers (NLC)*. Eur J Pharm Biopharm, 2008. **70**(2): p. 633-40.
207. Reddy, L.H., et al., *Preclinical toxicology (subacute and acute) and efficacy of a new squalenoyl gemcitabine anticancer nanomedicine*. J Pharmacol Exp Ther, 2008. **325**(2): p. 484-90.
208. Couvreur, P., et al., *Squalenoyl nanomedicines as potential therapeutics*. Nano Lett, 2006. **6**(11): p. 2544-8.
209. Ali, H.M., et al., *Effects of silencing the RET/PTC1 oncogene in papillary thyroid carcinoma by siRNA-squalene nanoparticles with and without fusogenic companion GALA-cholesterol*. Thyroid, 2014. **24**(2): p. 327-38.
210. Raouane, M., et al., *Synthesis, characterization, and in vivo delivery of siRNA-squalene nanoparticles targeting fusion oncogene in papillary thyroid carcinoma*. J Med Chem, 2011. **54**(12): p. 4067-76.
211. Massaad-Massade, L., et al., *New Formulation for the Delivery of Oligonucleotides Using "Clickable" siRNA-Polyisoprenoid-Conjugated Nanoparticles: Application to Cancers Harboring Fusion Oncogenes*. Bioconjug Chem, 2018. **29**(6): p. 1961-1972.
212. Keam, S.J., *Inotersen: First Global Approval*. Drugs, 2018. **78**(13): p. 1371-1376.
213. Ozaras, R., M. Yemisen, and Balkan, Il, *Current and future therapies for hepatitis C virus infection*. N Engl J Med, 2013. **369**(7): p. 679.

214. Watanabe, T., et al., *Liver target delivery of small interfering RNA to the HCV gene by lactosylated cationic liposome*. J Hepatol, 2007. **47**(6): p. 744-50.
215. Haussecker, D., *The Business of RNAi Therapeutics in 2012*. Mol Ther Nucleic Acids, 2012. **1**: p. e8.
216. Haussecker, D., *RNAi Arrives at the Bedside after a Mere Two Decades*. Mol Ther, 2018. **26**(11): p. 2533-2534.
217. Haussecker, D. and M.A. Kay, *RNA interference. Drugging RNAi*. Science, 2015. **347**(6226): p. 1069-70.
218. Tafer, H., et al., *The impact of target site accessibility on the design of effective siRNAs*. Nat Biotechnol, 2008. **26**(5): p. 578-83.
219. Tuschl, T., *Expanding small RNA interference*. Nat Biotechnol, 2002. **20**(5): p. 446-8.
220. Raouane, M., et al., *Synthesis, Characterization, and in Vivo Delivery of siRNA-Squalene Nanoparticles Targeting Fusion Oncogene in Papillary Thyroid Carcinoma*. Journal of Medicinal Chemistry, 2011. **54**(12): p. 4067-4076.
221. Hichor, M., et al., *Paraquat Induces Peripheral Myelin Disruption and Locomotor Defects: Crosstalk with LXR and Wnt Pathways*. Antioxid Redox Signal, 2017. **27**(3): p. 168-183.
222. Brooks, S.P. and S.B. Dunnett, *Tests to assess motor phenotype in mice: a user's guide*. Nat Rev Neurosci, 2009. **10**(7): p. 519-29.
223. Echaniz-Laguna, A., et al., *Electrophysiological studies in a mouse model of Schwartz-Jampel syndrome demonstrate muscle fiber hyperactivity of peripheral nerve origin*. Muscle Nerve, 2009. **40**(1): p. 55-61.
224. Bouhy, D. and V. Timmerman, *Animal models and therapeutic prospects for Charcot-Marie-Tooth disease*. Ann Neurol, 2013. **74**(3): p. 391-6.
225. Boutry, J.M., et al., *Establishment and characterization of a mouse Schwann cell line which produces myelin in vivo*. J Neurosci Res, 1992. **32**(1): p. 15-26.
226. Robertson, A.M., et al., *Comparison of a new pmp22 transgenic mouse line with other mouse models and human patients with CMT1A*. J Anat, 2002. **200**(4): p. 377-90.
227. Cooper, D.N., et al., *Where genotype is not predictive of phenotype: towards an understanding of the molecular basis of reduced penetrance in human inherited disease*. Hum Genet, 2013. **132**(10): p. 1077-130.
228. Guo, J., et al., *Abnormal junctions and permeability of myelin in PMP22-deficient nerves*. Annals of Neurology, 2014. **75**(2): p. 255-265.
229. Kamholz, J., et al., *Regulation of Myelin-Specific Gene Expression: Relevance to CMT1*. Ann N Y Acad Sci, 1999. **883**(1): p. 91-108.
230. Sobot, D., et al., *Circulating Lipoproteins: A Trojan Horse Guiding Squalenoylated Drugs to LDL-Accumulating Cancer Cells*. Mol Ther, 2017. **25**(7): p. 1596-1605.

APPENDIX

- I. Synthèse en française
- II. Article I: New Formulation for Delivery of oligonucleotides using Clickable siRNA-Polyisoprenoid-Conjugated Nanoparticles: Application to Cancers Harboring Fusion Oncogenes
- III. Review: Charcot Marie Tooth Disease Therapies: from the Classical Approach to Gene Regulation (submitted to journal Neurobiology of disease)
- IV. European Patent: Antisense RNA Targeting PMP22 For the Treatment of Charcot Marie Tooth 1A
- V. International extension of the Patent: Antisense RNA Targeting PMP22 For the Treatment of Charcot Marie Tooth 1A
- VI. Demande de mise en place d'accord de confidentialité sur le mémoire de soutenance de thèse, sans huis-clos

I. Synthèse en français

La Maladie de Charcot Marie Tooth (CMT) est la neuropathie héréditaire la plus fréquente au monde ; 1 personne sur 2500 est atteinte dans le monde. Elle est aussi appelée « neuropathie périphérique héréditaire sensitive et motrice » pour la distinguer de la maladie de Charcot ou sclérose latérale amyotrophique (SLA). Il existe plusieurs formes de CMT qui sont classées selon : 1) le mode de transmission autosomique dominant ou récessif et lié au chromosome X, 2) selon la mesure de la vitesse de conduction nerveuse et, 3) selon le gène impliqué, il en existe plus de 90 mais celui qui est fréquemment retrouvé chez 50% des patients est celui de la PMP22 (1/5000, CMT1A).

La CMT1A est donc due à une duplication interstitielle au niveau du bras court 17p12, entraînant la surexpression du gène codant pour la protéine de myéline périphérique de 22 kDa (PMP22). Il en résulte une détérioration de la gaine de myéline qui se reflète par un ralentissement de la vitesse de conduction nerveuse, provoquant une neuropathie et une atrophie musculaire. Cette neuropathie périphérique apparaît dans l'enfance ou à l'âge adulte avec une atteinte variable d'un patient à l'autre qui peut aller d'une simple gêne à la marche, jusqu'à l'usage d'un fauteuil roulant (10% des cas). Elle évolue lentement par poussées, l'espérance de vie n'est pas affectée mais la qualité de vie est très entravée.

Depuis la découverte de CMT au 19^{ème} siècle, aucun médicament n'a été mis sur le marché pour guérir ou soulager les symptômes de la maladie. Les seuls traitements reposent sur des mesures préventives mais non curatives, qui se limitent à la physiothérapie, au port de prothèses et à la chirurgie orthopédique qui peuvent apporter un soulagement et un maintien de la marche, mais n'arrête pas l'évolution de la maladie, d'où l'urgence pour les patients, leurs familles, les associations de patients et aussi les cliniciens de développer un traitement pour la maladie CMT1A.

L'absence d'un traitement efficace contre la maladie CMT1A nous a incités à développer une nouvelle approche thérapeutique basée sur l'interférence à l'ARN. Notre but est d'offrir une thérapie ciblée prometteuse en normalisant l'expression de PMP22 par un petit ARN interférent (small interfering RNA ou siRNA). Les siRNA sont des molécules nucléotidiques à double brin de 19-21 paires de bases dont le brin anti-sens est complémentaire de la séquence d'ARN messager (ARNm) d'un gène cible dont on souhaite inhiber ou normaliser l'expression. Nous avons conçu huit siRNAs pour couvrir la partie de l'ARNm de PMP22 commune à plusieurs espèces (humains, primates, rongeurs) en respectant les huit critères énoncés par Reynolds *et al.*, 2004. Ces siRNAs ont été testés *in vitro* dans un modèle de cellules de

Schwann immortalisées (MSC-80). La PMP22 et la Myelin Protein Zero (P0) sont deux glycoprotéines impliquées dans les stades précoces de la myélinisation et jouent un rôle prépondérant dans la compaction de la myéline. Notre objectif n'est pas d'inhiber fortement l'expression de la PMP22 mais de normaliser son expression. Une inhibition < 70% de la PMP22 serait responsable du développement d'une autre neuropathie périphérique. En ce qui concerne P0, elle assure la cohésion entre les tours de spires de la membrane plasmique des cellules de Schwann au cours de la formation de la myéline, une augmentation de son expression serait responsable du développement de CMT1B. Le siRNA qui répondait au mieux à nos critères d'inclusion (inhibition entre 30% et 50% de l'expression de PMP22, pas d'effet sur l'expression de P0) a donc été retenu.

Ensuite, nous avons déterminé la dose optimale du siRNA par PCR en temps réel après extraction de l'ARNm et son effet sur la viabilité cellulaire par test MTT. Nous avons testé différentes concentrations (25nM, 50nM et 100nM) et retenue celle capable de normaliser l'expression de PMP22 sans affecter l'expression de P0. Nos résultats montrent que la concentration optimale est de 50 nM, elle permet d'inhiber de 50% l'expression de PMP22 pendant 72h sans affecter l'expression de la P0 et la viabilité cellulaire. Le siRNA contrôle (siRNA Ct) ne modifie pas l'expression des deux gènes étudiés et la viabilité cellulaire.

Il est connu que les siRNA ont une demi-vie plasmatique courte due à une élimination rénale rapide et une forte dégradation par des enzymes contenues dans le sérum, sont hydrophiles et peuvent avoir des effets off-target (inhibition de l'expression d'un gène non ciblé) lorsqu'ils sont injectés à des fortes doses, d'où l'intérêt de les encapsuler. Nous avons opté pour une vectorisation chimique, qui, contrairement à la vectorisation physique (basée sur des interactions électrostatiques), a l'avantage de connaître précisément la quantité injectée de siRNA, puisqu'il est lié de façon covalente à son vecteur. Ceci permet d'avoir un taux de charge équimolaire entre la molécule active et le vecteur. Ceci empêcherait la libération rapide du principe actif et contournerait la toxicité et la résistance due à l'excès de charge du vecteur et/ou du principe actif.

Pour protéger et délivrer notre siRNA PMP22, nous l'avons conjugué au squalène, un polyterpène précurseur du cholestérol, par "chimie click sans cuivre". Cette réaction chimique s'effectue entre une fonction azide (lié au SQ) et une fonction alcyne incluse dans un dibenzocyclooctyne lié à la partie 5' - du brin sens du siRNA. La bioconjugaison du siRNA PMP22 au squalène est quasi complète (rendement de 95%). Les nanoparticules résultantes sont stables à 4°C pendant un mois. Les nanoparticules (NPs) siRNA PMP22-SQ inhibent ~50%

l'expression de PMP22, sans affecter l'expression de P0 et la viabilité cellulaire. De même, les NPs siRNA Ct-SQ ne modifient aucun des paramètres étudiés.

Nous avons testé les NPs siPMP22-SQ sur deux modèles de souris CMT1A JP18 B6 (simple transgénique) et JP18 / JY13 B6 (double transgénique). Après une dose cumulative de 2,5mg/kg, nos résultats montrent que les NPs siRNA PMP22-SQ restituent l'activité motrice chez les souris simple et double transgéniques. Ce traitement permet aussi de restaurer l'activité électrophysiologique, qui devient comparable aux souris sauvages. La normalisation de l'expression de PMP22 restaure également l'expression des protéines impliquées dans la myélinisation et la régénération axonale chez la souris simple et double transgénique.

Aussi, les NPs siRNA PMP22-SQ

En conclusion, nous avons réussi à obtenir une preuve de concept solide sur l'utilisation des siRNA dans deux modèles murins. Les NPs siRNA PMP22-SQ normalisent l'expression de PMP22, restaurant la myélinisation, la régénération axonale et l'activité électrophysiologique, permettant ainsi d'améliorer la locomotion. La rémission commence après la 3ème injection à partir de la concentration de 1.5 mg/kg et dure 2 semaine après la fin du 1er cycle de traitement. Elle reprend rapidement au cours du 2nd cycle de traitement.

En vue de passer aux phases précliniques et cliniques réglementaires, les études futures porteront sur l'optimisation du traitement. Nous injecterons des doses croissantes de 0,1 - 2,5 mg/kg pour déterminer la dose optimale capable d'induire une rémission à long terme, déterminerons la fréquence des injections et suivrons les souris jusqu'à 9 mois.

New Formulation for the Delivery of Oligonucleotides Using “Clickable” siRNA-Polyisoprenoid-Conjugated Nanoparticles: Application to Cancers Harboring Fusion Oncogenes

Liliane Massaad-Massade,^{*,†,‡,§,¶} Suzan Boutary,^{†,‡,§} Marie Caillaud,^{†,‡,§} Celine Gracia,^{†,‡,§} Beatrice Parola,[‡] Soukaina Bel Gnaouiya,[‡] Barbara Stella,[‡] Silvia Arpico,[‡] Eric Buchy,^{||} Didier Desmaële,^{||} Patrick Couvreur,^{||} and Giorgia Urbinati^{†,‡,§}

[†]Université Paris-Saclay, Laboratoire de Vectorologie et Thérapeutiques Anticancéreuses, UMR 8203, Villejuif, France-94805

[‡]CNRS, Laboratoire de Vectorologie et Thérapeutiques Anticancéreuses, UMR 8203, Villejuif, France-94805

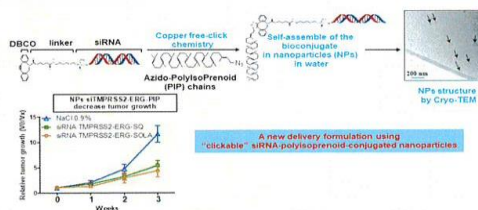
[§]Gustave Roussy, Laboratoire de Vectorologie et Thérapeutiques Anticancéreuses, UMR 8203, Villejuif, France-94805

^{||}Institut Galien, UMR CNRS 8612, Université Paris-Saclay, Faculté de Pharmacie, 5 rue J. B. Clément, 92296 Châtenay-Malabry, France

[¶]Università degli Studi di Torino, Dipartimento di Scienza e Tecnologia del Farmaco, Via Pietro Giuria 9, 10125 Torino, Italy

Supporting Information

ABSTRACT: The aim of the present study is to take advantage of the unique property of polyisoprenoid chains to adopt a compact molecular conformation and to use these natural and biocompatible lipids as nanocarriers of drugs to deliver siRNA. A new chemical strategy is applied here to conjugate squalene (SQ) and solanesol (SOLA) to siRNA consisting of an activated variant of the azide–alkyne Huisgen cycloaddition also known as copper-free (Cu-free) click chemistry. We conjugated siRNA against TMPRSS2-ERG, a fusion oncogene found in more than 50% of prostate cancers to SQ or SOLA. First, several parameters such as molar ratio, solvents, temperature, incubation time, and the annealing schedule between both siRNA strands were investigated to bioconjugate the SQ or SOLA via Cu-free click chemistry. The best parameters of the new bioconjugation approach allowed us to (i) increase the synthesis yield up to 95%, (ii) avoid the formation of byproducts during the synthesis, and (iii) improve the reproducibility of the bioconjugation. Then, the biological activity of the resulting nanoparticles was assessed. *In vitro*, all four formulations were able to decrease the corresponding oncogene and oncoprotein expression. *In vivo*, only two of the four nanoformulations showed anti-neoplastic activity that seems to be tightly related to their dissimilar biodistribution behavior. In conclusion, we performed a new approach easily transposable for pharmaceutical development to synthesize siRNA-SQ and siRNA-SOLA and to obtain efficient siRNA-nanoparticles. The robustness of the process could be extended to several other polyterpenes and likely applied to other siRNA targeting genes whose overexpression results in the development of cancers or other genetic diseases.



INTRODUCTION

Over the past two decades, the antisense oligonucleotides and in particular the small interfering RNAs (siRNA) have been extensively studied. They represent a potential powerful therapy for gene-specific diseases and, consequently, an efficient tool for gene modulation. The use of siRNA as a therapeutic approach is still under investigation for cancer treatment, in early and advanced clinical phases, as well as for noncancer diseases (i.e., macular degenerative disease, infections, and genetic disorders such congenital Pachyonychia) (<https://clinicaltrials.gov/ct2/results?term=siRNA&Search=Search>).^{1,2} However, despite the strong potential of siRNAs as therapeutic agents, none of them has been approved yet by the “Food and Drug Administration”.

In fact, *in vivo* delivery of siRNAs is a key challenge because their biological efficacy is hampered by short plasmatic half-life due to poor stability in biological fluids and by low intracellular penetration due to their highly hydrophilic characteristics.³ Thus, extensive research has been carried out to overcome those hurdles and to establish platforms for siRNA delivery. So far, a wide variety of delivery systems including viral-vectors and nonviral approaches have been developed.^{4,5} However, the cytotoxic effects of some of these vectors, often due to the use of cationic transporter materials, are now well documented.^{6,7}

Received: March 21, 2018

Revised: April 26, 2018

Published: May 4, 2018

There is, therefore, an urgent need to establish new strategies for delivering siRNA using new and safer nanocarriers. Hence, neutral lipid–oligonucleotide conjugates have become a subject of considerable interest to improve the half-life of siRNA and their delivery.⁸

Polyisoprenoids, a part of a large class of natural, flexible, and biocompatible biopolymers, have been described as being able to adapt to a wide variety of biologically active compounds due to their physicochemical characteristics.⁹ For example, siRNAs were conjugated to squalene, an acyclic triterpene, to target various fusion oncogenes, including RET/PTC frequently expressed in papillary thyroid carcinoma and TMPRSS2-ERG found in more than 50% of prostate cancer biopsies.^{10–15} The siRNA RET/PTC1 has been covalently linked to the acyclic isoprenoid chain of squalene, and the resulting bioconjugate was found to be able to self-assemble in water into nanoparticles (~165 ± 10 nm).¹³ Moreover, the resulting siRNA-squalene nanoparticles (siRNA-SQ NPs) were capable of extensively inhibiting the growth of papillary thyroid carcinoma xenografts in mice. Similar results were observed when siRNA TMPRSS2-ERG was conjugated to squalene (i.e., "squalenoylated"), nanoprecipitated, and the resulting nanoparticles were injected into mice bearing prostate cancer xenografts. Thus, the squalenoylation method may represent a new noncationic siRNA delivery system. Indeed, recent studies demonstrated the interaction of squalene derivatives with lipoproteins which suggest the role of low-density proteins as a Trojan horse to deliver squalene based nanoparticles within the tumor.^{16,17}

Nevertheless, the vectorization method mentioned above involving the hetero-Michael addition reaction of 3'-thiol-siRNA with squalene maleimide suffered from a moderate conversion that led to a laborious and low-yielding HPLC purification. With the objective of improving the overall yield and to shorten the synthetic scheme, we decided to explore the copper-free (Cu-free) click chemistry synthesis. This reaction is a mild and fast Huisgen cycloaddition between a strained-alkyne and an azide, enabling the selective formation of a triazol product.^{18,19} In this process, the use of highly strained alkynes abolishes the need for copper catalyst in the reaction that could degrade the siRNA and thus circumvents the difficulties of final purification of oligonucleotides.

Furthermore, with the aim of modulating the amphiphilic balance of the conjugate we used solanesol (SOLA), a natural nonaprenol isolated from tobacco leaves. SOLA is widely used for the synthesis of coenzyme Q10 and vitamin K2 and possesses many pharmacological activities.^{20,21} Recently, solanesol has also been described to have an inhibitory effect on the focal adhesion kinase protein, thus presenting anticancer properties.²² With a regular polyisoprenoid chain of 45 carbons, SOLA was expected to increase the hydrophobic characteristics of the conjugate with respect to SQ (C₃₂ chain). This increased lipophilicity was meant to increase the stability of the nanoparticles as well as provide a spontaneous uptake by tumor cells in vitro which is not observed for siRNA-SQ NPs except with the use of a cationic compound. Moreover, the presence of a terminal hydroxyl group makes it easy to introduce the required azide anchoring group.

This article describes the conjugation of the highly hydrophilic and fragile siRNA to the lipophilic SQ or SOLA by Cu-free click chemistry. In fact, this new type of chemistry applied conjugation of the SQ to siRNA allowing a much greater yield of the desired bioconjugate compared to the

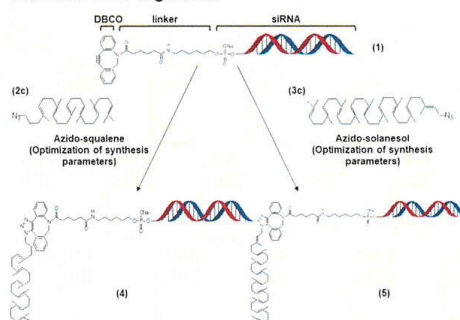
Michael addition employed before, and is a one-step reaction. In addition, the process is much faster and more reproducible. The high yield, the absence of byproducts, and the reproducibility of the synthesis allowed the application of this approach to two different siRNA sequences. Moreover, the Solanesol has never been conjugated before to siRNA and never studied as vector for oligonucleotides in vitro and in vivo. In conclusion, extensive characterization of the resulting nanoparticles and the biodistribution studies allowed, for the first time, one to highlight the importance of the structure and organization of the nanoassemblies to preserve the efficacy of the siRNA-SQ NPs in vivo.

RESULTS

Cu-Free Click Chemistry Strikingly Increases the Yield of the siRNA TMPRSS2-ERG Bioconjugates. In order to increase the yield of the bioconjugation previously obtained by a Hetero-Michael addition reaction,^{10,11,13–15} a new strategy based on the Cu-free click chemistry was investigated to conjugate the siRNA to polyisoprenoids. Thus, the siRNA TMPRSS2-ERG bioconjugates were synthesized according to the 1,3-dipolar cycloaddition of azides (squalene/solanesol) and dibenzocyclooctyne-modified siRNA as shown in Scheme 1 and Figure SI 1.

The *N*-(hexamethylenyl)-6-oxohexanamide spacer was introduced between the 5'-end of the sense strand of the siRNA and the reactive group dibenzocyclooctyne (DBCO) (Scheme 1 (1)) to allow functionalization and bioconjugation to azido-squalene (Scheme 1 (2c) and Figure SI 1) or azido-solanesol

Scheme 1. Cu-Free Click Chemistry to Synthesize siRNA TMPRSS2-ERG-SQ/SOLA^a



^a(1) The sense strand was modified by a DBCO residue at the 5'-end of the siRNA TMPRSS2-ERG. To avoid a steric hindrance, a linker was used. (2c) Squalene was modified by an azide (SQ-N₃) to react with the DBCO residue of the siRNA TMPRSS2-ERG. (2e) Solanesol was modified by an azide (SOLA-N₃) to react with the DBCO residue of the siRNA TMPRSS2-ERG. (3c) The bioconjugate siRNA TMPRSS2-ERG-SQ was obtained by applying the following parameters: (i) molar ratio of 1:50 of siRNA TMPRSS2-ERG and SQ-N₃ respectively; (ii) in the presence of DMSO/acetone/H₂O; (iii) at room temperature; (iv) incubating for 12 h under stirring. (5) The bioconjugate siRNA TMPRSS2-ERG-SOLA was obtained by applying the following parameters: (i) molar ratio of 1:50 of siRNA TMPRSS2-ERG and SOLA-N₃ respectively; (ii) in the presence of DMSO/acetone/H₂O; (iii) at room temperature; (iv) incubating for 18 h under stirring.

(Scheme 1 (3c) and Figure SI 1). The best parameters of the click chemistry reaction were investigated to conjugate the SQ and then applied to SOLA.

We observed that by modifying the parameters solvents, molar ratio, temperature, and time of incubation, it was possible to substantially increase the yield of the bioconjugates siRNA TMPRSS2-ERG-SQ (Scheme 1 (4)) and siRNA TMPRSS2-ERG-SOLA (Scheme 1 (5)) and to avoid the formation of byproducts. The different conditions tested for the Cu-free click chemistry reaction are listed in Figure SI 2.

H₂O/DMSO/Acetone Combination Improves the Bioconjugation of the siRNA TMPRSS2-ERG to SQ. To provide the best interaction between siRNA (highly hydrophilic) and SQ (highly hydrophobic), several solvents (H₂O, DMF, DMSO, methanol, acetone) were tested (Figure 1A and B).

When the DBCO-modified siRNA TMPRSS2-ERG (Figure 1A) was dissolved in water and then added to DMSO containing the azido-squalene, 87% of the starting product (Figure 1B, red chromatogram, siRNA elution time ~10–12

min) was converted into a more lipophilic compound (elution time ~18–20 min). The latter compound was then identified as the bioconjugate siRNA TMPRSS2-ERG-SQ by MALDI TOF MS analysis (7655 Da, Figure SI 3).

When the same modified siRNA was dissolved in H₂O and then added to a DMF/methanol solution of the azido-squalene, only 28% of the starting product (Figure 1B, black chromatogram, siRNA elution time ~10–12 min) was converted into the same lipophilic bioconjugate (elution time ~18–20 min) previously identified (please refer to Table 1, section A).

Moreover, the addition of acetone to the mixture H₂O/DMSO produced a bioconjugate free of byproducts when compared to the mixture H₂O/DMSO/ethanol (data not shown). Thus, all the conjugations were next routinely performed in the H₂O/DMSO/acetone solvent mixture.

Molar Ratio of 1:50 siRNA TMPRSS2-ERG:SQ Improves the Bioconjugation Yield. To improve the yield of the bioconjugation, several molar ratios ranging from 1:1 to 1:350 between the siRNA TMPRSS2-ERG and the squalene azide were assessed (Figure SI 4).

As shown in Figure 1C, the yield of the bioconjugation started to be affected when the molar ratio of the reagents drops from 1:50 to 1:5. Indeed, the 1:50 ratio (siRNA TMPRSS2-ERG:SQ, respectively) converted more than 95% of the starting siRNA TMPRSS2-ERG into the desired siRNA TMPRSS2-ERG-SQ bioconjugate (red chromatogram of Figure 1C). Below this threshold, a progressive decrease of the reaction yield was observed beginning from the 1:5 molar ratio and below (Figure 1C, black chromatogram, Table 1, section B and Figure SI 4).

Room Temperature Avoids the Degradation of the Bioconjugate. In order to prevent the formation of byproducts during the synthesis of the bioconjugate, the influence of the temperature was investigated. Two temperatures were tested, 37 °C and room temperature; those lower than 20 °C were not assessed as DMSO freezes below 18.5 °C.

We found that 37 °C strikingly increased the formation of byproducts, compared to the same synthesis performed at room temperature which reduced the yield of the desired bioconjugate (compare Figure 1D, black to red chromatograms, respectively, and Table 1, section C). Moreover, this was confirmed by MALDI-TOF-MS analysis showing that by-products were found in the reaction carried out at 37 °C (data not shown).

Twelve Hour Incubation Is Necessary for a Total Conversion of the Reaction. Finally, the reaction time of the bioconjugation was investigated. Figure 1E represents the conversion rate of the siRNA into the siRNA-SQ bioconjugate after 4 h (black chromatogram) and 12 h incubation (red chromatogram). Only ~60% of the initial siRNA TMPRSS2-ERG was conjugated to SQ after 4 h incubation, while a complete conversion into the desired bioconjugate siRNA TMPRSS2-ERG-SQ (>97%) was obtained after an overnight incubation (Table 1, section D).

Thus, for further studies the optimized conditions were as follows: incubation of the siRNA TMPRSS2-ERG with squalene at 1:50 molar ratio into a mixture of H₂O/DMSO/acetone, under stirring overnight at room temperature. This allowed the conversion of more than 95% of the siRNA TMPRSS2-ERG into the bioconjugate siRNA TMPRSS2-ERG-SQ.

Conjugation of siRNA TMPRSS2-ERG Can Be Extended to Solanesol by Cu-Free Click Chemistry. With the intent

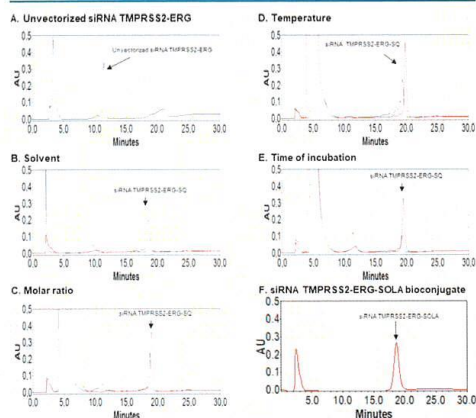


Figure 1. HPLC chromatograms of the bioconjugates after optimization of the Cu-free click chemistry. (A) Chromatograms of the unvectorized siRNA TMPRSS2-ERG showing that the elution time is around 12 min. (B) The siRNA TMPRSS2-ERG was dissolved in water; the squalene was added in the presence of DMF/MeOH (black chromatogram) or in DMSO/acetone (red chromatogram). For both solvents, the elution time of the bioconjugate is around 18 min but the yield is higher when the DMSO/acetone mixture (solvent used for further synthesis). (C) The siRNA TMPRSS2-ERG was added to squalene in a molar ratio of 1:5 (black chromatogram) or 1:50 (red chromatogram), respectively. For both molar ratios, the elution time of the bioconjugate is around 18 min, but the yield is higher when the molar ratio of 1:50 is applied. (D) The siRNA TMPRSS2-ERG was incubated with the squalene at 37 °C (black chromatogram) or at room temperature overnight (red chromatogram). The formation of byproducts was observed at 37 °C whereas they are quasi absent at room temperature. (E) The siRNA TMPRSS2-ERG was incubated with squalene for 4 h (black chromatogram) or overnight (red chromatogram). The elution time of the bioconjugate is around 18 min and the yield increased when the reaction held overnight. (F) The same parameters of the reaction were applied to bioconjugate siRNA TMPRSS2-ERG to SOLA and the elution time of the resulting bioconjugate was found to be around 18 min.

Table 1. Comparison of Areas under the Curve (AUC) of Unconjugated siRNA TMPRSS2-ERG vs Bioconjugate siRNA TMPRSS2-ERG-SQ Applying Different Cu-Free Click Chemistry Conditions^a

chromatogram	solvent of reaction	peaks	retention time	AUC	% area
A. Black chromatogram	H ₂ O/DMF/MeOH	Unconjugated siRNA TMPRSS2-ERG	9.5	2540093	72.0
A. Black chromatogram	H ₂ O/DMF/MeOH	Bioconjugate siRNA TMPRSS2-ERG-SQ	18.5	987935	28.0
A. Red chromatogram	H ₂ O/DMSO/Acetone	Unconjugated siRNA TMPRSS2-ERG	10.0	631597	10.1
A. Red chromatogram	H ₂ O/DMSO/Acetone	Bioconjugate siRNA TMPRSS2-ERG-SQ	18.5	5438762	87.4
	molar ratio of the reaction siRNA:SQ				
B. Black chromatogram	1:5	Unconjugated siRNA TMPRSS2-ERG	11.1	2197501	27.0
B. Black chromatogram	1:5	Bioconjugate siRNA TMPRSS2-ERG-SQ	18.7	5952826	73.0
B. Red chromatogram	1:50	Unconjugated siRNA TMPRSS2-ERG	12.6	347874	3.2
B. Red chromatogram:	1:50	Bioconjugate siRNA TMPRSS2-ERG-SQ	19.00	10249683	95.5
	temperature of the reaction				
C. Black chromatogram	37 °C	Unconjugated siRNA TMPRSS2-ERG	11.0	228551	4.8
C. Black chromatogram	37 °C	Bioconjugate siRNA TMPRSS2-ERG-SQ	19.4	3516956	73.6
C. Red chromatogram	Room temperature	Unconjugated siRNA TMPRSS2-ERG	10.4	193924	1.7
C. Red chromatogram	Room temperature	Bioconjugate siRNA TMPRSS2-ERG-SQ	19.8	10942393	96.0
	incubation time of the reaction				
D. Black chromatogram	4 h	Unconjugated siRNA TMPRSS2-ERG	19.2	2386118	33.5
D. Black chromatogram	4 h	Bioconjugate siRNA TMPRSS2-ERG-SQ	11.3	4742813	66.5
D. Red chromatogram	12 h	Unconjugated siRNA TMPRSS2-ERG	12.6	165802	1.6
D. Red chromatogram	12 h	Bioconjugate siRNA TMPRSS2-ERG-SQ	19.0	10108474	97.3

^aThe AUC of the chromatograms represented in Figure 1 has been calculated and the % of these areas is directly correlated to the yield of the reaction. Black chromatograms represent the not-yet-optimized reaction and red chromatograms represent the conditions where the desired bioconjugate siRNA TMPRSS2-ERG-SQ show a yield of $\sim \geq 90\%$.

to broaden the conjugation of siRNA to other polyisoprenoids, the SOLA, a more lipophilic compound, was chemically linked to the siRNA TMPRSS2-ERG by the Cu-free click chemistry approach. The bioconjugation of the siRNA TMPRSS2-ERG to SOLA was performed with the parameters previously described. The only difference is that the incubation time was extended to 18 h (vs 12 h for SQ) to obtain the complete conversion of siRNA TMPRSS2-ERG into the siRNA TMPRSS2-ERG-SOLA bioconjugate (Figure 1F). MALDI-TOF MS analysis confirmed the molecular weight of the expected bioconjugate (7830 Da, Figure SI 5).

Polyisoprenoid Conjugated siRNA TMPRSS2-ERG Self-Assemble into Stable Nanoobjects over Time with Different Shapes. The bioconjugates, whether annealed with the antisense strand of the siRNA TMPRSS2-ERG before or after the click chemistry step, were nanoprecipitated and the size of each nanoformulation was investigated by dynamic light scattering (DLS). Table 2 shows the data concerning the size, the polydispersity Index (PDI), as well as the zeta potential.

Interestingly, the bioconjugate siRNA TMPRSS2-ERG-SOLA was able to form nanoobjects similarly to siRNA TMPRSS2-ERG-SQ, whether the annealing with the antisense strand occurred before (Hb) or after (Ha) the bioconjugation. Herein, we observed that the size of the nanoparticles was stable over 3 weeks for all the studied nanoformulations. The PDI between 0.2 and 0.32 reflected the heterogeneity of the formulations which was observed also by others for macromolecules such as oligonucleotides.^{23,24}

Cryo-TEM analysis was performed on the same day of the nanoprecipitation and showed that the shape differs from one formulation to another (Figure 2). For squalene, when the annealing of both siRNA strands was performed before the conjugation (Hb), the cryo-TEM images showed spherical nanoobjects of about 100 nm surrounded by poorly defined objects, which may suggest that the siRNA could be exposed

outside of the nanoparticle (Figure 2A, dashed arrows). However, round and compact nanostructures were observed when the annealing was done after the bioconjugation (Ha) (Figure 2B). The formulation of the NPs siRNA TMPRSS2-ERG-SOLA for which the hybridization occurs before the conjugation (Hb) presented a well-defined object (Figure 2C). In contrast, when the formulation of the NPs siRNA TMPRSS2-ERG-SOLA was hybridized after the bioconjugation (Ha) a poorly defined nanoobject was observed evoking, for this formulation, the presence of micelles or aggregates (Figure 2D, dashed arrows).

Vectorized siRNA Is as Efficient as the Unvectorized siRNA in VCaP Cell Line for TMPRSS2-ERG Inhibition.

The annealing of both strands of the siRNA TMPRSS2-ERG was performed before (Hb) or after (Ha) the bioconjugation of the sense strand to SQ or SOLA; then, the bioconjugate was nanoprecipitated. Consequently, 4 nanoformulations (siRNA TMPRSS2-ERG-SQ Hb NPs, siRNA TMPRSS2-ERG-SQ Ha NPs, siRNA TMPRSS2-ERG-SOLA Hb NPs, siRNA TMPRSS2-ERG-SOLA Ha NPs) were tested for their ability to inhibit the TMPRSS2-ERG fusion oncogene transcriptional products in VCaP prostate cancer cell line over time (48, 72, and 96 h). Previously, we showed that the squalene based siRNA nanoparticles were not able to enter spontaneously into the cells without any cationic compound,^{11,14,25} thus, SQ/SOLA based siRNA TMPRSS2-ERG nanoparticles as well as the unvectorized siRNA TMPRSS2-ERG were transfected into VCaP cells by using lipofectamine iMAX. After 48 and 96 h, all nanoformulations were able to inhibit TMPRSS2-ERG products at both the mRNA and protein levels, similarly to the free siRNA TMPRSS2-ERG (Figure 3A,C for mRNA levels and Figure 3D,F for protein levels). Of note, at 72 h, when annealing of both strands occurred before the conjugation either to SQ or to SOLA, the inhibitory efficacy at mRNA level was slightly decreased, but this was not reflected at the protein

Table 2. Physicochemical Characterization of siRNA TMPRSS2-ERG-SQ/SOLA NPs by DLS Analysis^a

nanoparticle formulations	day	size (nm) \pm SD	PDI \pm SD	zeta potential (mV) \pm SD
A. siRNA TMPRSS2-ERG-SQ Hb NPs	0	337 nm \pm 71	0.27 \pm 0.00	-51 mV \pm 6
	7	358 nm \pm 12	0.26 \pm 0.04	
	14	342 nm \pm 41	0.25 \pm 0.01	
	21	331 nm \pm 2	0.25 \pm 0.01	
B. siRNA TMPRSS2-ERG-SQ Ha NPs	0	244 nm \pm 34	0.23 \pm 0.02	-48 mV \pm 1
	7	236 nm \pm 32	0.24 \pm 0.02	
	14	247 nm \pm 31	0.22 \pm 0.02	
	21	295 nm \pm 84	0.24 \pm 0.00	
C. siRNA TMPRSS2-ERG-SOLA Hb NPs	0	318 nm \pm 20	0.22 \pm 0.04	-61 mV \pm 3
	7	296 nm \pm 2	0.23 \pm 0.00	
	14	267 nm \pm 21	0.20 \pm 0.02	
	21	333 nm \pm 47	0.25 \pm 0.03	
D. siRNA TMPRSS2-ERG-SOLA Ha NPs	0	377 nm \pm 64	0.29 \pm 0.01	-51 mV \pm 2
	7	379 nm \pm 21	0.32 \pm 0.04	
	14	399 nm \pm 49	0.33 \pm 0.01	
	21	405 nm \pm 43	0.30 \pm 0.01	

^aSize, polydispersity index, and zeta potential of the four different nanoparticles formulations monitored over time (3 weeks). Samples were analyzed at 10 μ M in H₂O. Three measurements of 5 min for each sample were performed and the average diameter \pm S.D. of three independent samples was calculated.

levels (Figure 3B for mRNA levels and Figure 3E for protein levels). Noteworthy, the inhibitory activity of the siRNA NPs annealed with the antisense strand before or after the bioconjugation was comparable among all the different formulations regardless the incubation time of the transfection (Figure 3).

Moreover, siRNA Control nanoformulated or unvectorized did not affect TMPRSS2-ERG mRNA and protein expression when cells were transfected for 72 h (Figure SI 6 A and Figure SI 6 B for mRNA levels and Figure SI 6 C and Figure SI 6 D for protein levels).

Influence of the siRNA Annealing and the Length of the Isoprenoid Chain on the Antineoplastic Activity. As shown in Figure 4, two out of the four nanoformulations injected into mice bearing xenografted VCaP tumors showed significant antineoplastic activity. Especially, siRNA TMPRSS2-ERG-SQ Ha NPs and siRNA TMPRSS2-ERG-SOLA Hb NPs significantly inhibited tumor growth of \sim 60% compared to mice treated with saline solution ($p < 0.001$). In contrast, a nonsignificant difference was observed after treatment with siRNA TMPRSS2-ERG-SQ Hb NPs and siRNA TMPRSS2-ERG-SOLA Ha NPs. In addition, when mice were treated with nanoformulated siRNA Control-SQ Hb NPs, siRNA Control-SQ Ha NPs, siRNA Control-SOLA Hb NPs, siRNA Control-

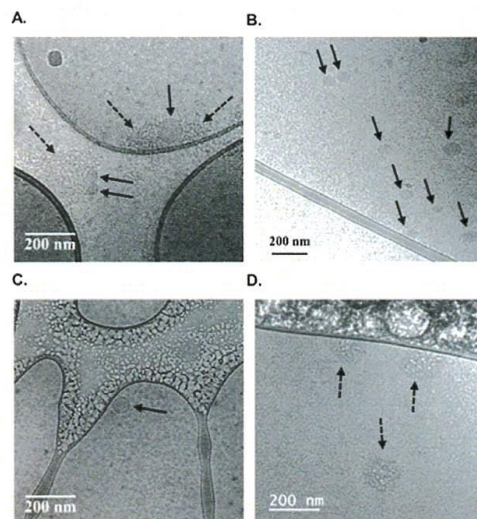


Figure 2. CryoTEM analysis of the siRNA TMPRSS2-ERG-SQ/SOLA NPs. CryoTEM images of (A) siRNA TMPRSS2-ERG-SQ Hb NPs; (B) siRNA TMPRSS2-ERG-SQ Ha NPs; (C) siRNA TMPRSS2-ERG-SOLA Hb NPs; (D) siRNA TMPRSS2-ERG-SOLA Ha NPs. Black arrows indicate the nanoobjects detected, dashed arrows indicate the nonwell-defined objects. The scale bar used is 200 nm. Ha: hybridization after the bioconjugation, Hb: hybridization before the bioconjugation.

SOLA Ha NPs, or unvectorized siRNA TMPRSS2-ERG, tumor growth was not significantly affected (Figure SI 6 E).

Biodistribution Study Reveals the Preferential Uptake of siRNA-SQ Ha NPs in Tumor. To explain the different antineoplastic effect of the nanoformulations obtained by the same method of hybridization (Ha), a biodistribution study was performed on two formulations, one efficient for tumor inhibition (siRNA-SQ Ha NPs) and the other lacking antitumor activity (siRNA-SOLA Ha NPs). When total radioactivity was counted, all treatment accumulated similarly mainly in the liver, then in kidney, urine, blood and tumors, and to even less extent in feces (Figure SI 7).

Interestingly, after RNA extraction that reflects the ³²P probe linked to the siRNA, the biodistribution changes within the organs and mainly in the tumor. An accumulation of the siRNA within the prostate tumor was observed when the siRNA NP was formulated with the squalene, whereas when formulated with SOLA it accumulated similarly to the unvectorized siRNA (Figure 5A). Moreover, these results were confirmed by electrophoresis gel performed on the extracted RNA where only the signal of the ³²P-siRNA-SQ Ha NPs was detectable at short time (3 h, Figure 5B, lane 3) and also at a longer time (16 h, Figure 5B, lane 7).

A major fraction of ³²P present in the extracted RNA was recovered in blood and in two organs of the excretory system: the liver and kidney. Notably, after 3 h we observed an excretion of siRNA through the feces and urine especially for the unvectorized siRNA (Figure 5A). The excretion of unvectorized siRNA and SOLA based nanoformulation increased after 16 h in the urine, while SQ-based nano-

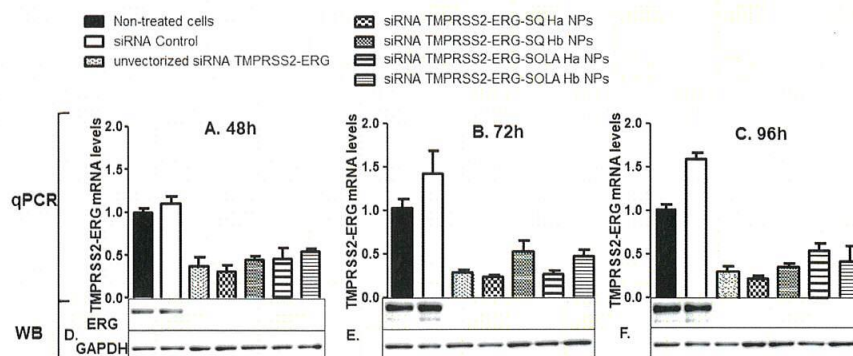


Figure 3. In vitro inhibitory efficacy of siRNA TMPRSS2-ERG-SQ/SOLA NPs. VCaP cells were transfected at 50 nM concentration with siRNA Control; unvectorized siRNA TMPRSS2-ERG; siRNA TMPRSS2-ERG-SQ Ha NPs; siRNA TMPRSS2-ERG-SQ Hb NPs; siRNA TMPRSS2-ERG-SOLA Ha NPs; siRNA TMPRSS2-ERG-SOLA Hb NPs. After 48 h (A and D), 72 h (B and E), and 96 h (C and F), cells were harvested, then mRNA and proteins were extracted to be analyzed for gene (A, B, C) and protein (D, E, F) knockdown. All nanoformulations inhibited TMPRSS2-ERG products similarly to the unvectorized siRNA TMPRSS2-ERG at either mRNA or protein levels over time (48, 72, and 96 h). The unvectorized siRNA is the siRNA TMPRSS2-ERG not bearing the vectors SQ or SOLA but transfected in the presence of Lipofectamine iMAX. Ha: hybridization after the bioconjugation, Hb: hybridization before the bioconjugation, qPCR: quantitative PCR, WB: Western blot.

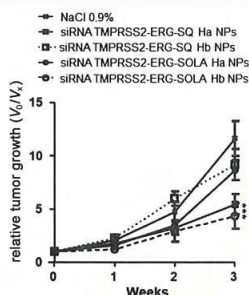


Figure 4. In vivo antineoplastic activity of siRNA TMPRSS2-ERG-SQ/SOLA NPs. Mice ($n = 5$ /group) bearing VCaP cells xenografted tumors were treated intravenously twice per week either with saline solution (NaCl 0.9%); siRNA TMPRSS2-ERG-SQ Hb NPs; siRNA TMPRSS2-ERG-SOLA Hb NPs; siRNA TMPRSS2-ERG-SQ Ha NPs and siRNA TMPRSS2-ERG-SOLA Ha NPs dispersed in 100 μ L of 0.9% NaCl solution at the cumulative dose of 1 mg/kg/mouse. The nanoformulations of siRNA TMPRSS2-ERG-SQ Ha NPs and siRNA TMPRSS2-ERG-SOLA Hb NPs significantly inhibited tumor growth of $\sim 60\%$ compared to mice treated with saline solution ($p < 0.001$), while siRNA TMPRSS2-ERG-SQ Hb NPs and siRNA TMPRSS2-ERG-SOLA Ha NPs only slightly inhibited tumor growth without significant difference. Ha: hybridization after the bioconjugation, Hb: hybridization before the bioconjugation; V_0/V_x = Volume of the tumor at day 0 of the treatment/Volume of the tumor at day X (X corresponds to the day of measurement of tumor volume during treatments, NaCl, siCT, and siTMPRSS2-ERG vectorized or not).

formulation was still observed upstream in the kidney suggesting a longer retention time when the SQ was used as a vector (data not shown).

Clickable siRNA-SQ Nanoparticles Approach May Represent a New Platform for siRNA Delivery. By applying the same parameters (molar ratio, solvents, temperature, and incubation time), the Cu-free click chemistry was performed to chemically link siRNA RET/PTC1 to SQ. A complete conversion of the initial siRNA RET/PTC1 (black

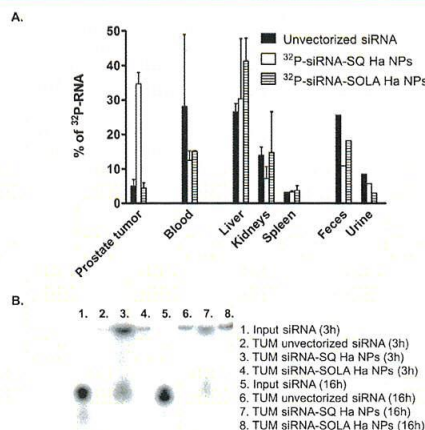


Figure 5. Biodistribution of vectorized or unvectorized ^{32}P labeled siRNA in mice bearing VCaP xenografts. Two mice bearing VCaP xenografted tumors were injected with 5 million cpm of unvectorized ^{32}P labeled siRNA or ^{32}P -siRNA-SQ Ha NPs or ^{32}P -siRNA-SOLA Ha NPs. (A) After 3 h mice were sacrificed, and tumors, organs, feces, and urine were collected. Total RNA was extracted from each organ and radioactivity present in the purified RNA was evaluated by Cherenkov counting. Results are expressed as the percentage of radioactivity in extracted RNA from each sample relatively to the total radioactivity of extracted RNA. Increased accumulation of radioactivity was found in tumors treated with ^{32}P -siRNA-SQ Ha NPs compared to unvectorized ^{32}P labeled siRNA or ^{32}P -siRNA-SOLA Ha NPs. (B) To assess the presence of intact ^{32}P -siRNA in extracted RNA, electrophoresis gel was performed on RNA extracted from tumors treated for 3 and 16 h with unvectorized ^{32}P labeled siRNA or ^{32}P -siRNA-SQ Ha NPs or ^{32}P -siRNA-SOLA Ha NPs. Tumors treated with ^{32}P -siRNA-SQ Ha NPs showed the presence of intact ^{32}P -siRNA mainly at 3 h and to a lesser extent at 16 h. Lanes 1 and 5 represent the input radiolabeled ^{32}P -siRNA. Ha: hybridization after the bioconjugation.

chromatogram) into the desired bioconjugate siRNA RET/PTC1-SQ (red chromatogram) with a high yield and absence of byproducts was observed (Figure SI 8A) and the nature of the bioconjugate was verified by MALDI-TOF MS (Figure SI 8B). The bioconjugate siRNA RET/PTC1-SQ was then annealed (Ha) and nanoprecipitated as previously described for siRNA TMPRSS2-ERG-SQ Ha NPs. As shown in Table 3,

Table 3. Physicochemical Characterization of siRNA RET/PTC1-SQ Ha NPs by DLS Analysis^a

nanoparticle formulation	day	size (nm) ± SD	PDI ± SD	zeta potential (mV) ± SD
siRNA RET/PTC1-SQ Ha NPs	0	232 ± 32	0.18 ± 0.03	-37 ± 7
	7	228 ± 32	0.18 ± 0.03	
	14	232 ± 35	0.16 ± 0.03	
	21	220 ± 31	0.17 ± 0.05	
	30	227 ± 46	0.18 ± 0.05	

^aSize and zeta potential of the nanoparticles were measured over 30 days. Each measure is the mean of 3 independent formulations and 3 independent technical measurements. Both size and zeta potential remain stable over time.

the DLS analysis revealed that the bioconjugate siRNA RET/PTC1-SQ was able to self-assemble into nanoparticles of ~230 nm in size with a PDI of ~0.175. The size and PDI of these nanoparticles are similar to the values obtained with the previous nanoformulations harboring the siRNA TMPRSS2-ERG sequence and in accordance with other studies.^{23,24} Herein, it was observed that the size of the nanoparticles was stable for at least 4 weeks.

Moreover, siRNA RET/PTC1-SQ Ha NPs were tested for their ability to inhibit the RET/PTC1 fusion oncogene transcriptional products in BHP 10-3 and TPC-1 papillary thyroid carcinoma cell lines for 24 and 48 h, respectively. Results have shown that siRNA RET/PTC1-SQ Ha NPs were as efficient as the unvectorized siRNA to inhibit the RET/PTC1 mRNA levels in both cell lines after 24 and 48 h (Table 4). However, the inhibition of the fusion oncogene RET/PTC1 observed was more important in BHP 10-3 cell line than in TPC-1 cells.

DISCUSSION

The aim of this study was to introduce a new targeted therapy for cancer patients with fusion oncogenes. In previous publications, we were able to develop specific siRNA against fusion oncogenes such as TMPRSS2-ERG found in 50% of patients with prostate cancers and RET/PTCs found in over 60% of patients with papillary thyroid carcinomas.^{10,11,14} Despite the efficacy of inhibiting the fusion oncogenes by siRNA-SQ NPs in vivo, the yield of the bioconjugation was low and poorly reproducible. In the present study, a new approach

is developed to protect the siRNA from degradation by using conjugation to polyisoprenoids via the Cu-free click chemistry. Indeed, Cu-free catalyzed Huisgen 1,3-dipolar cycloaddition has received tremendous interest as an established synthetic route to obtain tailor-made complex materials.¹⁸ Due to the very different physicochemical nature of the starting products (highly hydrophilic siRNA and lipophilic polyisoprenoid derivatives), the four main parameters of the reaction (solvents, molar ratio, temperature, and incubation time) were modified with respect to several articles describing the Cu-free click chemistry.^{26–28} Dimethyl sulfoxide and acetone were found to be the best solvents for performing the synthesis. Their ability to dissolve both polar and apolar compounds and to establish a chemical interface favored the interaction between siRNA and squalene thus leading to the complete conversion of the starting products into the desired bioconjugates. Concerning the molar ratio of the reagents, according to the literature, an equal molar ratio is generally applied. However, this could not be applied to the conjugation of siRNA (a high molecular weight hydrophilic molecule) with low molecular weight lipophilic molecules as squalene and solanesol. Herein, we showed that a molar ratio ≥1:50 of siRNA:SQ is necessary to obtain a complete conversion into the bioconjugate siRNA-SQ. This is directly linked with the kinetics of the reaction where the higher the amount of squalene, the faster the siRNA conversion.

Thus, the Cu-free click chemistry allowed us to substantially (i) increase the synthesis yield from ~35% to >95%, (ii) avoid the formation of byproducts during the synthesis, and (iii) improve the reproducibility of the bioconjugation. Despite the fact that this procedure is easy to handle and could be used as a platform for siRNA delivery, six steps were needed to obtain nanoparticles: (1) bioconjugation of siRNA to SQ/SOLA, (2) purification of the resulting bioconjugate siRNA-SQ/SOLA, (3) lyophilization of the purified bioconjugate, (4) hybridization of the bioconjugate with the antisense strand, (5) lyophilization of the hybridized bioconjugate, followed by (6) nanoprecipitation. Therefore, in order to further simplify and speed up the process by avoiding two steps (annealing and lyophilization of siRNA), it was tested to determine whether the conjugation to squalene could be performed on already hybridized siRNA in the double-stranded form. Moreover, to increase the siRNA lipophilicity, solanesol (SOLA), a longer polyisoprenoid compound, which possesses nine isoprenyl units instead of the six found in squalene, was used with the attempt of enhancing the nanoparticle stability. In this study, we showed that this polyisoprenoid behaves similarly to the squalene, regarding the stability and the reproducibility of the nanoformulation. The four bioconjugates produced were able to form nanoparticles in water. This result was expected for the squalene bioconjugates but has never been previously reported for the SOLA.

Table 4. Efficacy of siRNA RET/PTC1-SQ Ha NPs on RET/PTC1 Fusion Oncogene Inhibition^a

treatments	RET/PTC1 mRNA relative levels in BHP 10-3 cell line		RET/PTC1 mRNA relative levels in TPC-1 cell line	
	24 h	48 h	24 h	48 h
Nontreated cells	1.00 ± 0.00	1.00 ± 0.03	1.00 ± 0.00	1.00 ± 0.00
free siRNA RET/PC1	0.37 ± 0.02	0.26 ± 0.04	0.63 ± 0.09	0.70 ± 0.02
siRNA RET/PC1-SQ Ha NPs	0.39 ± 0.03	0.28 ± 0.06	0.64 ± 0.12	0.76 ± 0.06

^aBHP 10-3 and TPC-1 cells were transfected at 50 nM concentration with unvectorized siRNA RET/PTC1 or siRNA RET/PTC1-SQ Ha NPs. After 24 and 48 h, cells were harvested; then, mRNA was extracted and analyzed by RT-qPCR. The nanoformulation inhibits RET/PTC1 mRNA expression similarly to the unvectorized siRNA RET/PTC1 in BHP 10-3 and TPC-1 cells. Ha: hybridization after the bioconjugation.

As previously described, *in vitro*, the squalene based siRNA nanoparticles were not able to enter spontaneously into the cells and need a cationic compound to enter into the cells.^{11,14} Indeed, when VCaP cells were transfected with these nanoparticles in the presence of Lipofectamine iMAX, an inhibition of TMPRSS2-ERG mRNA expression and of ERG protein content was observed. This verified that the Cu-free click chemistry reaction applied to the conjugation of siRNA TMPRSS2-ERG to squalene, and solanesol polyisoprenoids did not compromise the efficacy of the siRNA TMPRSS2-ERG regardless of when the hybridization step occurs, *i.e.*, before or after the reaction.

On the contrary, different results were pointed out *in vivo* depending on the formulation administered to mice bearing VCaP prostate cancer xenografts. As discussed in our previous papers, the discrepancy between *in vitro* and *in vivo* nanoparticle uptake is probably related to the physicochemical properties of the nanoparticles that may change *in vivo* and the different enzymatic content present in the animal environment compared to simple culture medium.^{11,14,25} We observed a preserved efficacy of the siRNA to inhibit the tumor growth when siRNA TMPRSS2-ERG-SQ NPs (strands hybridized after bioconjugation, Ha) and siRNA TMPRSS2-ERG-SOLA NPs (strands hybridized before bioconjugation, Hb) were injected to mice intravenously. Cancer proliferation is due to deregulation of several signaling pathways that can act together to increase tumor growth, therefore the inhibition of ~50–60% of tumor growth by downregulating one oncogene (ERG) with a specific siRNA is noteworthy. Notably, in clinics, siRNA is often associated with other molecules to synergize with them and to allow decreasing the doses or the schedule of administration, thus diminishing the side effects. Interestingly, it seems that the *in vivo* efficacy of the nanoparticles was related to the nature of the terpene (SQ and SOLA) and to the hybridization step, both influencing the size and the nanostructural organization of the particles in aqueous solution. In fact, nanoparticles with a compact round shape and a size less than 300 nm resulted to be efficient *in vivo* suggesting that the conformation and the size may play a role in the activity as also observed recently by Jasinski *et al.*²⁹ In addition, biodistribution studies explain the different antineoplastic activity observed between the formulations. It is noteworthy that the counting of total radioactivity within the organs contemplates the accumulation of ³²P probe whether free or linked to the siRNA. In contrast, when the radioactivity is counted after RNA extraction, only the intact ³²P-siRNA is selected and showed the preferential uptake of siRNA-SQ Ha NPs in tumor compared to siRNA-SOLA Ha NPs and unvectorized siRNA, which reflects the antineoplastic activity found for this treatment. The accumulation of the formulation within the tumors may be explained by the fact that squalene-derived nanoparticles could interact preferentially with cholesterol-rich lipoproteins such as low-density lipoproteins (LDLs). LDLs are the main source of cholesterol for the peripheral tissues; thus, uptake of LDLs is often used by rapidly proliferating cancer cells to satisfy their cholesterol needs.³⁰ Interestingly, it has been shown that squalene bioconjugates strongly interacted with LDL conferring a so-called “indirect” targeting toward tumors.¹⁷ Thus, for the formulation siRNA-SQ Hb NPs the lack of antineoplastic activity would be due to the hybridization step that modulates the nanoparticle size and conformation, preventing the interaction with LDL and consequently determining the siRNA therapeutic outcome.

In conclusion, we developed a new chemical synthesis for the linkage of siRNA to two polyisoprenoids resulting in bioconjugates able to self-assemble as nanoparticles. Moreover, we show, for the first time, the opportunity to broaden the bioconjugation of siRNA to other polyterpenes such as SOLA. This approach was also extended to other siRNAs showing that this vectorization method can be applied to different sequences maintaining the same efficacy of the unmodified siRNA *in vitro*. The ease and flexibility of the proposed methodology, as well as the improved yield of the synthesis, are believed to facilitate further translation toward “clickable” siRNA-polyisoprenoid-conjugated nanoparticles targeting genes whose overexpression results in the development of cancers or other genetic diseases.

MATERIAL AND METHODS

Chemicals. All the chemicals used were of highest analytical grade and were purchased from Sigma–Aldrich unless otherwise noted. The anhydrous solvents were dried and distilled before their use (tetrahydrofuran (THF) on Na/benzophenone) and the reactions sensitive to air or humidity were performed under nitrogen pressure. TLC was done over Merck 60 F254 plates, thickness 0.25 mm. Kägi-Mischer (*p*-anisaldehyde 50 mL, CH₃COOH 10 mL, H₂SO₄ 50 mL, EtOH 900 mL) was used for spot visualization. SiO₂ (0.063 mm) was dried for flash chromatography.

¹H and ¹³C NMR spectra were registered on a Bruker ARX 300 spectrometer. 3-Hydroxypicolinic acid (3-HPA, used as the matrix for MALDI-TOF MS, was of the highest grade available and used without further purification) was purchased from Sigma-Aldrich Co. Modified siRNAs to perform the Cu-free click chemistry reactions were purchased from Eurogentec (France). Dulbecco's modified Eagle medium (DMEM), Opti-MEM, fetal calf serum (FCS), Lipofectamine iMAX, and PCR primers were purchased from Life Technologies (Saint Aubin, France). BD Matrigel (Basement Membrane Matrix Growth Factor Reduced - Reference 356234) was purchased from Corning (Amsterdam, The Netherlands). Bio-RAD protein assay was purchased from Bio-RAD Laboratories (Marnes-la-Coquette, France). Water was purified using a Milli-Q system (Millipore, Saint Quentin en Yvelines, France).

siRNAs Used and Chemical Modifications. The siRNA targeting TMPRSS2-ERG, RET/PTC1, and the irrelevant siRNA scrambled sequence used as a control in the experiments were previously described.^{10,14}

All single-stranded RNAs were synthesized, then characterized by matrix assisted laser desorption/ionization time-of-flight mass spectrometry (MALDI-TOF MS) and purified by RP-HPLC. Single-stranded RNAs were synthesized as 19-mers with two 3'-overhanging 2'-deoxynucleotide residues to provide stabilization against nucleases as described by Tuschl *et al.*³¹ To allow functionalization, a dibenzocyclooctyne (DBCO) reactive group was introduced at the 5'-end of the sense strand of each siRNA sequence through a *N*-(hexamethylenyl)-6-oxohexanamide spacer (C₆) (Scheme 1 (1)), purchased from Eurogentec, France). To generate siRNA from RNA single strands, equimolar amounts of both forward and reverse strands were annealed in annealing buffer [30 mM HEPES-KOH (pH 7.4), 2 mM Mg acetate, 100 mM K acetate] for 2 min at 95 °C and then kept 1 h at room temperature before storing at 20 °C.

Synthesis of Azido-Squalene and Azido-Solanesol. Azido squalene (SQ-N₃) (Scheme 1 (2c) and Figure SI 1A) was obtained by sequential mesylation and S_N2 displacement with sodium azide of the known alcohol (Scheme 1 (2c))

available in turn from squalene (SQ)³² (Figure SI 1A). Similarly, azido-solanesyl (SOLA-N₃, Scheme 1 (3c) and Figure SI 1A) was obtained from commercially available solanesol (SOLA) by bromination with PBr₃ in Et₂O followed by nucleophilic displacement of the bromine by sodium azide. The SOLA-N₃ (Scheme 1 (3c)) was obtained in 43% yield together with a minor amount of S_N2' product (15%) (Figure SI 1A).

¹H and ¹³C NMR spectra of azido-squalene 2c are reported in Figure SI 1B,C, respectively. ¹H and ¹³C NMR spectra of solanesyl azide 3c are reported as Figure SI 1D,E, respectively.

Bioconjugation of siRNAs to Azido-Squalene and Azido-Solanesol. Before any synthesis was undertaken, precautions were applied to avoid degradation of siRNA by contamination of ribonucleases. The bioconjugates siRNA TMPRSS2-ERG-squalene (siRNA TMPRSS2-ERG-SQ) (Scheme 1 (4)) and siRNA TMPRSS2-ERG-solanesol (siRNA TMPRSS2-ERG-SOLA) (Scheme 1 (5)) were obtained by the 1,3-dipolar cycloaddition of azides and dibenzocyclooctynes, also known as Cu-free click chemistry.

Investigation of the nature of the solvents, the temperature, the incubation time, and the molar ratios between the SQ-N₃ or the SOLA-N₃ and the modified sense strand (DBCO) of the siRNA TMPRSS2-ERG was assessed to obtain the best parameters of the synthesis giving an high yield of the desired bioconjugate.

The protocol to obtain the bioconjugates siRNA TMPRSS2-ERG-SQ and siRNA TMPRSS2-ERG-SOLA is described as follows. 1 nmol of the 5'-end modified sense strand DBCO-C₆ of the siRNA TMPRSS2-ERG (1 mg/mL in DNase/RNase-free water) was mixed with 50 nmol of SQ-N₃ or SOLA-N₃ (1 mg/mL in DMSO) in a glass vial. DMSO (286 μL) and acetone (65 μL) were added to the solution and incubated at room temperature for 12 h under stirring to obtain the bioconjugate siRNA TMPRSS2-ERG-SQ or 18 h to obtain the bioconjugate siRNA TMPRSS2-ERG-SOLA.

The progress of the reactions as well as the purification from the excess of unconjugated SQ and SOLA were performed by RP-HPLC on a polymeric column as described below. The coupling yield was determined based on the UV absorbance of the species. The identity of the bioconjugates siRNA TMPRSS2-ERG-SQ and siRNA TMPRSS2-ERG-SOLA was confirmed by MALDI-TOF mass spectrometry. Three independent reactions were carried out to verify the reproducibility of the synthesis. Purified products were lyophilized, then solubilized into RNase free water at the desired molar concentration.

To obtain the bioconjugate siRNA RET/PTC1-SQ, the protocol of Cu-free click chemistry and the processes described above were applied.

Hybridization of Both Strands of the siRNAs. The hybridization of both strands of the siRNA TMPRSS2-ERG was performed before (Hb) or after (Ha) the bioconjugation of the sense strand to SQ or SOLA according to the manufacturer's protocol. When the annealing of the driver strand was performed after the bioconjugation, the purified and lyophilized bioconjugates siRNA TMPRSS2-ERG-SQ and siRNA TMPRSS2-ERG-SOLA were used. For the siRNA RET/PTC1, the annealing was performed only after (Ha) the bioconjugation to squalene.

Purification of siRNA-SQ/SOLA Bioconjugates via HPLC Equipment. The HPLC separation was performed on a Waters high-performance liquid chromatography system

(Waters 2695) equipped with a photodiode array detector (Waters 2996) whose wavelength range was between 190 and 800 nm, a pump (model Waters 600 controller), and an automatic injector (Waters 717 autosampler). The stationary phase consisted of a nonporous, alkylated polystyrene divinylbenzene column (Hamilton 10 μm, 4.6–250 mm, PEEK) protected by precolumn (Hamilton). Empower was used for data acquisition. Flow rate was 1.2 mL/min. Injection volumes were 100 μL. A gradient of mobile phases A and B was applied. Mobile phase A was composed of 0.2 M TEAA (5%), pH 7.0. with 5% acetonitrile (v/v), water 90%, and mobile phase B consisted of 95% acetonitrile with 5% TEAA (v/v), 5% of water. The gradient conditions applied for purification were as follows: 0–8 min linear gradient from 0% to 24% of B; 8–16 min linear gradient from 24% to 90% of B; 16–18 min linear gradient from 90% to 100% of B; 18–30 min 100% of B; 30–32 min linear gradient from 100% of B to 100% of A, and 32–42 min re-equilibration with 100% of A. The chromatograms were recorded at a wavelength of 258 nm. Quantification of peaks was performed by integration of peak areas. Bioconjugates siRNA-SQ/SOLA were purified by manual peak collection. Fractions were collected for 3 min, corresponding to a fraction volume of 3.6 mL, and then lyophilized. All lyophilized siRNA fractions were reconstituted in DEPC-treated water.

MALDI-TOF Mass Spectrometry. A MALDI-TOF/TOF UltrafleXtreme mass spectrometer (Bruker Daltonics, Bremen) was used for all experiments. Mass spectra were obtained in linear positive ion mode. The laser intensity was set just above the ion generation threshold to obtain peaks with the highest possible signal-to-noise (S/N) ratio without significant peak broadening. All data were processed using the FlexAnalysis software package (Bruker Daltonics).

Preparation and Characterization of Nanoparticles siRNA-SQ and siRNA-SOLA. Nanoparticles siRNA-SQ or siRNA-SOLA were prepared by nanoprecipitation in acetone/water. One phase (aqueous or organic) was slowly added to the other, under magnetic stirring, then acetone was completely evaporated using nitrogen flux to obtain an aqueous suspension of pure siRNA-SQ or siRNA-SOLA nanoassemblies at 10 μM concentration. Control siRNA-SQ/SOLA NPs were prepared using the same protocol as described above.

Then, the hydrodynamic diameter (nm) was measured by dynamic light scattering (DLS) using the Nano Brook 90 Plus PALS with a DLS angle of 90° (Brookhaven Instrument) and the zeta potential (mV) was measured using a Zetasizer 4 (Malvern Instrument). Samples were analyzed at 10 μM concentration in H₂O. Three measures of 5 min for each sample were performed and the average diameter ± SD of three independent samples was calculated. The cryogenic transmission electron microscopy (cryo-TEM) was performed with the JEOL 2100 electron microscope at the Electronic Microscopy Platform (IBPS/Institut de Biologie Paris-Seine, Université P. et M. Curie, Paris, FRANCE). A 4 μL droplet of the samples (concentration of 2.2 mg/mL) hybridized before (Hb) or after the synthesis (Ha) [siRNA TMPRSS2-ERG-SQ Hb NPs, siRNA TMPRSS2-ERG-SQ Ha NPs, siRNA TMPRSS2-ERG-SOLA Hb NPs, siRNA TMPRSS2-ERG-SOLA Ha NPs] was deposited on a carbon-coated copper grid. Excess of the liquid was removed with blotting filter paper, and the samples were quickly vitrified by plunging them into liquid ethane using a guillotine-like frame. The samples were then transferred to a cryo-sample holder. Observations were

made at an acceleration voltage of 200 kV under a low electron dose. Analysis was performed with ImageJ software.

Cell Lines and Cell Culture. The VCaP is a prostate cancer cell line expressing TMPRSS2-ERG fusion oncogene. BHP 10-3 and TPC-1 are both papillary thyroid carcinoma cell lines harboring the fusion oncogene RET/PTC1. All cell lines were maintained at 37 °C in an atmosphere of 5% CO₂ and 95% humidity in Dulbecco's Modified Eagle Medium (DMEM) supplemented with FCS, 100 units/mL penicillin, and 100 µg/mL streptomycin.

In Vitro Cell Transfection. Our previous studies showed that NPs siRNA-SQ cannot spontaneously enter in vitro,^{10,13} therefore, Lipofectamine iMAX was used to assess the efficacy of siRNA bioconjugates compared to unvectorized siRNA and to decrypt if the conjugation was affecting the kinetic of the gene down regulation.

Briefly, 8×10^5 VCaP cells were seeded in six-well plates containing DMEM supplemented with 10% FCS, penicillin (100 U/mL), and streptomycin (10 µg/mL) and transient transfections were carried out using Lipofectamine RNAiMAX transfecting agent according to manufacturer's instructions. The following compounds were transfected at 50 nM concentration: (1) siRNA control; (2) unvectorized siRNA TMPRSS2-ERG; (3) siRNA TMPRSS2-ERG-SQ Hb NPs; (4) siRNA TMPRSS2-ERG-SOLA Hb NPs; (5) siRNA TMPRSS2-ERG-SQ Ha NPs; and (6) siRNA TMPRSS2-ERG-SOLA Ha NPs. After 48, 72, and 96 h, cells were harvested, and then mRNA and proteins were extracted to be analyzed for gene and protein knockdown. Each experiment was performed at least twice and in duplicate. Nanoparticles siRNA Control-SQ/SOLA Ha/b were also assessed as negative controls up to 72 h.

The papillary thyroid carcinoma cell lines BHP 10-3 and TPC-1 were also transfected with (1) siRNA RET/PTC-1 and (2) siRNA RET/PTC-1-SQ Ha NPs at 50 nM concentration.

Briefly, 4×10^5 BHP 10-3 and TPC-1 cells were seeded in six-well plates containing OPTIMEM and transient transfections were carried out using Lipofectamine-2000 transfecting agent according to manufacturer's instructions. Four hours later, the medium was replaced by DMEM supplemented with 10% FCS, penicillin (100 U/mL), and streptomycin (10 µg/mL). Twenty-four hours and 48 h later, cells were harvested and mRNA was extracted to be analyzed for gene expression. Each experiment was performed at least twice and in duplicate.

mRNA Extraction and Real Time PCR (RT-qPCR) Experiments. Total RNA was extracted from VCaP, BHP 10-3, and TPC-1 cells using RNeasy mini-kit (Qiagen, Courtaboeuf, France). First-strand cDNA was generated with M-MLV RT buffer pack (Invitrogen, Charbonnières-les-Bains, France). Real-time PCR (qPCR) was carried out with StepOnePlus PCR System (AB Applied Biosystems, Villebon-sur-Yvette, France) using Maxima Syber Green Rox qPCR master Mix (Thermo Scientific, Villebon-sur-Yvette, France) according to manufacturer's instructions. Samples were run in triplicate; gene regulation was determined by $2^{-\Delta\Delta C_t}$ method and normalized to GAPDH levels. For knockdown experiments, results are given as relative mRNA levels compared to nontreated cells.

Immunoblotting. Total protein extracts were obtained using M-PER reagent (Thermo Fisher Scientific Courtaboeuf, France) supplemented with a protease inhibitor cocktail (Roche, Neuilly sur Seine, France). Proteins were titrated by Bio-RAD Assay according to manufacturer's instructions. Samples were then loaded on 10% polyacrylamide gel

(NuPAGE Bis Tris Mini Gels 10%, Life technologies, Saint-Aubin, France) and proteins were transferred using the iBlotDry Blotting System (Invitrogen, France). Membranes were incubated overnight at 4 °C with either of the following primary antibodies: monoclonal rabbit ERG (EPR 3864 (2); 1:500. Abcam Biochemicals, Paris, France). Monoclonal mouse GAPDH-HRP (1:1000. Cell Signaling technology, Saint Quentin en Yvelines, France. ref: 3683) was used as internal control. Blots were then washed and incubated with corresponding secondary anti-rabbit antibody conjugated to HRP (horseradish peroxidase, 1:3000. Cell Signaling Technology). Bands were visualized by enhanced chemiluminescence reagent (Invitrogen, France).

Animal Studies. All animal experiments and the use of VCaP cells were approved by the institutional Ethics Committee of Animal Experimentation (CEEA) and research council (Integrated Research Cancer Institute in Villejuif, IRCIV), registered in the French Ministry of Higher Education and Research (Ministère de l'Enseignement Supérieur et de la Recherche; MESR) under the authorization number CEEA IRCIV/IGR no 26:94-226, no: 2011-09 and carried out according to French laws and regulations under the conditions established by the European Community (Directive 2010/63/UE). Investigation has been conducted in accordance with the ethical standards and according to the Declaration of Helsinki. All efforts were made to minimize animal suffering: administration of treatments was performed under isoflurane anesthesia and animals were sacrificed by CO₂. Five-week-old SCID/Beige mice were purchased from Harlan Laboratory. All animals were housed in sterilized laminar flow caging system. Food, water, and bedding were sterilized before being placed in the cages. Food and water were given ad libitum.

In Vivo Efficiency and Biodistribution of siRNA TMPRSS2-ERG Polyterpene Nanoparticles. VCaP cells were subcutaneously inoculated [10×10^6 cells/mouse in PBS (50 µL) mixed with Matrigel (50 µL)]. When tumors reached about 50 mm³, mice ($n = 5$ /group) were treated intravenously (i.v.) twice per week with either (1) saline solution (NaCl 0.9%); (2) siRNA TMPRSS2-ERG (or Control)-SQ Hb NPs; (3) siRNA TMPRSS2-ERG (or Control)-SOLA Hb NPs; (4) siRNA TMPRSS2-ERG (or Control)-SQ Ha NPs; (5) siRNA TMPRSS2-ERG (or Control)-SOLA Ha NPs; and (6) unvectorized siRNA TMPRSS2-ERG dispersed in 100 µL of 0.9% NaCl solution at the rate of 0.5 mg/kg for the first injection and 0.1 mg/kg for the rest of the injections (cumulative dose = 1.1 mg/kg/mouse). The administrated dose and schedule of treatments were selected based on previously published studies.^{10,11,13-15} Mice were monitored daily for tumor growth and body weight and then sacrificed at the end of the experiment (day 22) or when tumors reached a volume of 1000 mm³.

For biodistribution studies, the groups of mice treated with unvectorized siRNA, siRNA-SQ Ha NPs, and siRNA-SOLA Ha NPs received unvectorized ³²P-labeled siRNA or ³²P-siRNA-SQ Ha NPs or ³²P-siRNA-SOLA Ha NPs, respectively (5 million cpm), as the last injection. After 3 h, mice were sacrificed and excretory organs, urine, feces, and tumor were collected, and total radioactivity was counted by Cherenkov counting. Then, total RNA was extracted from each organ, urine, feces, and tumor, and radioactivity present in the purified RNA was evaluated by Cherenkov counting (mean ± SD). To assess the presence of intact ³²P-siRNA in extracted RNA, electrophoresis gel was performed on RNA extracted from tumors treated for 3

and 16 h with unvectorized ^{32}P labeled siRNA or ^{32}P -siRNA-SQ Ha NPs or ^{32}P -siRNA-SOLA Ha NPs.

Statistical Analysis. All data are presented as mean \pm standard deviation (SD). To compare the effects of the different treatments on tumor growth inhibition in mice, two-way ANOVA analysis followed by Bonferroni post-tests for multiple comparisons was applied using "Prism" software. $p < 0.05$ was considered as a statistically significant level.

■ ASSOCIATED CONTENT

Supporting Information

The Supporting Information is available free of charge on the ACS Publications website at DOI: 10.1021/acs.bioconjchem.8b00205.

Chemical synthesis and characterization of azido-squalene and azido-solanesol; Molar ratios, incubation time, temperature and solvent conditions of each reaction; MALDI-TOF MS spectrum; HPLC chromatograms; Biodistribution of total ^{32}P radioactivity (PDF)

■ AUTHOR INFORMATION

Corresponding Author

*E-mail: liliane.massade@gustaveroussy.fr. Phone: +33 1 42 11 51 28. Fax: +33 1 42 11 52 45.

ORCID

Liliane Massaad-Massade: 0000-0002-9636-4559

Barbara Stella: 0000-0001-8266-6604

Notes

The authors declare no competing financial interest.

■ ACKNOWLEDGMENTS

The research leading to these results has received funding from a public grant overseen by the French National Research Agency (ANR) as part of the "Investissements d'Avenir" program (Labex NanoSaclay, reference: ANR-10-LABX-0035), Ligue Contre le Cancer, Comité des Yvelines and de Val de Marne and PICS CNRS. We thank Ghislaine Frebourg for cryo-TEM observations and Vincent Guerneau for MALDI-TOF Mass Spectrometry analysis.

■ ABBREVIATIONS

AUC, area under the curve; DBCO, dibenzocyclooctyne; Ha, hybridization after bioconjugation; Hb, hybridization before bioconjugation; MALDI-TOF MS, matrix assisted laser desorption ionization–time of flight mass spectrometry; siRNA, small interfering RNAs; NPs, nanoparticles; SOLA, solanesol; SQ, squalene

■ REFERENCES

- (1) Chi, X., Gatti, P., and Papoian, T. (2017) Safety of antisense oligonucleotide and siRNA-based therapeutics. *Drug Discovery Today* 22, 823–833.
- (2) Stein, C. A., and Castanotto, D. (2017) FDA-Approved Oligonucleotide Therapies in 2017. *Mol. Ther.* 25, 1069–1075.
- (3) Whitehead, K. A., Langer, R., and Anderson, D. G. (2009) Knocking down barriers: advances in siRNA delivery. *Nat. Rev. Drug Discovery* 8, 129–38.
- (4) Bobbin, M. L., and Rossi, J. J. (2016) RNA Interference (RNAi)-Based Therapeutics: Delivering on the Promise? *Annu. Rev. Pharmacol. Toxicol.* 56, 103–22.

- (5) Burnett, J. C., Rossi, J. J., and Tiemann, K. (2011) Current progress of siRNA/shRNA therapeutics in clinical trials. *Biotechnol. J.* 6, 1130–46.

- (6) Akhtar, S., and Benter, I. (2007) Toxicogenomics of non-viral drug delivery systems for RNAi: Potential impact on siRNA-mediated gene silencing activity and specificity. *Adv. Drug Delivery Rev.* 59, 164–182.

- (7) Kanasty, R. L., Whitehead, K. A., Vegas, A. J., and Anderson, D. G. (2012) Action and reaction: the biological response to siRNA and its delivery vehicles. *Mol. Ther.* 20, 513–24.

- (8) Raouane, M., Desmaele, D., Urbinati, G., Massaad-Massade, L., and Couvreur, P. (2012) Lipid conjugated oligonucleotides: a useful strategy for delivery. *Bioconjugate Chem.* 23, 1091–104.

- (9) Desmaele, D., Gref, R., and Couvreur, P. (2012) Squalenoylation: a generic platform for nanoparticulate drug delivery. *J. Controlled Release* 161, 609–18.

- (10) Ali, H. M., Maksimenko, A., Urbinati, G., Chapuis, H., Raouane, M., Desmaele, D., Yasuhiro, H., Harashima, H., Couvreur, P., and Massaad-Massade, L. (2014) Effects of silencing the RET/PTC1 oncogene in papillary thyroid carcinoma by siRNA-squalene nanoparticles with and without fusogenic companion GALA-cholesterol. *Thyroid* 24, 327–38.

- (11) Ali, H. M., Urbinati, G., Chapuis, H., Desmaele, D., Bertrand, J. R., Couvreur, P., and Massaad-Massade, L. (2014) Effects of siRNA on RET/PTC3 junction oncogene in papillary thyroid carcinoma: from molecular and cellular studies to preclinical investigations. *PLoS One* 9, e95964.

- (12) Ali, H. M., Urbinati, G., Raouane, M., and Massaad-Massade, L. (2012) Significance and applications of nanoparticles in siRNA delivery for cancer therapy. *Expert Rev. Clin. Pharmacol.* 5, 403–12.

- (13) Raouane, M., Desmaele, D., Gilbert-Sirieix, M., Gueutin, C., Zouhiri, F., Bourgaux, C., Lepeltier, E., Gref, R., Ben Salah, R., Clayman, G., et al. (2011) Synthesis, Characterization, and in Vivo Delivery of siRNA-Squalene Nanoparticles Targeting Fusion Oncogene in Papillary Thyroid Carcinoma. *J. Med. Chem.* 54, 4067–4076.

- (14) Urbinati, G., Ali, H. M., Rousseau, Q., Chapuis, H., Desmaele, D., Couvreur, P., and Massaad-Massade, L. (2015) Antineoplastic Effects of siRNA against TMPRSS2-ERG Junction Oncogene in Prostate Cancer. *PLoS One* 10, e0125277.

- (15) Urbinati, G., de Waziers, I., Slamic, M., Foussigniere, T., Ali, H. M., Desmaele, D., Couvreur, P., and Massaad-Massade, L. (2016) Knocking Down TMPRSS2-ERG Fusion Oncogene by siRNA Could be an Alternative Treatment to Flutamide. *Mol. Ther.–Nucleic Acids* 5, e301.

- (16) Sobot, D., Mura, S., Rouquette, M., Vukosavljevic, B., Cayre, F., Buchy, E., Pieters, G., Garcia-Argote, S., Windbergs, M., Desmaele, D., et al. (2017) Circulating Lipoproteins: A Trojan Horse Guiding Squalenoylated Drugs to LDL-Accumulating Cancer Cells. *Mol. Ther.* 25, 1596–1605.

- (17) Sobot, D., Mura, S., Yesylevskyy, S. O., Dalbin, L., Cayre, F., Bort, G., Mouglin, J., Desmaele, D., Lepetre-Mouelhi, S., Pieters, G., et al. (2017) Conjugation of squalene to gemcitabine as unique approach exploiting endogenous lipoproteins for drug delivery. *Nat. Commun.* 8, 15678.

- (18) Jewett, J. C., and Bertozzi, C. R. (2010) Cu-free click cycloaddition reactions in chemical biology. *Chem. Soc. Rev.* 39, 1272–9.

- (19) Rostovtsev, V. V., Green, L. G., Fokin, V. V., and Sharpless, K. B. (2002) A stepwise Huisgen cycloaddition process: copper(I)-catalyzed regioselective "ligation" of azides and terminal alkynes. *Angew. Chem., Int. Ed.* 41, 2596–9.

- (20) Qin, B., Liu, L., Pan, Y., Zhu, Y., Wu, X., Song, S., and Han, G. (2017) PEGylated Solanesol for Oral Delivery of Coenzyme Q10. *J. Agric. Food Chem.* 65, 3360–3367.

- (21) Qin, B., Liu, L., Wu, X., Liang, F., Hou, T., Pan, Y., and Song, S. (2017) mPEGylated solanesol micelles as redox-responsive nanocarriers with synergistic anticancer effect. *Acta Biomater.* 64, 211–222.

- (22) Daneial, B., Joseph, J. P. V., and Ramakrishna, G. (2017) Molecular dynamics simulation analysis of Focal Adhesive Kinase

(FAK) docked with solanesol as an anti-cancer agent. *Bioinformation* 13, 274–283.

(23) Troiber, C., Kasper, J. C., Milani, S., Scheible, M., Martin, I., Schaubhut, F., Kuchler, S., Radler, J., Simmel, F. C., Friess, W., et al. (2013) Comparison of four different particle sizing methods for siRNA polyplex characterization. *Eur. J. Pharm. Biopharm.* 84, 255–64.

(24) Esmailzadeh Gharehdaghi, E., Amani, A., Khoshayand, M. R., Banan, M., Esmailzadeh Gharehdaghi, E., Amini, M. A., and Faramarzi, M. A. (2014) Chitosan nanoparticles for siRNA delivery: optimization of processing/formulation parameters. *Nucleic Acid Ther.* 24, 420–7.

(25) Ali, H. M., Maksimenko, A., Urbinati, G., Chapuis, H., Raouane, M., Desmaele, D., Yasuhiro, H., Harashima, H., Couvreur, P., and Massaad-Massade, L. (2014) Effects of Silencing the RET/PTC1 Oncogene in Papillary Thyroid Carcinoma by siRNA-Squalene Nanoparticles With and Without Fusogenic Companion GALA-Cholesterol. *Thyroid* 24, 327–338.

(26) Chang, P. V., Prescher, J. A., Sletten, E. M., Baskin, J. M., Miller, I. A., Agard, N. J., Lo, A., and Bertozzi, C. R. (2010) Copper-free click chemistry in living animals. *Proc. Natl. Acad. Sci. U. S. A.* 107, 1821–6.

(27) Jawalekar, A. M., Malik, S., Verkade, J. M., Gibson, B., Barta, N. S., Hodges, J. C., Rowan, A., and van Delft, F. L. (2013) Oligonucleotide tagging for copper-free click conjugation. *Molecules* 18, 7346–63.

(28) van Delft, P., Meeuwenoord, N. J., Hoogendoorn, S., Dinkelaar, J., Overkleef, H. S., van der Marel, G. A., and Filippov, D. V. (2010) Synthesis of oligoribonucleic acid conjugates using a cyclooctyne phosphoramidite. *Org. Lett.* 12, 5486–9.

(29) Jasinski, D. L., Li, H., and Guo, P. (2018) The Effect of Size and Shape of RNA Nanoparticles on Biodistribution. *Mol. Ther.* 26, 784–792.

(30) Versluis, A. J., van Geel, P. J., Oppelaar, H., van Berkel, T. J., and Bijsterbosch, M. K. (1996) Receptor-mediated uptake of low-density lipoprotein by B16 melanoma cells in vitro and in vivo in mice. *Br. J. Cancer* 74, 525–32.

(31) Tuschl, T. (2002) Expanding small RNA interference. *Nat. Biotechnol.* 20, 446–8.

(32) Othman, M., Desmaele, D., Couvreur, P., Vander Elst, L., Laurent, S., Muller, R. N., Bourgaux, C., Morvan, E., Pouget, T., Lepetre-Mouelhi, S., et al. (2011) Synthesis and physicochemical characterization of new squalenoyl amphiphilic gadolinium complexes as nanoparticle contrast agents. *Org. Biomol. Chem.* 9, 4367–86.

II. Review: Charcot Marie Tooth Disease Therapies: from the Classical Approach to Gene Regulation

Submitted to Journal Neurobiology of disease

Charcot Marie Tooth Disease Therapies: from the Classical Approach to Gene Regulation

Suzan Boutary¹, Andoni Echaniz-Laguna^{1,2}, David Adams^{1,2}, Michael Schumacher¹, Charbel Massaad³ and Liliane Massaad-Massade^{1*}

¹ U 1195, INSERM and Université Paris-Sud and Université Paris-Saclay, 94276 Le Kremlin-Bicêtre, France.

² Neurology Department, AP-HP, Paris-Sud University and French Referent Center for Familial Amyloid Polyneuropathy and other rare peripheral neuropathies (CRMR-NNERF), Bicêtre Hospital, Le Kremlin-Bicêtre, France.

³ Faculty of Basic and Biomedical Sciences, Paris Descartes University, INSERM UMRS 1124, 75006 Paris, France.

***Corresponding author:** Liliane Massade, PhD, U 1195, INSERM and Université Paris-Sud and Université Paris-Saclay, 94276 Le Kremlin-Bicêtre, France. Email : liliane.massade@inserm.fr, phone : + 33 1 49 59 18 30

Abstract

Charcot-Marie-Tooth disease is the most common inherited neuropathy in the world. Nevertheless, it has no cure. This review focuses on the mechanisms underlying the development of this disease and the potential therapies that are developed. First, the basic elements involved in myelination are deeply exposed. Then, the CMT pathology and the genes involved in its development are displayed with a focus on CMT-1A. The second part of this review discuss the most frequently used animal models as well as the molecules used to attempt a recovery from this unmet medical neuropathy. Finally, we highlight the latest therapeutic innovation in this field including RNA interference.

Key words: Peripheral Nervous System, Charcot Marie Tooth, Schwann Cells, Peripheral Myelin Protein 22, CMT1A, RNA interference

Funding: This work is supported by a public grant overseen by the French National Research Agency (ANR) as part of the “Investissements d’Avenir” program (Labex NanoSaclay, reference: ANR-10-LABX-0035).

III. European Patent: Antisense RNA Targeting PMP22 For the Treatment of Charcot Marie Tooth 1A



2, Place d'Estienne d'Orves - 75441 Paris Cedex 09 - France
Tél. : 33 (0)1 53 20 14 20 - Fax : 33 (0)1 53 20 14 91 - paris@lavoix.eu

CNRS
3, rue Michel-Ange
75794 PARIS CEDEX 16
FRANCE

A l'attention de M. Ludovic HAMON

Email (dire.valorisation@cnrs.fr), sans confirmation

Paris, le 27 septembre 2018

V.Réf. 11542-01/Liliane MASSADE et al
N.Réf. BET 18P2848 (IH/DK)

Utilisateur d'IP DATA², retrouvez votre dossier en cliquant [ici](#)

Dépôt - Pour action

Objet : Demande de brevet européen No. 18306241.3
ANTISENSE RNA TARGETING PMP22 FOR THE TREATMENT OF CHARCOT-M
Titulaire(s) : Centre national de la recherche scientifique
INSTITUT NATIONAL DE LA SANTE ET DE LA RECHERCHE MEDICALE
(INSERM)

Cher Monsieur,

Nous nous référons à nos correspondances antérieures et vous informons avoir fait le nécessaire pour protéger l'invention rappelée en rubrique par le dépôt ci-après :

Europe n° 18306241.3 du 25 septembre 2018.

Les taxes de désignation et d'extension ne sont plus à régler lors du dépôt de la demande, mais six mois après la publication du rapport de recherche, de sorte que nous reverrons avec vous la portée géographique de l'invention le moment venu.

Nous vous remettons ci-joint une copie de la demande telle que déposée. Notre facture correspondante vous sera adressée ultérieurement.

Par ailleurs, cette demande étant une première demande, si vous souhaitez bénéficier de la priorité de cette première demande pour protéger cette invention à l'étranger, de tels dépôts étrangers devront intervenir au plus tard le **25 septembre 2019**. Bien entendu, nous ne manquerons pas de vous rappeler cette échéance en temps opportun.

Nous vous rappelons par ailleurs que l'article L611-7 du Code de la Propriété Intellectuelle impose désormais à l'employeur d'informer chaque inventeur-salarié, auteur d'une invention de mission, du dépôt d'une demande de brevet.

Cabinet LAVOIX - SPE des professions de Conseils en Propriété Industrielle et d'Avocats - SAS au capital de 681 250 € - 331 829 754 R.C.S. Paris - N. TVA FR02331829754 - Toque E1626 inscrit au barreau de Paris - Siège Social : 2, place d'Estienne d'Orves, 75441 Paris Cedex 09 - France - Deutsche Niederlassung LAVOIX Munich - Antisgengch HRB 177666 - Cabinet LAVOIX (Milano) - REA 2106082 - Reg. Imp. MI e C.F. 09676230985 - Piazza IV Novembre 7, 20124 Milano



www.lavoix.eu

Nous vous prions d'agr er, Cher Monsieur, nos salutations distingu es.

PO : Audrey BIGEL

A handwritten signature in black ink, appearing to read 'Audrey Bigel', is written over the typed name 'Audrey BIGEL'.

Isabelle HAY

PJ. : Demande d pos e

Cc : MASSADE Liliane (Inventeur CNRS) par email, INSERM TRANSFERT
Copie(s)   CNRS INNOVATION - Mme Sabrina ONG (Email sabrina.ong@cnrsinnovation.fr)

IV. International extension of the Patent : Antisense RNA Targeting PMP22 For the Treatment of Charcot Marie Tooth 1A



2, Place d'Estienne d'Orves - 75441 Paris Cedex 09 - France
Tél. : 33 (0)1 53 20 14 20 - Fax : 33 (0)1 53 20 14 91 - paris@lavoix.eu

CNRS
3, rue Michel-Ange
75794 PARIS CEDEX 16
FRANCE

**A l'attention de Mme Marie-France
DAUMAS-LADOUCÉ**

**Email (noreply@lavoix.eu), sans
confirmation**

Paris, le 24 septembre 2019

V.Réf. 11542-01/Liliane MASSADE et al
N.Réf. BET 19P3966 (EMO/APE)

Utilisateur d'IP DATA², retrouvez votre dossier en cliquant [ici](#)

Dépôt - Pour information

Objet : Demande internationale PCT No. PCT/EP2019/075736
Priorité : EP 18306241.3
ANTISENSE RNA TARGETING PMP22 - TREATMENT OF CHARCOT-MT1A
Titulaire(s) : Centre national de la recherche scientifique
INSTITUT NATIONAL DE LA SANTE ET DE LA RECHERCHE MEDICALE
(INSERM)

Chère Madame,

Nous vous informons que, conformément à vos instructions, une demande internationale (PCT) a été déposée avec désignation de tous les pays membres, comme indiqué ci-dessous :

Date de dépôt: 24 septembre 2019
Numéro de dépôt : PCT/EP2019/075736
Titulaire(s) : Centre national de la recherche scientifique
INSTITUT NATIONAL DE LA SANTE ET DE LA RECHERCHE
MEDICALE (INSERM)
Inventeur(s) : MASSADE Liliane
MASSAAD Charbel
BOUTARY Susan
URBINATI Giorgia Maria Laura
COUVREUR Patrick
DESMAËLE Didier

Cabinet LAVOIX - SPE des professions de Conseils en Propriété Industrielle et d'Avocats - SAS au capital de 681 250 € - 331 829 754 R.C.S Paris - N TVA FR02331829754 - Toque E1626 inscrit au barreau de Paris - Siège Social 2, place d'Estienne d'Orves, 75441 Paris Cedex 09, France - Deutsche Niederlassung LAVOIX Munich - Amtsgericht HRB 177666 - Cabinet LAVOIX (Milano) - REA 2106082 - Reg. Imp. MI e C.F. 09676230965 - Piazza IV Novembre 7, 20124 Milano



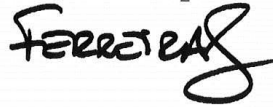
www.lavoix.eu

Nous vous remettons ci-joint une copie de la demande telle que déposée. Notre facture correspondante vous sera adressée ultérieurement.

Nous vous rappelons par ailleurs que l'article L611-7 du Code de la Propriété Intellectuelle impose désormais à l'employeur d'informer le ou chaque inventeur-salarié, auteur d'une invention de mission, du dépôt d'une demande de brevet.

Nous vous prions d'agréer, Chère Madame, nos salutations distinguées.

PO : Sandra FERREIRA_S

A handwritten signature in black ink, appearing to read 'FERREIRA_S' with a stylized flourish at the end.

Eva MORGADO

P.J. : Copie de la demande

Cc : MASSADE Liliane (Inventeur CNRS) par email, INSERM TRANSFERT, SATT IDF INNOV
Copie(s) à CNRS INNOVATION - Mme Daniela BREBION (Email daniela.brebion@cnrsinnovation.fr, sans confirmation)

V. Demande de Confidentiality

université
PARIS-SACLAY

-1-

Demande de mise en place d'accord de confidentialité sur le mémoire de soutenance de thèse, sans huis-clos

Nous soussignés,

Civilité : Mme

Nom : Massade

Prénom : Liliane

directeur de thèse,

et

Civilité : Mme

Nom : Boutary

Prénom : Suzan

doctorant(e),

sollicitons, de Monsieur le Président de l'Université Paris-Saclay, la mise en place d'accords de confidentialité, pour une thèse de doctorat présentant un caractère confidentiel avéré :

Titre de la Thèse : Développement d'une thérapie ciblée pour la maladie Charcot Marie Tooth 1A (CMT1A) par des nanoparticules siRNA PMP22 squalénées.

Spécialité : recherche clinique, innovation technologique, santé publique

ECOLE DOCTORALE : Signalisations et Réseaux Intégratifs en Biologie

ETABLISSEMENT DE PREPARATION DE LA THESE : Université Paris-Sud

Date de soutenance prévisionnelle: ...13.../...12...../...2019.....

Nous sommes informés que ce caractère confidentiel impose la mise en place d'accords préalables de confidentialité avec les rapporteurs et les membres du Jury et que les aspects confidentiels de la thèse ne pourront être présentés lors de la soutenance.

La date prévisionnelle de la soutenance est le :

Nous sommes également informés que cette confidentialité doit s'accompagner de restrictions sur la diffusion de la thèse.

La durée de confidentialité demandée est de : 24 mois

www.universite-paris-saclay.fr
Espace Technologique / Immeuble Discovery
Route de l'Orme aux Merisiers RD 128 / 91190 Saint-Aubin, France

Nous certifions que les toutes les alternatives ont bien été explorées¹ et qu'elles ne permettent pas d'évaluer les travaux de manière satisfaisante ou qu'elles ne permettent pas de garantir la confidentialité des travaux.

Motif(s) de la demande² :

1. Dépôt de brevet Européen Nombre : 18306241.3-1111 le 25/09/2018
Title : Antisense RNA Targeting PMP22 For the Treatment Of Charcot-Marie-Tooth 1A Disease.
2. Extension de brevet international Nombre: PTC/EP2019/075736. Date 24/09/2019
3. Publication : not yet submitted

A Kremlin-Bicêtre le 17/10/2019

Signature du doctorant



Signature du directeur de thèse



Dr Liliane MASSADE
INSERM U1195 CHU BICETRE
Bât. Grégory PINCUS
80 rue du Général LECLERC
94270 LE KREMLIN BICETRE

¹ Par exemple : regroupement des informations confidentielles dans une annexe, soumise à une clause de confidentialité, la thèse restant alors libre de toute confidentialité.

² Fournir tout élément permettant de justifier cette demande – copie d'un engagement de confidentialité sur des données reproduites dans la thèse (données personnelles de patients..), par exemple.

Avis du directeur de l'unité de recherche

avis favorable à la confidentialité de la thèse

avis défavorable à la confidentialité de la thèse

Nom, prénom, date et signature

Michael Schumacher
Directeur U 1195
17/10/2019



Observations :

Avis du directeur de l'école doctorale

avis favorable à la confidentialité de la thèse

avis défavorable à la confidentialité de la thèse

Nom, prénom, date et signature

Professeur
O. NÜSSE
Université Paris-Sud 11

18/10/2019



Observations :

ECOLE DOCTORALE 568 Signalisations et Réseaux Intégratifs en Biologie Université Paris-Saclay
--

Autorisation de confidentialité³

Le président de l'Université Paris-Saclay déclare que :

La thèse de doctorat de

Civilité :

Nom :

Prénom :

Pour la date prévue du :

/ /

Titre de la thèse :

Spécialité :

Ecole doctorale :

Etablissement opérateur d'inscription :

présente un caractère confidentiel avéré, requiert la mise en place d'accords de confidentialité et devra faire l'objet de restrictions sur sa diffusion

ne présente pas un caractère confidentiel avéré et ne requiert pas la mise en place d'accords de confidentialité

En cas d'autorisation la durée de confidentialité accordée est de (mois)

A , le

Nom, prénom, signature du chef d'établissement, cachet de l'établissement

³ Une copie de cette autorisation doit impérativement être transmise au service documentaire en charge du dépôt légal des thèses de l'établissement

Titre : Développement d'une thérapie ciblée pour la maladie Charcot Marie Tooth 1A (CMT1A) par des nanoparticules siRNA PMP22 squalénées

Mots clés : Charcot Marie Tooth 1A, PMP22, siRNA, Nanoparticules

Résumé : La maladie de Charcot Marie Tooth (CMT) 1A est la neuropathie héréditaire la plus fréquente au monde. Elle est dû à la duplication du gène *PMP22*. A ce jour, la majorité des traitements testés sont plutôt d'ordre palliatifs non curatifs. L'objectif de ce projet est de développer un nouveau traitement pour CMT1A basé sur la normalisation de la surexpression du produit du gène *PMP22* par une thérapie ciblée par siRNA. Dans cet objectif, huit siRNA *PMP22* ont été conçus et testés dans la lignée cellulaire MSC-80. *In vitro*, le siPM22 n°7 a montré une inhibition de 50% du gène de *PMP22* et de l'expression de la protéine correspondante sans affecter la viabilité cellulaire. Cet siRNA a été choisi pour des études ultérieures. Afin de protéger le siRNA *PMP22* de la dégradation et d'améliorer l'internalisation, nous l'avons couplé à un précurseur du cholestérol, le squalène (SQ), qui a la particularité de former des nanoparticules (NP) dans l'eau. Après bioconjugaison, obtention et caractérisation des NPs siRNA *PMP22*-SQ nous montrons que leur caractère lipophile reste stable au cours du temps et qu'ils restaient biologiquement actif. *In vitro*, les NPs siRNA *PMP22*-SQ inhibent, tout comme le siRNA *PMP22* transfecté dans les cellules MSC-80, l'expression du gène de *PMP22* à 50%. *In vivo*, les NPs siRNA *PMP22*-SQ injectées par *i.v.* resituent l'activité motrice dans deux modèles de souris transgéniques de CMT1A, portant une copie supplémentaire (JP18 B6) ou deux copies supplémentaires de (JP18/Y13 B6) de *PMP22* ainsi que la vitesse de conduction nerveuse et le potentiel d'action musculaire. Après sacrifice des souris, par microscopie confocale, nous montrons que les 2 facteurs de transcription KROX 20 et SOX10 ainsi que les neurofilaments sont augmentés dans les coupes de nerf sciatique traitées par les NPs siRNA *PMP22*-SQ témoignant d'une myélinisation et une régénération axonale. En microscopie électronique, nous observons une normalisation du phénotype qui se traduit par une compaction de la myéline due à l'internalisation des NPs siRNA *PMP22*-SQ dans les cellules de Schwann ainsi que dans les axones. En conclusion, nous montrons qu'un traitement ciblé par des NPs siRNA *PMP22* normalisant l'expression de la *PMP22* pourrait faire l'objet d'une future thérapie de la maladie CMT1A. Des études précliniques toxicologiques seront effectuées pour confirmer leur utilisation clinique.

Title : Development of a Targeted Therapy for Charcot Marie Tooth 1A (CMT1A) Neuropathy Based on siRNA PMP22 Squalene Nanoparticles

Keywords : CMT1A, PMP22, siRNA, Nanoparticles

Abstract: Charcot Marie Tooth disease 1A (CMT1A) is the most common inherited neuropathy worldwide. It is due to a duplication in the *PMP22* gene. Up to date, most of the tested drugs are rather symptomatic and not effective in reversing CMT neuropathy scores. Hence, the goal of this project is to develop new treatment for CMT1A using a targeted therapy against *PMP22* by siRNA. Eight siRNA *PMP22* were designed and tested on mouse Schwann cells. *In vitro*, siPM22#7 showed 50% inhibition of *PMP22* gene and protein expression and did not affect cell viability therefore, it was chosen for further studies. To protect this siRNA from degradation and improve its internalization, we used a precursor of cholesterol, squalene (SQ), that have the particularity to give nanoparticles (NPs) in water. After bioconjugation and characterization of the resulting siPMP22-SQ NPs we depicted that their lipophilic characteristic remained stable with time, and most importantly, still biologically active. *In vitro* they were able to inhibit *PMP22* gene expression of about 50 % similar to naked transfected siPMP22. In two CMT1A transgenic mice models carrying one extra copy (JP18 B6) or 2 extra copies (JP18/JY13 B6) of *PMP22*, we showed that siPMP22-SQ NPs normalized the motor activity. Moreover, nerve conduction velocity and compound muscle action potential revealed improvement in the siPMP22-SQ NPs treatment group in both mice models. Histologically, the effect of the siPMP22-SQ NPs was clear in electron microscopy images that displayed a proper alignment of myelin around the axon. In addition, KROX 20, SOX10 and neurofilament levels were normalized thus indicating that myelin and axonal regeneration can take place in the groups treated with siPMP22-SQ NPs. Interestingly, we found that siRNA-SQ NPs reached Schwann cells and axons. To conclude, a treatment using siRNA against *PMP22* can be the future therapy for CMT1A once it proved its safety and tolerability.

